TRANSPORTATION RESEARCH

RECORD

No. 1277

Soils, Geology, and Foundations

Modern Geotechnical Methods: Instrumentation and Vibratory Hammers 1990

A peer-reviewed publication of the Transportation Research Board

TRANSPORTATION RESEARCH BOARD
NATIONAL RESEARCH COUNCIL
WASHINGTON, D.C. 1990

Transportation Research Record 1277
Price: $23.00

Subscriber Category
IIIA Soils, geology, and foundations

Modes
1 highway transportation
3 rail transportation

Subject Areas
25 structure designs and performance
33 construction
61 soil exploration and classification
62 soil foundations
63 soil and rock mechanics

TRB Publications Staff
Director of Publications: Nancy A. Ackerman
Senior Editor: Naomi C. Kassabian
Associate Editor: Alison G. Tobias
Assistant Editors: Luanne Crayton, Kathleen Solomon, Norman Solomon
Production Coordinator: Karen Waugh
Graphics Coordinator: Diane Ross
Office Manager: Phyllis D. Barber
Production Assistant: Betty L. Hawkins

Printed in the United States of America

Library of Congress Cataloging-in-Publication Data
National Research Council. Transportation Research Board.

Modern geotechnical methods : instrumentation and vibratory hammers, 1990.
p. cm.—(Transportation research record ISSN 0361-1981 ; no. 1277)
ISBN 0-309-05057-X
1. Soil mechanics. 2. Foundations. 3. Construction equipment. 4. Piling (Civil engineering) I. National Research Council (U.S.). Transportation Research Board. II. Series: Transportation research record ; 1277.
TE7.H5 no. 1277
[TA710]
388 s—dc20
[624.1'5] 90-20118
CIP

Sponsorship of Transportation Research Record 1277

GROUP 2—DESIGN AND CONSTRUCTION OF TRANSPORTATION FACILITIES
Chairman: Raymond A. Forsyth, Sacramento, California

Soil Mechanics Section
Chairman: Michael G. Katona, Tyndall AFB

Committee on Soils and Rock Instrumentation
Chairman: John L. Walkinshaw, Federal Highway Administration, U.S. Department of Transportation
Loren R. Anderson, Harold E. Beeston, Joseph A. Caliendo, Barry R. Christopher, Brian J. Dawes, Charles N. Easton, John B. Gilmore, Gordon E. Green, William H. Hansmire, Neil F. Hawks, John L. Henkes III, Kenneth A. Jackura, Richard H. Ledbetter, P. Erik Mikkelsen, Dewayne L. Misterek, Soheil Nazarian, Gary W. Rhodes, A. J. Simmonds, Anwar E. Z. Wissa, Duncan C. Wyllie

Committee on Transportation Earthworks
Chairman: Richard P. Long, University of Connecticut
Loren R. Anderson, Thomas A. Bellatty, Jerome A. Dimaggio, Raymond L. Gemme, Robert D. Holtz, J. M. Hoover, Ilan Juran, James E. Kelly, Philip C. Lambe, Richard E. Landau, Robert M. Leary, C. William Lovell, David P. McKittrick, Victor A. Modeer, K. Jeff Nelson, Walter C. Waidelich, David E. Weatherby, Gary C. Whited

Committee on Foundations of Bridges and Other Structures
Chairman: Richard S. Cheney, Federal Highway Administration, U.S. Department of Transportation
Secretary: Richard P. Long, University of Connecticut
Francois J. Baguelin, Jean-Louis Briaud, Bernard E. Butler, Murty S. Devata, Albert F. Dimillio, Victor Elias, Richard L. Engel, Bengt H. Fellenius, George G. Goble, Richard J. Goettle III, James S. Graham, Robert C. Houghton, Alan P. Kilian, Hugh S. Lacy, Robert M. Leary, John F. Ledbetter, Jr., Larry Lockett, Randolph W. Losche, Lyle K. Moulton, Peter J. Nicholson, Michael Wayne O'Neill, Harvey E. Wahls, John L. Walkinshaw, Gdalyah Wiseman

Committee on Subsurface Soil-Structure Interaction
Chairman: J. Michael Duncan, Virginia Polytechnic Institute and State University
George Abdel-Sayed, Baidar Bakht, Sangchul Bang, Timothy J. Beach, Mike Bealey, Lester H. Gabriel, James B. Goddard, John Owen Hurd, Michael G. Katona, Kenneth K. Kienow, Richard W. Lautensleger, L. R. Lawrence, Donald Ray McNeal, Samuel C. Musser, Thomas D. O'Rourke, Raymond B. Seed, Ernest T. Selig, H. J. Siriwardane, Mehdi S. Zarghamee

Committee on Mechanics of Earth Masses and Layered Systems
Chairman: Tien H. Wu, Ohio State University
Walter R. Barker, Richard D. Barksdale, J. Michael Duncan, Deborah J. Goodings, John S. Horvath, Ilan Juran, Gerald P. Raymond, Cheryl A. Richter, Robert L. Schiffman, H. J. Siriwardane, Harry E. Stewart, Robert D. Stoll, Harvey E. Wahls, John L. Walkinshaw

Committee on Geosynthetics
Chairman: Verne C. McGuffey, New York State Department of Transportation
Richard D. Barksdale, Robert K. Barrett, Laurinda T. Bedingfield, John A. Bove, Calvin G. Burgess, Robert G. Carroll, Jr., Jerome A. Dimaggio, James B. Farris, Graham Ford, S. S. Dave Guram, Neil F. Hawks, Gary L. Hoffman, Robert D. Holtz, Thomas C. Kinney, Robert M. Koerner, Larry Lockett, James H. Long, R. Gordon McKeen, Bernard Myles, Malcolm L. Steinberg, John E. Steward, Harry H. Ulery, Jr., Dennis B. Wedding, David C. Wyant

Geology and Properties of Earth Materials Section
Chairman: C. William Lovell, Purdue University

Committee on Environmental Factors Except Frost
Chairman: Robert L. Lytton, Texas A & M University
Warren T. Bennett, Michael L. Bunting, Samuel H. Carpenter, Fu Hua Chen, Koon Meng Chua, Judith B. Corley, Barry J. Dempsey, Gary L. Fitts, Donald G. Fohs, Donald J. Janssen, Lawrence D. Johnson, Amos Komornik, C. William Lovell, Joseph Massucco, Said Ossama Mazen, R. Gordon McKeen, Thomas M. Petry, Miguel Picornell, Rogel H. Prysock, Albert C. Ruckman, Larry A. Scofield, Malcolm L. Steinberg, Jacob Uzan, Gdalyah Wiseman

G. P. Jayaprakash, Transportation Research Board staff

Sponsorship is indicated by a footnote at the end of each paper. The organizational units, officers, and members are as of December 31, 1989.

Transportation Research Record 1277

Contents

Foreword

The 19 papers included in this Record are of interest to geotechnical and foundation engineers. The first 13 papers are on geotechnical instrumentation used for design and monitoring of construction and performance of transportation facilities. The next four papers contain discussions of laboratory and field performance of vibratory-driven piles. Also included in this Record are papers by Brown on drilled shaft construction and by Juang and Ulshafer on an expert system for pile selection.

Of the first 13 papers on geotechnical instrumentation, 4 are on investigation of swelling clays; the next 6 are on monitoring and analysis of data on construction, settlement, and performance of caissons, culverts, tunnels, and so forth; and the remaining 3 are on the instrumentation of geosynthetics used in earthworks.

The installation of piling has been accomplished for many years by impact hammers. Volumes of research have been published on the behavior of impact-driven piles. Rational dynamic formulas were developed over 100 years ago to estimate as-driven pile capacity from the blow count. The more recent use of wave equation analyses, developed about 50 years ago, has improved verification of as-driven capacity while providing information about pile stresses during driving. However, until recently, the behavior of piling driven by vibratory equipment has not received detailed study. Public agencies have been hesitant to permit vibratory installation of production piles because proven methods did not exist to determine either capacity or pile damage. This void in the available information is partially filled by the four papers included in this Record that relate to the behavior of bearing piles driven by vibratory hammers. Additional information on vibratory pile installation was published in *NCHRP Report 316: Laboratory Evaluation of Piles Installed with Vibratory Drivers*.

On the Characterization of Suction in Swelling Clay

I. KEISSAR, J. UZAN, AND R. BAKER

The analysis of wetting and consequent swelling of unsaturated clays requires the specification of water potential in the unsaturated regime. Conventional characterization of water potential in unsaturated soils is done in terms of "retention curves" that specify a relation between suction and water content. In all conceptual models of unsaturated soils, suction is assumed to depend on the geometry of the "water-filled pore space." A first order characterization of this geometry is proposed in terms of water content, void ratio, and initial conditions. Despite this fact, conventional retention curves are presented as a relation between suction and water content, regardless of the void ratio. Moreover, in conventional laboratory techniques for the determination of suction there is no control over the void ratio, and each point on the retention curve corresponds to a different void ratio if swelling soil is tested. The present paper presents a laboratory technique for the determination of suction as a function of water content, void ratio, and initial conditions. Preliminary experimental results show that void ratio may have a substantial effect on suction, particularly in the low suction range. It is also demonstrated that the dependence of suction on void ratio has a significant effect on the analysis of the flow and swelling processes, to the extent that use of conventional suction curves in the analysis may lead to unreasonable results.

Design of structures in swelling soils represents one of the most challenging engineering problems. This problem occurs mainly in unsaturated clay soils in temperate climatic conditions consisting of wet and dry seasons. Generally the process involves migration of water from wet to relatively dry regions in the soil mass. This migration is accompanied by volume changes and, if mechanical constraints are present, a buildup in the state of stress. Thus the problem is a multifield process involving simultaneous changes in void ratio, water content, and stress as a result of a change in the environmental boundary conditions. Migration of water is an indication of spatial variation in the energy level of the soil water. Consequently, one of the preconditions for rational analysis of the swelling process is the establishment of a constitutive law which characterizes the energy state of water in unsaturated clay soils in a way that is meaningful under conditions that exist during a process of constrained swelling. The present work represents an attempt of such characterization. The paper includes the following elements:

1. Discussion of some physical facts relevant for the formulation of a constitutive model of water potential in unsaturated swelling soils;
2. A detailed description of equipment which was built for the purpose of experimental determination of the model;
3. Preliminary experimental results which were obtained for a particular Israeli clay at a given initial condition; and
4. A demonstration of the significance of the present characterization vis-à-vis the classical formulation, which is based on the concept of retention curves.

Faculty of Civil Engineering, Technion-Israel Institute of Technology, Haifa, Israel.

THE CONSTITUTIVE MODEL

The essential feature of the swelling process is the simultaneous change of void ratio, water content, and stress. Hence a proper characterization of the energy state of water in an unsaturated swelling clay soil should reflect the dependence of the energy on the parameters that change during the process, namely void ratio, water content, and stress. The following discussion uses the term "water potential" (h) as an abbreviation for the "energy state of water in the soil." When h is negative, it is usually called "suction."

In the classical approach, using the pressure or suction plates procedures [ASTM D3152 (*1*)], retention curves are determined without control of void ratio. In nonswelling soils this feature of the classical procedure is not a limitation, because void ratio does not change during the process. However, when dealing with swelling soils it is important to quantify the dependence of the potential on the void ratio. The existence of such a dependence is implied by all models that relate suction to the "geometry of the pore space" [e.g., Yong and Warkentin (*2*), Bear (*3*), and many others].

In view of this argument, we propose the following constitutive model for the specification of water potential:

$$h = p_a + p_{w0} + p_{w\sigma} + \gamma_w Z - \phi(w,e,I_0) \quad (1)$$

where

h = total water potential,
w = current water content,
e = current void ratio,
I_0 = "initial conditions," including w_0 and e_0 (the initial values of w and e) but also the method of sample preparation (compaction) and other factors of similar nature,
$\phi(w,e,I_0)$ = physico-chemical potential (suction), a term representing the effect of the clay matrix on the energy of the water mechanisms by which such effects take place (include capillary, absorption, osmotic, etc.),
p_a = air pressure (present in an equation defining the potential of water because ϕ includes a capillary component, which is defined relative to the air pressure),

p_{w0} = static component of pore water pressure, related to the depth of the element below water table,
$p_{w\sigma}$ = excess pore water pressure due to external mechanical loading,
Z = elevation,
γ_w = unit weight of water, and
$\gamma_w Z$ = potential energy of the water.

Since the interaction between soil and water depends on the position of water elements relative to the clay particles, the value of ϕ must depend on the geometry of the water-filled pore space. As a first approximation this geometry can be characterized by the void ratio and water content. It is evident, however, that these two scalar variables cannot describe all the details of the pore geometry. Consequently, there may exist two samples with the same e and w but having different ϕ values due to the difference in the "pore size distribution function," or in other words difference in "soil structure." Failure to include such high-order geometrical variables in the constitutive relations manifests itself as a "history dependence," that is, the potential ϕ will show a dependence on the total time history of e and w, rather than the final values of these variables. One of the well-known manifestations of such history dependence is the phenomenon of hysteresis. In the present work we avoid the need to model hysteresis by considering the wetting process only. Other aspects of the history dependence are described in an approximate way by allowing ϕ to depend not only on the current values of w and e but also on the initial conditions, I_0. In other words, we allow different functions $\phi(w,e)$ for samples with different initial conditions, and therefore write $\phi(w,e,I_0)$.

Equation 1 is essentially a constitutive assumption, and as such its validity must be judged on the basis of the correspondence between predictions obtained using this equation and experimental results. In general this equation is not controversial, except perhaps the role of the term $p_{w\sigma}$, representing the effect of external loads on the water potential. Therefore, further discussion of Equation 1 is restricted mainly to this term.

In saturated soils Equation 1 simplifies to

$$h = p_{w0} + p_{w\sigma} + \gamma_w Z \tag{2}$$

corresponding to $p_a = 0$ and $\phi(w_s,e,I_0) = 0$, where w_s is the moisture content at complete saturation. Equation 2 states that the total water potential is the sum of the gravity potential, the static water pressure, and the mechanical potential due to external loading. The existence of $p_{w\sigma}$—generally called excess of pore pressure due to mechanical load—is well known in saturated soils where undrained conditions prevail. However, when the water is allowed to drain, $p_{w\sigma}$ will dissipate with time, with the external load being now supported by the particles (principle of effective stress).

In unsaturated soils, all terms of Equation 1 may exist simultaneously. However, in the case of low degree of saturation, when both the air and the water are continuous, one may argue whether $p_{w\sigma}$ develops or not under load application. If $p_{w\sigma}$ develops it is anticipated that due to the existence of the continuous air phase within the material (corresponding to internal drainage), $p_{w\sigma}$ will certainly dissipate, and may do so at a fast rate. Therefore, for practical purposes and since processes of wetting and swelling are relatively slow, $p_{w\sigma}$ may be assumed to equal zero. This argument breaks down at sufficiently high degree of saturation (90 percent and higher), when the air in the soil exists probably in the form of air bubbles [Barden (*4*)]. At these high degrees of saturation, $p_{w\sigma}$ probably dissipates at a rate similar to or slightly slower than that of a completely saturated soil.

The above discussion suggests that $p_{w\sigma}$ dissipates with time, probably at a faster rate in unsaturated soils than in the completely or almost completely saturated soils. It should be noted that $p_{w\sigma}$ can be attributed to a variety of sources, such as foundations loading, changes in overburden pressure, etc. Due to these external loads, $p_{w\sigma}$ develops and dissipates, resulting in void ratio changes and consequently changes in the water potential. The effect of external load on the water potential is obtained here naturally, in contrast with the approach taken by Philip (*5*), who included a separate "overburden potential" term in Equation 1.

THE PRINCIPLE OF THE PROPOSED TESTING METHOD

In principle the proposed procedure for the determination of the function $\phi(w,e,I_0)$ is similar to the conventional pressure plate test [ASTM D-3152 (*1*)], or Zur's osmotic cell (*6*), except for the fact that the soil sample is enclosed in a rigid cell, hence in a wetting process the volume of the sample and also the void ratio remains constant. In fact, each point of the function $\phi(w,e,I_0) = \phi(w,e=e_0,I_0)$ is determined by running a swell pressure test under controlled suction. The suction is controlled either by the concentration of the osmotic solution or by the magnitude of the externally applied air pressure. Tests of similar type have been performed previously by Kassiff and Ben Shalom (*7*) for the purpose of estimating swelling pressure under controlled suction rather than quantifying the suction function. On the basis of the discussion presented in the previous section, the mechanical pressure (swell pressure) that is developed during such a test has no effect on the results of the measurements, because by its very nature the test is run under "drained" conditions. One of the added advantages of running suction tests at constant volume is that the pore size distribution function (soil structure) remains approximately constant during the test.

More specifically, consider the osmotic version of the test, in which the following procedure is used:

1. A series of soil samples are compacted in a rigid cell to the same initial conditions w_0, e_0.
2. Each sample is allowed to come to equilibrium with an osmotic solution of different concentration. Let h_s be the potential of the water in the solution. During the test p_a is kept equal to atmospheric pressure. The sample is prevented from swelling by the rigid cell, so that the void ratio remains at its initial value, i.e., $e = e_0$.
3. At equilibrium the total water potential of the sample equals h_s, the known potential of the water in the osmotic solution; p_{w0}, $p_{w\sigma}$, and $\gamma_w Z$ are zero; and Equation 1 reduces to $h = -\phi(w,e_0,I_0) = h_s$, or:

$$\phi(w,e_0,I_0) = -h_s \tag{3}$$

4. At the end of the test the water content at equilibrium is determined. Repeating this procedure with a series of sam-

ples, all having the same initial conditions, using different concentrations of the osmotic solution with each sample, results in a function $\phi = \phi(w,e_0,I_0)$, which is a "retention curve" for a condition of constant void ratio.

In a second version of this procedure, the water potential at equilibrium is controlled by applying a known air pressure p_a to the sample rather than the osmotic solution. In this case the water potential at equilibrium equals the energy of free water (i.e., $h = 0$), and p_{w0}, $p_{w\sigma}$, and $\gamma_w Z$ equal zero. Hence Equation 1 reduces to

$$h = p_a - \phi(w,e_0,I_0) = 0 \tag{4.1}$$

or

$$\phi(w,e_0,I_0) = p_a \tag{4.2}$$

EQUIPMENT

The test equipment is composed of a specimen box, a supply system for water or osmotic solution, and an air pressure supply system. The specimen box (Figure 1) is made of stainless steel and it may be considered as rigid. The box consists of two parts:

1. The box body, in which the specimen is compacted (part A). At the bottom of the box there is a porous stone and a connection to air pressure, or (as an alternative) an atmospheric pressure opening.

2. The box cover (part B). Two stainless steel meshes are embedded in this cover, No. 80 on top and under it No. 20. The surface of the top mesh creates a plane with the area of the cover box.

Water or osmotic solution is supplied through two connections at the top of the box cover. This arrangement provides the supply of water or osmotic solution to the stainless steel meshes and through them to the top of the specimen. The osmotic solution (or water) is circulated continuously.

The two parts of the box are separated by semipermeable membrane. The membrane separates the sample from the circulating free water or osmotic solution. When suction is controlled by air pressure, fresh water is supplied, and the semipermeable membrane that is used is pervious to water but impervious to air. When suction is controlled by osmotic solution, the air pressure in the soil specimen is atmospheric, and the semipermeable membrane used is pervious to water but impervious to salt molecules in the solution.

One of the advantages of this arrangement is that water penetrates into the sample on one side, while air leaves the system on the other side. This prevents air from being trapped inside the sample and reduces the time required in order to achieve equilibrium. The principal disadvantage of this testing procedure is that tests can be conducted in a wetting process only. This limitation is due to the fact that it is not possible to prevent shrinkage or to keep the void ratio constant during a drying process.

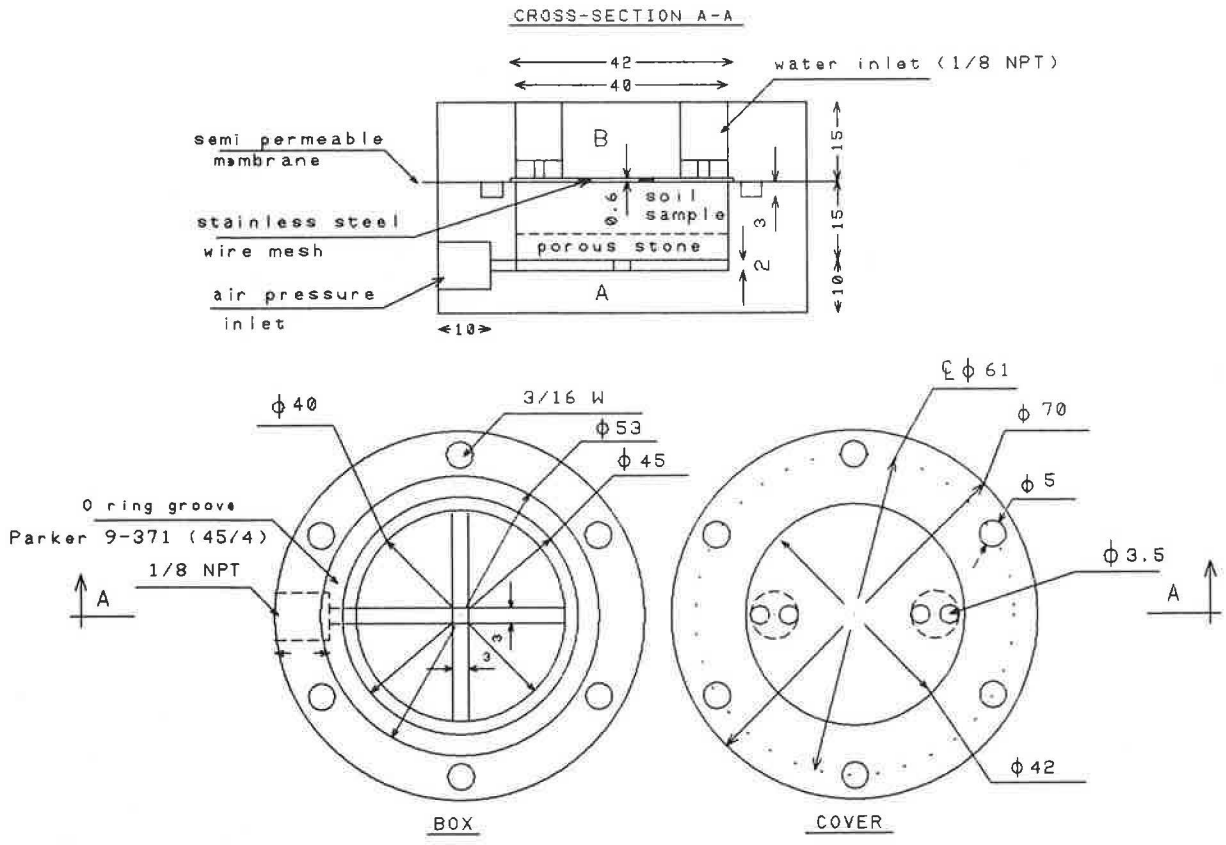

FIGURE 1 Equipment for measuring retention curve in constant void ratio (dimensions in mm).

TEST PROCEDURE

The soil specimen can be compacted or undisturbed (in this research only compacted samples were tested). The samples are statically compacted directly in the specimen box to a desired initial void ratio and water content. The initial conditions should be such as to ensure a wetting of the specimen during the test. The specimen dimensions are 4 cm diameter and 0.5 cm height. The specimen height is relatively small in order to reduce the time required to reach equilibrium.

When suction is controlled using air pressure, the test procedure is as follows:

1. Specimen is compacted to the desired initial void ratio and water content directly in the specimen box. The suitable semipermeable membrane is placed on the sample and the box is closed tightly.
2. The desired air pressure is applied to the specimen. This air pressure is kept constant. Since the specimen is relatively dry, equilibrium between the air pressure and the sample water pressure is reached almost instantaneously.
3. The water supply is connected to the box cover. The water fills the mesh holes, and flows to the soil specimen through the semipermeable membrane. The specimen water content is increased until equilibrium is established.
4. The test is stopped and the water content of the soil specimen is measured.

Using this procedure the following problems were encountered:

- There is small but constant diffusion of air through the membrane from the specimen chamber to the box cover. This diffusion slows the rate of water flow into the soil specimen. Consequently, the time required for equilibrium was of the order of 2 to 3 weeks.
- Although the membrane is supported by the box cover, there were many cases where it was punctured by the applied air pressure.

Where suction is controlled by an osmotic solution, the test procedure is similar to the one described above. The differences between the two procedures are as follows:

- The air pressure in the soil specimen is atmospheric (the opening at the bottom of the cell is opened to the atmosphere).
- The membrane used is pervious to water but impervious to the salt molecules.
- Osmotic solution in a certain concentration is circulated through the box cover and the stainless steel meshes. The salt used is Carbowax-Polyethylenglycol 6000, which has also been used by Zur (*6*), Kassiff and Ben Shalom (*7*), and Samocha (*8*). In order to keep the concentration of the solution at a constant value, a large volume of solution is used and the solution is circulated constantly through the box cover.

Using osmotic solution in order to control suction has several advantages:

- The time needed to reach equilibrium is just 3 or 4 days.
- There were almost no cases of membrane failures.
- Test can be conducted up to 3000 kPa of suction (*6*).

A potential disadvantage of using osmotic solution is the possibility of membrane corrosion. It was found by Samocha (*8*) and Ben Shalom (*9*) that after about a week the membrane is torn by corrosion. Because the proposed equipment reaches equilibrium after 3 to 4 days, however, it appears that this problem is not relevant in the present case.

TEST RESULTS

All tests were made on "Mizra clay," a typical Israeli expansive clay. The basic properties of this clay are

- Liquid limit (LL) 78 percent;
- Plastic limit (PL) 29 percent;
- Percent fines (passing No. 200) 98 percent; and
- Specific gravity (*Gs*) 2.78.

The initial water content in all the tests was 10 percent.

Test results, conducted with air pressure up to 700 kPa and osmotic solution up to 1962 kPa are given in Table 1 and Figure 2. Some tests were conducted with pure water, keeping the air pressure in the sample at atmospheric value. Equilibrium was reached after 3 days. Water contents in equilibrium were equal to the expected water content at full saturation, which is equal to e/Gs. An additional series of tests was performed using osmotic solution and varying the testing time. It was found that maintaining the sample in the cell longer than 3 to 4 days did not affect the results in any systematic way.

Table 1 shows that there is a good agreement between results of tests made with air pressure and tests made with osmotic solution (in the range of 0 to 700 kPa where air pressure tests could be conducted). Figure 2 shows that the retention curves depend on the void ratio. The separation between curves of different void ratios is more pronounced at high water contents (low suction values). A possible explanation of this trend is that, in relatively wet soils, small voids are filled with water and suction is controlled by the bigger voids. The size of the large voids is changed with void ratio, and hence in this range the suction shows strong dependence on the void ratio. In relatively dry soils, the bigger voids are empty of water, and suction is determined by the size of the smaller voids. Changes in void ratio have only a small effect on the size of the small voids; hence in this water content range the suction is almost independent of the void ratio.

A comparison was made between the retention curves obtained in this research and the results obtained by Livneh et al. (*10*) using the pressure plate apparatus, and the same Mizra clay. It should be emphasized that the results of Livneh et al. (*10*) correspond to a drying process starting from saturation. From Figure 2 it appears that, in general, the void ratio of the tests conducted by Livneh et al. (*10*) were very high. The initial void ratio (at saturation) is greater than 1.5.

It may be of interest to point out that the retention curves in Figure 2 are by definition loci of constant effective stresses. Adding a facility for measuring the swelling pressure developed in this test will make this type of equipment extremely useful for studying the principle of effective stress in unsaturated swelling soils.

TABLE 1 SUCTION MEASUREMENT RESULTS

e_o	suction (Kg/cm²)	w(%) (air press.)	w(%) (Carbowax)
1.1	0	41.8 40.1	
	2	26.8 26.4	27.2
	4	26.3 26.2	25.6
	6	25.2	23.9
	8		24.9
	15		21.8
	20		20.6
1.0	0	35.3 38.1	
	2	28.4	25.6 28.4
	4	28.1 27.6	27.0
	6	26.0	23.0
	8		24.2
	15		20.8
	20		19.8
0.9	0	33.7 33.3	
	2	25.7 26.1	25.4
	4	24.8 24.6	24.2
	6	25.4 24.1	23.4
	8		24.0
	15		20.8
	20		20.1
0.8	0	29.4	
	2	28.0	
	4	24.1	
	6	23.5	
	8		23.6
	15		20.2
	20		19.7

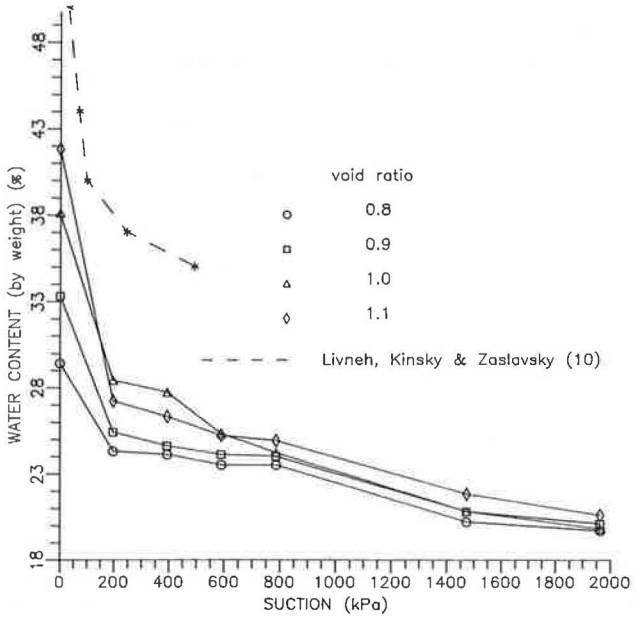

FIGURE 2 Suction versus water content and void ratio (Mizra clay).

SIGNIFICANCE OF THE PRESENT SUCTION CHARACTERIZATION

In order to study the implications and significance of the dependence of suction on both void ratio and water content, a one dimensional free swell flow problem in expansive soil was analyzed. The method of analysis is an extension of the approach presented by Uzan, Baker, and Frydman (*11*). Complete details of this procedure can be found in the work of Keissar (*12*).

The numerical implementation of this procedure requires an iteration solution of flow and stress-deformation problems in each time step. Both of these problems are solved using finite element technique. The geometry of the finite element mesh used for the analysis of the one dimensional free swell problem is given in Figure 3. The boundary conditions of this problem are as follows:

- Zero water potential at the bottom of the sample (boundary AB);
- Zero flux through the boundaries AD, DC, and CB; and
- No external stresses on the specimen top (boundary DC).

The problem defined by these boundary conditions is one dimensional for both flow and deformation, and it corre-

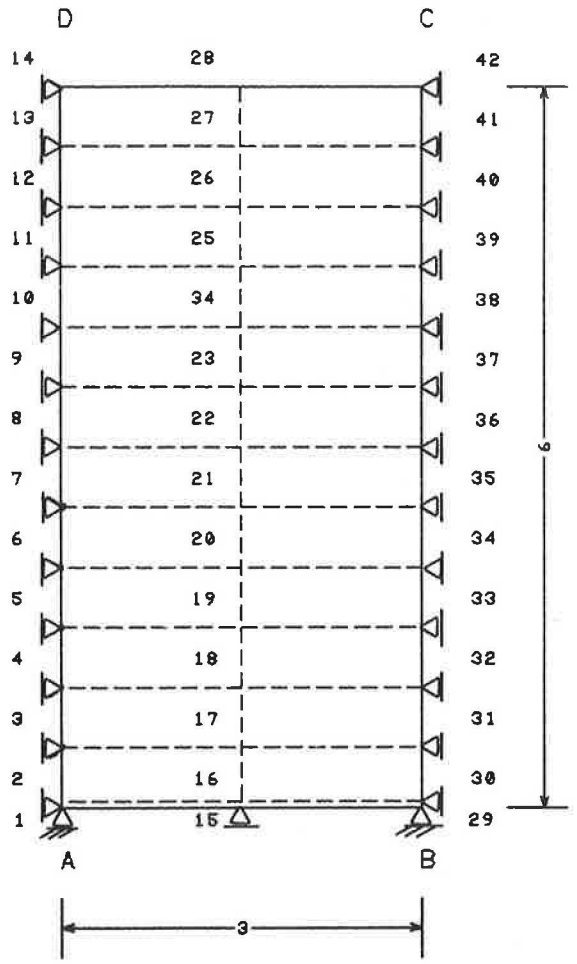

FIGURE 3 One-dimensional problem—geometry and elemental mesh (dimensions in cm).

sponds to a "free swell" test in an odometer. The problem was solved for the following initial conditions:

- Initial void ratio is 1.0;
- Initial water content is 0.21; and
- Distribution of initial water potential as implied by the initial conditions and the nature of the suction function.

Three different models of the suction function were analyzed:

Case 1. Suction is assumed to depend on both water content and void ratio, according to the approach presented in this paper. The experimental values given in Figure 2 were used for the purpose of the analysis. These curves were measured at w_0 = 10 percent, compared with the initial water content of 21 percent assumed in the analysis. Further tests conducted with the same equipment, using the same soil at w_0 = 21 percent, showed no significant effect on the retention curves (*13*).

Case 2. Suction is assumed to depend on water content only. This case is included in order to establish the significance of the relation between suction and void ratio to the results of the analysis. The suction function for e = 1.0 in Figure 2 was used for the purpose of the analysis. This suction function is consistent with the assumed initial void ratio of 1.0.

Case 3. Conventional suction curve as a function of water content. This case is included in order to illustrate some of the difficulties that result from the use of conventional retention curves for the analysis of flow in swelling soils. The experimental function found by Livneh et al. (*10*) and given in Figure 2 was used for the purpose of the analysis.

A number of additional parameters and constitutive relations are required in order to completely specify the problem. These parameters are related to the stress-deformation behavior of the material, interaction between the flow and deformation regimes, and dependence of permeability on the state of the system (w,e). Since the purpose of the present section is to investigate the significance of the new characterization of suction on a swelling problem, these variables are the same for all three suction curves presented above. Actual values for these parameters were established for Mizra clay and are presented in the work of Keissar (*12*).

For the initial conditions given above and from the suction functions found in this research, the initial suction is 1670 kPa. For the same initial water content, the initial suction based on Livneh et al. (*10*) is approximately 34,000 kPa. This last value is obtained at an unknown void ratio, and it is probably not consistent with an initial void ratio of 1.0. The use of classical retention curves always results in this type of inconsistency when flow in swelling soils is considered.

The results of the analysis for the three models of suction function described above are presented in Figure 4. On the basis of this figure, it may be concluded that

- The dependence of suction on void ratio has a considerable influence on the flow regime. This influence is seen both in Case 2 (suction independent of void ratio) and Case 3 (classical retention curve) as compared with Case 1 (present characterization).
- Using the retention curve found with the pressure plate apparatus (Case 3), the flow rate is much greater than the flow rate resulting using the suction functions based on the proposed measurement technique (Cases 1 and 2). The reason for this difference is the much higher initial value of suction inferred in Case 3, which implies a large gradient on wetting and therefore very high flow rates.
- The water contents obtained in Case 3 are very high, exceeding the water content at saturation at the calculated void ratios. The reason for this erroneous result is that the retention curve of Livneh et al. (*10*) corresponds to an unrealistically high void ratio, as discussed above.

It is seen that the dependence of suction on void ratio has a significant effect on the analysis of flow and deformation in swelling soils. If one does not use suction values that are consistent with the actual void ratio of the sample (as is the case when classical retention curves are used) then the results may contain large errors and inconsistencies.

SUMMARY AND CONCLUSIONS

It is natural to assume that the potential of water in unsaturated soils is a function of the geometry of the water field pore

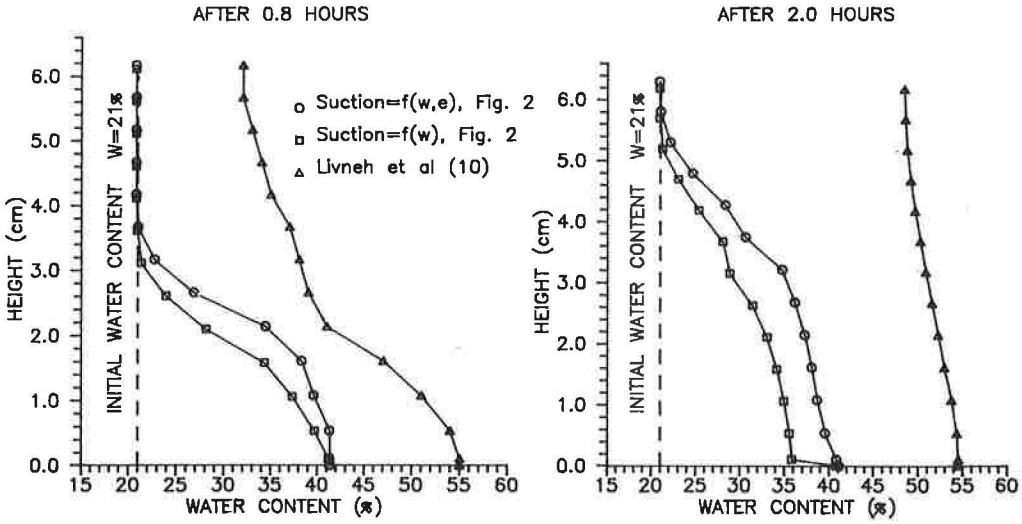

FIGURE 4 One-dimensional free swell flow and expansion problem—results.

space, and hence depends on both water content and void ratio. A new experimental procedure was developed in order to characterize the dependence of water potential on the void ratio. In this procedure, suction is measured under constant volume conditions, essentially in a type of "swelling pressure" test. It is argued that the mechanical swelling pressures that developed during such a procedure have no effect on the measured values of suction, due to the "drained" nature of the test.

Preliminary test results show that, as expected, suction depends on the void ratio. This dependence is particularly significant in the range of small suctions. The implications of this new characterization of water potential on the analysis of flow and deformation in swelling soils are demonstrated in a number of case studies. It is shown that the dependence of suction on void ratio may have a significant effect on the results of such an analysis. Moreover, the use of conventional retention curves, which are obtained without control of the void ratio, may result, with inconsistencies in the calculated results.

REFERENCES

1. ASTM. *Annual Book of ASTM Standards*, Vol. 4, No. 8, 1988, pp. 381–386.
2. R. N. Yong and B. P. Warkentin. *Introduction to Soil Behavior*. Macmillan, New York, 1966.
3. J. Bear. *Dynamics of Fluid in Porous Media*. American Elsevier New York, 1972.
4. L. Barden. Consolidation of Compacted and Unsaturated Clays. *Geotechnique*, Vol. 15, 1965, pp. 267–286.
5. J. R. Philip. Moisture Equilibrium in the Vertical in Swelling Soils I. Basic Theory. *Australian Journal of Soil Research*. Vol. 7, 1969, pp. 99–120.
6. B. Zur. Osmotic Control of the Matrix Soil-Water Potential: I. Soil Water System. *Soil Science*. Vol. 102, 1966, pp. 394–398.
7. G. Kassiff and A. Ben Shalom. Experimental Relationships Between Swell Pressure and Suction. *Geotechnique*, Vol. 21, No. 3, 1971, pp. 245–255.
8. S. Samocha. *A Method for Measuring Three-Dimensional Swell and Shear Strength of Clay Specimens Under Controlled Unsaturated Conditions*. M.S. thesis. Technion Israel Institute of Technology, Haifa, Israel, 1971.
9. A. Ben Shalom. *Laboratory Method for Measuring Swell Potential Under Conditions of Partial Saturation*. M.S. thesis. Technion Israel Institute of Technology, Haifa, Israel, 1970.
10. M. Livneh, I. Kinsky, and D. Zaslavsky. *The Relationship Between the Suction Curves and Atterberg Limits*. Research Report CV-194. Technion Israel Institute of Technology, Haifa, Israel, 1967.
11. J. Uzan, R. Baker, and S. Frydman. Characterization of Constrained Swelling of Clay. In *Transportation Research Record 1137*, TRB, National Research Council, Washington, D.C., 1987, pp. 52–58.
12. I. Keissar. *The Development of a Model for the Prediction of Flow, Strains and Stresses in Expansive Soils*. D.S. thesis. Technion Israel Institute of Technology, Haifa, Israel, 1989.
13. E. Weisberg. One Dimensional Development of Swelling and Wetting of Heavy Clay Samples in the Laboratory and Centrifuge. M.S. thesis. Technion Israel Institute of Technology, Haifa, Israel, 1989.

Publication of this paper sponsored by Committee on Environmental Factors Except Frost.

Study of Flow in Compacted Columns of Swelling Clay

E. WEISBERG AND S. FRYDMAN

Part of a research program aimed at studying the advance of the wetting front and the development of swell during flow through a compacted, active clay is described. The study included tests on compacted soil columns tested both under laboratory conditions and under an increased acceleration field in a centrifuge. Special instrumentation was employed, including gamma ray scanning, high-speed photography, and moisture transducers. Test results indicated differences in the wetting process for soil compacted wet and dry of plastic limit. In the latter case, a sharp wetting front was observed, whose rate of advance was unaffected by the high suction in the soil. In the columns compacted wet of plastic limit, the wetting front was less sharp, and its advance was significantly affected by soil suction. In all cases, the coefficient of permeability dropped continuously following wetting. These observations led to a model for the process of flow through swelling soil in which flow advances through the large, inter-aggregate pores of the soil. As the aggregates become wet, they swell, the pores close, and permeability decreases.

Prediction of the behavior of swelling-soil embankments and subgrades on wetting requires an understanding of the coupled effects of saturated and unsaturated flow, swell, and the stress-strain response of the soil. Such predictions are of importance in many fields (e.g., performance of pavements on expansive clays, stability of water reservoir embankments, development of lateral pressure on structures retaining expansive soils, performance of foundations located in or near expansive soils). Several simplified modeling approaches have been developed for estimation of soil movements as a result of wetting and consequent swelling. These generally involve a decoupling of the flow and stress-strain problems [e.g., Justo et al. (*1*), Picornell and Lytton (*2*), Uzan et al. (*3*)]. Richards (*4*) presented a more sophisticated approach that employs a coupled analysis, leading to a more realistic modeling of the physical processes involved. However, he concluded that "current knowledge of the interaction between water flow and load-deformation processes is not sufficient for the accurate analysis of the response of swelling soils in the field."

This paper describes part of a research program aimed at studying the advance of the wetting front, and the accompanying development of swell, during flow through a compacted, active clay. The overall study included tests on compacted soil columns performed both under laboratory conditions and under increased accelerations in a centrifuge, with the purpose of clarifying the modeling laws governing the coupled flow-swell process.

Technion-Israel Institute of Technology, Haifa, Israel.

THE SOIL TESTED

The soil used in the investigation was a highly plastic, brown clay known in Israel as Mizra clay, from a location about 20 km east of Haifa. This clay has been used for many previous research studies carried out in Israel on the swelling mechanism [e.g., Kassiff et al. (*5*), Komornik and Zeitlen (*6*), Ben Shalom (*7*), Samoocha (*8*), Pachas (*9*), Keissar (*10*)], and its basic geotechnical properties have been well established. The soil contains about 70 percent clay-sized particles; the predominant clay mineral is montmorillonite, rich in adsorbed calcium cations. The consistency limits of the sample used for the tests were liquid limit (LL) 78 percent and plasticity index (PI) 53 percent. Specific gravity of the particles was 2.75. Maximum dry density and optimum moisture content as obtained in a standard compaction test (Proctor energy, ASTM D698-78) were 12.6 kN/m^3 and 33 percent, respectively. All tests were performed on soil compacted to a dry density of 13.5 kN/m^3; most tests were performed on columns compacted at a moisture content of 21 percent (i.e., slightly below the plastic limit), but columns at 16 percent (very dry) and 30 percent (slightly above the plastic limit) were also tested.

ONE-DIMENSIONAL FLOW TESTS

General

Tests were performed on soil compacted in perspex columns of internal diameter 112 mm and height 300 mm. The soil was placed and compacted in layers of 20 mm; the bottom layer was sand, providing a drain for water that would eventually flow downward during the test. The weight and height of each compacted layer were carefully monitored during preparation, and this, together with moisture content determinations, provided a check on the initial total and dry densities of the soil column.

Two series of tests were carried out—one under laboratory conditions, and the second under increased acceleration conditions in a centrifuge. The purpose of the centrifuge tests was to simulate the stress conditions that exist in a prototype situation. The use of centrifugal modelling in geotechnical engineering has been extensively described in the literature [e.g., Craig et al. (*11*)]. In particular, the use of the method for simulating flow through stable soils has been demonstrated [Cargill and Ko (*12*), Goodings (*13*), Arulanandan et al. (*14*)]. In such cases, as the soil structure and properties remain unchanged during flow, time effects are scaled according to clear scaling laws; the time required for flow to occur between

two points at similar geometrical locations in a prototype and in a small model tested in a centrifuge will be in the ratio of n^2, where n is the ratio between both the prototype and model dimensions, and the accelerations acting on the model and the prototype.

In the case of flow through swelling soils, a more complex situation exists. As flow advances through the soil, swelling occurs, altering the structure and properties (presumably including the coefficient of permeability) of the wetted soil. The swelling process itself is time dependent and, as a result, the properties of the soil in the wetted zone continue to change with time until an equilibrium condition is reached. The scaling of time effects in small models will, therefore, be complicated by the superposition of a permeability change, the rate of which is not, a priori, clearly connected to the governing acceleration field. The purpose of the research, of which the present paper describes part, was to study the implications of these effects with regard to the possibility of using small models for simulating flow through prototypes of swelling soils. This paper does not discuss the modeling consequences of the results of the tests performed in the centrifuge; these will be presented elsewhere. The paper makes use of these results in order to develop a better understanding of the flow/swell phenomenon in expansive soil.

In order to monitor both the advance of the wetting front and the development of swell within the soil columns, special techniques were employed. The techniques used for the two test series are presented below. In all cases, the height of water above the base of the soil column was held constant during a test.

Columns Tested Under Laboratory Conditions

In order to monitor changes in moisture content and dry density in the columns, they were scanned with gamma rays during flow. Gamma radiation attenuation has been used since the early 1960s for measuring density and moisture content in porous materials and during flow through them [e.g., Davidson et al. (*15*), Gurr (*16*)]. Tsur and Pazi (*17*) built a scanning system for laboratory samples, and this system was employed for the present investigation. In essence, the system consists of a source (Cs^{137}, with an energy of 0.662 MeV, producing a narrow ray of 1 mm depth and 20 mm width) and a scintillation counter detector. The spacing between the source and detector is 30 cm. The soil column is placed between the source and detector, and a reading of gamma ray transmission is taken at desired stages of the flow test. The column is seated on a base that can be raised or lowered, with height monitoring being carried out using a linear variable differential transformer (LVDT), so that the location of the section at which readings are being obtained is known at any time. A scan over the column height may be made at various stages of the test by taking a series of readings, in between which the column is raised or lowered as required. Figure 1 shows the equipment, and Figure 2 shows a soil column being scanned.

The single count obtained at the detector during a reading is generally correlated to the bulk density of the soil. Consequently, if moisture content is known, dry density can be calculated; alternatively, if dry density is known, moisture content can be calculated. In the case of the study of flow through stable soils, the dry density of the soil may be con-

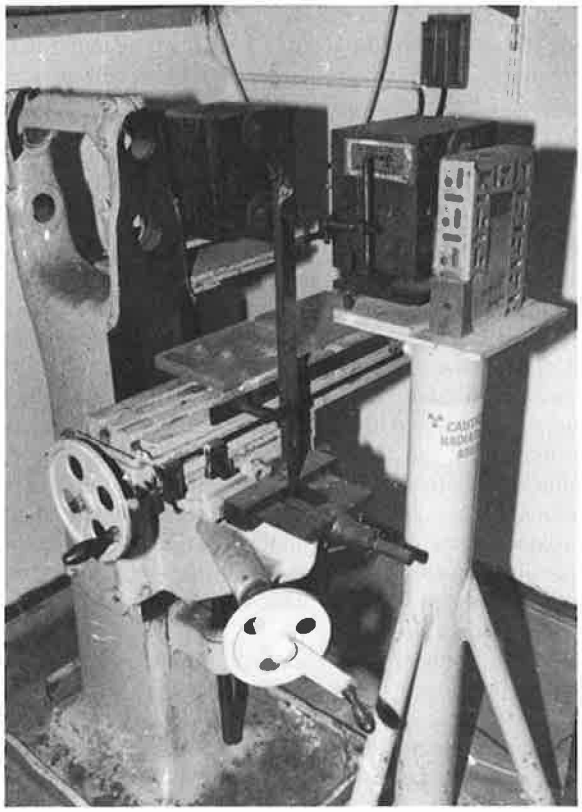

FIGURE 1 Gamma ray device (source on right, detector on left).

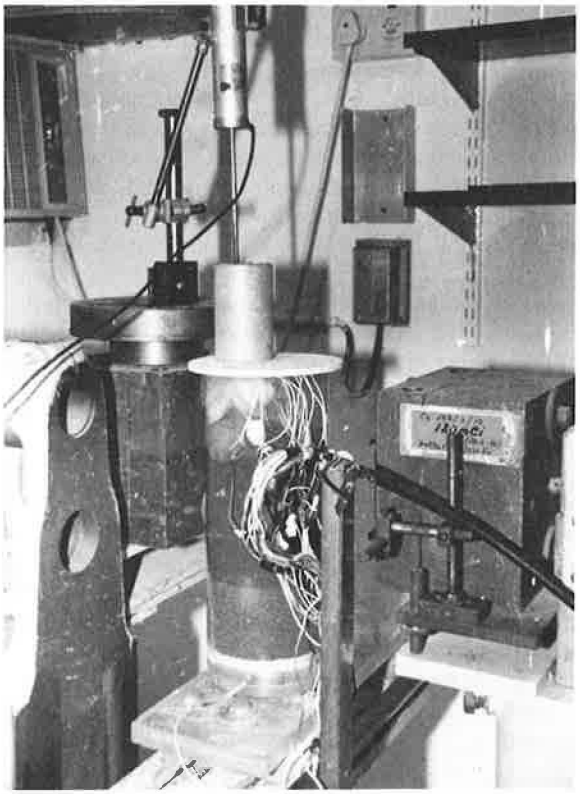

FIGURE 2 Soil column being scanned during wetting test (leads are connected to moisture transducers).

sidered constant, and so the change in moisture content (and hence the advance of the wetting front) can be monitored as flow progresses through the soil column. However, in the case of associated flow and swell, where both moisture content and dry density are changing simultaneously, one reading of gamma ray transmission is insufficient to enable the estimation of these two unknowns. This problem may be solved by using, for example, two sources of different energies; each reading would then provide two transmission counts enabling the evaluation of the two unknowns.

In the present investigation, a different approach was employed. During compaction of the soil columns, a small lead disk, 1 mm thick and 20 mm in diameter, was placed between each layer. On completion of compaction, the soil column was scanned. The locations of the lead disks, easily identifiable by the extreme attenuation they cause, were established relative to a fixed point on the perspex column. Additional count readings were made in each compacted layer, approximately midway between the lead disks. Using the measured initial moisture content of the soil sample, these readings made possible the calculation of the initial dry density over the column height.

A head of water was then applied to the top of the column, and flow developed downward through the soil. At various stages of advance of the wetting front (usually visible on the wall of the column), further series of readings were made of the locations of the disks and of the count at layer centers. As the dry weight of soil located between any pair of disks could be assumed to remain constant, the relative movement between neighboring disks was used to calculate the amount of swell and the change in dry density of the relevant soil layer. The count readings at layer center, together with the calculated dry densities, made possible the calculation of the moisture content in each layer and the degree of saturation of the layer. Several of the tests were continued for some time after the wetting front reached the bottom of the column, in order to facilitate the evaluation of the "saturated" coefficient of permeability of the soil, and to study the variation with time of degree of saturation, permeability, and swell. Some of the soil columns were carefully extruded from the perspex container on completion of the test, and moisture contents of the layers were determined by the oven-drying procedure; these values were compared to those obtained from the gamma ray scan carried out at the end of the test.

Columns Tested in the Centrifuge

The centrifuge used for the study (Figure 3) has been described previously [Leshchinsky et al. (*18*), Frydman and Keissar (*19*)]. It has an arm radius of 1.6 m, develops a maximum acceleration at the sample center of 100 *g*, and can take a maximum payload of 5,000 kg-*g* (i.e., 5,000 kg at 1 *g* up to 50 kg at 100 *g*).

In order to monitor the advance of the wetting front and the development of swell in the soil, the following techniques were used:

1. During preparation of the soil columns, a number of small steel balls, 3 mm diameter, were placed at the top of each compacted layer, in contact with the perspex container.

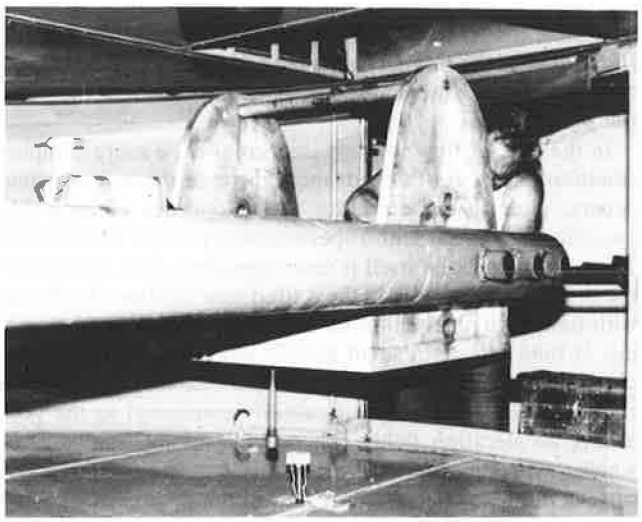

FIGURE 3 The centrifuge.

During the test, the columns were photographed at different stages of the wetting process while in flight in the centrifuge. Analysis of the movements of the balls, obtained from the resulting photographs, allowed the calculation of the development of swell during the test. The photography and analysis procedures have been described previously (*18,19*).

2. During preparation of the soil columns, an electrical resistance transducer was placed between each compacted layer. The transducer consisted of a pair of wires, spaced 7 mm from each other and supported on a plastic mesh. During the test, alternating current was applied between the wires, and the electrical resistance of the soil between them was measured. When the wetting front reached a transducer, the measured resistance dropped markedly. These readings provided a means for monitoring the advance of the wetting front.

3. The above inclusions were additional to the lead disks placed between layers in the laboratory-tested columns. The columns were scanned by gamma ray transmission before and after each test. The data so obtained provided information on the overall change in moisture content and dry density during the test. They also provided a check on the measurements carried out in flight in the centrifuge.

4. Water level was held constant during a test by use of a control system including a solenoid valve activated by a float mounted at the desired water level.

Figure 4 shows a photograph of the top of a soil layer during compaction of a column for centrifuge testing; the steel balls, moisture transducer, and lead disk are clearly seen. Figure 5 shows three stages in the wetting of a column compacted at 21 percent moisture content; the photographs were taken while the column was in flight in the centrifuge, at an acceleration of 15 *g*. The wetting front is clearly visible at all stages.

A SIMPLIFIED MODEL FOR THE ADVANCE OF THE WETTING FRONT

A simplified model for the advance of the wetting front during one-dimensional flow was presented by Uzan et al. (*3*). Mod-

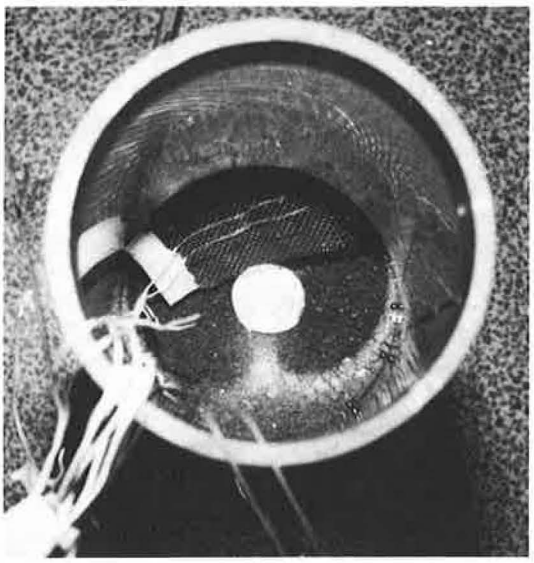

FIGURE 4 View of the top of a soil layer during compaction of a column for centrifuge testing.

ified to take account of centrifugal acceleration, this model is used as the basis for analyzing the tests. The model assumes a sharp wetting front, as shown in Figure 6, with saturated flow within the wetted zone. For flow downwards through the soil column shown in Figure 6, the time t for the wetting front to reach depth h may be considered, for the case in which the suction at the wetting front is ψ, as follows:

Define the effective porosity $n' = n - \theta$, where θ is the volumetric water content (i.e., the ratio between volume of water to total volume); n' represents the relative volume of pores not filled with water.

The rate of advance v of the wetting front is given by

$$v = q/n' = (-Ki)/n' \tag{1}$$

where K is the coefficient of permeability of the wet soil, i (the hydraulic gradient) equals $-[H_A - H_B]/h$, and H_A and H_B are the heads at levels A and B.

Taking level B as reference elevation, the head at A is $N(H_0 + h)$, and at B is $-\alpha\psi$, where N is the centrifugal acceleration and α is a coefficient with value between 0 and 1. The hydraulic gradient i is then

$$i = \frac{-[N(h + H_0) + \alpha\psi]}{h} \tag{2}$$

Two limiting cases may be considered, the first when the suction at the wetting front is zero, and the second when the suction, ψ, is much greater than the value $N(h + H_0)$. In the former case, the rate of advance of the wetting front is given by

$$v = \frac{dh}{dt} = \frac{KN(h + H_0)}{n'h} \tag{3}$$

For an increment of time from $t = 0$ to t, in which h increases from 0 to h, Equation 3 yields

$$t = \frac{n'}{KN}\left[h + H_0 ln \frac{H_0}{(h + H_0)}\right] \tag{4}$$

where K represents an average coefficient of permeability over time t and depth h.

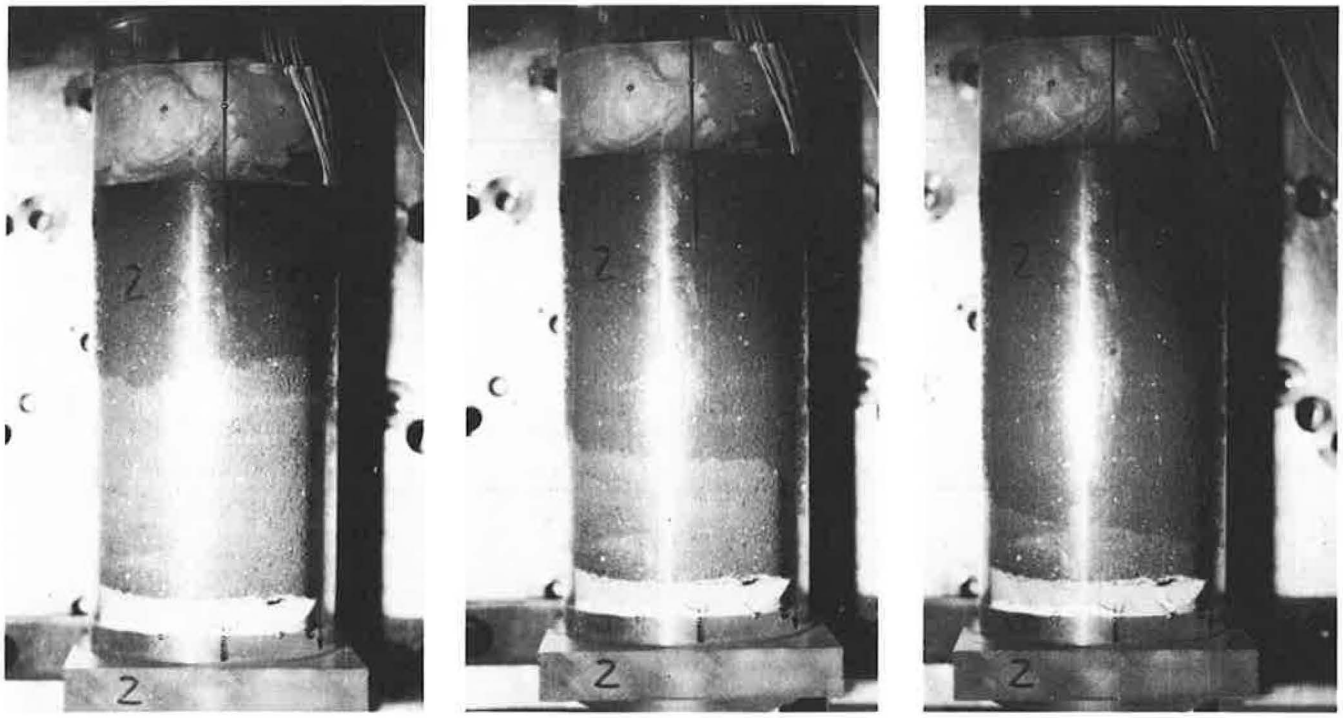

FIGURE 5 Three wetting stages in a column tested in the centrifuge at 15 *g* (compaction moisture content 21 percent).

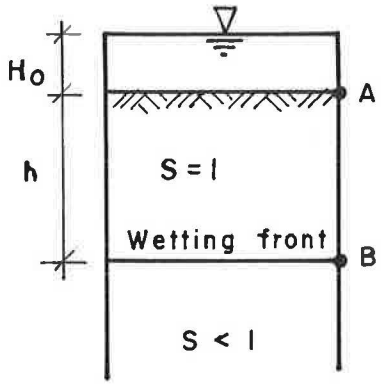

FIGURE 6 Simplified one-dimensional flow model.

In the second case, with $\psi >> h + H_0$,

$$v = \frac{dh}{dt} = \frac{K\alpha\psi}{n'h} \tag{5}$$

which leads, for time interval 0 to t, to

$$t = \frac{h^2 n'}{2K\alpha\psi} \tag{6}$$

with K again representing a value averaged over time and depth.

Uzan et al. (*20*) suggested that α be taken as 0.5. Using this value, Equation 6 can be written

$$t = \frac{h^2 n'}{K\psi} \tag{7}$$

In this second case, in which the driving head is controlled mainly by the extremely large suction, the rate of advance of the wetting front is dependent neither on the acceleration field nor on the level of water above the soil surface.

TEST RESULTS

Figure 7 shows a comparison between the moisture contents obtained by gamma ray scan and those obtained by oven drying. Despite the existence of some outliers, there is seen to be generally good correspondence between the values, providing a basis for confidence in the moisture content values obtained from the gamma ray scans in all the tests.

Figures 8–10 show the degree of saturation, S, and the amount of swell as a function of depth in the soil column and

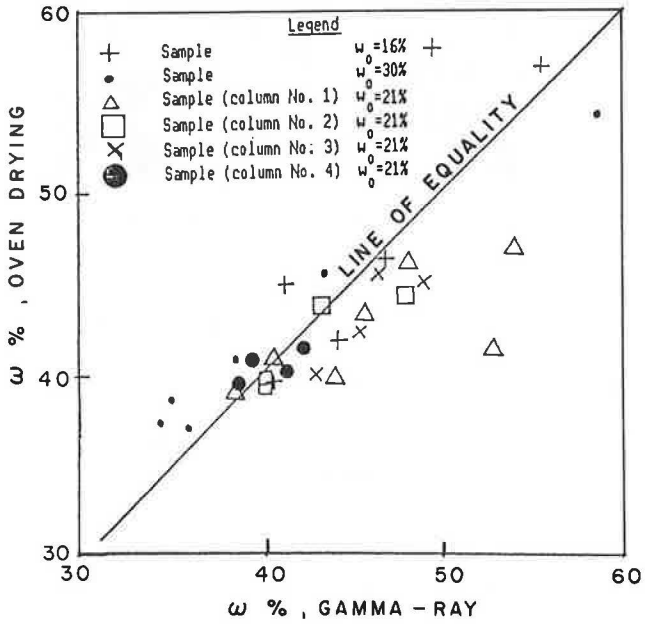

FIGURE 7 Comparison of moisture content values obtained by oven drying and by gamma ray scanning.

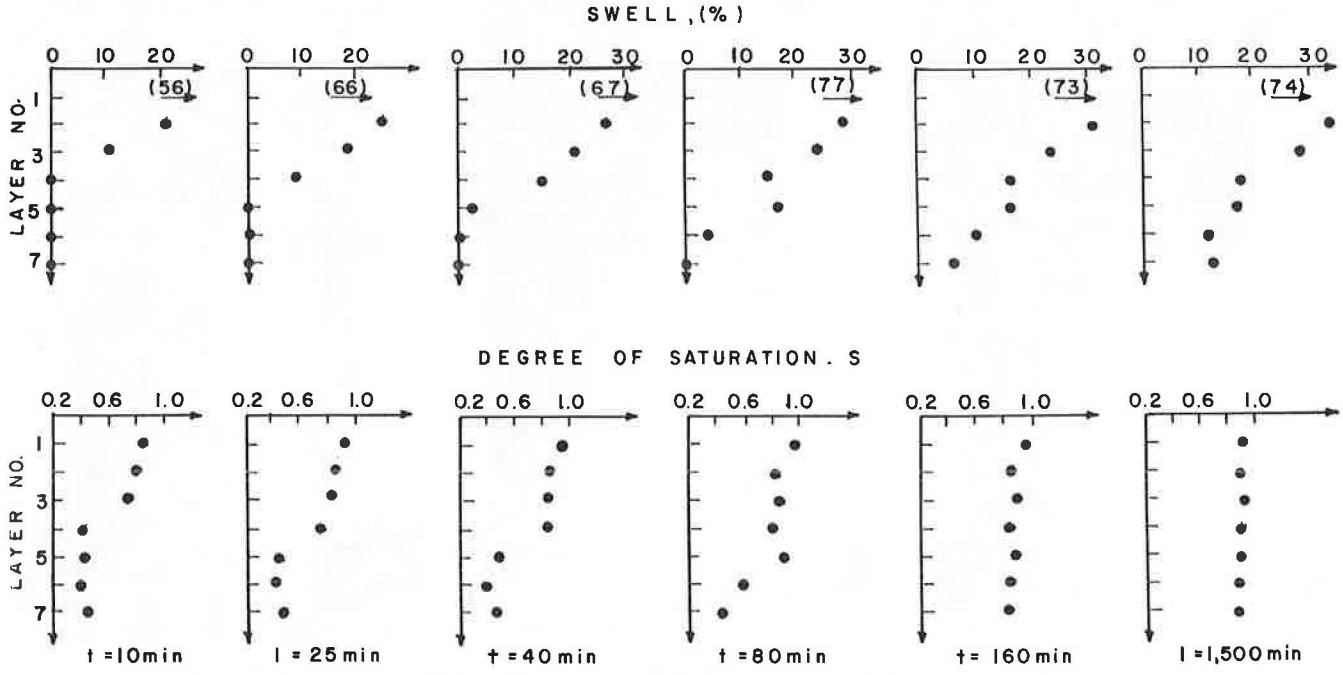

FIGURE 8 Distribution of degree of saturation and swell with depth during laboratory test (compaction moisture content 16 percent).

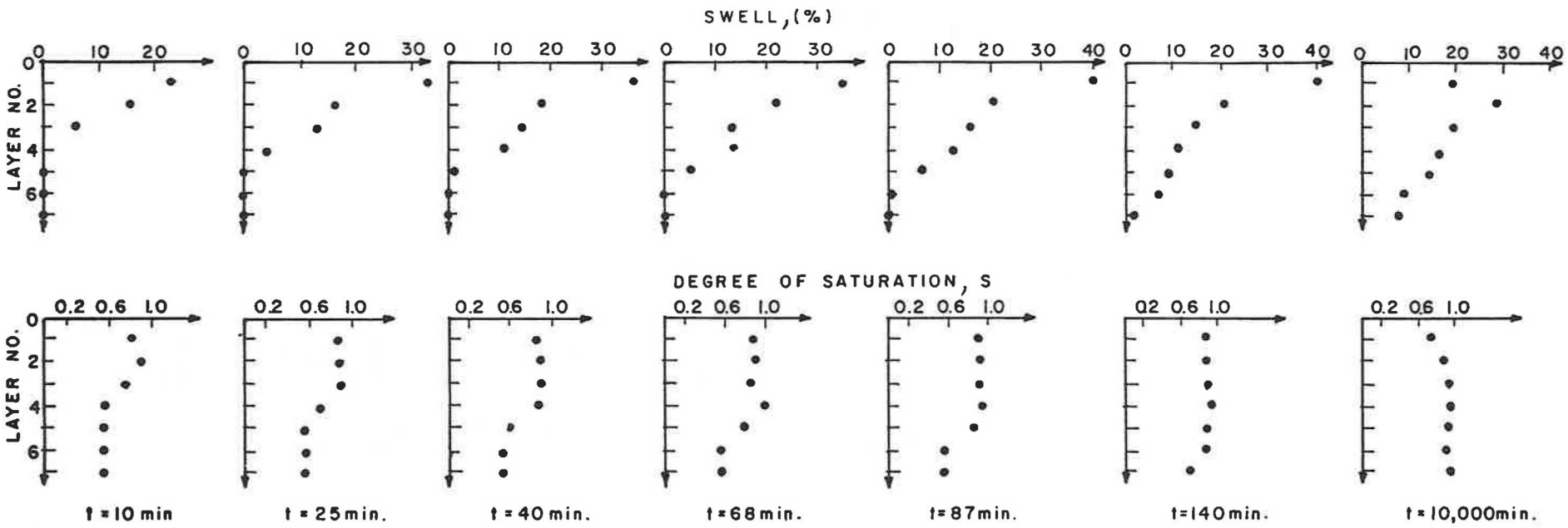

FIGURE 9 Distribution of degree of saturation and swell with depth during laboratory test (compaction moisture content 21 percent).

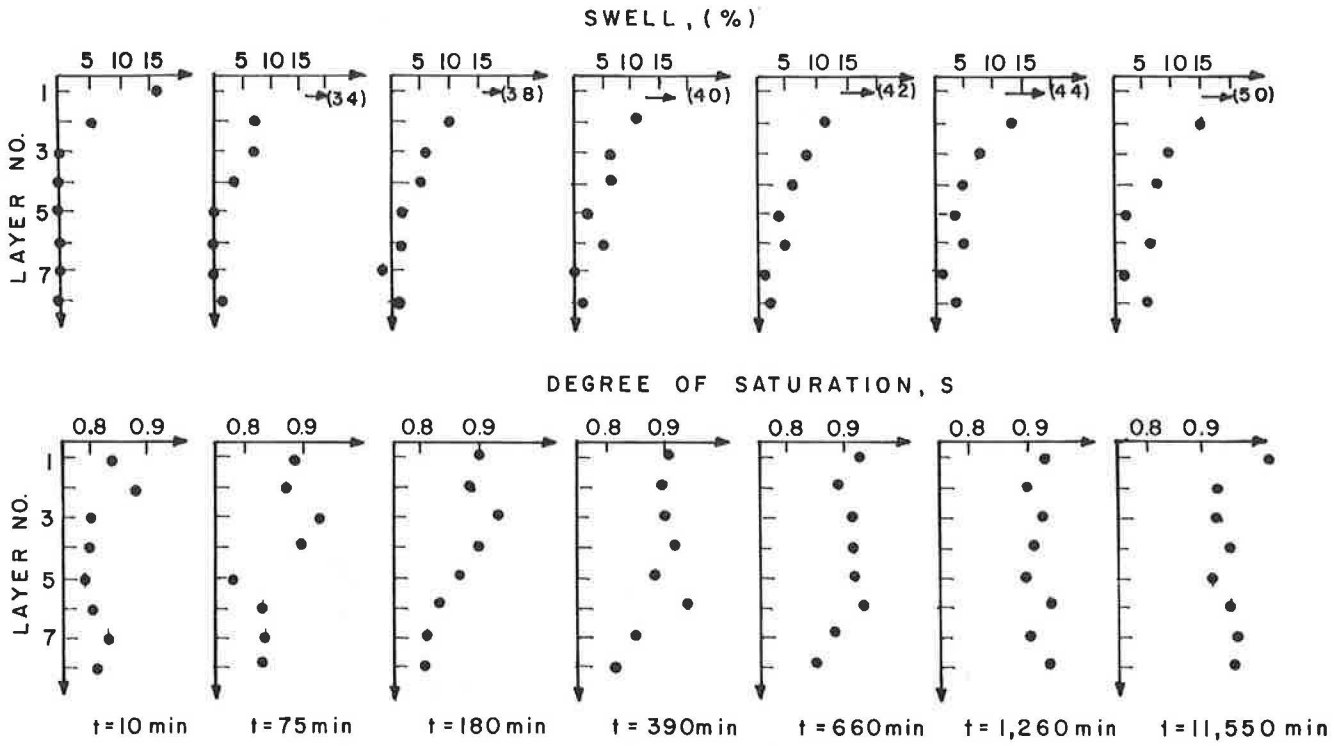

FIGURE 10 Distribution of degree of saturation and swell with depth during laboratory test (compaction moisture content 30 percent).

time for three tests performed in the laboratory—one at each preparation moisture content. From these figures, the following observations may be made:

1. In the columns prepared at the lower moisture contents of 16 and 21 percent, corresponding to degrees of saturation of 0.42 and 0.56, respectively, a sharp wetting front could be identified, associated with a sharp increase in the degree of saturation. It was observed in the tests that the sharp wetting front was clearly visible in the columns prepared at these lower moisture contents (as in the case of the centrifuge columns—see Figure 5). In the column prepared at 30 percent moisture content, corresponding to a degree of saturation of 0.8, the wetting front was less sharp. On the basis of these results, the sharp wetting front model presented in Figure 6 appears reasonable, at least for the lower moisture contents.
2. In all cases, the degree of saturation of the wetted zone increased with time, but never reached 1.0; the maximum value attained was in the range 0.90 to 0.96.
3. Swelling began to develop concurrently with wetting and increased with time. A steep gradient of swell was observed along the column height, despite the small magnitude of the overburden pressures.

Figure 11 shows the advance of the wetting front as a function of time for soil columns compacted at 21 percent moisture content and tested under both laboratory and centrifuge conditions. In general, the rate of advance of the wetting front increases with centrifugal acceleration and with height of water above the soil surface, H_0. The suction corresponding to the compaction conditions of these columns was evaluated using the method developed by Keissar (*10*) and was found to be of the order of 2 MPa. For the test conditions applied, the value of 0.5 ψ is clearly much larger than $N(H_0 + h)$, and so, as seen from Equation 7, neither the centrifugal acceleration, N, nor the water height, H_0, would be expected to have such an effect. On the contrary, the trend noted in Figure 11 is consistent with the case in which the effect of suction is insignificant (Equation 4).

It appears, then, that the high suction measured in the soil is not effective in influencing the advance of the wetting front. This observation is considered further, and its implications are discussed in the next section. At this stage, attention is focused on the columns compacted slightly dry of the plastic limit (21 percent moisture content), which represented the bulk of the testing program. Following discussion of the results of these tests, and their consequences, the comparative behavior of columns compacted wet of plastic limit (30 percent moisture content) is considered.

SOIL COMPACTED DRY OF PLASTIC LIMIT

The results shown in Figure 11 suggest that the rate of advance of the wetting front in the soil columns compacted at 21 percent moisture content was not affected by suction. In order to investigate this observation further, it was assumed that the suction was insignificant, and Equation 4 was used to calculate the variation of K with time during the wetting process. The result of these calculations is shown in Figure 12. It should be noted that K, as used in Equation 11 and shown in Figure 12, represents an average value over time (from time zero up to time t) and depth of wetting front (from depth zero to depth h). Of the 9 tests performed, the results of 7

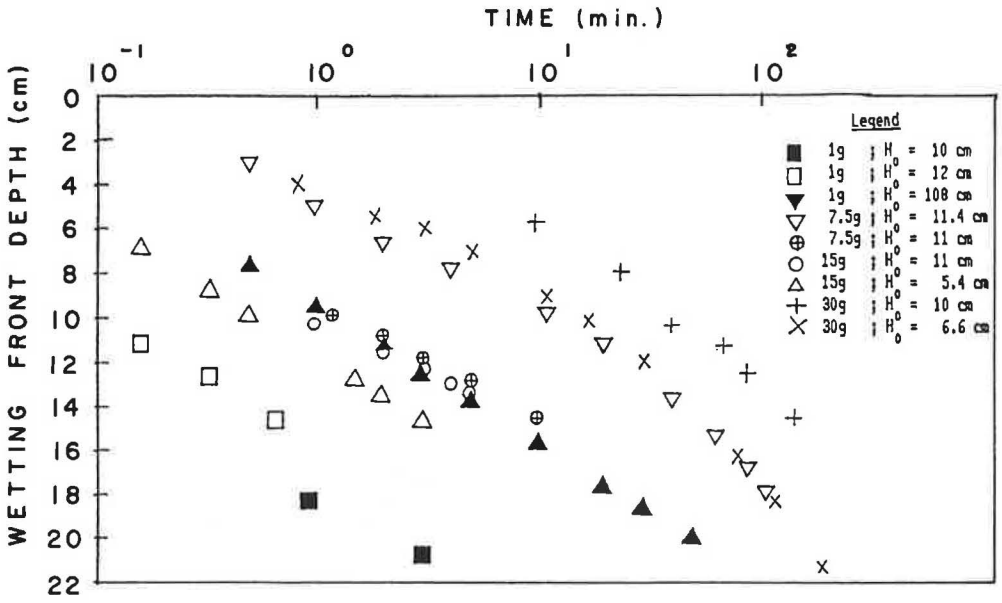

FIGURE 11 Depth of wetting front versus time (compaction moisture content 21 percent).

lie very close to each other. The overall scatter in values of K at any time is less than one order of magnitude. This consistency in the value of K adds credance to the assumption that suction was insignificant in the flow process.

Figure 12 also shows that K decreases continuously with time; the inverse relationship between K and time is approximately linear on a log-log basis. The K values at the start of wetting appear extremely high (the order of 10^{-2} mm/sec) compared to values considered typical for highly plastic clays (the order of 10^{-5} mm/sec and less). In order to obtain an indication of the feasibility of these high values, the intrinsic permeability, k, of soil columns was evaluated by testing the rate of air flow through them. Terzaghi (*20*) expressed the coefficient of permeability K by the expression

$$K = k\gamma/\mu \tag{8}$$

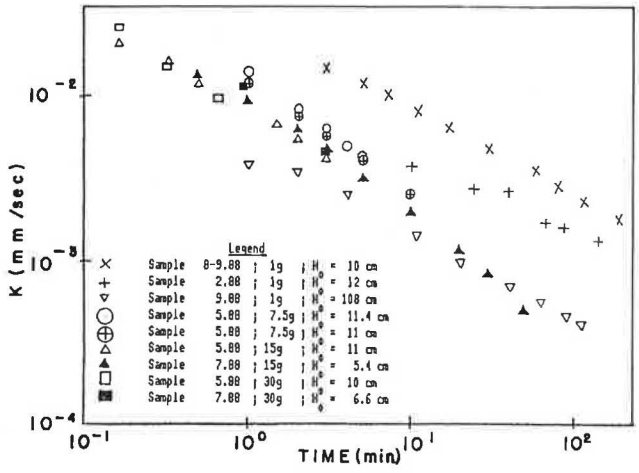

FIGURE 12 Time dependence of average coefficient of permeability of wet soil (compaction moisture content 21 percent; soil suction assumed zero).

where k is a constant for the soil, independent of the fluid flowing through it, γ is the unit weight of the fluid, and μ is the dynamic viscosity of the fluid.

The air permeability tests were performed by measuring the time required to flow 1 liter of air through the soil column under a given pressure gradient, i_p. Terzaghi (*20*) expressed the discharge velocity, v, by the expression

$$v = \frac{k}{\mu} i_p \tag{9}$$

From these tests, k was found to be between 3×10^{-7} and 9×10^{-7} mm^2, giving K a value between 3×10^{-3} and 9×10^{-3} mm/sec. This range is consistent with the values indicated at the start of wetting, as seen in Figure 12.

Further light may be shed on the source of this high permeability and apparent lack of effective suction by estimating the "effective particle size," d, which would be expected for a soil with the above range of permeability. Bear (*21*) suggested the following relationship between k and d:

$$k = 0.617 \times 10^{-9} d^2 \tag{10}$$

where k is in mm^2 and d is in microns. The effective particle size of the columns compacted at 21 percent moisture content is found to be in the range 0.02 to 0.04 mm. Clearly, these values represent the sizes of particle aggregates, and not of the individual clay particles.

Finally, for a porous medium with pore size of the order of 0.03 mm, the classical capillary model [e.g., Terzaghi (*20*)] may be used to estimate the suction which can exist within the pores from the following expression:

$$\psi = \frac{2T_s}{0.5d} \tag{11}$$

where T_s is the surface tension between water and soil; it may be taken as 7 dyne/mm, resulting in an estimated suction of

about 9 kPa. This is a very small suction, in contrast to the value of 2 MPa measured in suction tests. It would appear that the high suction is developed within the soil aggregates, but is not relevant to the interaggregate pores where the flow apparently takes place.

On the basis of the above considerations, it is suggested that the advance of the wetting front in highly swelling clay, compacted dry of the plastic limit, involves the following process. Flow occurs through the large, interaggregate pores and is not significantly affected by suction head. As wetting develops, swelling occurs at the surface of the aggregates, resulting in a decrease in the size of the interaggregate pores and consequently in the permeability of the wetted portion of the soil. The process of decreasing permeability continues with time, accompanied by swelling of the soil. This suggested model is consistent with the observations of Tovey et al. (*22*) from scanning electron micrographs prepared both before and after swelling tests on a clay compacted dry of the plastic limit. These showed that although the overall porosity of the soil increased during swelling, the sizes of the interaggregate pores decreased.

SOIL COMPACTED WET OF PLASTIC LIMIT

Only three soil columns compacted at 30 percent moisture content were tested, two under laboratory conditions and one in the centrifuge. Although these are sufficient to warrant clear-cut conclusions, their results are presented and discussed in the light of the observations made with regards the drier columns.

Figure 13 shows the advance of the wetting front with time. The observation that the rate of advance was similar for all columns immediately suggests that the suction may have been significant at this compaction moisture condition. If the suction ψ is assumed to be zero, and Equation 4 is used to calculate the average coefficient of permeability, K, at different stages of the wetting process, the values shown in Figure 14 result. In this case, in contrast to the dry soil, the assumption of $\psi = 0$ does not result in a consistent estimate of K. Suction tests performed on soil compacted at 30 percent moisture content indicated values of the order of 200 kPa. In Figure 15, the K values have been recalculated from the results of

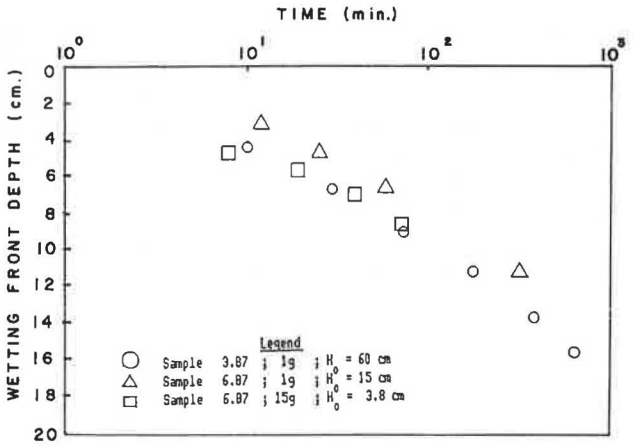

FIGURE 13 Depth of wetting front versus time (compaction moisture content 30 percent).

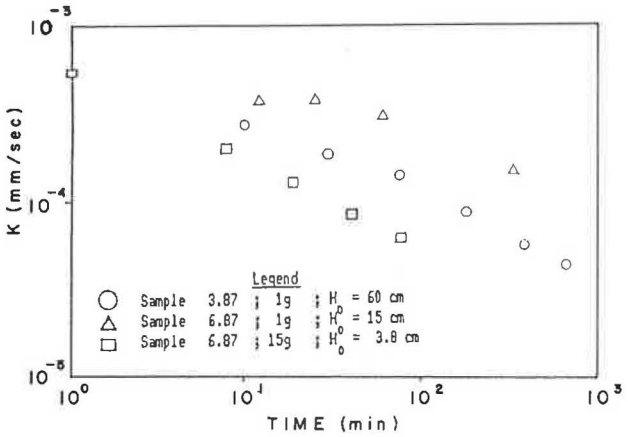

FIGURE 14 Time dependence of average coefficient of permeability of wet soil (compaction moisture content 30 percent; soil suction assumed zero).

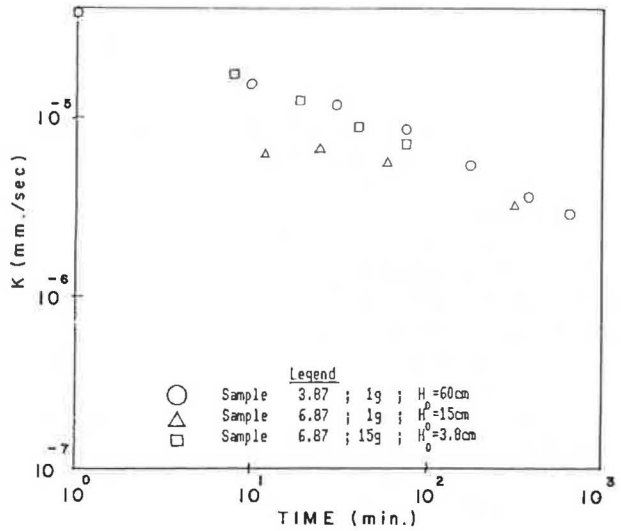

FIGURE 15 Time dependence of average coefficient of permeability of wet soil (compaction moisture content 30 percent; soil suction assumed 200 kPa).

the three tests, using Equation 2 for hydraulic gradient, with $\alpha = 0.5$ and $\psi = 200$ kPa. For these conditions, consistent values of K are obtained from the three tests. It would appear, then, that for soil compacted wet of plastic limit, the suction that is measured in a suction test is effective in the pores through which flow occurs. This observation, if demonstrated by further testing, would suggest a basic difference between the role of suction, as measured by conventional techniques, in the wetting of soils compacted dry and wet of the plastic limit.

Figure 15 again shows K decreasing almost linearly with time on a log-log plot. It appears that the mechanism of swell suggested for the dry soil may also be pertinent for the wetter condition.

CONCLUSIONS

The results of the tests reported in this paper indicate some features of flow through compacted, swelling clay that should

be considered when carrying out analyses of field situations. It is clear that generalizations cannot be made on the basis of the limited number of tests performed, but the following observations, which should be verified by further investigations, appear pertinent:

1. There appear to be differences in the flow process in soils compacted below and above the plastic limit. Below the plastic limit, the wetting front is relatively sharp, but it becomes difficult to define the wetting front as a sharp interface between wet and unwet zones as compaction moisture content increases above the plastic limit. Below the plastic limit, suctions appear to have insignificant effect on the rate of advance of the wetting front. The high suctions measured at these moisture contents are apparently developed in the small pores within the soil aggregates, whereas flow advances through the larger, interaggregate pores where the suctions are extremely small. As the compaction moisture content increases above the plastic limit, the size of the aggregates increases and that of the interaggregate pores decreases, and the suctions in the interaggregate pores apparently approach those in the intraaggregate pores. The measured suctions are then significant in controlling the rate of advance of the wetting front. This finding is of major significance in analysis and design of field situations, where the in situ value of soil suction represents one of the basic items of input data.

2. The coefficient of permeability of compacted, swelling soil decreases with time following wetting, despite the fact that the overall porosity of the soil increases due to swelling. It is suggested that the source of this permeability decrease lies in the fact that flow develops through the larger interaggregate pores, leading to swelling on the aggregate surfaces and a resulting decrease in the sizes of these pores. This decrease in pore size results in a decrease in permeability that is approximately linear with time on a log-log scale. At the same time, the intragranular pores increase in size, resulting in an overall increase in the porosity of the soil. The decrease in permeability with time should be taken into account in analysis.

ACKNOWLEDGMENT

The research described in the paper was partially financed by the Department of Soil Conservation and Drainage in the Israeli Ministry of Agriculture. The support of Ezra Henkin, head of the department, is gratefully acknowledged.

REFERENCES

1. J. L. Justo, J. Saura, J. E. Rodriguez, A. Delgado, and A. Jamrillo. A Finite Element Method to Design and Calculate Pier Foundations in Expansive Collapsing Soils. *Proc., Fifth International Conference on Expansive Soils*, Adelaide, Australia, 1984, pp. 119–123.
2. M. Picornell and R. L. Lytton. Modelling the Heave of a Heavily Loaded Foundation. Proc., *Fifth International Conference on Expansive Soils*, Adelaide, Australia, 1984, pp. 104–108.
3. J. Uzan, R. Baker, and S. Frydman. Characterization of Constrained Swelling of Clay. *Transportation Research Record 1137*, TRB, National Research Council, Washington, D.C., 1987, pp. 52–58.
4. B. G. Richards. Finite Element Analysis of Volume Change in Expansive Clays. *Proc., Fifth International Conference on Expansive Soils*, Adelaide, Australia, 1984, pp. 141–148.
5. G. Kassiff, M. Livneh, and G. Wiseman. *Pavements on Expansive Clays*. Jerusalem Academic Press, Jerusalem, 1969.
6. A. Komornik and J. G. Zeitlen. An Apparatus for Measuring Lateral Soil Swelling Pressure in the Laboratory. *Proc., Sixth International Conference on Soil Mechanics and Foundation Engineering*, Vol. 1, 1965, pp. 278–281.
7. A. Ben Shalom. *Laboratory Method for Measuring Swelling Potential under Partial Saturation Conditions*. M.Sc. thesis, Technion, Israel Institute of Technology, 1970 (in Hebrew).
8. S. Samoocha. *A Method for Measuring Three Dimensional Swell and Shear Strength of Clay Specimens Under Controlled Unsaturated Conditions*. M.Sc. thesis. Technion, Israel Institute of Technology, 1971 (in Hebrew).
9. G. Pachas. *Swelling of Israeli Clays Under Triaxial Stress Conditions*. M.Sc. thesis, Technion, Israel Institute of Technology, 1986.
10. I. Keissar. *The Development of a Model for the Prediction of Flow, Strains and Stresses in Expansive Soils*. D.Sc. thesis. Technion, Israel Institute of Technology, 1989 (in Hebrew).
11. W. H. Craig, R. G. James, and A. N. Schofield (eds.). *Centrifuges in Soil Mechanics*. Balkema, Rotterdam, Netherlands, 1987.
12. K. W. Cargill and H. Ko. Centrifugal Modelling of Transient Water Flow. *Journal of Geotechnical Engineering*, ASCE, Vol. 109, No. 4, 1983, pp. 536–555.
13. D. J. Goodings. Relationships for Modelling Water Effects in Geotechnical Centrifuge Models. *Proc., Symposium on the Application of Centrifuge Modelling to Geotechnical Design*, University of Manchester, 1984.
14. K. Arulanandan, P. Y. Thompson, B. L. Kutter, N. J. Meegoda, K. K. Muraleetharan, and C. Yogachandran. Centrifuge Modelling of Transport Processes for Pollutants in Soils. *Journal of Geotechnical Engineering*, ASCE, Vol. 114, No. 2, 1988, pp. 185–205.
15. J. H. Davidson, J. W. Biggar, and D. R. Nielsen. Gamma Radiation Attenuation for Measuring Bulk Density and Transient Water Flow in Porous Materials. *Journal of Geophysical Research*, Vol. 68, No. 16, 1963, pp. 4777–4783.
16. C. G. Gurr. Use of Gamma Rays in Measuring Water Content and Permeability in Unsaturated Columns of Soil. *Soil Science*, Vol. 94, 1962, pp. 224–230.
17. B. Tsur and B. Pazi. *The Measurement of Density and Moisture Content of Soil Samples Using Gamma Radiation*. Agricultural Engineering Faculty, Technion, Israel Institute of Technology, Haifa, 1969, (in Hebrew).
18. D. Leshchinsky, S. Frydman, and R. Baker. Study of Soil Structure Interaction Using Finite Elements and Centrifugal Models. *Canadian Geotechnical Journal*, Vol. 3, 1981, pp. 345–359.
19. S. Frydman and I. Keissar. Earth Pressure on Retaining Walls Near Rock Faces. *Journal of Geotechnical Engineering*, ASCE, Vol. 113, No. 6, 1987, pp. 586–599.
20. K. Terzaghi. *Theoretical Soil Mechanics*. John Wiley and Sons, New York, 1943.
21. J. Bear. *Dynamics of Fluids in Porous Media*. Elsevier, New York, 1972.
22. N. K. Tovey, S. Frydman, and K. Y. Wong. A Study of a Swelling Clay in the Scanning Electron Microscope. *Proc., Third International Conference on Expansive Soils*, Haifa, Israel, Vol. 2, 1973, pp. 45–54.

Publication of this paper sponsored by Committee on Environmental Factors Except Frost.

Field Monitoring of Expansive Soil Behavior

HSIU C. LEE, PATRICIA S. POMPER, AND WARREN K. WRAY

Two field test sites were constructed to monitor the behavior of slab-on-ground foundation models constructed over expansive soils and the change in soil moisture conditions as a function of climate. One site was constructed in a dry climate (Amarillo) and the second site in a relatively wet climate (College Station); both sites were monitored monthly for 3 years. Immediately following construction of the Amarillo site, a 3 year drought ended and the subsequent 3 years were much wetter than normal. Because of the increased soil moisture content, the east end moisture cells stopped working, but the psychrometers on the west end of the slab model worked well over the full study period. Similarly, a 1½ year drought at College Station ended the month following site installation and the whole site experienced a general heave of the soil surface, including the slab model. The site continued to experience above average rainfall for approximately 24 months, after which a new period of drought began. During this wet period, nearly all of the 84 moisture cells stopped working because soil conditions were too wet, and more and more of the 160 psychrometers failed to yield suction readings as the study period continued. Fewer than 20 of the psychrometers were yielding readings by the end of the second year; however, the number of instruments providing readings had increased to more than 50 during the drought of the third year of the study.

Two field test sites were constructed to monitor the behavior of slab-on-ground foundation models constructed over expansive soil and the change in soil moisture conditions at each site as a function of climate. One site was constructed in a dry climate in Amarillo, Texas, and the second site was constructed in a relatively wet climate in College Station, Texas. The two sites were both constructed in 1985 and were monitored monthly subsequent to construction.

Two types of soil moisture monitoring instrumentation were installed at each site. One type of instrumentation was to measure the change in soil water content using a fiberglass moisture sensor. The second type of instrument was a thermocouple psychrometer to measure soil suction. In addition to the soil moisture monitoring instrumentation, more than 230 surface elevation points were established at each site to monitor the change in surface elevation, which was expected to occur as a result of the changing soil moisture conditions.

This paper describes the characteristics of the test sites, the instrumentation installed to monitor changes in soil moisture conditions, the success of the instrumentation, and the validity of the results obtained from these instruments. It also presents some conclusions regarding the success of this instrumentation in achieving the desired objectives of (1) frequently measuring climate-induced changes in soil moisture conditions, (2) measuring the corresponding changes in surface elevations both on and outside the slab model, and (3) relating the observed changes in surface elevation to predicted shrink/swell magnitudes based on the measured changes in soil suction.

Department of Civil Engineering, Texas Tech University, Lubbock, Tex. 79409.

DESCRIPTION OF TEST SITES

Amarillo Site

The "dry" climate site was in Amarillo, Texas, on the eastern edge of the grounds of the Family Hospital Center. The site sloped approximately one percent from northwest to southeast. Initial surface vegetation included short grasses and common lawn weeds. The hospital kept the grounds mowed but did not irrigate. All watering of the site was from natural precipitation. The groundwater table was not found within 27.5 ft of the ground surface and was reported to be at least 50 ft deep at this location by city officials. Thus, the groundwater table was deep enough not to affect the changes in soil moisture content caused by seasonal changes.

Four separate soil strata were identified at the site. The first stratum was a reddish brown silty clay approximately 18 in. thick. This soil was composed of fill material that was partially topsoil and partially construction residue. The second stratum was a dark gray silty clay approximately 2 ft thick. Both of the first two layers were classified as CL in the Unified Soil Classification System (USCS) or A-6 in the American Association of State Highway and Transportation Officials (AASHTO) Soil Classification System. The third layer was a light gray silty clay approximately 3 ft thick. Underlying the third stratum, to a depth of at least 27.5 ft, was a very similar light gray clay that was slightly more sandy and slightly less plastic. The third and fourth strata were both classified as CH in the USCS system and either A-7-5 or A-7-6 in the AASHTO system. Table 1 reports soil characterization results as determined from multiple tests for Atterberg limits, percent passing the No. 200 sieve, and the clay content of the total sample as determined by the hydrometer test for each foot of depth.

The in situ moisture content and the in situ soil suction were determined at each foot of depth for each of the 17 continuously sampled, 9 ft deep borings. The mean and the range of the 17 moisture contents at each depth are also shown in Table 1. The moisture contents indicated that, at the time of installation, the soil at the site was very dry near the surface but got progressively wetter to a depth of approximately 6 ft, whereupon the moisture content became a fairly constant value.

The in situ soil suction tests were accomplished using the filter paper method suggested by McQueen and Miller (*1*).

TABLE 1 SOIL PROPERTIES AT VARIOUS DEPTHS FOR THE AMARILLO TEST SITE

DEPTH (ft)	MOISTURE CONTENT (%)		PLASTIC LIMIT (%)		LIQUID LIMIT (%)		PLASTICITY INDEX (%)		PERCENT PASSING No. 200 SIEVE (%)		PERCENT CLAY (<0.002 mm) (%)		FILTER PAPER SOIL SUCTION (pF)	
	Mean	(Range)	Mean	(Range)	Mean	(Range)	Mean	(Range)	Mean	(Range)	Mean	(Range)	Mean	(Range)
0-1	8.3	(4.9-9.8)	23.2	(19.8-25.7)	37.3	(35.6-39.8)	14.1	(11.5-16.7)	62	(49-66)	47	(43-50)	5.3	(5.0-5.5)
1-2	10.5	(7.1-13.1)	19.8	(18.4-21.9)	35.0	(32.2-37.1)	15.3	(13.7-18.4)	57	(55-61)	46	(43-47)	5.0	(4.9-5.1)
2-3	13.8	(8.2-18.0)	20.5	(17.7-24.8)	33.9	(32.4-36.8)	14.1	(11.9-15.5)	59	(50-65)	42	(38-47)	5.0	(4.7-5.8)
3-4	17.8	(15.8-19.8)	26.0	(21.8-33.8)	64.3	(57.9-73.3)	38.4	(35.6-40.0)	82	(64-96)	62	(49-70)	4.8	(4.7-4.9)
4-5	19.7	(17.3-22.2)	29.3	(27.1-30.6)	77.2	(67.4-83.1)	54.2	(52.5-56.2)	75	(66-87)	59	(50-68)	4.7	(4.5-4.8)
5-6	21.7	(17.5-24.5)	36.5	(26.9-44.2)	75.8	(69.5-81.3)	39.3	(31.1-54.3)	83	(83-89)	63	(57-67)	4.6	(4.4-5.0)
6-7	24.2	(20.9-27.0)	31.0	(26.3-38.4)	74.3	(72.0-77.3)	43.4	(33.6-49.1)	83	(79-87)	64	(61-66)	4.4	(4.2-4.7)
7-8	22.7	(20.8-25.7)	28.6	(25.4-34.6)	68.7	(64.3-72.9)	40.1	(29.7-47.0)	78	(77-80)	64	(62-66)	4.4	(4.2-4.7)
8-9	23.5	(16.8-26.8)	27.4	(25.8-30.3)	66.3	(54.2-76.9)	34.8	(15.8-51.1)	81	(80-84)	61	(59-64)	4.3	(4.1-4.7)

The values were determined using S&S No. 589 White Ribbon filter paper and the McKeen calibration curve (*2*). The means and ranges of the 17 suction values are also reported in Table 1. The in situ soil suction values also indicated that the soil near the surface was very dry; the suction to a depth of 3 ft exceeded 5.0 pF. ("pF" nomenclature is used to define soil suction in terms of the common logarithm of the height in centimeters of a column of water needed to give an equivalent suction pressure; 5.0 pF is equivalent to 98.06 bars; see Appendix for other soil suction conversion factors.) The soil became wetter with increasing depth, but was still quite dry at a depth of 9 ft, the maximum depth of the continuous sampling. X-ray diffraction analysis of each soil strata was also performed. The results from this test indicated that smectite was the principal clay mineral constituent for each stratum.

College Station Site

College Station, Texas, was chosen as the "wet" site. The actual location was within the farm equipment compound of the Texas A&M University College of Agriculture. The area sloped at approximately three percent from east to west. At the time of installation, the surface of the site was covered with tall grasses and weeds. Three tall, mature trees shaded the site for parts of the day. The site was not irrigated; all precipitation occurring at the site was the result of natural rainfall.

Three separate soil strata were identified on the site. The top stratum consisted of 2 ft of a silty fill material mixed with large aggregate. The second stratum was a dark gray medium stiff silty clay approximately 5 ft thick. Underlying the second stratum was a grayish brown silty clay that extended to approximately the 16 ft depth. Both soils classified as CL in the USCS system and A-7-6 in the AASHTO system. At a depth of 16 ft, a thin lens of clean white sand was encountered. A grayish brown silty clay similar to the third stratum, classifying as CH and A-7-6, extended to the limit of the deepest boring of 25 ft. The groundwater table was not encountered within 25 ft of the surface. Table 2 reports soil characterization results as determined from multiple tests for Atterberg limits, percent passing the No. 200 sieve, and the clay content of the total sample as determined by the hydrometer test for each foot of depth.

The in situ moisture content and the in situ soil suction were determined at each foot of depth for each of the 17 continuously sampled, 9 ft deep borings. The mean and the range of the 17 moisture contents are also shown in Table 2. The moisture contents indicate that at the time of site installation, the soil was relatively dry. The soil suction values also indicated that the soil was relatively dry near the surface. However, at the 2–3 ft depth, the suction reduced to 4.3 pF, a value that remained unchanged to the 8–9 ft depth. This value is also approximately equal to the wilting point of plants. X-ray diffraction analysis of each soil strata was also performed. The results from these tests indicated that smectite was the principal clay mineral for each layer.

INSTRUMENTATION

Objectives

The two principal objectives from a data collection viewpoint were to collect information on vertical shrink/heave and changes in soil moisture conditions as the climate changed over a period of several seasons. The changes in surface elevation were ultimately to be related to the changes in the soil moisture conditions at the sites. To express quantitatively the soil moisture conditions, two variables—gravimetric moisture content and total soil suction—were selected for measurement. These soil moisture variables can be measured in situ with several commercially available sensors. Instrumentation selected for this study consisted of fiberglass fiber sensors manufactured by Soiltest, Inc., to measure changes in gravimetric moisture content, and thermocouple psychrometers manufactured by J.R.D. Merrill Co. to measure changes in

TABLE 2 SOIL PROPERTIES AT VARIOUS DEPTHS FOR THE COLLEGE STATION TEST SITE

DEPTH (ft)	MOISTURE CONTENT (%) Mean	(Range)	PLASTIC LIMIT (%) Mean	(Range)	LIQUID LIMIT (%) Mean	(Range)	PLASTICITY INDEX (%) Mean	(Range)	PERCENT PASSING No. 200 SIEVE (%) Mean	(Range)	PERCENT CLAY (<0.002 mm) (%) Mean	(Range)	FILTER PAPER SOIL SUCTION (pF) Mean	(Range)
0-1	6.4	(3.3-14/4)	16.7	(16.2-17.4)	26.1	(23.3-30.9)	9.4	(6.7-15.5)	33	(29-39)	23	(18-28)	4.9	(4.6-5.1)
1-2	8.9	(2.7-23.6)	20.3	(17.9-23.5)	40.0	(21.2-63.1)	19.7	(3.3-39.6)	36	(33-39)	23	(18-29)	4.5	(3.0-4.9)
2-3	18.7	(2.8-29.4)	22.4	(19.5-24.4)	51.9	(46.9-59.7)	29.4	(22.5-36.3)	62	(60-65)	52	(48-56)	4.3	(2.3-4.8)
3-4	17.4	(10.7-31.7)	19.6	(18.7-20.7)	45.1	(40.2-48.2)	25.5	(20.9-28.1)	62	(57-69)	49	(40-57)	4.3	(4.0-4.7)
4-5	16.9	(10.0-21.2)	23.3	(21.6-25.0)	48.0	(40.1-54.5)	24.7	(18.5-31.3)	62	(58-67)	48	(40-61)	4.3	(3.9-4.5)
5-6	17.9	(14.5-20.3)	18.7	(18.6-19.0)	45.5	(36.9-52.8)	26.8	(18.3-33.9)	65	(59-69)	42	(37-48)	4.3	(4.2-4.4)
6-7	20.8	(12.8-26.2)	23.2	(20.5-27.9)	48.8	(42.8-54.4)	25.6	(22.3-28.1)	64	(63-66)	50	(44-53)	4.3	(4.0-4.5)
7-8	23.9	(16.8-30.7)	29.3	(25.9-31.8)	57.6	(50.6-65.8)	28.3	(20.5-39.9)	79	(74-88)	59	(46-68)	4.3	(4.1-4.6)
8-9	29.1	(24.5-30.7)	30.5	(25.4-33.0)	64.4	(46.1-78.5)	34.0	(20.6-45.5)	94	(86-98)	72	(63-82)	4.2	(4.1-4.5)

soil suction and soil temperature; the psychrometer was covered with a No. 400 mesh stainless steel protective tip.

Moisture Cells

The concept behind the fiberglass electrical soil moisture instrument is described in Colman (*3*) and Colman and Hendrix (*4*). The instrument operates on the principle that the electrical resistivity of porous material (e.g., fiberglass) is related to its moisture content. When embedded in the soil, it absorbs soil water until equilibrium with the soil is reached. The resistivity reading is then calibrated against the moisture content of the soil. The fiberglass moisture cell is a sandwich composed of two monel screen electrodes separated by two layers of fiberglass cloth and wrapped around with three layers of the same material. The electrical resistance between screens, through the fiberglass cloth, varies in response to changes in moisture content of the soil in which it is placed.

The moisture cell calibration procedure followed that suggested by the manufacturer:

1. A moisture cell was placed in an approximately 1,000 g soil specimen, which was then wrapped in nylon fabric to prevent loss of soil during inundation.
2. The soil-moisture cell-nylon composite was weighed to the nearest 0.01 g.
3. Because the specimens were principally dry, the soil-moisture cell-nylon composite was then inundated in distilled water for a period of several hours.
4. At the end of the soaking period, the soil-moisture cell-nylon composite was removed, the surface blotted dry, a cell reading taken, and the composite weighed.
5. Step 4 was repeated several times until constant weights and moisture cell readings were obtained. This saturating process typically took several days.
6. Once stable soil wetness conditions were attained, the soil-moisture cell-nylon composite was allowed to air dry in a position that permitted air to have access to nearly all surfaces simultaneously.
7. Readings and weighings were taken at intervals that were based on the technician's experience. The composite was rotated after each weighing to ensure equal access to the composite surface by the room air and to negate the effects of gravity.
8. As the soil specimen dried, the drying process was assisted by an electric fan to ensure that the dry end of the calibration scale was reached (i.e., that the soil moisture content was drier than that which the instrument could detect).
9. At the conclusion of the wetting/drying cycle, approximately 100 g of the specimen was removed to determine a representative weight of the soil solids for each specimen. Then soil moisture contents were determined for each sensor reading and the results plotted on 5-cycle semilog paper. If the calibration curve lacked sufficient definition at any location, then the remainder of the calibration specimen was rewetted and the required additional calibration points were determined. Typically, 4 to 6 weeks were required to satisfactorily complete a calibration curve for the CH soil, although soils of smaller sample size and with less clay content can be calibrated in approximately 2 weeks. Figure 1 shows a typical moisture cell calibration curve.

The fiberglass moisture cell was selected in the study because of the apparent wide range of moisture contents over which the cell is useful and its apparent sturdiness. Moisture contents as high as pore-space saturation and moisture contents below the wilting point have been detected, according to the literature with the sensor. Its fiberglass cloth is more resistant to deterioration than are other porous materials (e.g., gypsum, which is soluble in soil water). Finally, its sturdy construction indicated that it would not require special handling or placement procedures because of its being delicate. A continuous record of in situ soil moisture changes can be easily obtained from an ohm readout device.

Thermocouple Psychrometers

Soil Suction

Unlike pure free water, water in soil is subjected to several forces that restrict or direct the movement of soil moisture

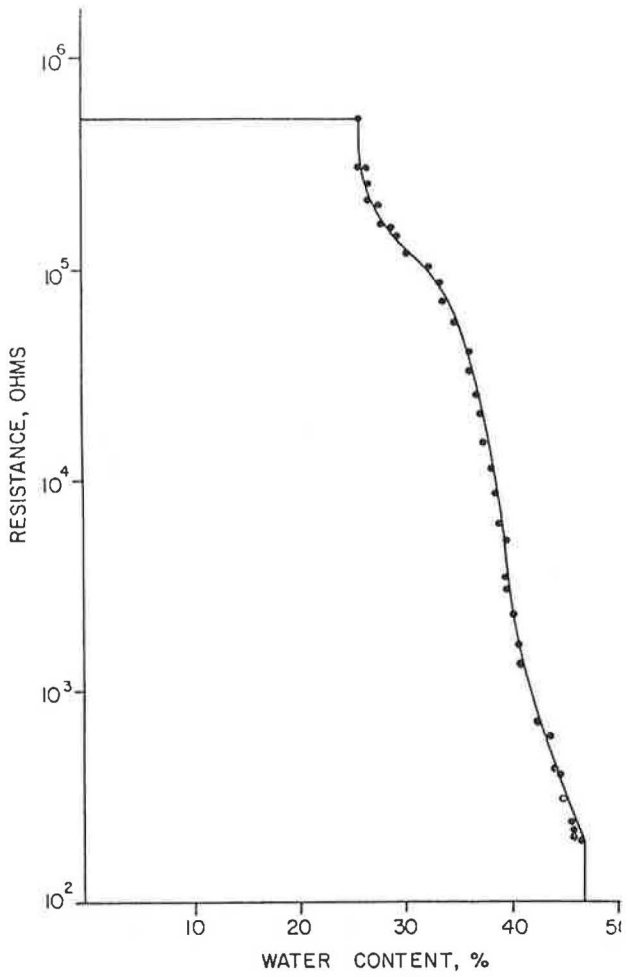

FIGURE 1 Typical calibration curve for a Soiltest moisture cell.

and result in a reduction of free energy. The difference in free energy between soil water and pure free water is termed soil water potential. A more precise definition is given by the International Society of Soil Science (ISSS) (*5*): "The amount of work that must be done per unit quantity of pure water in order to transport reversibly and isothermally an infinitesimal quantity of water from a pool of pure water at a specified elevation at atmospheric pressure to the soil water (at the point under consideration)." As suggested by ISSS, the soil water potential can be subdivided into components on the basis of the forces responsible for the difference in free energy between the soil moisture and pure free water, namely, matrix potential, osmotic potential, gravitational potential, and potential due to external gas pressure (pneumatic potential).

When gravitational and external gas pressure potentials are negligible, the soil water potential is termed "soil suction." This is the tensile pressure that must be applied to a unit area of water to prevent the water from entering the soil. In laymen's terms, it can be described as a measure of a soil's affinity for water (*6*). In general, the drier the soil, the greater is the soil suction.

Total soil suction, or difference in free energy, is related to the relative humidity of air in equilibrium with the soil water—a ratio of water vapor pressure of air in equilibrium with soil water to that of air in equilibrium with pure free water at the same temperature and pressure—by the following thermodynamic equation:

$$h = \frac{-RT}{g} \ln \frac{p}{p_0} \tag{1}$$

where

h = soil suction,
R = universal gas constant,
T = absolute temperature,
g = acceleration due to gravity,
p = vapor pressure of air in equilibrium with the soil water,
p_0 = vapor pressure of free water at the same temperature and pressure, and
p/p_0 = relative humidity.

The relative humidity ($H = p/p_0 \times 100$) will be less than 100 percent because the vapor pressure of soil water is less than that of pure free water. The reduction of vapor pressure in soil water over pure free water is the combined effect of matrix suction and osmotic suction. Thus, the soil suction value given by Equation 1 is a measure of the sum of the matrix suction and the osmotic suction and is termed "total suction."

Thermocouple Psychrometers

A thermocouple psychrometer (TCP) determines the relative humidity of soil moisture using the Peltier effect (i.e., production or absorption of heat at the junction of two dissimilar metals when a current is passed through the junction). Basically, the thermocouple is constructed using chromel and constantan wires, which together form a measuring junction. Two reference junctions are created slightly behind the measuring junction by attaching each of the constantan and chromel wires to separate copper wires of a larger diameter. Electrical current is then passed through the thermocouple to cool the measuring junction and condense a small bead of water on the junction. After the current is switched off, the condensed bead of water begins to evaporate, further cooling the junction. The change in voltage caused by cooling from the evaporation of the bead of water is then measured with a microvolt readout device. The microvolt readings are then calibrated with soil suction by using solutions of known water potential.

Calibration

Each thermocouple psychrometer was individually calibrated in the following manner:

1. The TCP was suspended in one end of a closed stainless steel calibration chamber that was compatible with the Merrill psychrometers. This chamber could be sealed to prevent the exchange of the atmosphere of known relative humidity inside the chamber with that of the ambient laboratory room atmosphere.
2. A piece of No. 40 Whatman filter paper was saturated in an NaCl solution of known molality and water potential

and then sealed in the opposite end of the calibration chamber used in Step 1.

3. The sealed calibration chamber was then immersed in a large tank of water. The ambient temperature of the room was controlled to remain at 65° ± 2°F. The water bath prevented sudden changes in temperature caused by air conditioning/heating equipment starting and stopping and fluctuations caused by doors to the laboratory opening and closing. The water bath temperature consistently remained at 65° ± 0.5°F.

4. The relative humidity in the small calibration chamber was permitted to come into equilibrium. The period typically required to reach equilibrium was approximately 1 hr; however, the minimum period employed was 2 hr, to ensure that complete equilibrium had been attained before proceeding to the next step.

5. The microvolt output from the readout device was checked periodically, beginning at an elapsed time of approximately 1 hr into the equilibration period. If the microvolt output remained constant, then a recorded calibration reading was taken at an elapsed time of 2 hr.

6. The microvolt reading was then plotted as a function of the water potential corresponding to the molality of the NaCl solution used in each calibration step.

7. The calibration chamber was removed from the water bath, opened, the filter paper removed, and the chamber cleaned and dried. Another piece of filter paper saturated in a different molal NaCl solution was then inserted into the calibration chamber and the procedure repeated until a definitive curve was produced. A typical calibration curve is shown in Figure 2.

The psychrometer is reported to have a measurable range of 3.0 to 6.2 pF (*6*). Thus, it becomes unreliable when the soil moisture content approaches saturation (≈3.0 pF). However, its range is such that it was judged to be able to provide reliable measurements over most soil moisture conditions expected to be encountered in this study. The psychrometer can measure only total suction; thus, if the matrix or osmotic components are desired, other methods of measurement must be employed. In certain subsurface conditions, the thermocouple can become corroded and fail to function, particularly in soils with high salinity; however, high-salinity soils were not the case in either location in this study. Relative humidity (and thus the psychrometer reading) is dependent on temperature. Therefore, thermocouple psychrometers were selected for this study. The thermocouple provided the temperature within a few millimeters of the tip of the thermocouple. This temperature measurement permitted the psychrometric reading to be corrected for temperature. Because of the possibility of instrument loss from thermocouple corrosion, damage during installation, or other unforeseen reasons, 100 percent redundancy in instrumentation was employed at each test site.

Surface Elevation Changes

Movement of the ground surface, both beneath as well as outside the slab-on-ground foundation model, was to be an important measurement of the study. To measure these changes in surface elevation, elevation points were established in a grid pattern with measurement points 3 ft on-center in each direction, including points 3 ft and 6 ft outside the perimeter of the slab model. The Amarillo site had a total of 247 elevation points with a line of points on the transverse centerline, whereas the College Station site totalled 234 points with no measurement points installed along the transverse centerline. The points outside the slab model consisted of 16d nails driven into the ground with red plastic flagging identifying each location. The points on the membrane were constructed of 6 in. high by ½ in. diameter PVC pipe glued to a 3 in. square plastic plate. The vertical PVC pipe was cut on a diagonal at

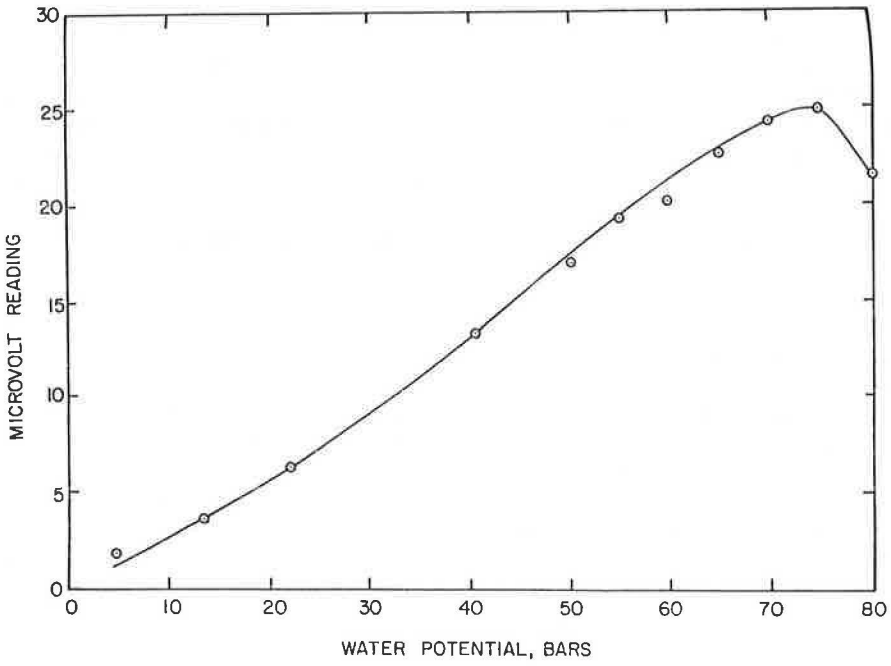

FIGURE 2 Typical thermocouple psychrometer calibration curve.

the top, so that a definite high point was provided for consistent elevation measurement points. The flat plate bottom of the elevation points was placed directly on the plastic membrane on 3 ft centers and covered with approximately 2 in. of sand. Surface elevations were measured along conventional engineering surveying equipment. All elevations were referenced to a permanent bench mark set at an elevation of 27.5 ft (Amarillo) or 25 ft (College Station). Details of the bench mark construction is presented elsewhere (*8*).

Instrumentation Layout

The instrumentation was placed beneath the covered surface in two identical parallel rows spaced 2 ft north and 2 ft south, respectively, of the longitudinal centerline. The rows were aligned parallel to the longitudinal dimension of the slab model and were symmetrical about the transverse centerline. The plan view of the instrument locations is shown in Figure 3.

Instrumentation Installation

Thermocouple psychrometers were placed in each location at depths of 1, 3, 5, 7, and 9 ft below the surface. All but the three centermost instrument locations in each row also had moisture cells installed at depths of 1, 3, and 5 ft below the surface. Figure 4 shows the vertical arrangement (termed a stack) of one row of the instrumentation. Each instrumentation location was augered using a truck-mounted auger, capturing and separating the removed soil in 1 ft increments. An egg-sized "ball" of soil from the appropriate depth was then molded around each sensor and carefully lowered back into the hole to the proper depth. Then the soil was carefully compacted back into the hole at the depth from which it was removed (at least to the nearest foot). The instrumentation was checked frequently to ensure that it was still operating before backfill and compaction proceeded too far, to prevent removal and replacement of a damaged device. The instrumentation holes were advanced by commercial testing lab personnel. Texas Tech University personnel performed all other installation activities.

CLIMATE

Amarillo Test Site

Amarillo has a dry steppe climate marked by mild winters. The average annual precipitation is 19.10 in. More than three-quarters of this annual amount typically occurs in the period May through October, usually in the form of thunderstorms. Monthly and annual precipitation amounts are extremely variable. Winter is usually a dry season, with most precipitation occurring as light snow. The mean daily high and low temperatures in the summer months are 88°F and 64°F, respectively. The mean daily high and low temperatures during the winter months are 50°F and 25°F, respectively.

The 5 years preceding site installation were drier than normal. This drought ended in August, 1985 (Month 1 of the study), and, although seasonal fluctuations were present, conditions during the study period were overall much wetter than normal. The 44-year historical Thornthwaite Moisture Index (TMI) for Amarillo is −21.9 in./yr. The five years preceding the study had an average TMI of −27.3 in./yr, but the TMIs for the three 12-month periods of this study were a very wet −7.4, −12.5, and −2.1 in./yr, respectively. KGNC radio station, located less than one-quarter mile from the site, re-

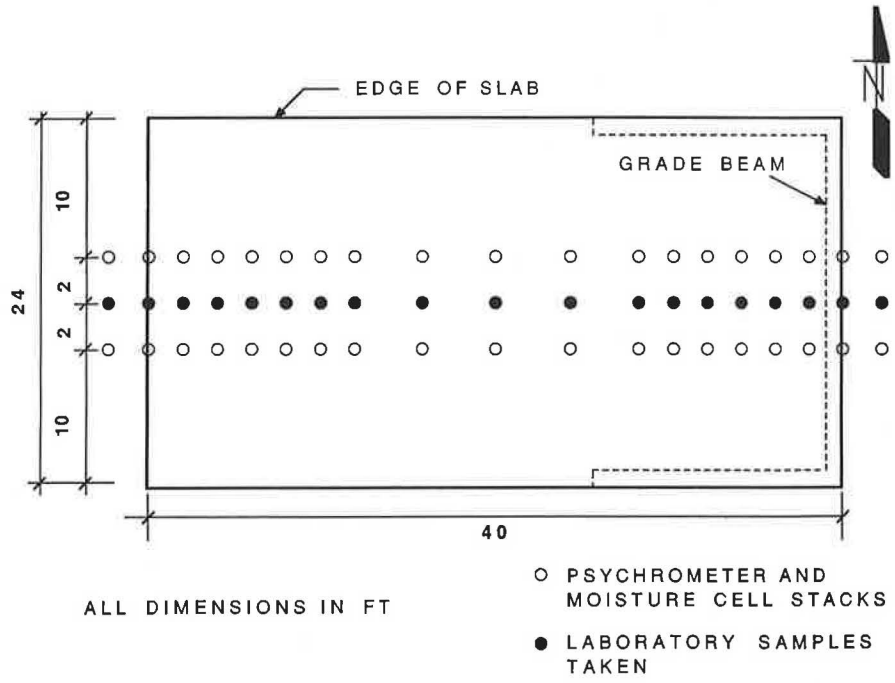

FIGURE 3 Test site layout showing dimensions of the test slab model, instrumentation stacks, and sampling locations.

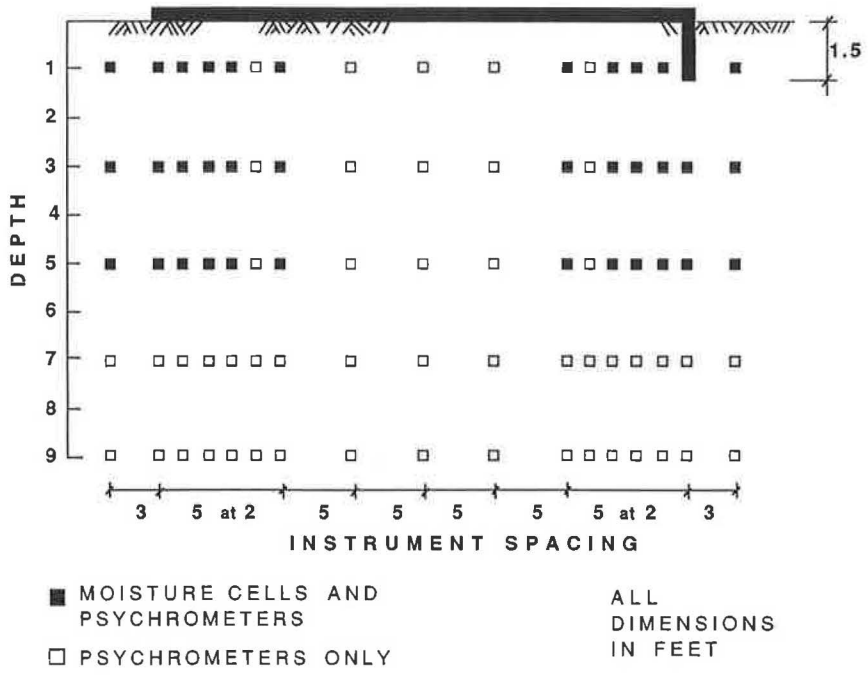

FIGURE 4 Vertical location and distribution of the instrumentation installed at the Amarillo site.

corded daily temperature and precipitation values for the period of this study. Thus, the climatological data was considered to be site specific.

College Station Test Site

College Station has a warm-temperate, humid, continental climate that is modified by breezes from the Gulf of Mexico. The summers are long, warm, and dry. The winters are short and mild and characterized by short periods of clear cold weather that is freezing at times. The average temperature during the summer months is 83°F, and during the winter months it is 52°F. The annual precipitation averages approximately 38.8 in. Droughts of varying duration and severity occur during the months of July, August, September, and October. Although the rainfall averages more than 2.4 in./month during these months, it may fall in only one or two events and with such intensity that a large part of it runs off before it has an opportunity to infiltrate the soil. The greatest rainfall historically occurs in May, but during January, February, and sometimes December, when the humidity is high and the rate of evaporation low, the ground becomes saturated and remains so for several days. Rain usually falls more slowly in winter than at other times of the year.

College Station was under drier than normal conditions in the months immediately preceding site construction. Subsequent to site installation, the climate became wetter than normal for the first 2 years. The final year experienced drought conditions. The 74 year mean TMI for College Station is a nearly neutral −0.5 in./yr. The TMIs for the three 12 month periods of this study were +5.3, +28.1, and −19.5 in./yr. The Texas A&M College of Agriculture weather station, located approximately 100 yd southeast of the research site, recorded daily temperature and precipitation data. Thus, the climatological data used in this study was considered to be site specific.

MEASUREMENTS AND RESULTS

Moisture Cell Measurements

Amarillo Site

The soil moisture content change measurements obtained during the period of this study were disappointing. The moisture cell measurements failed to provide any significant contribution to the study, apparently because of the extreme weather conditions experienced at each site. The in situ soil moisture content exceeded the range of the sensors, apparently as a result of the extended rainy period at the beginning of the study. Brief drought periods experienced later at the site also made the instruments fail to function when the soil dried out and lost contact with the moisture cells.

College Station Site

As with the moisture cell readings obtained at the Amarillo site, the College Station site also initially encountered soil moisture conditions that were beyond the wet end of the cells' sensitivity. Then came the drought period, during which some moisture cells reactivated and began to give readings. Because of the sporadic nature of the results obtained during each measurement visit, the moisture cell readings were judged to be of little assistance in understanding the changes that were observed to occur at the site.

Thermocouple Psychrometer Measurements

The soil suction data were collected by calibrated thermocouple psychrometers and, as one form of data presentation, plotted in the form of contour lines of constant suction value using units of pF. All measurements were taken by university personnel. A typical contoured suction value presentation is shown in Figure 5. Each psychrometer was read at least three times during each measurement visit; a consistency in readings was taken to be a valid reading. Each psychrometer reading was corrected for temperature. Two psychrometers were installed at each depth; thus, if both sensors were operating, one provided a check on the other. Typically, "sister" psychrometers yielded readings within ± 0.2 pF of each other. However, sister readings occasionally exceeded this differential range. In these instances, judgment had to be used to determine which reading was invalid

Another check on the data was available. Since theoretical wet and dry steady state soil suction conditions, based solely on changes in climate, could be developed for each site, any data falling outside this envelope could be considered to be either in error or influenced by factors other than only climate (e.g., trees at the College Station site during the hot, dry summer months) (*7,8*). The influence of surface cracks, particularly during periods of drought, can often influence a psychrometric reading, even if the sensor is several feet inside a covered surface. A precipitation event immediately preceding a measurement also was found to have a significant influence on the readings obtained from some psychrometers (*8,9*).

A comparison of rainfall versus the number of working psychrometers is shown in Figures 6 and 7. Although it is likely that more factors are involved in the failure of the TCPs than just rainfall, the figures show a definite correlation between long-term wet and drought conditions and the number of psychrometers yielding readings each month.

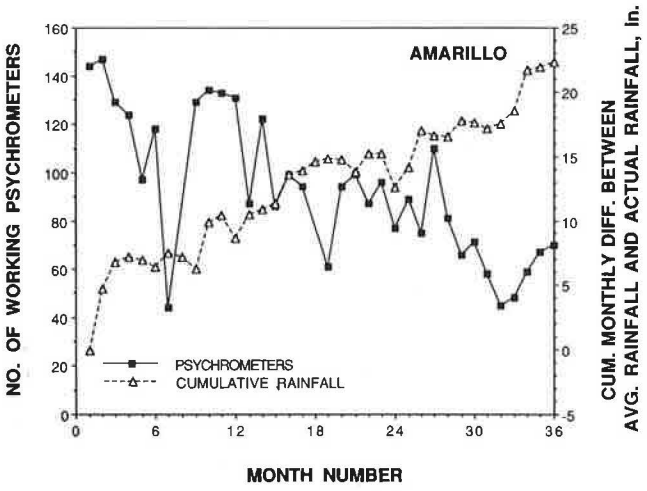

FIGURE 6 A comparison between the number of thermocouple psychrometers yielding readings during each monthly measurement visit to the Amarillo site and the surplus or deficit of precipitation each month with respect to the average precipitation for that month.

Amarillo Site

The soil at the site was very dry and nearly desiccated at the time of site installation. This condition was indicated by the in situ soil suction values ranging from a very dry 5.3 pF at a depth of 0 to 1 ft to a still quite dry reading of 4.3 pF at a depth of approximately 9 ft.

Two observations can be made from Figure 5, which depicts soil suction variations beneath the slab model one month after site installation. First, the soil immediately beneath the cover has become slightly wetter than the soil at a greater depth. This increase in moisture is attributed to the suction gradient continuing to draw moisture from depth as it was doing before installation of the impervious cover interrupted the moisture transfer to the atmosphere at the surface. Second, the essentially horizontal contour lines have been disturbed outside the cover by moisture entering the soil as a result of the rainfall occurring immediately after the site construction.

For most of the first 30 months of the study, the soil suction remained a fairly constant 4.2 to 4.4 pF at the soil surface

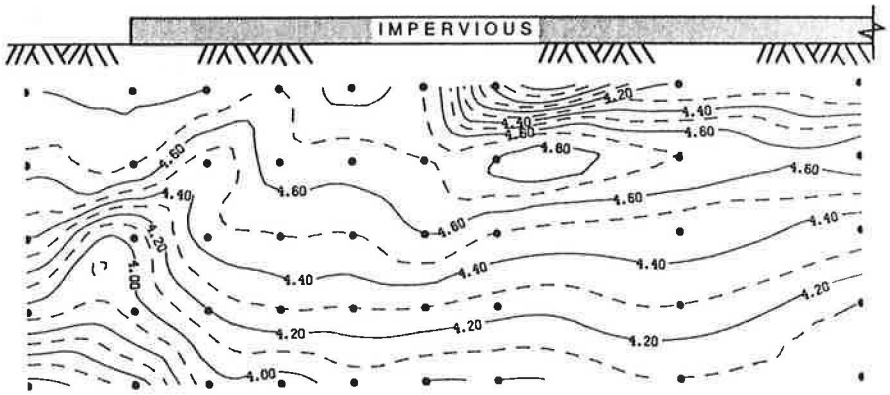

FIGURE 5 Lines of constant soil suction occurring beneath the west half of the slab model, as measured during the first measurement visit to the Amarillo site following test site construction.

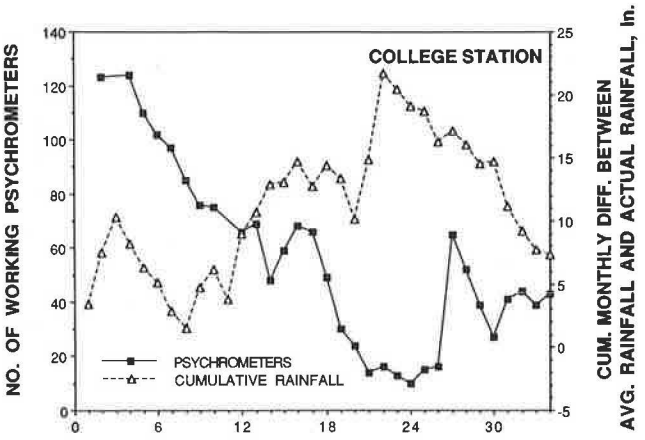

FIGURE 7 A comparison between the number of thermocouple psychrometers yielding readings during each monthly measurement visit to the College Station site and the surplus or deficit of precipitation each month with respect to the average precipitation for that month.

beneath the center region of the cover. Beginning at about Month 30, the soil suction data begins to indicate a wetting trend, with suction values trending to the 3.8–3.9 pF range. This wetting trend is consistent with the gradual development of a center lift mound at about this time (*8*).

College Station Site

The soil at the College Station site also was initially very dry. The soil suction near the surface was 4.9 pF, but the initial soil suction rapidly decreased to 4.3 pF at a depth of 2–3 ft and remained at this value until the average reduced slightly to 4.2 pF at the 8–9 ft depth. The contour lines for the College Station site (Figure 8) are not nearly as well defined as those at the Amarillo site. The poorly defined soil suction changes beneath the slab model are attributed to the influence of three mature trees located some 25 ft away from the edge of the site. As both the period of the study lengthened and the extended period of wet climate continued, more and more

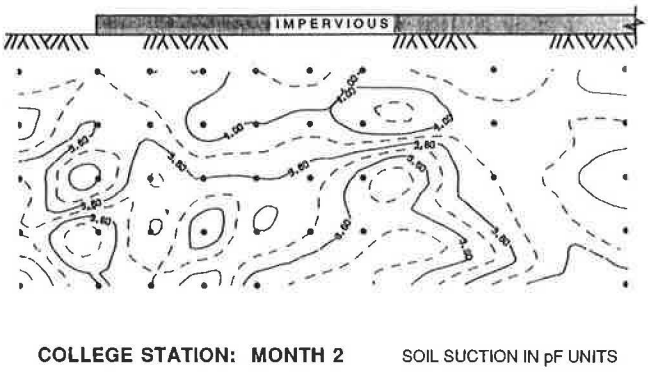

FIGURE 8 Lines of constant soil suction occurring beneath the west half of the slab model as measured during the first measurement visit (Month 2) to the College Station site following test site construction.

psychrometers failed to respond during measurement visits (Figure 8). During the Month 24 readings, as few as 10 of the 160 psychrometers yielded readings. However, drought conditions returned at about Month 25, and the number of working psychrometers subsequently began to increase, especially those located outside and near the edge of the slab model. These TCPs continued to report drying soil moisture conditions as the drought persisted. As many as 50 TCPs "revived" to yield readings over the last 8 months of the study.

Surface Elevation Changes

All elevation points were determined and referenced to the 25-ft deep benchmark at each site of the time of site installation. The actual elevations of each site were then corrected to an assumed elevation of 10.00 ft in order to provide a horizontal reference plane. All subsequent elevation measurements were then referenced to this horizontal plane in order to better visualize the changes in the surface elevations as they occurred. Measurements were made using conventional engineering surveying techniques with an accuracy to the nearest 0.01 ft.

Amarillo Site

Four days after installation, 1.53 in. of rainfall fell on the site; a total of 5.31 in. fell on the site during the 39 days between installation completion and the first measurement. The dry soil had begun to respond to this rainfall by the time of the first measurement. Heave was being exhibited around the perimeter of the cover (edge lift distortion pattern). The greatest heave measured was 0.8 in., which occurred at the east end of the slab model, the end with the 18-in. deep perimeter grade beam. The climate continued to be wetter than normal over this period, resulting in a very definite edge lift. The heave at the east edge of the slab model reached 2.3 in., while the heave experienced by the west edge of the covered surface was 1.0 in. The large heave measured on the east end of the slab model stayed between 2.0 and 2.5 in. throughout the study period, although the actual heave did reflect slight seasonal changes. Beginning at about Month 24, a mound began to develop beneath the center of the cover (center lift distortion). This mound continued to grow both laterally and in height throughout the remainder of the study period, reaching a maximum heave of 1.8 in. (*8*).

College Station Site

The month in which the site was constructed (August 1985) was very dry. Twelve of the 17 months preceding the site installation had recorded a moisture deficit. However, the period September–November 1985 was very rainy. As a result of this wet period immediately following the site installation, the ground heaved and did so fairly uniformly. Heaves between 0.5 and 1.0 in. were prevalent beneath as well as outside the cover. By Month 11, a center lift distortion started to be exhibited, particularly on the west, south, and east sides of the cover. Maximum heave occurred in the southwest quad-

rant of the cover and was 1.7 in. The maximum heave recorded each month remained in the 1.9–2.3 in. range. The maximum heave recorded during the 36-month study period was 2.5 in. in Month 29. Beginning with Month 32, a gradual general reduction in surface elevations was noted through Month 36 when the study terminated and a definite center lift condition was present (*8*).

Predictions Based on Measurements

One of the principal objectives of the study was to determine if reasonable estimates of shrink or heave of expansive soils could be made using soil suction data. Using soil suction theory (*7,8*), an estimate of the maximum heave to be expected at each site was made. This estimate was predicted on soil properties at each site and the initial soil suction profile. An estimate of each month's shrink or heave was also made using the monthly psychrometer (soil suction) measurements. Figures 9 and 10 show a comparison between the theoretical predictions and the actual measurements using psychrometer measurements taken beneath the center of the covered surface at each test site. Each figure also indicates the estimated maximum heave to occur at each location; as can be seen, the theoretical maximum heave has been approached but not exceeded. The predicted monthly heaves for the College Station site (Figure 10) stop at Month 18. Subsequent to this date, soil moisture conditions became too wet for the instrumentation and no further readings were obtained from this instrumentation "stack." Nonetheless, both figures indicate good correlation between predicted and actual heaves.

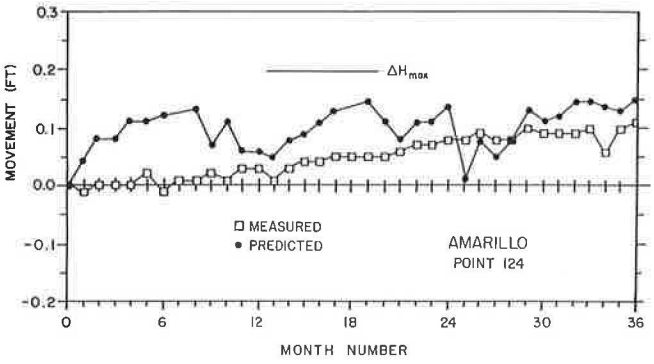

FIGURE 9 A comparison of the predicted month-by-month change in surface elevation with the measured surface elevation change at a point located at the intersection of the longitudinal and transverse centerlines of the Amarillo test site slab model [the maximum expected heave (ΔH_{max}) is also shown].

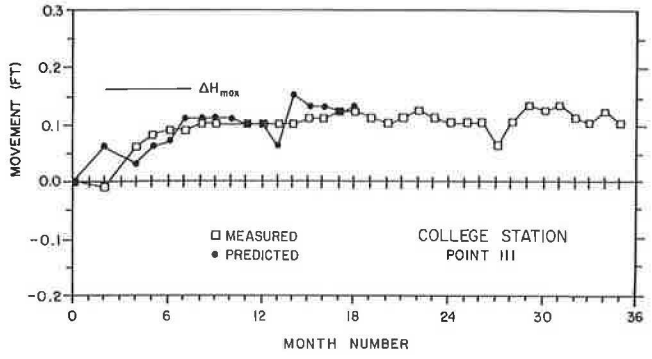

FIGURE 10 A comparison of the predicted month-by-month change in surface elevation with the measured surface elevation change at a point located 2 ft west of the transverse centerline and on the longitudinal centerline of the College Station test site slab model [the maximum expected heave (ΔH_{max}) is also shown].

CONCLUSIONS

Some conclusions can be made about the success of the instrumentation used on this study and the validity of the measurements obtained from these sensors.

1. Although the vendor of the fiberglass moisture cells has cited successful applications of this device in heavy clays, it appears that caution should be exercised when using this device in field applications in such clays unless soil moisture conditions are reasonably certain not to exceed the sensing bounds of the instrument. The use of this instrument in this field study must be considered to be a poor selection.
2. Use of thermocouple psychrometers on a study such as the one described above must be considered as being partially successful. The instrumentation provided monthly readings at the dry climate site without any significant problems under drought conditions. However, when saturation conditions were approached, the readings became either unobtainable or unreliable. Invariably, the sensors began functioning again or began to give reliable measurements once the wet conditions causing the loss of the instrument measurements began to become drier. Thus, the selection of thermocouple psychrometers for the dry climate site was, in retrospect, a good decision.
3. Use of thermocouple psychrometers proved to be a poor selection with respect to the wet climate site. Based on a review of prior year precipitation data, it appeared at the outset of the study that psychrometers would likely perform well over the duration of the measurement period. Although some localized or brief failure period due to excessively wet soil conditions was anticipated, it was expected that the sensor would soon recover and function once again when the wet conditions passed. Employing 100 percent redundancy in instrumentation was also thought to provide some hedge against any total loss in measurements. However, this was proven to be wrong when extremely wet weather persisting over a 2-year period plagued the site. It was also believed that the fiberglass moisture cell would provide some measure of the soil moisture conditions, should the soil approach saturation and become too wet for psychrometric readings. However, it was subsequently learned that the soil moisture conditions also exceeded the operating range of the moisture cell. Thus, the selection of the thermocouple psychrometer for the wet climate site proved to be a poor selection, although good data was obtained over approximately the first 18 months of the study.
4. Using the psychrometer measurements, converted to soil suction, to predict surface shrink and heave of the soil showed reasonably good comparisons between the predicted surface

elevation changes and the measured surface changes. Thus, it appears that reasonable predictions of the expected shrink and heave at an expansive soil site can be made if the proper soil characterization properties and if some knowledge of the in situ soil suction conditions are known.

At the time of instrumentation selection, a convenient device for making wet moisture condition measurements at depth was not commercially available. Thermal blocks, the precursor of the Moisture Control System (MCS) and Agwatronics sensors, were not considered to be practical for this installation. The MCS heat dissipation matrix soil sensor became commercially unavailable in 1979, and the Agwa-II heat dissipation matrix soil sensor was only introduced commercially at about the time of the site construction. The currently available Agwa-II sensor reportedly has a sensing range from approximately 0.1 bar to approximately 3 bars (higher potential sensors are reportedly available but require several months to acquire). Thus, were this study to be performed now it would be desirable to install both thermocouple psychrometers and heat dissipation sensors at the wet climate site to ensure that wet soil conditions are also captured.

SOIL SUCTION CONVERSION FACTORS

1,000 cm H_2O = 0.9806 bars
= 0.9678 atm
= 14.2234 psi
= 98.0665 kPa
= 980.6650 dyne/cm^2
= 3.0000 pF

ACKNOWLEDGMENTS

The investigation described above was performed under a grant provided by the U.S. National Science Foundation. The authors are also indebted to the Family Hospital Center for providing the Amarillo experimental site; to Texas A&M University for providing the College Station site; and to Amarillo Engineering & Testing, Inc., Dyess Testing Laboratories, and KGNC Radio (all of Amarillo), Allen Drilling, Inc. (of Austin), and N.L. Baroid Co. (of Lovington, N.M.), all of whom donated services or materials to the project.

REFERENCES

1. I. S. McQueen and R. F. Miller. Calibration and Evaluation of a Wide-Range Gravimetric Method for Measuring Moisture Stress. *Soil Science*, Vol. 106, 1968, pp. 225–231.
2. R. G. McKeen. *Design and Construction of Airport Pavements on Expansive Soils*. Report FAA-RD-76-66. Federal Aviation Administration, U.S. Department of Transportation, Washington, D.C., 1976, Appendix D, pp. 116–120.
3. E. A. Colman. The Place of Electrical Soil-Moisture Meters in Hydrologic Research. *Transactions* (American Geophysical Union), Vol. 27, No. VI, 1946, pp. 847–853.
4. E. A. Colman and T. M. Hendrix. The Fiberglass Electrical Soil Moisture Instrument. *Soil Science*, Vol. 67, No. 6, 1949, pp. 425–438.
5. International Society of Soil Science. *Soil Physics Terminology*. Bulletin No. 23. ISSS, 1963, pp. 7–10.
6. W. K. Wray. The Principle of Soil Suction and Its Geotechnical Engineering Application. *Proc., Fifth International Conference on Expansive Soils*, Adelaide, Australia, 1984, pp. 114–118.
7. W. K. Wray. Evaluation of Static Equilibrium Soil Suction Envelopes for Predicting Climate-Induced Soil Suction Changes Occurring Beneath Covered Surfaces. *Proc., Sixth International Conference on Expansive Soils*. New Delhi, India, 1987, pp. 235–240.
8. W. K. Wray. *Mitigation of Damage to Structures Supported on Slab-on-Ground Foundations*. Report ECE-88-20493, Vol. I. National Science Foundation, Washington, D.C., 1989.
9. W. K. Wray. Field Measurement of Edge Moisture Variation Distance. *Proc., XII International Conference on Soil Mechanics and Foundation Engineering*, Rio de Janeiro, Brazil, 1989.

Publication of this paper sponsored by Committee on Environmental Factors Except Frost.

Use of Dual Tube Nuclear Gauge for Crack Detection in Expansive Clay Soils

JUDITH B. CORLEY AND MARY ANNE RODRIGUEZ

Dual tube instrumentation was installed at vertical barrier projects in Texas to determine the spacing of horizontal cracks that transmit water through expansive clay soils. Site selection was contingent on roadway rehabilitation that included installation of a vertical moisture barrier. To date, six dual tube sites in Texas have been instrumented and readings taken. Field problems encountered were manufacturing defects with the sensor probe, moisture damage to the scintillation probe, and difficulty in extending readings to required depths due to poor design of the extension rods. The scaler ratemeter is susceptible to damage during normal transport. Data obtained in the field consisted of depths and count ratios for the source and sensor in the field-installed dual tubes. Density was determined using calibration curves of density versus count ratio supplied by the manufacturer. Plots of the density versus depth for each location were prepared and were studied to determine the crack pattern. Crack spacings of between 4 and 5 in. were obtained for four sites in climatic zones III-C and II-C, while spacings of 7 in. were obtained for two sites in or near climatic zone III-B.

Two types of pavement damage are commonly noted in pavements founded on expansive clay soils: pavement undulations, and longitudinal edge cracks. Pavement undulations consist of periodic areas of heave that normally extend across the pavement width and result in pavement roughness and concomitant decline in ride quality (*1*). Longitudinal edge cracks extend along the edge of pavement and result in a decrease in lateral support and an increase in evaporation at the pavement edge. Often the cracking phenomenon develops progressively, with a series of "parallel" cracks extending inward from the edge of pavement. This type of damage often results in a subsidence of the edge of pavement from the initial cross section.

The type and severity of pavement damage are affected by the subgrade moisture conditions. Site moisture conditions can vary from very dry conditions to wet conditions. When the subgrade is very dry prior to construction, the soil will have a fully developed array of horizontal and vertical cracks that divide the soil mass into blocks. Water may flow in the cracks as free water at a rate that is several orders of magnitude higher than that indicated by the low permeability of the intact clay. Thus the sides of the blocks are exposed to free water and are able to swell, while the centers of the blocks are not exposed to free water and remain very dry due to the low permeability of the clay within the block (*2*).

At the opposite end of the moisture spectrum, the subgrade could be initially in the wet condition, where the soil is "swelled" and the crack structure is closed. When the wet subgrade is covered with a pavement, evaporation occurs at the edge of pavement but cannot now occur from the covered soil. Shrinkage occurs at the pavement edge, and the marked difference in moisture conditions results in the development of a longitudinal crack. Once the longitudinal crack develops, it allows increased and deeper evaporation to occur, exacerbating the situation.

A wide variety of treatments have been used in efforts to control one or both of these classical damage mechanisms. One such method is to remove the expansive clay soil to a calculated depth and replace it with a compacted select fill. In addition to being expensive, the method had a tendency to result in rapid moisture availability to the subgrade through the select fill. Reed (*3*) reported that the method was unsuccessful in preventing pavement undulations.

A variation of the "remove and replace" method is the construction of a compacted fill of in situ soils. This approach has several positive aspects. There is no significant permeability difference between the subgrade and the compacted fill, so that no water source is created. In addition, the process of removing the soil, breaking it up into workable form, and recompacting in lifts destroys the crack structure. Time would be required for a new crack structure to reform, and the pavement would prevent drying. This approach is consistent with the observation that severe undulations are most often observed in cut sections and only after many moisture cycles in fill sections. A combination of both select fill and a layer of recompacted site clays was utilized on reconstruction of 131 miles of I-90 in South Dakota. Improved pavement performance with reduced maintenance expense was noted over a 13-year period (*4*).

An extension of the idea of compacting in situ soil above optimum moisture content is to prewet or preswell the subgrade without removal or recompaction. This technique may be carried out by ponding water at the surface or by multiple pass water injection (*3*,*5*,*6*). The soil is wetted using the existing crack structure, which is not affected by this process. These techniques are time consuming, create a difficult working environment, and do not prevent longitudinal edge cracking.

Horizontal barriers have been used and will continue to be used, both to improve highway safety and to control moisture stability in the driving lanes. The common horizontal barrier consists of the paved and sealed shoulder, which reduces evaporation from the edges of the driving lanes, thereby reducing longitudinal cracking within the lanes of traffic. Use of impermeable membranes below unpaved shoulders is an alternative to the paved shoulder horizontal barrier (*5*).

Texas Transportation Institute, Texas A&M University, College Station, Tex. 77843.

To achieve pavement stability on expansive clay subgrade, it is necessary to control both edge evaporation and water movement through the crack structure. Use of vertical moisture barriers offers promise to achieve control over both types of pavement distress (*1*). Providing that the barrier extends below the depth of the crack structure, free water flow will be controlled from entering or leaving the soil mass beneath the pavement. Evaporation will still occur beyond the vertical barrier, but the flow path for the soil beneath the pavement will be lengthened so that change in soil volume will be minimized. Unlike prewetting and horizontal barriers that are used in new construction, the vertical moisture barrier can be installed in existing distressed pavements as part of pavement rehabilitation efforts (*6*).

VERTICAL MOISTURE BARRIER PROJECTS

The Texas State Department of Highways and Public Transportation (DHPT) has a considerable history of installing and evaluating vertical moisture barriers for pavements founded on expansive clay. One of the early efforts was I-410 in San Antonio. This pavement had required repeated levelling efforts from the time of construction in 1960 until installation of the vertical barrier in 1978 (*6*). Additional moisture barriers were placed at I-37 and U.S. 90 in order to improve construction techniques and to decrease damage due to expansive clay subgrade. In all cases, the installation of the vertical barrier was part of a pavement rehabilitation project on a pavement already known to exhibit significant distress due to expansive clays. Favorable results were obtained for the early San Antonio projects, with maintenance costs for the barrier sections reduced from a minimum of $50,000 per year to zero (*7*).

Following the beneficial installations in San Antonio, a research project was undertaken by DHPT and the Texas Transportation Institute to consider several different types and depths of vertical barriers. This project was installed on I-30 in Greenville, Texas. Barrier tests included 8 ft deep fabric, 6 ft deep fabric, 8 ft deep pressure-injected lime slurry, and 8 ft deep pressure-injected lime/flyash slurry. Results of this project showed that test sections with the vertical moisture barrier deformed more than the control sections. The difference between the initial and the equilibrium suction conditions were considered to be the cause of the difference in performance of the Greenville sections. The more effective barriers permitted the equilibrium suction condition to be approached more rapidly (*8*).

An additional site has been installed and monitored in Sierra Blanca, in far west Texas. This site has demonstrated the effects of highly variable subgrade conditions, with surficial sands being underlain by expansive clays at depths ranging from 2.5 ft to 20.0 ft.

With succeeding efforts at installing and monitoring vertical moisture barriers in Texas, the level of understanding has improved. Efforts are now aimed at maximizing performance and predicting the behavior of installed barriers.

CURRENT PROJECT DESCRIPTION

Installation of dual tubes and monitoring of vertical density variations was performed as part of a project to control moisture variations under pavement sections founded on expansive clay soils using vertical moisture barriers. The project, which is still in progress, is funded by the DHPT and involves test sites throughout Texas. The project team consists of researchers from the Materials Division of the Texas Transportation Institute, Texas Tech University, and the University of Texas at El Paso. The project consists of several distinct phases:

- Coordination with highway engineers to select suitable sites;
- Instrumentation of sites and control sections where possible during installation of vertical barrier;
- Monitoring of pavement performance and subgrade suction conditions to evaluate effectiveness of vertical barriers;
- Preparation of a computer model to allow evaluation of sites for use of vertical barriers;
- Recommendations regarding suitability of vertical barriers for various regions in Texas and rational sizing methods to assure adequate performance; and
- Recommendations of construction improvements to facilitate installation of the barriers and minimize deterioration of pavement conditions due to construction.

Each dual tube installation is a permanent part of the pavement instrumentation and is generally located adjacent to the holes in which suction and temperature sensors were installed outside the vertical barriers. A schematic of a typical site installation is shown in Figure 1.

Installation of the dual tubes and monitoring of density with depth was conducted in order to provide input for the computer model. The computer model considers moisture flow in expansive clay soils to consist of free flow in vertical and horizontal cracks, followed by gradual infiltration of the water into the clay clods. Determination of the size of the clay clods and the depth of cracking of the expansive clay is necessary in order to utilize the computer model. The model also is capable of handling multiple soil layers that may be present in some locations.

Figure 2 shows the types of elements used in the computer model, with each element consisting of a relatively homogeneous soil clod. Horizontal lines on Figure 2 may indicate changes in geometry, changes in material characteristics, or locations of horizontal cracks. Vertical lines indicate changes in geometry, locations of vertical cracks, physical barriers, or convenient locations to obtain rectangular elements of reasonable size. The purpose of using the dual tube system was to define the crack spacing.

The presence of either shrinkage cracks or thin layers of different material will result in changes in density with depth. It was believed that these changes would be detectable using

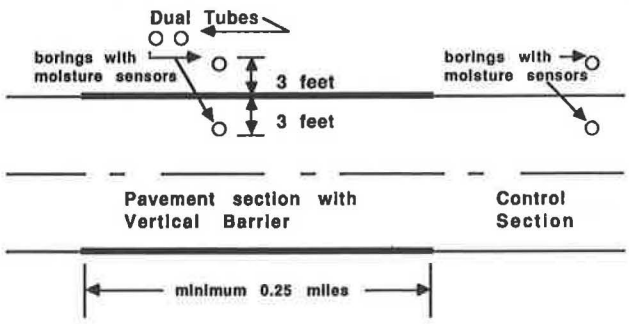

FIGURE 1 Schematic of field instrumentation.

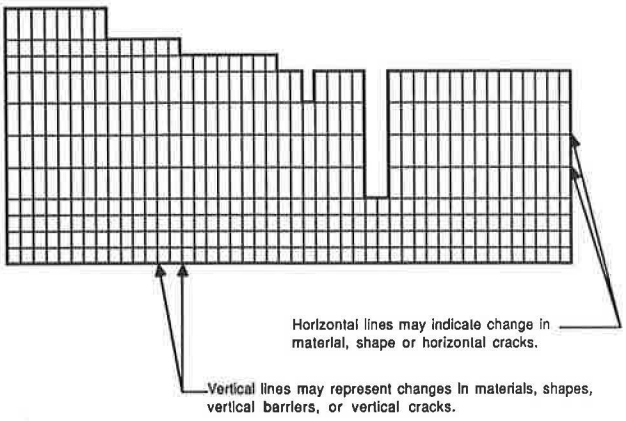

FIGURE 2 One possible configuration of computer model of moisture flow through cracked clay.

the dual tube nuclear gauge. The purpose of the installation was to allow determination of density at frequent depth intervals, in order to determine the size of the clods formed by shrinkage of the expansive clay soils. This information is required so that a vertical barrier is extended to a sufficient depth to prevent moisture flow in horizontal cracks, which would result in significant moisture variation beneath the pavement.

SITE SELECTION

Instrumentation of any site for this project was contingent on installation of the vertical barrier by a local highway district. Site selection thus required coordination of efforts with local maintenance engineers so that desirable sites were considered for rehabilitation. Local district personnel were asked to submit candidate sites having the following characteristics:

- Site should be founded on expansive clay soil. Sites that have interbedded layers of sand, silt, gravel or shale are included in this group.
- Site should have a history of repeated maintenance requirements. These pavements may have sagging shoulders, extensive cracking, or a "roller coaster" ride.
- Roadway must be in cut, at natural grade, or in a minimal fill. Roadways that are placed on extensive clay fill do not exhibit the same degree of moisture movement through a developed crack system and were therefore excluded.
- Distressed length of the pavement section must be at least 0.25 miles.
- Site may have either high or low groundwater conditions. Moisture conditions beneath a pavement with a vertical barrier will stabilize more rapidly for a high groundwater table.
- Maintenance or pavement rehabilitation must be planned within the duration of the project.

Based on these characteristics, highway personnel suggested a total of 48 sites. Each of these sites was visited by a research project engineer, and a list of "most suitable" sites was prepared. In addition to the characteristics above, the research team was also interested in having sites present in a variety of climatic zones and geographic areas within the State.

To date, six dual tube sites have been instrumented and readings taken. These sites are located in College Station, Seguin, Converse, Irving, Wichita Falls, and Snyder, Texas, as shown on the map in Figure 3. Also shown in Figure 3 are the climatic zones in the State of Texas. Results of the project in Greenville have suggested that climatic conditions are an important variable to barrier performance, so it was desirable in the current project to test the barriers for a variety of climate types. The variability of the size and spacing of soil cracks, or the degree to which the cracks are open for water flow at the time of construction, may also be a function of climatic zone. Additional sites are anticipated, and additional readings will be taken at existing sites where the dual tubes are not damaged during construction.

All of the sites listed above are located either at natural grade or in cut sections. The site in Seguin, part of a major rehabilitation project of I-10, is a roadway section subjected to heavy traffic loads and a particularly high percentage of truck traffic. The site located near Converse is a pavement improvement and capacity enlargement project of a farm-to-market (FM) road that previously consisted of two lanes with no shoulders. The site for the dual tube installation in College Station is the soils research area at the research annex at Texas A&M University.

The site in Wichita Falls is on I-44 and is unusual in that the barrier has been installed at the inclination of the slopes past the shoulder. This resulted in ease and economy of installation but significantly less vertical penetration of the barrier. The Irving site is located on the outer urban traffic loop of the Dallas metropolitan area in a soil formation that is extremely expansive. The dual tube is installed at MacArthur Boulevard, where Loop 635 is located approximately 25 feet below natural grade and the exit roadway rises to the level of the uncut soil. The Snyder site is a four-lane divided highway located approximately 18 miles north of Snyder. The dual tubes are installed at natural grade in what appears to be undisturbed clay soils.

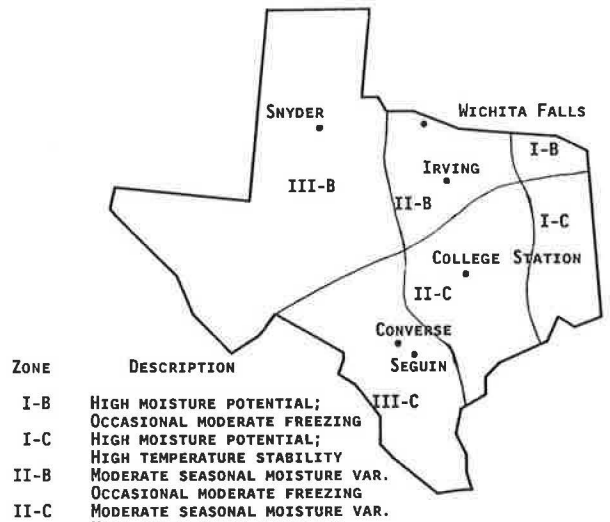

FIGURE 3 Site locations and climatic zones for highway technology.

DESCRIPTION OF INSTRUMENTS

The dual tube nuclear system consists of two parallel aluminum tubes, a nuclear source and sensor, and a scaler ratemeter. The field installation consists of drilling and placing the aluminum tubes, and the field monitoring involves inserting the source and sensor and obtaining the resultant readings on the scaler ratemeter.

The dual tubes used for this project are 10 ft aluminum tubes having an outside diameter of 2 in. Borings for placement of the tubes were made using a truck-mounted probe with a 2 in. diameter auger. A template is used during drilling to ensure that the two holes are parallel and are separated by a distance of 12 in. Prior to insertion, a rubber plug was placed into the lower end of each aluminum tube. Each tube was sealed at the surface with a steel banded rubber cap to minimize water entrance into the tube. Following the installation process, a minimum of two days was allowed prior to taking readings, in order to allow the soil to achieve good contact with the installed tubes.

The instruments used on this project consisted of Model 2376 two-probe density gauge, Model 2651 scaler ratemeter, and extension rods, all manufactured by Troxler Electronic Laboratories. The scaler ratemeter consists of three portions: a timer/counter for taking readings; a ratemeter module used to calibrate the unit; and a power supply module. The source consisted of a 5 mCi unit of cesium 137, which screwed onto the source probe from its lead-encased travel container. The source produces gamma photons of 662 KeV energy by radioactive decay. The sensor consists of a scintillation probe, which produces pulses proportional to the energy of the gamma radiation striking it.

Field readings were obtained at each of the six installations to within six in. of the termination depth of the tubes by research engineers from the Texas Transportation Institute. The scaler ratemeter was calibrated at each location by placing the source probe and the sensor probe into a calibration frame and obtaining readings. Following calibration, the source was inserted into one aluminum tube and the sensor was inserted into the other. A bubble level was used to ensure that both source and sensor were at the same elevation prior to each reading. A reading was taken over a period of one minute. The various components of the field instrumentation are shown in Figure 4. The arrangement between the source and sensor probes while taking readings is shown in Figure 5. Readings, in the form of a count, were taken at 1 in. intervals by carefully lowering both source and sensor in the dual tubes.

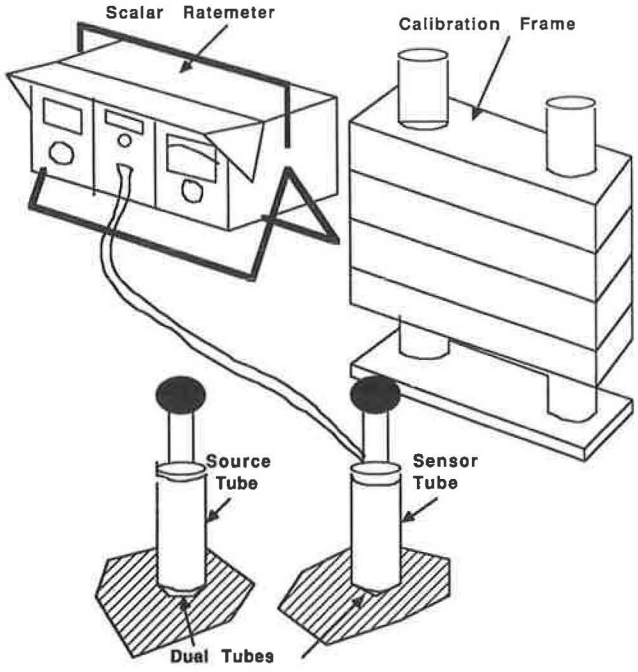

FIGURE 4 Field instruments for dual tube operations.

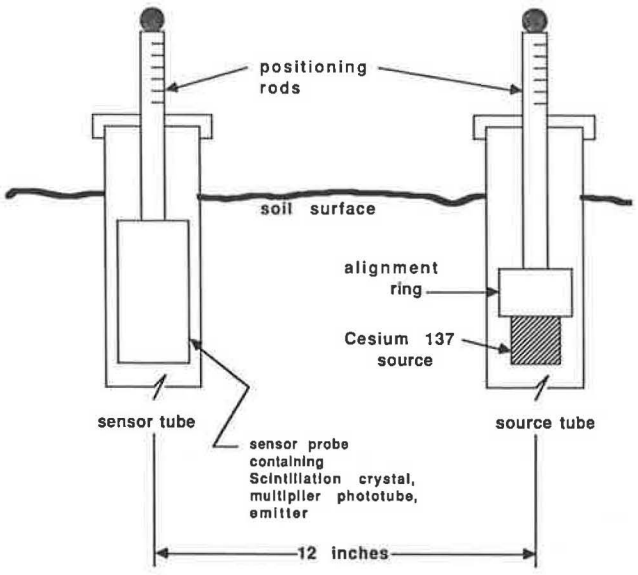

FIGURE 5 Source and sensor probes during field readings.

DATA ANALYSIS AND RESULTS

Data obtained in the field consisted of the count for the source and sensor placed in the magnesium standard and depths and counts for the source and sensor in the field-installed dual tubes. The standard count was taken four times using a one minute reading for each count, and the average of the standard count was used in data analysis.

Following completion of field work at each site, count ratios were obtained for each field reading by dividing the field reading by the average standard count. The density was determined using calibration curves of density versus count ratio that were supplied by the manufacturer.

Plots of the density versus depth for each location are prepared. A typical plot is shown in Figure 6 for the density versus depth results at Converse, Texas. Several things can be observed in this plot. First, there is a significant increase in density at a depth of 28 in. This change in density corresponds almost exactly to the depth of material added at the pavement shoulder in order to widen FM 1516 from a two-lane to a four-lane roadway. It is important to note that fill is present even at a site that is essentially at natural grade due to the change in section geometry. The dual tube system is sensitive to these density changes and shows a dramatic

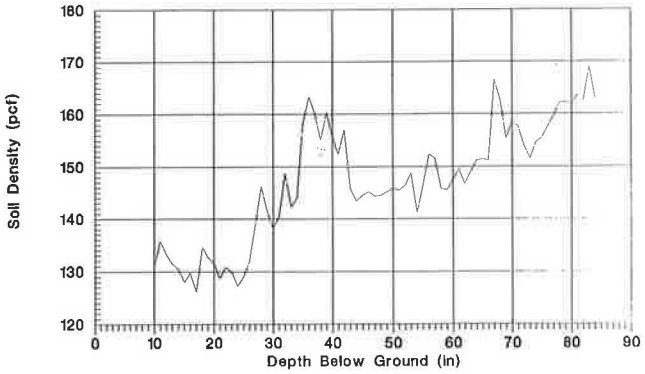

FIGURE 6 Soil density vs. depth below ground, FM 1516, Converse, Texas.

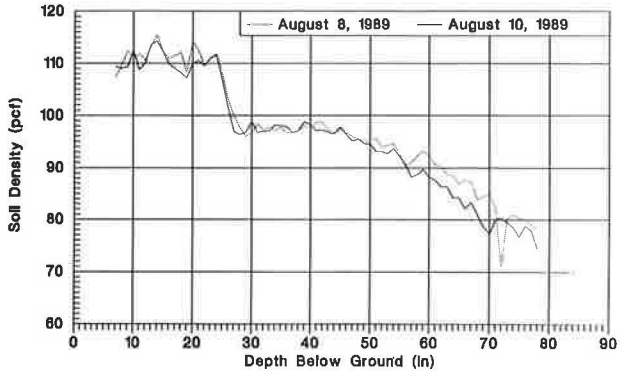

FIGURE 7 Soil density vs. depth below ground, Texas A&M research annex, College Station, Texas.

response in cases where the compaction specification results in a significantly different density condition.

Peak densities are observed in the fill material at about 5 in. increments and undoubtedly reflect both the quality assurance increment and the finished lift increment at the site. Several relatively low densities are observed in the fill material and show the ability of the dual tube system to detect densities that are below specifications. The feasibility of using the system for construction quality assurance is limited, however, due to the fixed location of the tubes and expense of the installation.

The purpose of the dual tube installation on this project was to determine the spacing of horizontal cracks that transmit water in expansive clay soils. To determine this crack spacing, the plot of density versus depth is observed for the subgrade below the fill. Depths associated with low density are listed and are combined into a single low point in cases where a trend toward lower density occurs. For example, two low points are observed on the Converse plot at depths of 15 and 17 in. These were combined into a single low point at 17 in. for the purpose of evaluating clod size. All significant low points were listed and included depths of 10, 17, 21, 24, 30, 33, 38, 41, 44, 54, 59, 63, 69, and 74 in. The difference between successive low points represents a soil clod, so clod sizes of 7, 4, 3, 6, 3, 5, 3, 3, 10, 5, 4, 6, and 5 in. were obtained. The average clod size for the Converse site was 5.3 in. Clod sizes of 4.7 in. appear to be suitable for modelling of the overlying fill material as previously described.

A similar evaluation of data was done for the site located at the Texas A&M research annex. The plot of density versus depth for this site is shown in Figure 7 and shows approximately 23 in. of dense material underlain by much less dense material. Readings at the site were repeated on two occasions to verify this finding, and the two plots show excellent repeatability. Density readings were evaluated to detect low-density locations, which were noted at depths of 11, 16, 19, 22, 28, 31, 36, 43, 51, 55, 63, 66, 70, and 77 in. Based on these depths to low-density areas, an average crack spacing of 5.1 in. is obtained. The average for the upper seven low-density peaks was 4.85 in., while the average for the seven deeper low-density peaks was 5.85 in.

The plot of density versus depth for the site on Loop 635 in Dallas indicates continued increase in density with depth. This site is located approximately midway in a 25 ft deep cut along an exit ramp from the loop onto MacArthur Boulevard. Dual tube readings were made on two site visits and resulted in average crack spacings of 4.8 and 5.0 in., respectively. Slightly higher average crack spacing was obtained when considering the upper low-density peaks as compared to the deeper peaks, with averages of 5.0 and 4.57 in., respectively. The range of crack spacings for the Dallas site was between 3 in. and 8 in.

Evaluation of the plots from Seguin resulted in an average crack spacing of 4.8 in., while those from Wichita Falls and Snyder yielded average crack spacings of 7.0 and 7.3 in., respectively. A significantly different crack spacing with depth was observed only for the Wichita Falls site, where the upper spacing was 6.6 in., while the deeper crack spacing was 9.0 in. The range of crack spacing values for the Seguin site was 3 to 10 in., while that for Snyder was 5 to 12 in. Crack spacings as low as 3 in. and as high as 14 in. were observed for the Wichita Falls site.

Based on results to date, it appears that crack spacings of between 4 and 5 in. apply to sites in the eastern and southern part of the State of Texas. Larger crack spacings of 7 in. or above are indicated for the two sites located in or near climatic zone III-B. The spacings may be related to the activity of the clay mineral as well as the climatic zone. Additional sites will be installed and monitored to test the validity of these conclusions.

FIELD DIFFICULTIES WITH DUAL TUBE SYSTEM

Several field problems have been encountered with use of the dual tube system. Among these problems are manufacturing defects in the sensor probe, susceptibility of the scintillation probe to moisture, and difficulty in extending readings to depths required for engineering applications.

Initial efforts at using the dual tube system met with severe difficulty in lowering the sensor probe into the installed dual tube. The sensor probe had been manufactured out-of-spec with regard to encasement diameter. Replacement of the sensor housing was required in order to correct the problem.

The high level of pressure initially required to lower the sensor probe into the dual tube resulted in damage to the housing seal. Moisture present in the tube entered the sensor

and damaged the scintillation probe, despite the fact that the probe was not lowered below the level of the groundwater table. As a result of this costly damage, great care is now taken to ensure that the sensor probe is not exposed to water. As previously mentioned, both top and bottom caps are used during installation. Prior to taking any readings, each tube is checked for water. Water that is present is removed using a system of sponges on rope until a dry hole is achieved. No warning of water susceptibility was provided by the manufacturer. This problem may limit use of the dual tube system in very wet environments or will require redesign of the sensor probe with an improved water seal.

Transportation of the scaler ratemeter to take field readings has also been a problem. The instrument is very sensitive and must be transported in a level position. Despite considerable care to ensure that the equipment is not subject to jarring, the electronic boards in the ratemeter have loosened and required maintenance. It will be necessary to provide a less sensitive system before widespread use of the dual tube system will be feasible in civil engineering applications.

The dual tube system has been used up to the present time primarily by soil scientists in agricultural applications, which has limited its use to the upper 3 to 4 ft of soil. Engineering applications for pavements have required installations that have varied from 7 to 10 ft. The extension system for lowering the source probe and the sensor probe beyond the depth of 2 ft consists of multiple 2 ft rods that screw into the probe units. It was noted that rotation of the extensions during lowering loosened the connections between successive extensions and the weight of the extensions made it difficult to control lowering of the sensor probe beyond 9 ft. While these problems were overcome on this project by teamwork and care during connection of the extensions, greater difficulties may be encountered in applications requiring deeper tube installations.

As is the case with all instruments having radioactive elements, all personnel using the instrument must wear radiation badges to monitor exposure. In addition to normal training in the use of the typical density gauge, the dual tube system requires significantly more training and care in operation. The instrument must be field calibrated at each location, and the procedure to prepare the instrument prior to taking readings is detailed. Approximately 2.5 hours was required to set up and take readings at 1 in. intervals at each site.

CONCLUSIONS

Based on preliminary findings, it appears that the dual tube system can be used to characterize the clay clods and the locations of shrinkage cracks that determine moisture flow in the clay mass. This information has not been available previously due to the practical sample size required to obtain soil density in the laboratory. Location of the cracks requires obtaining density over short depth intervals so that changes are pinpointed.

Once installed, the dual tubes can be read repeatedly to observe seasonal variations. While limited data are available at this time, this may provide useful information for areas like Texas that have dramatic seasonal variations in moisture availability. Changes in the size of soil clods may also be an indicator of the depth of seasonal moisture variation. This depth is an important design parameter for a variety of transportation structures.

Problems associated with the dual tube system will limit its use for engineering applications until design changes are made. The most critical problem is the susceptibility of the scintillation probe to moisture, which limits use of the system to holes above the groundwater table. Improvement of the water seal in the sensor probe is necessary for most engineering projects where dry conditions cannot be guaranteed. An improved extension system should also be provided to facilitate use of the dual tube at depths greater than 9 ft. The development of a locking mechanism over the screw fitting and a lighter extension unit are also desirable.

Results have demonstrated that the dual tube system produces results that are consistent with the design and construction processes at a site. It is possible to detect weak layers, lift thicknesses, and fill thicknesses. In addition to this transportation application, the system may prove useful in solid waste management applications where detection of these items is essential and permanent monitoring systems are required.

REFERENCES

1. M. Picornell and R. L. Lytton. Behavior and Design of Vertical Moisture Barriers. In *Transportation Research Record 1137*, TRB, National Research Council, Washington, D.C., 1987, pp. 71–81.
2. R. L. Lytton, R. L. Boggess, and J. W. Spotts. Characteristics of Expansive Clay Roughness of Pavements. In *Transportation Research Record 568*, TRB, National Research Council, Washington, D.C., 1976, pp. 9–23.
3. R. F. Reed. Roadway Performance in an Expansive Clay. In *Transportation Research Record 1137*, TRB, National Research Council, Washington, D.C., 1987, pp. 36–41.
4. E. B. McDonald. Construction Methods to Control Expansive Soils in South Dakota. In *Transportation Research Record 1089*, TRB, National Research Council, Washington, D.C., 1986, pp. 57–62.
5. D. H. van der Merwe, F. Hugo, and A. P. Steyn. The Pretreatment of Clay Soils for Road Construction. *Proc., Fourth International Conference on Expansive Soils*, Vol. 1, ASCE, New York, 1980, pp. 361–382.
6. M. L. Steinberg. Deep Vertical Fabric Moisture Seals. *Proc., Fourth International Conference on Expansive Soils*, Vol. 1, ASCE, New York, 1980, pp. 383–399.
7. M. L. Steinberg. Controlling Expansive Soil Destructiveness by Deep Vertical Geomembranes on Four Highways. In *Transportation Research Record 1032*, TRB, National Research Council, Washington, D.C., 1985, pp. 48–53.
8. D. D. Gay and R. L. Lytton. Pavement Roughness on Expansive Clays Altered by Vertical Moisture Barriers. *Proc., Annual National Meeting*, ASCE, Memphis, Tenn., 1988.

Publication of this paper sponsored by Committee on Environmental Factors Except Frost.

Construction Control Testing of Slurry-Assisted Soldier Wall Caissons with Inclinometer and Nuclear Density Probes

MICHAEL L. RUCKER

A foundation system for the new Terminal 4 building at Sky Harbor International Airport in Phoenix, Arizona, incorporated subsurface support and space for a proposed rapid transit tunnel, which may be constructed beneath the groundwater table in a sand-gravel-cobble horizon after the building is finished and in use. Two walls consisting of slurry-assisted drilled shaft caissons were constructed along the sides of the proposed tunnel to provide foundation support for the terminal and to provide stability for possible future tunnel excavation. An inclinometer verified clearance tolerances for the proposed tunnel space that necessitated tight vertical plumbness specifications for the drilled shaft caissons. Placement of concrete in the slurry assisted caissons was verified using nuclear density probes. The presence of rebar splices and varying access tube positions relative to rebar steel required detailed analysis of nuclear density probe response characteristics, special calibration blocks and procedures, and interpretation of density data based on knowledge of the rebar and access tube geometries.

The objective of this paper is to describe the methodologies used to monitor slurry-assisted caisson (drilled pier) construction at the Sky Harbor International Airport Terminal 4 in Phoenix, Arizona. Foundation design included elements to permit future construction of a rapid transit tunnel (RTT) under the terminal building. The RTT space was flanked by two walls, each consisting of about 115 drilled piers on 10 ft centers connected by a grade beam located at building basement level. These walls were designed to serve as part of the foundation system with the tunnel in place.

Each wall pier consisted of a straight, drilled shaft with a neat diameter of 54 in. advanced to a depth of about 55 ft below the basement excavation. The shafts were installed in the Salt River sand-gravel-cobble (SGC) deposits underlying the site. Overbreakage of shaft excavations was anticipated due to the dense packing of cobbles and boulders in this material. Groundwater was present at depths of about 25 to 30 ft below construction grade, requiring bentonite slurry construction techniques be used to maintain hole stability.

CONSTRUCTION MONITORING OBJECTIVES

The proposed RTT placed unusually strict constraints on the true subsurface location and geometry of the caissons immediately adjacent to the proposed tunnel. A distance of only 21 in. separated the proposed tunnel walls from the caisson neat lines. A caisson could theoretically encroach on the space in either of two ways. Caissons with diameters in excess of 96 in. could encroach upon the RTT space, perhaps requiring partial demolition for future tunnel construction. Caissons with somewhat smaller diameters that drifted towards the proposed tunnel could also impact tunnel construction. Therefore, it was especially important to accurately document the as-built diameter and orientation of each caisson. The use of slurry dictated that caisson density monitoring be performed to verify the integrity of the concrete, especially at the caisson rebar cages.

Approximate caisson diameters were determined by monitoring concrete height gain versus concrete volume placed during caisson installation. The approximate orientation of each caisson was determined by measuring the verticality of the caisson rebar cage using an inclinometer. Downhole nuclear density gauges were used to verify concrete integrity in the caissons (*1*,*2*).

Instrumentation access was provided by PVC tubing installed by the contractor on the steel reinforcement (rebar) cages and cast into the caissons. These access tubes were tied adjacent to selected vertical rebar members during the cage fabrication. This positioning minimized both bending and crimping of the access tubes and the potential for restricting concrete flow around and through the rebar cages during concreting.

Daily field observations, instrumentation readings and initial field inclinometer data interpretations were performed onsite by engineering technicians. Final data analysis and interpretation was performed by the instrumentation engineer as construction proceeded. The engineer was continuously available for telephone consultation with the field technicians or, when necessary, site inspection visits.

CAISSON DIAMETER

The as-drilled diameters of caissons immediately adjacent to the proposed RTT were estimated by measuring concrete volume and height changes between each truckload of concrete tremied into each caisson. Using a weighted measuring tape, the technician would initially measure and record the depth of the hole prior to concrete placement. After each truckload of concrete was tremied into the hole, the technician

Sergent, Hauskins & Beckwith, 3232 West Virginia Ave., Phoenix, Ariz. 85009.

would measure and record the depth to the top of the concrete, compute the change in height, and record the quantity of concrete placed (from the truckload). This procedure was repeated until completion of concrete placement for the caisson.

Given the change in height due to the volume of each truckload of concrete, and assuming a cylindrical shape for each section of caisson, an average diameter was computed. If a given caisson section did not have a uniform diameter, this assumption could underestimate the greatest diameter in that section. Such a condition was likely if, for example, a portion of the borehole wall in a section collapsed or caved.

CAISSON PLUMBNESS

Caisson plumbness was measured using an inclinometer in conjunction with casing referenced to the caisson rebar cage. A standard biaxial inclinometer sensor and readout was utilized, permitting simultaneous measurements in two directions. There was a possibility of damage to the inclinometer casing during lifting and handling of the caisson rebar cages. Therefore, inclinometer casing was temporarily assembled in a 4 in. diameter PVC access tube securely attached to each cage after the cage was set.

For purposes of construction control, accuracy of horizontal measurements to the full capability of the inclinometer system was not required. The accuracy was limited by the verticality of the access tube alignment on the rebar cage and the 0.5 in. play between the inclinometer casing spacers and the access tube. Inclinometer measurements consisting of a single set of readings at 5 ft intervals from the bottom to the top of the casing, completed in a few minutes, were found to be sufficient for monitoring purposes. Cages not meeting the verticality specification of 6.75 in. in 55 ft, some of which were in excess of 10 in. out of plumb, were quickly identified and corrected before placement of concrete. Plumbness measurements in caissons adjacent to the proposed RTT were repeated after placement of concrete in order to document the final position of the rebar cage in those caissons relative to potential future tunnel construction.

DENSITY MEASUREMENTS

The continuity of the caisson concrete was verified by density measurements using nuclear density gauges passed through 2 in. diameter Schedule 40 PVC access tubes attached to the caisson rebar cages. Four access tubes were installed along the length of each wall pier rebar cage. To assist in making density interpretations, the locations of PVC density access tubes relative to the vertical No. 14 bars were documented for 65 rebar cages. This information was utilized in evaluating the quantitative effects of the rebar on density data.

Standard downhole nuclear density and moisture gauges were used on this project. Density measurements were generally made at 2 ft depth intervals along the access tubes. Measurements were alternated between even and odd depths at adjacent tubes. Where measurements indicated a potential problem, density measurements were repeated at 1 ft intervals within the zone of interest. After initial verification of sampling time periods, reading periods of 32 seconds were deemed to provide sufficiently accurate results. Because of the large volume of testing required and equipment problems, four different nuclear density gauges were used. Differences in instrument response between the four gauges complicated density interpretations.

NUCLEAR DENSITY GAUGE RESPONSE CHARACTERISTICS

Although the qualitative response patterns and characteristics of individual density gauges were consistent, the quantitative density values reported by individual gauges varied widely. Consistent interpretation of the density data required that individual gauge readings be referenced to a known set of material densities, and that the nuclear density gauge response behavior to the materials in the caissons be sufficiently understood.

Density measurements were influenced by the materials immediately adjacent to access tubes. PVC pipe, concrete, and steel with densities of about 64, 145, and 490 pounds per cubic foot (pcf), respectively, were the materials encountered within a properly constructed caisson. Water or slurry, with a density range of about 64 to 75 pcf, or native soils, having a wet density in the range of 130 to 135 pcf, were expected to be encountered in a cutoff or other failure zone within a caisson.

Density readings were profoundly influenced by the response characteristics of the nuclear density probe technology. The typical range in density measurement for the type of instruments utilized (*1*,*3*) was about 70 to 170 pcf. Densities of PVC, water, and slurry were at the bottom end of this range, while the density of steel was far in excess of the upper limit. It was further assumed that the location and high density of steel would cause the rebar to act as a nuclear particle shield, with a "shadow zone" behind the rebar.

Instrument response was, of course, also dependent on the distance from the probe. The nuclear density probe was designed so that 95 percent of the response was from a roughly cylindrical volume of material within a distance of 2 in. of the edge of the probe (Mancusa, unpublished data). Detailed performance data concerning the probe response as a function of distance was not available. However, a general downhole nuclear probe response pattern as a function of distance was obtained from a study by Champion (unpublished data) and scaled to fit the 95 percent response at 2 in.

FIELD CALIBRATION OF DENSITY GAUGES

To ensure that representative density readings were obtained, three field calibration blocks fabricated from 55 gallon drums filled with caisson concrete and with a PVC access tube in the center were used both to verify and to monitor the nuclear density gauge response. In addition, one block had a single No. 14 bar tied adjacent to the PVC, and one block had two No. 14 bars tied adjacent to the PVC. The three field calibration blocks were designed to represent "normal" caisson density conditions: an access tube without adjacent steel, an access tube with a single adjacent bar, and an access tube

with two adjacent bars. Due to the assumed shielding effect of steel, it was deemed unnecessary to fabricate barrels with spliced bundles of three or four bars.

Once the calibration blocks were fabricated, the nuclear density gauges were checked on a regular basis. The first set of calibration block readings were used to develop a simplified model to predict and interpret various normal and abnormal caisson conditions. Continued calibration block readings were used to verify instrument readings for interpretation purposes. These readings also documented changes in instrument performance during the intensive construction monitoring, control, and documentation process.

DENSITY RESPONSE MODEL

In order to determine and analyze acceptable and unacceptable density conditions in the caissons, a simple model for prediction of the nuclear density probe response characteristic was developed. Incremental 5 percent response "rings" were intersected by rays at 5 degree intervals to generate a field of equal response points around a "probe." Response was analyzed only in the radial plane; a three dimensional analysis was not attempted. One-fourth of the response field, along with outlines of typical materials such as access tube and rebar that might be found within the response field, is presented in Figure 1.

This model yielded 1,440 points of equal response. The total density reading was a weighted average of the material densities for the 1,440 points. Seventy-two points were in the air gap between the probe and PVC access tube, and 216 points were in the PVC access tube. Where PVC access tubing was joined by a PVC coupler, the coupler contained another 216 points. Including a "shadow zone" behind the steel, a single No. 14 bar adjacent to the access tube contained 135 points, allowing for the space occupied by the rebar corrugations. The same bar at 0.5, 1.0, and 1.5 in. from the access tube contained 74, 38, and 20 points, respectively. An annular space which contained no concrete aggregate, leaving only slurry, was generated when two bars were placed adjacent to the access tube; this space contained 38 points. If the access tube was placed adjacent to the borehole side, as many as 338 points may have fallen within native soils, and another 64 points may have been contained in an annular space between the tube, bar, and hole sidewall.

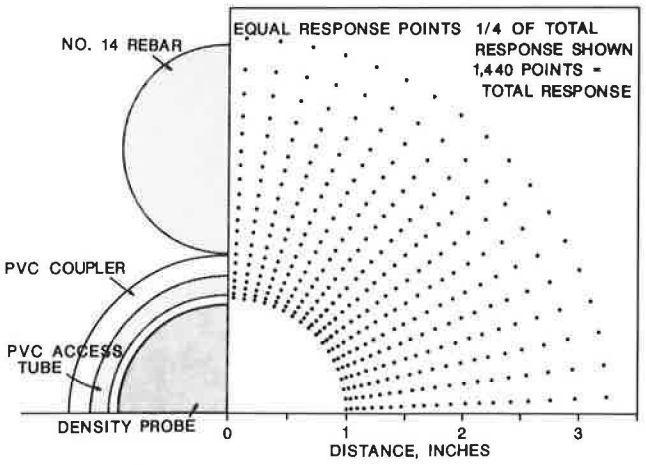

FIGURE 1 Density response model for equal response points and typical material sizes.

Initial readings from the field calibration blocks were used to calibrate the density response model. Material densities for PVC pipe, concrete, slurry, and wet native soils of about 64, 145, 64 to 70, and 130 to 135 pcf, respectively, were expected to be accurately measured by the density probes. Air was assumed to have a density of zero and was ignored. The steel rebar density of 490 pcf was not expected to be measured accurately by the probe. An "equivalent rebar density" of about 335 pcf was backcalculated from the readings in the no-bar, one-bar, and two-bar field calibration blocks.

Once the density response model was calibrated, different anticipated material configurations representing normal and abnormal conditions within a caisson were analyzed. For example, the model of concrete around an access tube with one adjacent rebar included 72 air gap points, 216 access tube points at 64 pcf, 135 steel rebar points at 335 pcf, and 1,017 concrete points at 145 pcf, resulting in a total or average density of 143.4 pcf. Normal conditions included one, two, or no bars; bars at different distances; and a PVC coupler at the access tube. Abnormal conditions included wet sand or native soils around the access tube or an access tube adjacent to the boring sidewall. Results of the density response model are presented in Table 1.

Finally, the field calibration data was analyzed to verify the relationship between the measured densities of the field calibration blocks for different reported densities and the instrument calibrations. Densities for concrete with no rebar varied from 98.8 to 137.5 pcf, depending upon the instrument and the selected calibration for that instrument. However, instrument responses followed the same trend, and density readings could be related to actual density conditions in the caissons. A plot of the measured densities for cases of one and two

TABLE 1 CALCULATED DENSITIES FOR POSSIBLE CAISSON CONDITIONS

Condition	Density Reading (pcf)	
	Actual	Calculated
Rebar adjacent to PVC access tube		
Wet sand only, no concrete	—	116.1
Concrete with PVC coupler	—	114.3
Concrete only	125.2	125.6
Concrete & one bar	143.4	143.4
Concrete & two bars	156.8	—
Concrete in annular space	—	159.2
Slurry in annular space	—	157.1
One bar at 0.5 in. from PVC access tube		
Wet sand only, no concrete	—	126.4
Concrete only	—	135.4
Against boring sidewall	—	128.9
One bar at 1 in. from PVC access tube		
Concrete only	—	130.6
One bar at 1.5 in. from PVC access tube		
Concrete only	—	128.2

NOTE: From initial field calibration block readings and density response model from Figure 2. No. 14 rebar is assumed. Annular spaces with both concrete and slurry are presented. Densities of 64, 133, 145, 335, and 64 pcf are assumed for PVC, wet sand or native soils, concrete, rebar, and slurry, respectively.

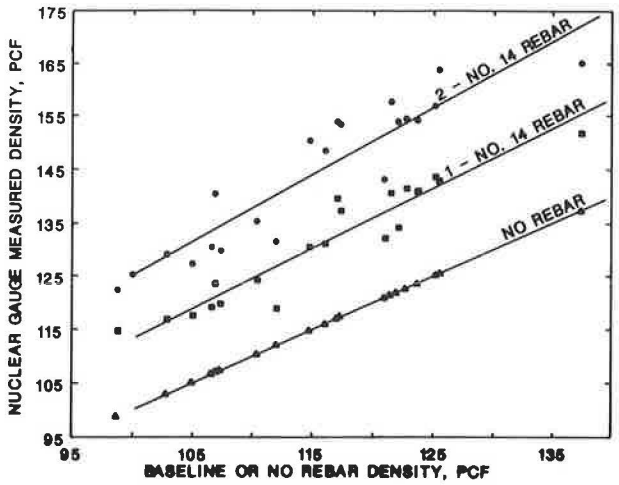

FIGURE 2 Field calibration block readings and characteristics.

bars versus the measured densities for the case of no rebar are presented in Figure 2.

DENSITY ANALYSIS AND INTERPRETATION

Density data collected in the field was processed and analyzed in the office using a spreadsheet computer program before final interpretation was performed. The first step in the interpretation process was to determine the appropriate "baseline" density for the caisson, that is, the density reading with no rebar. The density data was examined to find a consistent low density value that was close to the particular instrument field calibration. In all but a few cases, the baseline was readily identified. Where possible, readings from access tube sections with no nearby vertical rebar (shown by rebar cage maps) were used to determine the baseline density.

Once the baseline density was determined, expected densities for different conditions in the caisson were determined. In general, the conditions presented in Table 1 at a baseline density of 125 pcf were adjusted to levels appropriate to the caisson baseline density using the relationships shown in Figure 2. Any density significantly lower (by at least 5 pcf) than the caisson baseline density represented a potential abnormality. However, a single, isolated point of very low density could be due to a PVC coupler. Low density readings across a set of access tubes, with some readings at even and some readings at odd depths, would confirm that an abnormality was present. Lastly, two contiguous vertical low density readings in one access tube eliminated the possibility of a PVC coupler as the cause.

Significant portions of each access tube were near or adjacent to bundles of vertical rebar. Interpretation of these sections could potentially prove very complex. A length of access tube in wet sand without concrete, but with rebar at a distance of 0.5 in., was expected to exhibit a density at or above the caisson baseline density. Rebar cage mapping significantly aided density interpretations of normal and abnormal conditions in these situations. For example, in areas where a vertical bar splice ended, an access tube suddenly had no nearby steel instead of two adjacent bars, with a resulting density drop of more than 20 pcf. Such conditions were often noted for several tubes in a given caisson. Changes in density for normal caisson conditions were anticipated by knowing where rebar splices were located; familiarity with such typical project details (through mapping) simplified interpretation. Alternatively, when readings were not at a bar splice, a 15 to 20 pcf drop in density for two or more contiguous vertical readings, with density drops in the same vicinity at adjacent access tubes, indicated a seriously abnormal caisson condition.

DATA INTERPRETATION AND ANALYSIS

Caisson diameter, plumbness and density data collected in the field required varying degrees of interpretation and analysis for construction monitoring and documentation purposes. As shown in Figure 3, severe abnormal density conditions were identified in one caisson. These conditions were in the vicinity of severe borehole caving, as indicated by caisson diameter measurements. Based on the density information, the caisson was rejected. Subsequent coring of the caisson confirmed voids in the concrete, and another caisson was placed adjacent to the rejected caisson. It was postulated that the concrete placement tremie pipe was raised at the normal rate through the isolated zone of very large hole diameter. Concrete filling the large void did not rise sufficiently in the hole at that point. The tremie pipe was exposed above the concrete level and a cutoff was created.

CONCLUSIONS

The integrity, plumbness, and in-place geometry of slurry-assisted caissons was verified through a comprehensive construction monitoring program. Special procedures were required to effectively interpret density data obtained from nuclear density gauges. By applying these procedures, caisson integrity in the vicinity of each caisson rebar cage was assured.

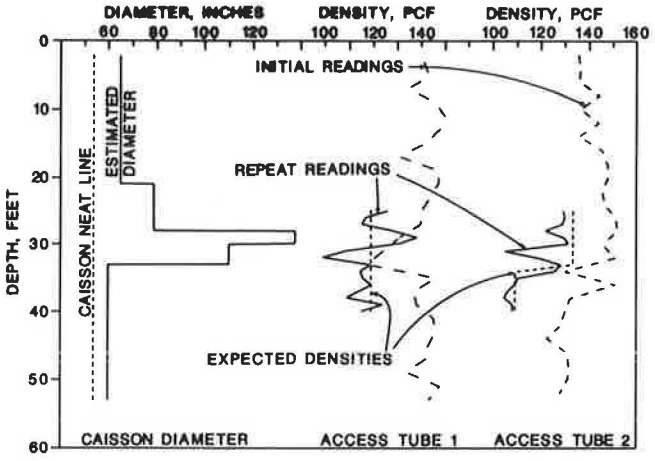

FIGURE 3 Diameter and density data showing abnormal caisson condition.

ACKNOWLEDGMENTS

The field data for this work was collected by technicians led by Ronald L. Wilson, upon whose vigilant efforts the success of the monitoring and testing program depended. The encouragement of Albert C. Ruckman and the editorial comments and reviews by Lawrence A. Hansen and Nickolas J. LaFronz are appreciated.

REFERENCES

1. B. R. Christopher, C. N. Baker, and D. L. Wellington. Geophysical and Nuclear Methods for Non-Destructive Evaluation of Caissons. In *Foundation Engineering: Current Principles and Practices* (F. H. Kulhawy, ed.), ASCE, New York, 1989.
2. J. W. Priess and A. Caiserman. Non-Destructive Integrity Testing of Bored Piles by Gamma Ray Scattering. *Ground Engineering*, Vol. 8, No. 3, 1975, pp.
3. *Operator's Manual, 501DR Depthprobe Moisture/Density Gauge*. Campbell Pacific Nuclear Corporation, Pacheco, Calif., 1983.

Publication of this paper sponsored by Committee on Environmental Factors Except Frost.

Instrumentation of Deep Corrugated Steel Box Culverts

ALAN F. RAUCH, SHAD M. SARGAND, GLENN A. HAZEN, AND JOHN O. HURD

The design procedure for predicting the structural performance of deep corrugated box culverts was investigated. Load capacity and deflection measurements were conducted on a fully instrumented, steel box culvert. Response due to the construction sequence was monitored, as was response to static loads of 16, 32, and 42 kips applied with a loaded dump truck.

Several researchers have reported on the design and performance of metal box culverts in the last few years (*1–3*). All of the culverts reported on were made of corrugated aluminum or steel plate. Their moment capacity was increased with transverse reinforcement using angle sections or corrugated sections. There is much controversy as to whether this structural system acts as composite or noncomposite during construction and application of live loads. The dispute can be avoided by utilizing a deep corrugated plate to provide additional moment of inertia without additional stiffening elements.

In this study, a deep corrugated steel culvert was installed on S.R. 554 in Gallia County, Ohio, in May, 1988. This box culvert had a span of 15 ft, a rise of 4 ft 11 in., and a length of 44 ft. The culvert was fully instrumented to monitor the responses due to the construction sequence and live load.

CULVERT DESCRIPTION AND INSTRUMENTATION

The dimensions of the culvert plate, shown in Figure 1, are corrugation width, 15.0 in.; depth, 5.5 in.; and thickness, 0.133 in. This deep corrugated steel culvert is not stiffened by ribs. Because the deep corrugated plates are difficult to bend, haunches are fabricated by welding at the intersections of the formed crown plate and the side plates. This results in a very stiff connection, as shown in Figure 2. The longitudinal supporting edges of the culvert are anchored into reinforced concrete footings. The culvert was placed in position across the creek with reinforced concrete headwalls at both ends.

An instrumentation scheme was planned to determine strains in the culvert structure and the backfill material and deflections at critical sections of the culvert. In this study it is assumed that the stress states of corrugated structural plates were biaxial. Thus the bending moment and thrust were determined using biaxial electrical strain gauge readings. To supplement the electric gauges, vibrating wire strain gauges were also mounted because of their better long-term stability and lesser sensitivity to environmental effects. A total of 52 biaxial gauges and 8 strain gauge rosettes were mounted inside the plate at sections, as shown in Figure 1. Ten vibrating wire gauges were installed at sections 2, 4, 7, 10, and 12, as shown in Figure 2.

Four horizontal rod extensometers were positioned to monitor horizontal movements of the soil near the culvert sides and in the soil cover at the top of the culvert, as shown in Figure 2. Deflection of the culvert was measured at 13 points around the inside culvert periphery at mid-length with respect to two reference points firmly embedded in concrete in the stream bed. Displacement monitoring points were marked by attaching eyebolts to the culvert, and displacements were measured with a tape extensometer. By taking two precise measurements to each eyebolt, the vertical and horizontal movements could be calculated.

Backfilling of the deep corrugated steel culvert was begun on May 16, 1988. Granular backfill material (standard #310 graded sand) was placed in lifts of 4 in. Each lift was compacted to at least 90 percent of the standard Procter maximum density using a hand-operated tamper. The compaction of soil was monitored with a Troxler nuclear density gauge.

A height of 80 in. of fill above the top of the footing was completed by May 19. The next day a 5 in. subbase of crushed limestone was placed, leveled, and compacted. This was followed by three lifts of asphalt paving. Five in. was placed in the first lift on May 23 and 3 in. added after three days. An additional lift of 1.75 in. was placed later.

One week after the completion of the pavement construction, three static live loads consisting of 16, 32, and 42 kips (1 kip equals 1,000 lb) were applied at positions shown in Figure 3. The loads were applied with the rear axle of a gravel-filled dump truck by deflating the tires on the central axle as shown in Figure 4. This was done to simulate 0.5, 1.0, and 1.5 times AASHTO H20-44 loading conditions. A complete load test was conducted by moving the rear axle wheels to five locations on the culvert. The positions of loading were arranged to take advantage of symmetry, since the fill depth was level. Locations at which loads were applied were chosen to simulate static traffic situations.

Recordings of strain gauge readings were taken with a Model HP 3497A data acquisition system in conjunction with an HP personal computer. An initial set of all gauge readings was recorded prior to backfilling. The electric strain gauge (uniaxials, biaxials, and rosettes) were read at the completion of each lift. The reading used for purposes of analysis was the average of five individual readings, which were recorded on

A. F. Rauch, S. M. Sargand, and G. A. Hazen, Department of Civil Engineering, Ohio University, Athens, Ohio 45701-2979. J. O. Hurd, Ohio Department of Transportation, Columbus, Ohio, 43215.

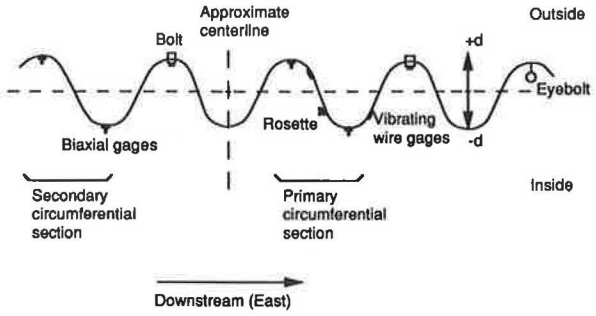

FIGURE 1 Typical section of deep corrugated steel (*d* is the distance to the neutral axis).

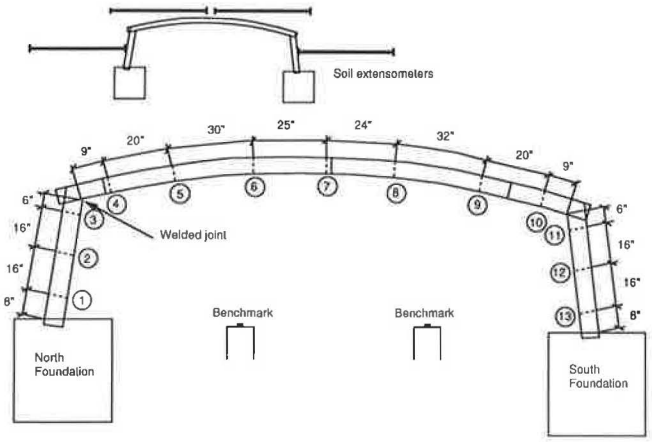

FIGURE 2 Cross section of test culvert showing 13 instrument locations and 4 soil extensometer locations.

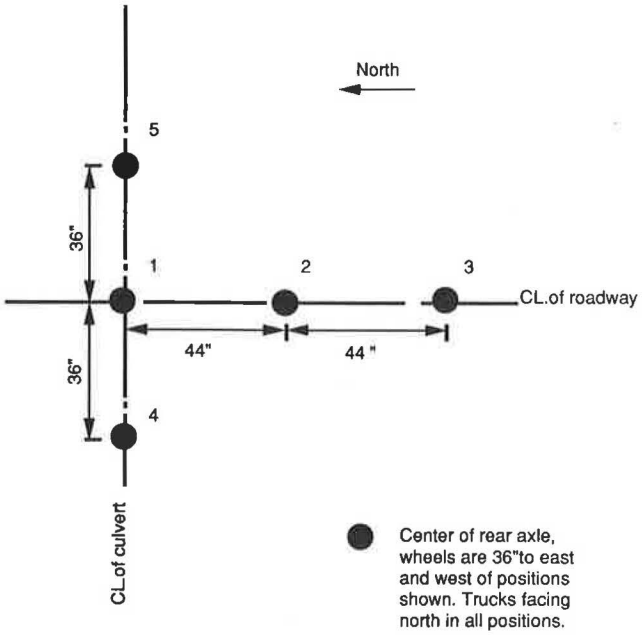

FIGURE 3 Live load application points (center of rear axle; wheels are 36 in. east and west of positions shown; truck facing north in all locations).

FIGURE 4 Application of live load (note flat tires on central axle to shift weight to rear axle).

a diskette and printed out on paper. This average was used in subsequent calculations as one reading. The average scanning time per gauge was 1.2 seconds in order to eliminate any undesirable noise in the readings. The vibrating wire gauges and the rod extensometers were also read at the end of each lift. Deflection measurements, on the other hand, were recorded every second lift, because construction had to be halted each time deflection readings were made. A hose level was used to monitor movement of the internal reference points as well as the culvert foundations. The hose level consists of a long plastic hose filled with colored water connected to a measuring scale on a rigid rod. One end of the level was fixed to a bench mark located outside the culvert on firm ground. This simple apparatus had an accuracy of 1/16 in. and permitted measurements to be made quickly and easily.

Since the thickness of the culvert plate with respect to the corrugation depth was small, a dial gauge was mounted to monitor the change in corrugation depth, as shown in Figure 5. The highest point in the culvert center was selected for monitoring, as it was expected to give the largest distortion. The maximum change in corrugation depth recorded was 0.014 in.

RESULTS

The change of the culvert shape during the construction sequence is shown in Figure 6. Examination shows a slight

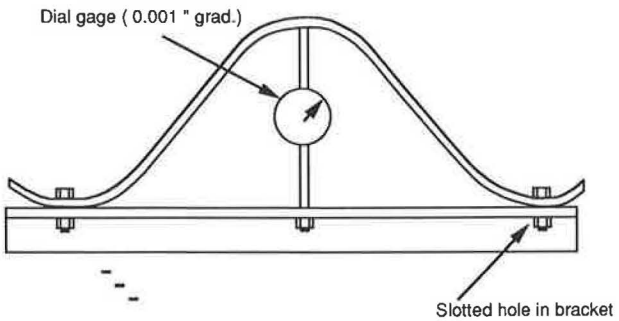

FIGURE 5 Attachment to measure change in corrugation depth.

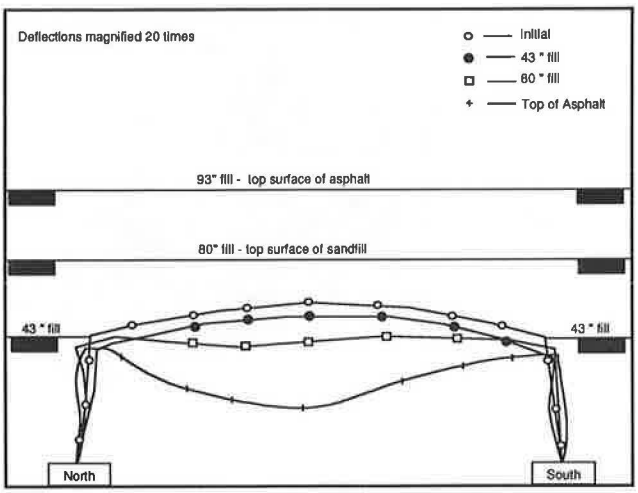

FIGURE 6 Changes in culvert shape during construction sequence (deflections magnified 20 times).

shift of the culvert during backfill. This shift might be due to the sequence of placing and compacting fill. Such deflection illustrates the importance of proper backfill and compaction procedures.

The results of the crown deflections are shown in Figure 7. During the first few lifts the culvert did not move significantly. This result contrasts with previously reported investigations (*1*,*2*), where the crown deflected upward. This culvert was initially composite, whereas the other culverts reported on were initially noncomposite. Most of the large downward vertical movement was recorded during the placement of asphalt and subsequent roller compaction. The maximum deflection under a 42 kip live load was 0.21 in.

Electric strain rosettes were mounted between the centroid and the peaks and valleys of the plate corrugations to determine if this structure can be modelled as a beam or a folded plate. Figures 8 and 9 confirm a beam response as indicated by the linearity of strains with respect to depth. During the analysis it was noticed that strain readings obtained with the vibrating wire gauges and the electric strain gauges gave almost identical results.

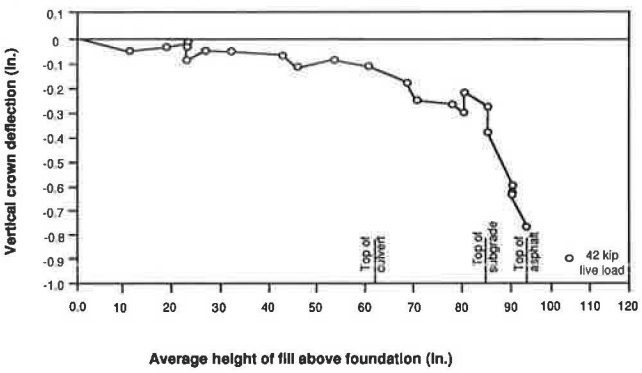

FIGURE 7 Crown deflection of culvert during construction sequence and under 42 kip static live load.

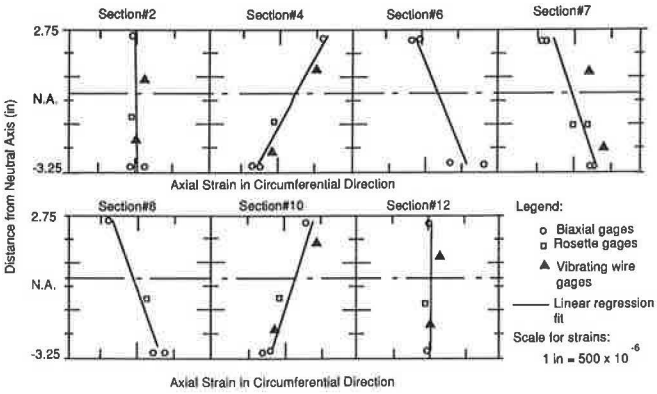

FIGURE 8 Strain measurements compared to beam response for 78 in. of backfill.

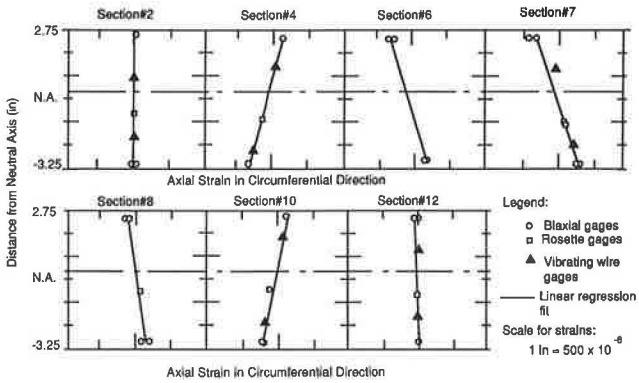

FIGURE 9 Strain measurements compared to beam response for 32 kip static live load at Position 1.

Settlement of the foundations, as observed with the hose level, was monitored independent of the interior bench marks. The reference points in the stream bed did not move appreciably in the vertical direction and moved only slightly in the horizontal direction. Accuracy of settlement was 0.02 in. Deflection measurements recorded for the culvert were taken to be the vector difference of foundation settlement and culvert deflections.

Moment and thrust due to the live load are shown in Figure 10, where they are plotted with respect to position of loading. Positions 1, 2, and 3 were centered over the culvert, midway between eyebolts and strain gauge section. Positions 4 and 5 were such that one wheel is located directly over the center of the culvert.

For live loads, the two instrumented cross sections behaved differently. As expected, maximum moment occurred at the section most directly under the wheels. This occurred in the primary section when loaded at positions 4 and 5, and in the secondary section (Figure 1) when loaded at position 1. Thrust also responded differently at the two sections due to the same

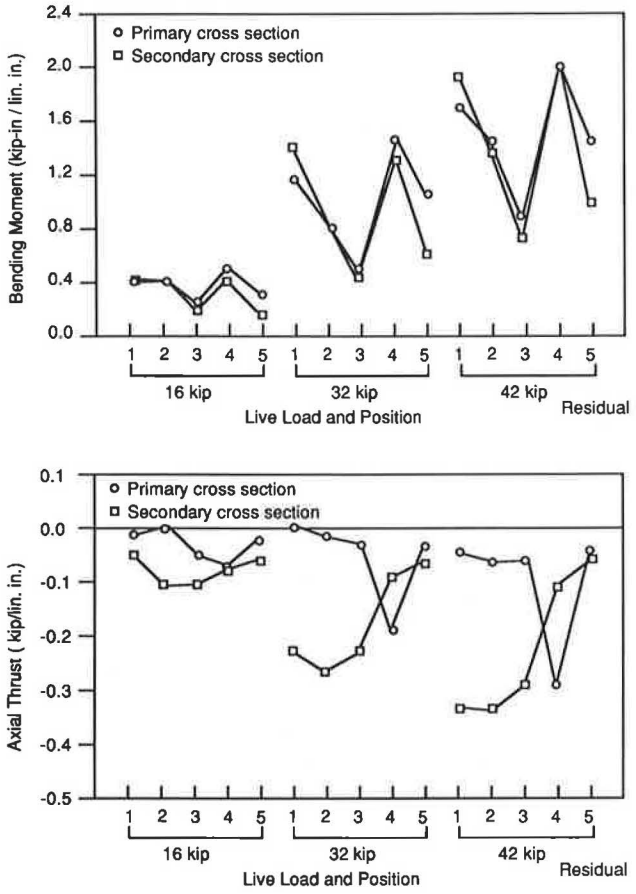

FIGURE 10 Bending moment (top) and axial thrust (bottom) due to varying static live load at five positions.

effect. The maximum moment and thrust recorded were 24 kip-in. and −3.5 kip per linear foot.

CONCLUSIONS

Based on the field instrumentation results, the deep corrugated culvert behaves as a beam. Furthermore, there is no major distortion of corrugation geometry during construction sequence or live load application, and the moment of inertia can be kept constant. This type of structure does not deflect upwards at the crown in early construction; most vertical deflection occurs as pavement is placed. The foundation movement was significant, however, and must not be ignored. The true deflection must take into account the foundation movement, otherwise results will be conservative.

REFERENCES

1. J. M. Duncan, R. B. Seed, and R. H. Drawsky. Design of Corrugated Metal Box Culverts. In *Transportation Research Record 1008*, TRB, National Research Council, Washington, D.C., 1985, pp. 33–41.
2. D. B. Beal. *Behavior of a Corrugated-Metal Box Culvert*. Research Report No. 90. Engineering Research and Development Bureau, New York State Department of Transportation, Albany, 1986.
3. E. T. Selig, J. T. Abel, F. H. Kulhawy, and W. E. Falby. *Review of the Design and Construction of Long-Span, Corrugated-Metal, Buried Conduits*. Report FHWA-RD-77-131. FHWA, U.S. Department of Transportation, Washington, D.C., 1977.

Publication of this paper sponsored by Committee on Subsurface Soil-Structure Interaction.

Instrumentation for Measuring Earth Pressures due to Compaction

ALLEN L. SEHN AND J. MICHAEL DUNCAN

The Instrumented Retaining Wall Facility at Virginia Polytechnic Institute and State University (Virginia Tech), developed to study the factors that control the magnitudes of earth pressures induced by compaction of soil, is described. Previous investigations of earth pressures induced by compaction have shown that measuring earth pressures due to compaction is difficult because (1) earth pressure cells sometimes give erroneous readings, depending on their stiffness and how they are installed; (2) compaction-induced earth pressures vary rapidly with depth, resulting in misinterpretation if fill elevations are not accurately determined; (3) the large inherent variability in earth pressures results in possible erroneous evaluations if too few measurements are made; and (4) walls must be stiff and mounted on unyielding supports to measure earth pressures that are not influenced by wall movements. The experimental facility at Virginia Tech has been designed to overcome these problems and to achieve accurate measurements of compaction-induced earth pressures at a scale approaching field scale. The electronic instruments and the data acquisition system in the facility make it possible to perform efficient and accurate studies of earth pressures during and at the end of backfilling and their variation with time after backfilling. This facility offers promise for investigating aspects of the horizontal and vertical earth loads on retaining walls that are not reflected in conventional earth pressure theories but have significant effects on the stability and performance of retaining walls.

The Instrumented Retaining Wall Facility at Virginia Polytechnic Institute and State University (Virginia Tech) has been developed to study the factors that control the magnitudes of earth pressures induced by compaction of soil. Previous investigations of earth pressures induced by compaction have shown that measuring earth pressures due to compaction is difficult because:

- Earth pressure cells sometimes give erroneous readings, depending on their stiffness and how they are installed;
- Compaction-induced earth pressures vary rapidly with depth, resulting in misinterpretation if fill elevations are not measured with sufficient accuracy;
- There appears to be large inherent variability in earth pressures, resulting in possible erroneous evaluations if too few measurements are made; and
- Small wall movements can change earth pressures very significantly, requiring walls to be stiff and mounted on unyielding supports to measure earth pressures that are not influenced by wall movements.

A. L. Sehn, Department of Civil Engineering, Virginia Polytechnic Institute and State University, Blacksburg, Va. 24061. Current Affiliation: Department of Civil Engineering, The University of Akron, Akron, Ohio 44325. J. M. Duncan, Department of Civil Engineering, Virginia Polytechnic Institute and State University, Blacksburg, Va. 24061.

The experimental facility at Virginia Tech has been designed to overcome these problems, and to achieve accurate measurements of compaction-induced earth pressures at a scale approaching field scale.

DESIGN FEATURES

The instrumented retaining wall is 7 ft high and 10 ft long. Figure 1 shows the principal features of the wall, and Figure 2 shows the wall before and after backfilling. The bottom of the wall is 3 ft below floor level, and the top is 4 ft above. The area in back of the wall, where the backfill is placed, is 6 ft wide. A 6 ft wide ramp leading into the area provides access for loading and compacting equipment.

The wall is divided into four panels, each 2.5 ft wide and 7 ft high, as shown in Figure 3. Each of these panels is mounted on two vertical load cells that support the weight of the panels and measure the vertical shear loads exerted on them by the backfill. Each panel is supported horizontally by three load cells, two located 20 in. above the bottom, and one located 60 in. above the bottom. These load cells are used to measure the magnitude and position of the resultant horizontal force exerted on each panel by the backfill.

All four wall panels are attached through the horizontal load cells to a stiff steel frame, as shown in Figure 4. The frame is supported vertically by bearings that can slide and rotate and horizontally by jacks that can be used to induce translational or rotational movements. Because the frame is very stiff, the four wall panels always move together, remaining in the same plane.

A total of 17 earth pressure cells (11 Gloetzl cells, 4 Carlson cells, and 2 Geonor cells) are mounted on the center two wall panels, as shown in Figure 3. These pressure cells are all quite stiff, and are mounted flush with the faces of the wall panels. They are located at 6.0 in. vertical spacings in four vertical strips on the two wall panels. They thus provide closely spaced points for determining variations of earth presssure with depth, as well as redundancy with respect to pressure cell elevation and pressure cell type.

The elevation of the surface of the fill is measured after each lift is compacted using an array of 12 ultrasonic distance measuring devices (UDMDs) mounted on a frame that rotates down into the horizontal position over the fill. The frame is shown in Figure 1 and is visible in Figure 2. The UDMDs can sense the position of the fill after compaction, but they cannot be used to measure the position of the loose fill because the ultrasonic signals are scattered rather than reflected.

Movements of the wall panels are measured by 8 linear variable differential transformers (LVDTs), one near the top

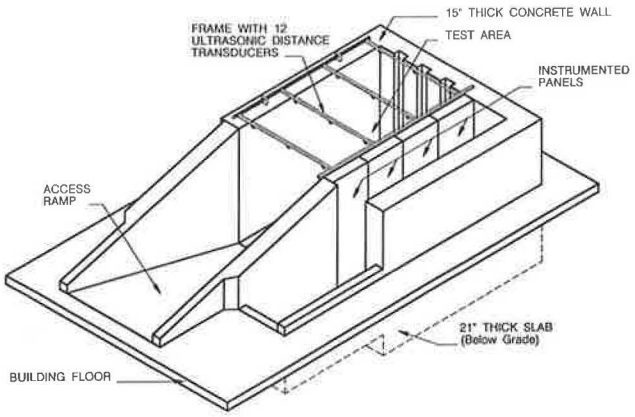

FIGURE 1 The Instrumented Retaining Wall Facility.

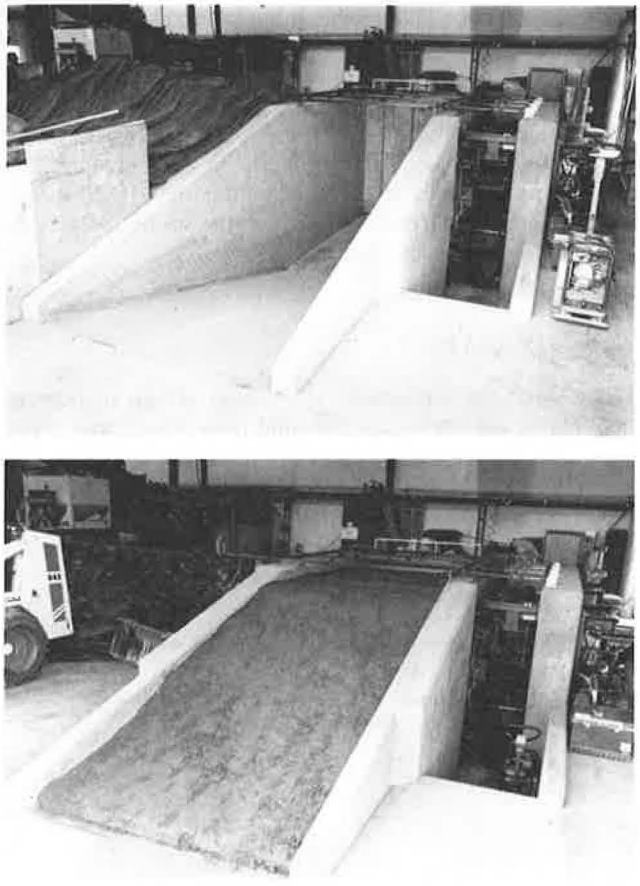

FIGURE 2 Facility before and after backfilling.

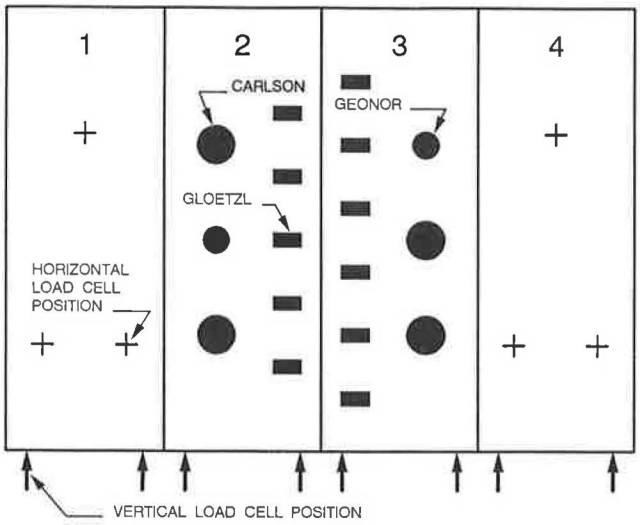

FIGURE 3 The four panels of the instrumented wall.

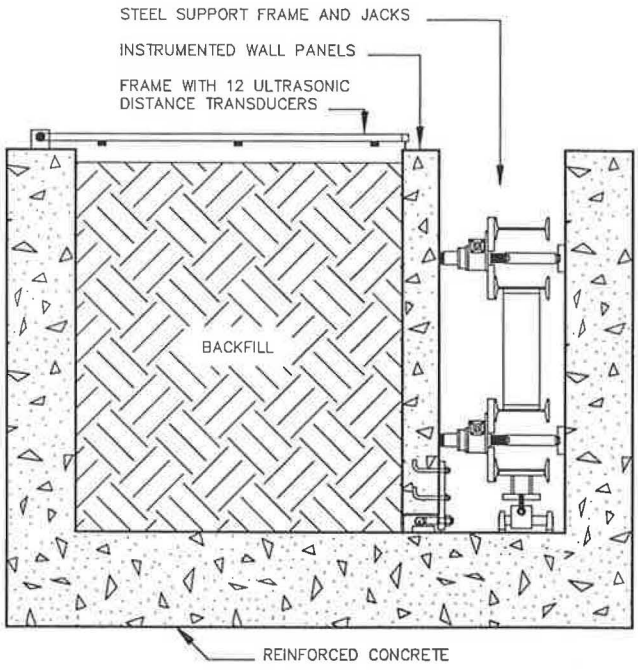

FIGURE 4 Cross-section through the instrumented wall.

and one near the bottom of each wall panel. These are mounted on unstressed reference frames attached to the reinforced concrete wall that supports the steel frame. A ninth LVDT, mounted on the floor slab of the building, is used to measure possible movements of the reinforced concrete wall. The floor slab is isolated from the concrete wall by an expansion joint. Two thermocouples are used to measure the temperature of the LVDT support, in order to determine possible temperature effects on the readings.

The temperature of the wall panels is measured at three locations, one near the bottom of the wall, one near the middle, and one near the top. These measurements provide the information needed to adjust the Gloetzl cell readings for temperature-induced zero shift.

All of the instruments are monitored by a computer-controlled data acquisition system. Measurements are made after each lift has been placed loose and again after it has been compacted. Two independent sets of readings are made each time and stored in different data files. This provides security in case one set of readings should be destroyed accidentally, as well as redundancy in case some of the measured values appear questionable. Making two sets of readings takes about 5 minutes.

The process of placing fill behind the wall and compacting it is recorded on videotape to provide a detailed record of each test. The video camera operates for 3 seconds in each 30 second period. This provides a record of 15 hours of activity on a 90 minute tape. On fast forward, the record can be scanned in 9 minutes.

TECHNICAL CHARACTERISTICS OF THE INSTRUMENTATION SYSTEM

Vertical Load Cells

The vertical forces on the wall panels are measured by means of the load cells that support the panels. As shown in Figure 5, these load cells are 4 in. long cantilever beams that are bolted to brackets at the bottoms of the panels. The free end of each beam has a roller bearing wheel that can move back and forth on a hardened steel pad epoxied to the concrete floor. This permits free lateral movement of the wall panels. The vertical forces are measured by means of bonded strain gauges attached to the cantilever beams. The accuracy of the load cells is about 15 lb, or about 30 lb per panel.

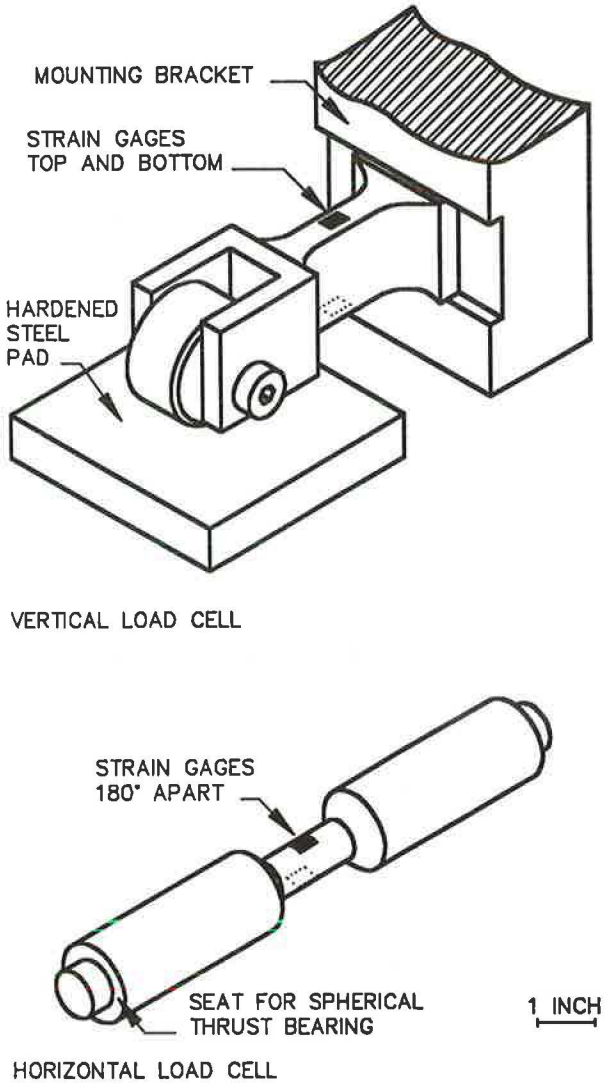

FIGURE 5 Vertical and horizontal load cells.

Horizontal Load Cells

The horizontal reaction forces on the wall panels are measured using column load cells with bonded strain gauges. As shown in Figure 5, the ends of the columns are seated in spherical bearings to minimize bending moments. The accuracy of the load cells is about 50 lb, resulting in overall accuracy of about 150 lb for the horizontal force on a single wall panel. With two load cells at the bottom of each panel and one at the top, it is possible to determine both the magnitude and the position of the resultant force acting on each panel. Comparing these to the same quantities determined from the earth pressure cell readings provides an independent check on accuracy.

The horizontal load cells work only in compression. During the early stages of filling, when fill is being placed and compacted below the bottom load cells, the top load cells tend to go into tension and become loose in their bearings. To prevent this, they are prestressed in compression by springs located at the top of 2 ft above the bottom of the wall panels. These springs hold the horizontal load cells in compression at all times. The load cells are so much stiffer than these springs that there is no appreciable change in the spring force as the forces in the load cells change.

Earth Pressure Cells

The Gloetzl earth pressure cells consist of two rectangular steel plates welded together around their edges, with a thin film of oil between them, as shown in Figure 6(a). They are 5.5 in. long, 2.75 in. wide, and 0.18 in. thick. The front face is flat. The oil pressure is transmitted to a pressure transducer by means of a heavy gauge steel tube that extends from the back of the cell. The cells used in this were fitted with electrical pressure transducers so that they could be read using the data

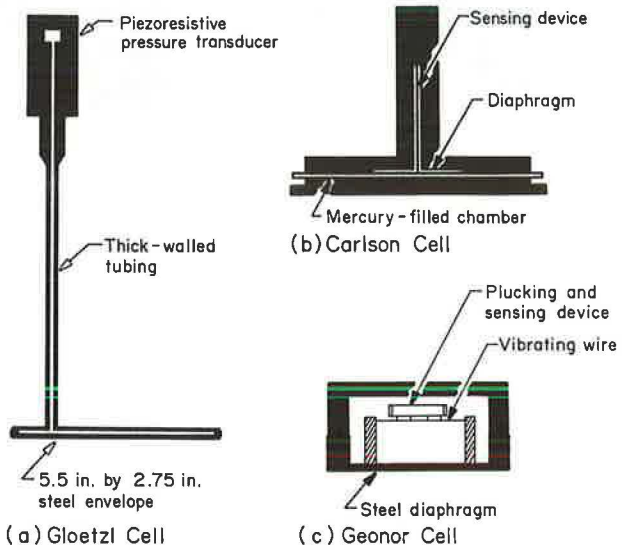

FIGURE 6 Earth pressure cells.

acquisition system. The transducers were purchased in the United States and were attached to the pressure cells at the Gloetzl factory in Germany.

The Carlson earth pressure cells are 7.4 in. in diameter and about 1 in. thick, as shown in Figure 6(b). Behind a heavy metal faceplate they contain a thin film of mercury. The pressure in the mercury is measured using an extensometer contained in a cylindrical housing attached to the back of the cell. The pressure readings are sensitive to the temperature of the cell, and the temperature is measured each time a pressure reading is made.

The Geonor earth pressure cells are 6.5 in. in diameter and 1.8 in. thick. As shown in Figure 6(c), the face of the gauge is a stiff metal diaphragm. The diameter of the active portion of this diaphragm is 2.95 in. Attached to the back of the diaphragm is a taut wire that is caused to vibrate at its natural frequency by an electrical magnet, which is switched on and off at intervals. As the pressure on the face of the cell changes, the tension in the wire and the natural frequency of its vibration also change. The vibration of the wire is picked up by a small pickup device in the cell and transmitted as an electrical signal to the data acquisition system. The frequency of vibration is determined by counting the number of signal pulses for a set period, like one second.

Ultrasonic Distance Measuring Devices (UDMDs)

As illustrated in Figure 7, the UDMDs send out a burst of ultrasound at a signal frequency and measure the length of time for the first reflected wave to reach the instrument. This interval of time, divided by the speed of sound, is twice the distance from the instrument to the surface causing the reflection. The speed of sound in the atmosphere is affected by temperature and humidity. To correct for these effects, another measurement is made with a UDMD aimed at a target located at a fixed distance from the device. This measurement provides a calibration reading each time a set of measurements is made, resulting in accuracy of about 0.1 in. in the measured values of fill depth. The maximum range of the UDMDs is about 30 ft, which is considerably longer than required for this application.

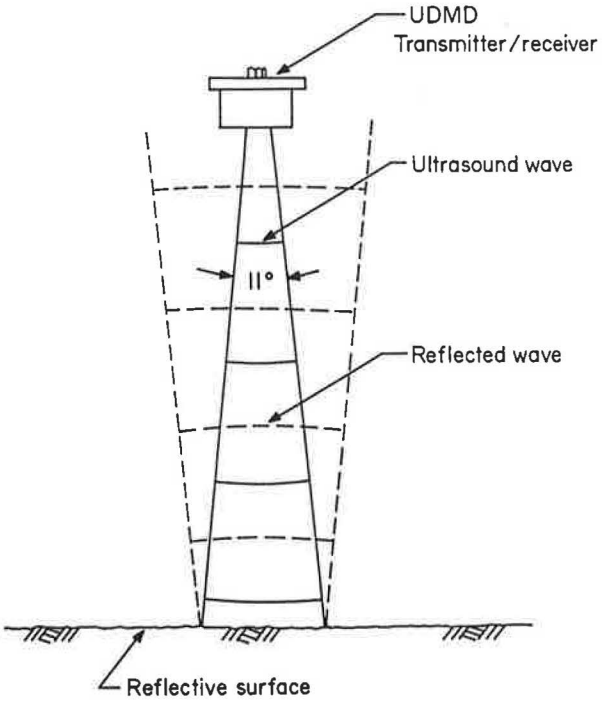

FIGURE 7 Ultrasonic distance measuring device (UDMD).

Linear Variable Differential Transformers (LVDTs)

The LVDTs are powered by direct current. Their range of measurement is 1.0 in. By accounting for output nonlinearity, accuracies on the order of 0.0005 in. are achievable.

Thermocouples

The thermocouples are conventional copper-constantan devices capable of measuring temperature with an accuracy of 0.5 degree Fahrenheit.

DATA ACQUISITION SYSTEM

Computer

The data acquisition system is controlled by the IBM XT microcomputer shown in Figure 8. Three data acquisition cards in expansion slots in the computer control the selection of the data channels and the reading of the instruments. The cabinet to the left of the computer in Figure 8 contains the multiplexing cards that are connected to each of the instruments. The data acquisition cards in the computer select the channel to be read and read the signals from the instruments.

Power Supply

The power supply for the instruments is located in the cabinet with the multiplexing cards. It is connected to a digital voltmeter that is used to regulate its output with an accuracy of 0.02 percent before each set of readings.

FIGURE 8 The computer and the cabinet containing the multiplexing cards.

Voltage Measurements

The reading of instruments that produce voltage signals is controlled by a MetraByte DAS-8 card in the computer. This card is connected to seven MetraByte EXP-16 multiplexing cards by a 37 conductor ribbon cable. Cold junction compensation for thermocouples is provided by circuitry on the EXP-16 cards. The load cells, the Gloetzl cells, the Carlson cells, the LVDTs, and the thermocouples (a total of 51 instruments) all produce voltage signals that are transmitted through the multiplexing cards connected to the DAS-8 controller card. Under software control, the DAS-8 selects each channel in turn, converts the analog signal to digital form, and transmits it to computer memory. The 12 bit analog to digital conversion is capable of dividing a signal into as many as 4,096 parts.

Frequency Measurements

The Geonor earth pressure cells produce oscillating voltage signals, the frequency of which vary depending on the pressure. These instruments are read under the control of a MetraByte CTM-05 card in the computer. Each Geonor cell is connected to a separate channel on the CTM-05 controller card. The Geonor cells have their own control circuits, which are connected to the power supply and produce signals continually. Under software control, the CTM-05 card selects each channel in turn and measures the frequency by counting cycles for a fixed period of time, about one second.

UDMD Measurements

The basic measurement for the ultrasonic distance measuring devices is the interval of time required for a reflected ultrasound signal to return to the instrument. A UDM-PC controller card in the computer is connected to a UDM-MUX multiplexer card in an external cabinet by a 14 conductor cable. Each of the UDMDs is connected to a separate channel on the multiplexing card. Under software control, the UDM-PC card selects each channel in turn, causes the UDMD to transmit an ultrasound signal, and measures the length of time required to receive a return signal of the same frequency.

Software Control

The data acquisition system is controlled by a computer program written in Microsoft QuickBASIC 4.5. The subroutines in this program address the data acquisition controller cards in the computer and relay instructions for the sequence of reading the instruments and the number of times each is to be read. In cases where instruments are read more than once, the subroutines average the readings and provide logical procedures for eliminating erroneous readings. They also store the data acquired in files on hard and floppy disks and add identifying labels specified by the user.

Each of the voltage measurements is repeated 20 times, and the average of these 20 readings is calculated. The voltage readings for the load cells, the Gloetzl cells, the LVDTs, and the thermocouples are multiplied by their calibration constants to convert the readings to engineering units, and the result is stored. Four separate voltage readings are required for each Carlson cell. These are used in a series of equations that determine a raw pressure reading uncorrected for temperature, the temperature of the cell, the temperature correction, and finally the pressure corrected for temperature.

The frequency of the signal from each Geonor cell is monitored twice, for one second each time, and the two values are averaged. The average frequency is multiplied by a constant to convert it to pressure, and the value is stored in the data file.

The logic governing the reading of the UDMDs is the most complex of any of the instruments. This is necessary because sometimes a reflected signal is not detected. The software addresses each of the instruments 10 times. If a reflected sound wave is detected, the time interval for wave return is recorded. If a return wave is not detected any of the 10 times the instrument is addressed, that is noted. After the tenth attempt, the average return time is calculated. A calibration factor is calculated based on the return time for the UDMD that is aimed at a fixed target. This calibration factor is used to reduce the measured time intervals to distance values. These are stored in the data file together with the number of successful attempts to read the instrument. With this procedure for data acquisition, the system performs well.

Operation

Two routines are used to make readings. The first is used when a loose lift of backfill has been placed behind the wall, before it has been compacted. This routine does not include UDMD measurements, because they are not effective in measuring the elevation of the nonreflective loose earth. It does include readings of all the other instruments. Making two sets of readings with this routine takes about 3 minutes.

The second routine is used after a lift has been compacted. It includes readings of the UDMDs as well as the other instruments. Making two sets of readings with this routine takes about 5 minutes.

System Development

The suppliers of the instruments and data acquisition hardware used in the Instrumented Retaining Wall facility are listed in Table 1. The load cells for measuring horizontal and vertical forces were designed by the first author and were built in the Civil Engineering Department shops at Virginia Tech. The computer programs that control the operation of the data acquisition system were written by the first author.

CALIBRATIONS AND ACCURACY OF INSTRUMENTS

Calibrations

The load cells were calibrated twice, once in a universal testing machine in the geotechnical engineering laboratory, and once

TABLE 1 SUPPLIERS OF INSTRUMENTATION HARDWARE

Item	Manufacturer
Gloetzl Earth Pressure Cells Type: E 7/14 K3.5 Z4 Model: C, with adaptor for Omega pressure transducers, special order	Gloetzl Gesellschaft fur BaumeBtechnik GmbH 7512 Rheinstetten 4-Fo. WEST GERMANY US Representative: Geo Group, Inc. 2209 Georgian Way #12 Wheaton, MD 20902
Carlson Earth Pressure Cells Model: S-25	Carlson/RST Instruments 1190-C Dell Avenue Campbell, CA 95008
Geonor Earth Pressure Cells Model: P100 0-5 Bar	Geonor A/S P. O. Box 99 - ROA 0701 Oslo 7 NORWAY US Representative: Geonor,Inc. 1454 Van Houten Ave. Clifton, NJ 07013
Ultrasonic Distance Measuring Devices and Interfacing Hardware	Contaq Technologies Corp 15 Main Street Bristol, VT 05443
LVDTs Models: 353-000 351-000	Trans-Tek, Inc. Route 83 P. O. Box 338 Ellington, CT 06029
Pressure Transducers (used with Gloetzl cells) Model: PX236 Thermocouples type T	Omega Engineering, Inc. One Omega Drive Stamford, CT 06907
Data Acquisition Hardware Models: DASH-8, EXP-16, CTM-05	MetraByte Corporation 440 Myles Standish Blvd. Taunton, MA 02780

in place after installation in the experimental facility. The two calibrations of the horizontal load cells differed by about 2.0 percent, due to the fact that larger voltage drops occurred at various locations after all of the instruments were installed in the instrumentation circuit. The two calibrations of the vertical load cells differed by about 6.0 percent for the same reason. The second set of calibrations, which were made using the same data acquisition system used in the tests, is used in reducing the data.

The earth pressure cells were calibrated after they were installed on the wall by placing a pressure cylinder against the wall panel at the location of each earth pressure cell and pressurizing a rubber membrane in contact with the face of the cell. During calibration it was found that the readings of the Carlson cells drifted with time, and this was traced to heating of the cell due to the electrical current flow during the measurements. To overcome this problem, the applied voltage was reduced and the length of time the voltage was applied was standardized.

The LVDTs were calibrated using a micrometer in a bench-top calibrating frame. The readings of the thermocouples were checked against a thermometer and an ice bath. Finally, as mentioned previously, a calibration factor for the UDMDs is measured each time a new set of readings is made.

Accuracy of Instruments

The estimated accuracies of the instruments are listed in Table 2. These values reflect the influence of all of the factors that determine the repeatability of measurements over a period as long as the several days involved in a test, as well as the intrinsic accuracy of the instruments. It takes into account the use of multiple readings to improve the resolution of each set of readings.

COST OF THE FACILITY

Approximate costs for the components of the Instrumented Retaining Wall facility are listed in Table 3. The total is about $173,000. It is interesting to compare the cost of this facility with the cost of a similar facility built by Terzaghi at MIT in about 1930. Terzaghi (*1*) stated that the total investment in the MIT facility was about $50,000. Using the change in the Engineering News Record Construction Cost Index as a guide, the comparable current cost would be about $1,200,000 in 1990. The difference in cost is largely attributable to the availability of smaller and less costly devices for measuring the forces on the wall. Terzaghi's facility had intricate and elab-

TABLE 2 ESTIMATED INSTRUMENT ACCURACIES

Instrument	Estimated Accuracy[a]
Gloetzl Cells	± 0.25 psi
Carlson Cells	± 0.50 psi
Geonor Cells	± 0.25 psi
Horizontal Load Cells	± 50 lbs
Vertical Load Cells	± 15 lbs
Ultrasonic Distance Measuring Devices	± 0.10 in
LVDTs	± 0.0005 in
Thermocouples	± 0.5° F

[a] Estimate based on consideration of overall system performance as installed in the Instrumented Retaining Wall Facility at Virginia Tech. May not reflect the accuracy of the instrument alone or under different conditions.

TABLE 3 APPROXIMATE COST OF INSTRUMENTED RETAINING WALL FACILITY

Item	Cost
Reinforced Concrete Sidewalls, Floor, and Ramp	$15,500
Gloetzl earth pressure cells + transducers (11)	5,300
Carlson earth pressure cells (4)	3,100
Geonor earth pressure cells (2)	1,500
Jacks to move walls (4)	2,500
Horizontal load cells (materials + labor for 12)	8,400
Vertical load cells (materials + labor for 8)	8,000
Ultrasonic Distance Measuring Devices (16, not all deployed)	3,500
LVDTs (9)	4,100
Thermocouples (5)	200
Video camera, VCR, TV and controller	1,400
Analog to Digital card DASH-8 (1)	400
Frequency to Digital card CTM-05 (1)	300
Multiplexing cards EXP-16 (7)	2,600
Computer IBM XT (1)	1,500
Bobcat Loader	11,000
Wacker BPU 2440A Compactor	3,000
Santo SV-104 Compactor	1,400
Wacker BS 60Y Compactor	1,900
Rototiller	600
Soil delivery & conditioning	4,000
Building & crane (half of 2400 ft^2 bldg)	45,000
Miscellaneous materials	5,000
Design	25,000
Fabrication	6,000
Assembly	10,000
Calibration	2,000
Total:	$173,200

orate force measuring systems based on the principle of balance beam scales. Today these are replaced by more compact and less expensive electrical measuring devices.

The cost of operation of the new facility is probably also much lower, due to the fact that power equipment greatly reduces the amount of time required for material handling, automatic data acquisition reduces the time for collecting data, and computer programs reduce the time required for processing and plotting the information.

MEASURED EARTH PRESSURES AND SHEAR LOADS

The first experiments in the Instrumented Retaining Wall facility were performed using a silty sand from the foundation of Yatesville Dam in Kentucky. About 45 percent of this material passes the #200 sieve, and the fines are nonplastic. It has a Standard AASHTO maximum dry density of 120 lb/ft^3, and an optimum water content of 12.5 percent.

In the first tests the backfill was placed behind the wall at a water content of about 14.5 percent, and compacted with a Wacker BPU 2440A vibratory plate compactor. The lifts were 4 in. thick after compaction. The compacted density was 120 lb/ft^3. The water content was approximately 2.0 percent wet of the line of optimums, and a small amount of water drained from the fill during a 2 day period after placement. Although the fill was compacted to 100 percent of the Standard AASHTO maximum dry density, it remained sufficiently deformable after compaction that the vibrating plate compactor left a track about 0.5 in. deep on the final pass, and the Bobcat tractor loader left tire prints about 1.0 in. deep on the compacted fill.

Earth pressures measured after compaction are shown in Figure 9. Integration of the measured pressure distribution indicates that the horizontal resultant force is about 5600 to 5800 lb, depending on how the pressures are assumed to vary above the top and below the bottom pressure cells. The sum of the horizontal force transducers for panel 3 indicates a horizontal resultant force of 5400 lb, about 4 percent to 7 percent less than indicated by integration of the pressure diagram. The resultant force acts at 0.38(H) based on the force transducer data and at 0.34(H) based on the pressure cell data.

Figure 9 includes a theoretical earth pressure variation that was calculated using the method of Duncan and Seed (*2*) and the computer program NCOMP, developed by Seed and Duncan (*3*). The measured and calculated values agree well on average. The measured values are smaller than the calculated values near the top of the fill, however, and larger than the calculated values near the bottom.

The differences between the measured and the calculated values can be attributed to two factors:

1. It seems likely that the dynamic force applied by the vibrating compactor is smaller than the manufacturer's rated force of 5400 lb, perhaps because the moist silty sand is not very firm even after compaction to 100 percent of the Standard AASHTO maximum dry density. This would explain the fact that the measured values are smaller than the calculated values in the upper 3 ft.
2. The measured total stress coefficient of earth pressure at rest for the moist silty sand is about 0.8, rather than the expected value of 0.5 used in calculating the theoretical variation shown in Figure 9. This high value of K_0 may be related to pore pressure effects within the backfill during compaction. A small amount of water drained from the fill after compaction, and the pressure decreased about 35 percent within a 5 day period after compaction, bringing the value of K_0 down to about 0.5.

It is planned to study these effects further through experiments to measure the dynamic forces applied by vibratory compactors and laboratory tests to study the factors that influence the value of K_0 for compacted fill.

Vertical shear loads measured during backfilling and for a period of about 5 days after compaction are shown in Figure

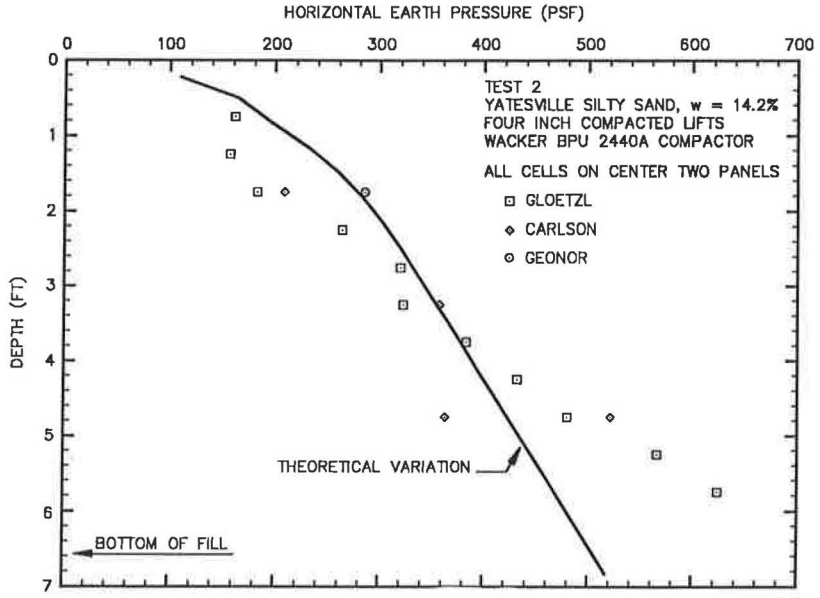

FIGURE 9 Measured and calculated horizontal earth pressure—Test No. 2.

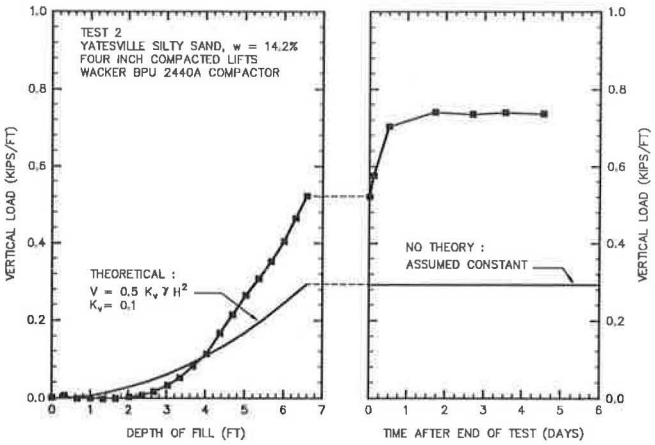

FIGURE 10 Measured and calculated vertical shear loads—Test No. 2.

10. The "theory" used to calculate the theoretical values shown in Figure 10 is quite rudimentary. The theoretical variation shown in the figure is based on the results of finite element analyses of a number of 40 ft high walls. These analyses indicated that the value of the vertical shear coefficient (K_v) is not less than about 0.1 for a wide range of conditions of wall geometry and backfill properties.

It can be seen that the equation shown in the left side of Figure 10 underestimates the vertical shear load for fill depths greater than about 4 ft. Since the shear load results from settlement of the backfill relative to the wall, and since the amount of settlement increases with increasing fill depth, it seems probable that the shear load (V) should be proportional to fill depth (H) raised to a power larger than two. More experimental and theoretical work is needed to develop improved means for estimating shear loads on walls.

As shown at the right side of Figure 10, the measured shear load increased by about 40 percent over a period of about 5 days after backfilling. This increase in shear load is believed to result from settlement of the fill over this period, although no measurements of the settlement were made in Test No. 2. Settlements as small as 0.1 in. would be sufficient to mobilize significant shear loads on the wall. Further study is planned to investigate the factors causing changes in shear loads with time after compaction.

CONCLUSION

The Instrumented Retaining Wall Facility at Virginia Tech has been developed to study the factors that influence normal and shear loads on retaining walls. The electronic instruments and the data acquisition system in the facility make it possible to perform efficient and accurate studies of earth pressures during and at the end of backfilling and their variation with time after backfilling. This facility offers promise for investigating aspects of the horizontal and vertical earth loads on retaining walls that are not reflected in conventional earth pressure theories, but which have significant effects on the stability and performance of retaining walls.

ACKNOWLEDGMENTS

The authors wish to express their appreciation to the many people who have assisted with the development of the Instrumented Retaining Wall Facility. These include Tom Brandon, Glen Thomas, Brett Farmer, Clark Brown, George Filz, and Eric Zeimer of Virginia Polytechnic Institute and State University; Ed Brylawski of Geonor, Inc.; and Brian Dawes of Geo Group, Inc. They also wish to express their appreciation to the National Science Foundation, to Nikken Sekkei Corporation of Japan, to the U.S. Army Corps of Engineers, and to Virginia Polytechnic Institute and State University, which supported the development of the facility. Reed Mosher of the U.S. Army Engineer Waterways Experiment Station and Don Dresler and Lucian Guthry of the Office of the Chief of Engineers have provided valuable suggestions regarding the use of the facility to measure shear loads on walls.

REFERENCES

1. K. Terzaghi. Record Earth-Pressure Testing Machine. *Engineering News Record*, Vol. 109, No. 13, 1932, pp. 365–369.
2. J. M. Duncan and R. B. Seed. Compaction-Induced Earth Pressures Under K_0-Conditions. *Journal of Geotechnical Engineering*, ASCE, Vol. 112, No. 1, 1986, pp. 1–22.
3. R. B. Seed and J. M. Duncan. *Soil-Structure Interaction Effects of Compaction-Induced Stresses and Deflections*. Geotechnical Engineering Research Report No. UCB/GT/83-06. Civil Engineering Department, University of California, Berkeley, 1983.

Publication of this paper sponsored by Committee on Subsurface Soil-Structure Interaction.

Instrumentation of Cumberland Gap Pilot Tunnel

RICHARD W. HUMPHRIES, W. RANDALL SULLIVAN, AND ROBERT M. LEARY

The Cumberland Gap twin highway tunnels are currently under construction. In 1986 a pilot tunnel was excavated at the crown of the southbound tunnel to investigate the geologic conditions along the 4,200 ft length of the twin tunnels. This paper describes the evolution of the instrumentation program associated with the excavation of the pilot tunnel. The instrumentation program as initially conceived had research as a primary objective. The initial program was reduced to a moderate number of extensometers, convergence points, strain gauges on steel sets, piezometers, and groundwater flow weirs for the bid documents for the pilot tunnel excavation. After about 15 percent of the tunnel had been excavated, the instrumentation program was again reduced substantially because the initial data indicated that the scope of the program could be reduced while still providing sufficient data for designing support of the main tunnels. The paper presents the results of the instrumentation program and concludes with recommendations regarding instrumentation programs for pilot tunnels.

The Cumberland Gap has been a transportation route since before Daniel Boone led settlers through the Gap to Kentucky. Currently, U.S. Highway 25E carries more than 18,000 vehicles per day between Cumberland Gap, Tennessee, and Middlesboro, Kentucky, on a winding alignment that has steep grades. To reduce the accident rate along this section of steep terrain and to allow restoration of the wilderness road in the Cumberland Gap National Historic Park, twin tunnels 4,200 ft long are planned through Cumberland Mountain.

Planning for the tunnels started in the 1950s, but financial restrictions delayed initial design until 1980, when work started in earnest. Investigations for the tunnels have included:

- Geologic literature review (1980–1982);
- Extensive outcrop mapping on the surface and in the nearby railroad tunnel through Cumberland Mountain (1981–1983);
- Extensive core drilling at both portals (1981–1983);
- A 2,000 ft horizontal core boring from the Kentucky portal along the alignment of the southbound tunnel (1983); and
- Excavation of a 10 ft by 10 ft pilot tunnel as a crown drift in the southbound tunnel (1985–1986).

This paper describes the evolution of the instrumentation for the pilot tunnel, the results obtained from the instrumentation program, the implications of the instrumentation results on the design of the main tunnels, and general recommendations for instrumentation of pilot tunnels.

The prime objectives of the pilot tunnel were to investigate the ground conditions along the tunnel alignment, to evaluate how the ground will behave during the construction of the main tunnels, and to expose the geology for first-hand evaluation by main tunnel designers and contractors bidding on the main tunnels (*1*). The importance of understanding ground behavior in tunnel construction is illustrated by the difficulties that were encountered during the excavation of the Eisenhower Tunnel in Colorado (*2*), where ground behavior proved to be much different than expected. Severe squeezing conditions were encountered in a major regional fault zone, resulting in substantial changes in the contractor's planned operations and substantial cost overruns.

GEOLOGY

Cumberland Mountain is an overthrust block near the junction of the Valley and Ridge and Appalachian Plateau provinces. The rocks along the tunnel alignment range from Silurian to Pennsylvanian age formations. Rock conditions vary significantly and range from uniform shales and limestones to interbedded sandstone, shales, and coals. Bedding dips at 35 to 50 degrees toward Kentucky and strikes nearly perpendicular to the tunnel alignment. Figure 1 shows a generalized geologic profile along the tunnel alignment.

The strength, jointing, and engineering characteristics of these units vary significantly. The limestones and some of the sandstone units are massive, without prominent bedding planes and with relatively few joints, while some of the claystones, mudstones, and shale units are weak, with closely spaced bedding partings and numerous slickensided joints. Extensive cave systems and mudfilled solution cavities were encountered in one of the limestone units during excavation of the pilot tunnel. One of these cave systems carries significant quantities of water across the tunnel alignment.

EXPECTED GROUND BEHAVIOR

The behavior of the ground depends on the engineering characteristics of the ground and the construction process. Ground behavior of rock tunnels is often characterized as follows (*3*):

- Structural control or loosening (rock displacing under its own weight along preexisting discontinuities);

R.W. Humphries and W.R. Sullivan, Golder Associates Inc., 3730 Chamblee Tucker Road, Atlanta, Ga. 30341. R.M. Leary, Federal Highway Administration, Harrogate, Tenn. 37752.

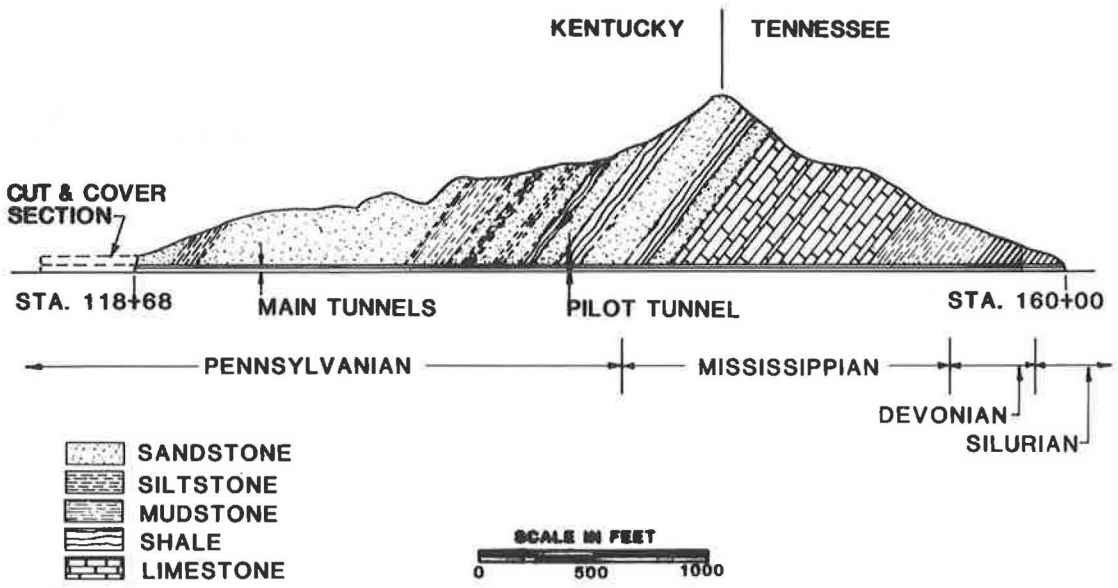

FIGURE 1 Geologic profile of Cumberland Gap tunnels.

- Stress slabbing (formation of new fractures and slabs as a result of stress concentrations around the opening);
- Squeezing (creep without volume change due to stresses that exceed the strength of the rock mass);
- Swelling (volume increase); and
- Slaking (volume change and deterioration due to changes in the physical environment, including freeze-thaw cycles and changes in the confining pressure, humidity, and moisture content.

Actual ground behavior often involves a combination of several of the types described above.

The maximum overburden or rock cover above the Cumberland Gap tunnels is approximately 750 feet. Uniaxial compressive strengths of the units in the tunnel were estimated to exceed the in situ stresses by more than a factor of six, the level at which stress-slabbing may begin to develop (*4*). Squeezing was not expected, because even lower strength-to-stress ratios are required to produce squeezing. No rocks with swell-susceptible minerals were expected, but the shales were expected to be susceptible to slaking. Thus, the types of ground behavior of concern on this project were expected to be structurally controlled loosening, due to the prominent bedding and jointing, and slaking in the shale units.

DESIGN OF THE INSTRUMENTATION PROGRAM

The design of the instrumentation program for the pilot tunnel evolved over the period from 1981 through pilot tunnel construction in 1986. Through this period, a number of key personnel changes occurred within the Federal Highway Administration (FHWA) and their consultants. The personal philosophies of the people involved often differed concerning the purposes and benefits of instrumentation on the project. Consequently, the actual instrumentation program differed considerably from the program planned at the beginning of construction, which, in turn, was radically different from that originally conceived in 1981.

At the outset of the design of the pilot tunnel, research into rock mass behavior, ground-support interaction, and advances in tunneling technology was envisioned as one of the primary objectives of instrumentation in the pilot tunnel. However, subsequent funding restrictions eliminated research as an objective in the pilot tunnel instrumentation, and the modified program was redirected to provide data for the design of the main tunnels.

In the modified program, it was decided to monitor ground displacements with respect to heading location and time, loads on steel rib supports, and groundwater flows and pressures. Construction plans for the pilot tunnel called for five instrumented test sections within the tunnel, plus instrumentation to measure crown and sidewall displacements at both portals. Tentative locations of the test sections were indicated in the plans, but the locations could be varied to provide data on the range of ground conditions encountered. Typical instrumentation planned at each test section is shown in Figure 2. In addition to the test sections and portal instrumentation, the plans also included the following devices:

- Convergence points in sets of four, as shown in Figure 2, at about 25 locations;
- Strain gauges to measure loads on steel ribs at 2 locations, with three instrumented ribs at each location;
- Weirs installed at 7 locations in the ditch carrying groundwater from the tunnel; and
- An automatic flow recording device at the portal.

The contractor was paid at the contract unit price for each instrument type and for standby time when tunneling or instrument installation activities were interrupted.

Experience has shown that instrument selection, if left to a low bid process, is often less than satisfactory (*6*). For this

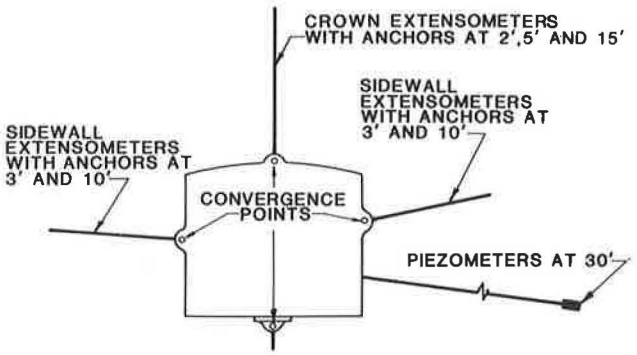

FIGURE 2 Planned instrumented test section.

reason, the procurement and assembly of instruments for this project were done through a geotechnical assistance contract between Golder Associates and the FHWA. With this arrangement, specific hardware with proven accuracy, reliability, and longevity was obtained from preferred sources and furnished to the construction contractor. This procurement process was successful in securing the contractor's cooperation and achieving high-quality installations. Although it was successful here and is recommended by the authors, this procedure requires aggressive management and a liberal interpretation of the acquisition regulations for federal projects.

In addition to the usual language on materials and construction procedures found in most instrumentation specifications, Table 1 was included as part of the contract. This table specifically shows the division of work and responsibility between the contractor and the engineer for each type of instrumentation used on this project. Experience in the pilot tunnel with this specification was satisfactory, and the authors recommend that no matter what procurement procedures are used, a table similar to Table 1 be included in any instrumentation specifications to assure that the division of responsibilities is clearly defined in advance.

TABLE 1 BREAKDOWN OF TUNNEL INSTRUMENTATION WORK

	Responsibilities	
Instrumentation	Contractor	Engineer
Strain gauge	Locate clean steel, and install gauges, sensors and leads Furnish, weld, and paint protective covers to gauges and leads	Furnish gauges, leads, readout unit, and junction box Do final electrical connectors
Stainless steel weir	Prepare site Supply mortar Maintenance cleaning Install weirs	Select location Provide weirs Check calibration
Automatic flow recording device	Furnish and install concrete pipe Install weirs and flow reading devices	Furnish weirs and flow reading devices Calibrate
Convergence measurement	Drill and clean hole Furnish rebar, epoxy, and invert covers	Furnish eyebolts, protective pipes, and cap; tape extensometers; and calibration bar Indicate location and calibrate Take initial readings
Convergence measurement (*continued*)	Install eyebolts Install invert covers, protective pipe, and caps Furnish and install lockable metal enclosure in tunnel	
Extensometer	Drill and clean hole Furnish drillers log, core boxes, grout, grout machines, protective covers, and locks Grout assembly in hole	Locate position, log core Furnish complete MPBX units and readout equipment Assemble in borehole Take initial readings
Piezometer	Drill and clean hole Furnish drillers log, core boxes, bentonite grout, and grout machine Grout instrument in hole	Locate position and log core Furnish piezometer, tubing, readout box, and accessories Assemble unit in hole Calibrate and take readings
Settlement inclinometer	Drill and clean hole Furnish drillers log, core boxes, grout, grout machine, protective covers, and locks Grout assembly in hole	Locate position Log cores Furnish complete downhole units and readout equipment Assemble in borehole Take initial readings

PREDICTED INSTRUMENTATION RESULTS

For structurally controlled behavior, displacements measured with extensometers and convergence points were expected to:

- Exceed the theoretical elastic displacement only by the amount required for loosening to mobilize the support capacity (i.e., very small displacements were expected);
- Be less than 0.5 to 1.0 in. at the tunnel periphery, unless a failure occurs (*5*); and
- Stabilize when the heading advances two to three equivalent tunnel diameters (20 to 30 ft) beyond the instrument location (i.e., no creep or long-term displacement, provided the support prevents further loosening).

The need for steel rib support was anticipated only near the portals, where the loading from structurally controlled loosening would be no larger than the overburden pressure. No sidewall pressures were expected.

EARLY PILOT TUNNEL EXPERIENCE

Excavation of the pilot tunnel started in December 1985 from the Kentucky portal. Support through most of the pilot tunnel is shown in Figure 3. Steel ribs (Figure 4) were installed at the portals and in short sections through the tunnel. Ribs were often used along with the rockbolt-shotcrete support shown in Figure 4. In some sections where bolt anchorage was questionable or not available, ribs provided the only ground support. Ribs were blocked to the rock using unseasoned hardwood; in some cases a thin layer of shotcrete (less than 1 in.) was applied to the blocking in the crown. As with most steel rib installations, blocking was irregularly spaced and sometimes loosened by subsequent blasts.

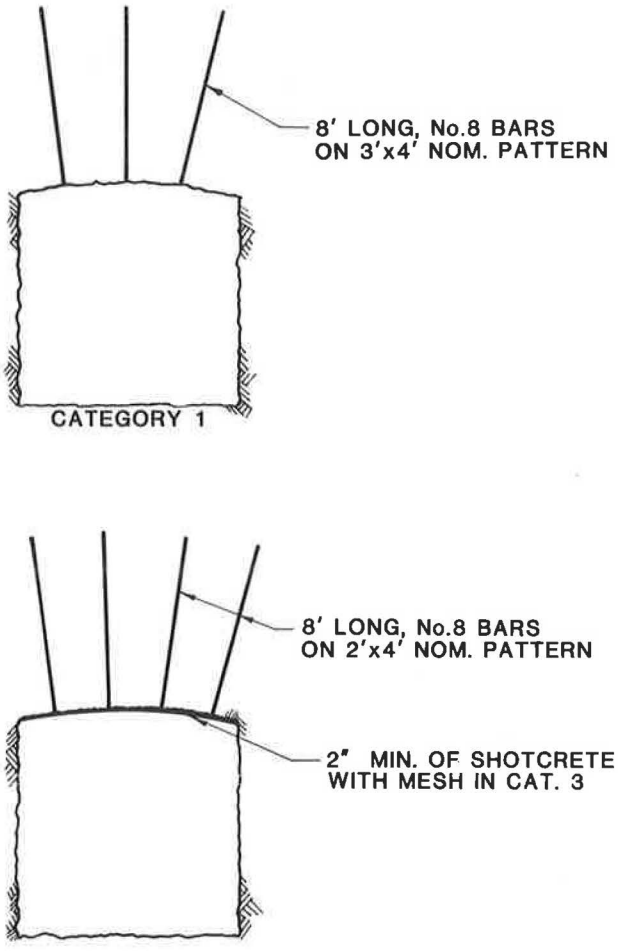

FIGURE 3 Pilot tunnel support—categories 1, 2, and 3.

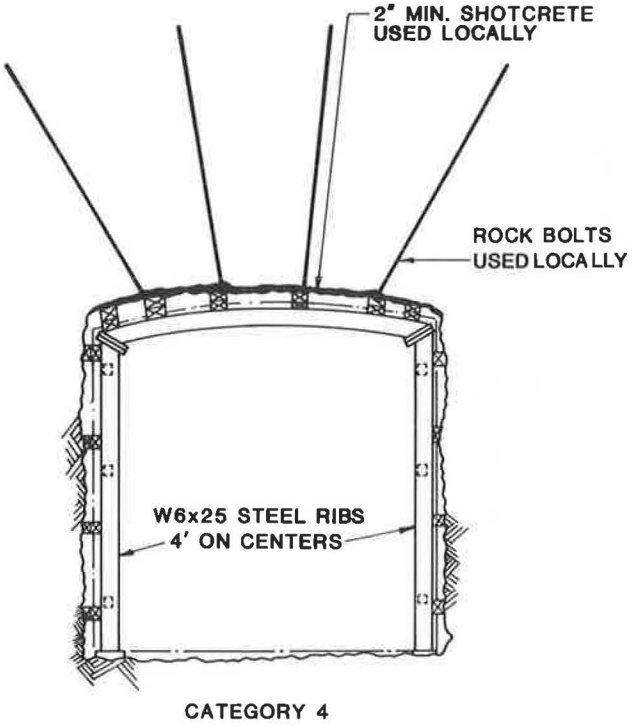

FIGURE 4 Pilot tunnel support—category 4.

As the excavation proceeded, the ground behavior was being evaluated regularly by both direct visual observation and instrumentation data. Once the excavation reached a point about 600 ft into the mountain, these data prompted a reevaluation of the instrumentation program. At that point, rock conditions ranging from a weak, sheared claystone to a thin-bedded sandstone to a relatively massive sandstone had been encountered.

Data were available from an extensometer and inclinometer at the portal, three convergence stations, and five instrumented steel ribs. Data on a thin-bedded sandstone from the portal extensometer showed about 0.1 in. of total crown displacement (see Figure 6). The inclinometer in the sidewall of the tunnel at the portal showed just under 0.2 in. of total lateral displacement toward the tunnel. Convergence data showed movements of 0.2 in. or less, except at one location where the convergence point was anchored in a sandstone block in the crown that rotated and settled on the blocking above the steel ribs. Strain gauge data on the steel ribs indicated less than 1 ft of rock load. All the instruments showed the movements or loads stabilized by the time the heading was about 30 ft ahead of the instrument location.

The data indicated that, although some inelastic movements occurred, they were small and stabilized quickly. This confirmed the initial expectation that the ground behavior would be structurally controlled. It was agreed that structurally controlled displacements and loads in the rest of the tunnel were likely to depend on small-scale, local geologic structures, and

that instrumentation data would be of little use in quantitatively extrapolating to main tunnel behavior. For the remainder of the tunnel, it was agreed that instrumentation would be used to (1) verify structurally controlled behavior, and (2) monitor stability during construction.

The revised instrumentation program included a crown extensometer in a relatively massive sandstone unit and Tennessee portal instruments, as originally planned; strain gauges on representative steel ribs; and convergence stations in each major rock unit. The remaining crown and sidewall extensometers called for at each instrumented test section were eliminated from the plan. It was believed that the combination of convergence measurements and visual observations would provide sufficient data to evaluate ground behavior. If either of these indicated that the ground behavior might not be structurally controlled, more extensive instrumentation would be installed.

This revised program proved to be adequate for the remainder of the tunnel, except in the Chattanooga shale. Unlike the other rock encountered in the tunnel, the Chattanooga shale is highly fractured and sheared. Because of these factors, a crown extensometer was installed to allow a more thorough evaluation of ground behavior.

As a result of timely on-site interpretations, the total instrumentation cost was substantially reduced. The final instrumentation costs were only about 5 percent of the original estimate. Although much of this cost saving was due to lower than estimated unit prices, a significant portion was due to the lesser quantity of instrumentation installed. Major cost reductions were realized in reduced standby time and cost of installations, as well as reduced time for data collection, evaluation, and reporting of results, most of which would have been only slightly beyond the detectable level of the various instruments.

LOAD MEASUREMENTS ON STEEL RIBS

Geokon Model VSM-4000 vibrating wire strain gauges were used to monitor strain in selected steel ribs. This particular type of strain gauge can be welded to the ribs using conventional welding equipment. It proved to be reliable under the rough handling and adverse conditions of nearby blasting in the tunnel environment. Protective plates were installed, however, to shield the gauges against direct impact by miners' tools and flyrock. Instrumented ribs were installed in groups of two or three to minimize the effects of local variations due to blocking details and overbreak. Strain gauges were attached to the ribs before the ribs were used in the tunnel; instrumented ribs were installed less than 4 ft behind the heading.

The performance of the strain gauges was evaluated by monitoring 12 strain gauges over a two month period on one of the steel ribs while it was stored in the contractor's shop. The purpose of these measurements was to determine how much variation occurred in reading with no change in load. Initial readings were used as a reference value, and six subsequent readings were compared to the reference reading. The data showed an apparently random variation of about 10 microstrains, which corresponds to about one ton of thrust or about 4 in. of average rock load (*7*).

Of 120 gauges installed on 30 steel ribs, only 8 became inoperable during the 12 month monitoring period following installation. On one occasion, an instrumented steel rib was severely damaged by flyrock from the heading advance, rendering 4 of the gauges inoperable.

Approximately twice as many steel ribs were used for pilot tunnel support as anticipated in the original design. Short sections of poor ground conditions were more frequent than expected, and there were obvious differences in support bid prices, which made it advantageous for the contractor to recommend steel ribs rather than shotcrete support whenever possible. The data obtained from the strain gauges were used during the construction to verify that some contractor-installed sets were unnecessary and that the rockbolt-shotcrete support was adequate.

Groups of steel ribs were instrumented at five locations in the tunnel. Groups 1 and 5 were at the Kentucky and Tennessee portals, respectively. The other groups were located in some of the poorest quality rock encountered, to determine whether high loads were developing. Data from the instrumented steel ribs are summarized in Figure 5.

The rock loads shown in Figure 5 were calculated according to the method described by Proctor and White (*7*), by summing the loads measured in the two legs of the steel ribs. Except for one of the ribs in Group 3, all of the measured rock loads were less than 3 ft. Side pressures appeared to be negligible at all instrumented locations, but ravelling of weak rock in the side walls was frequently observed and invert struts were required at two locations to resist lateral pressures from the ravelled material that accumulated behind the ribs.

For comparison, Terzaghi's predicted rock loads (*7*) for a 10 ft by 10 ft tunnel are as follows:

Ground Description	*Road Load (ft)*	*Remarks*
Moderately blocky and seamy	2.5 to 7	No side pressure
Very blocky and seamy	7 to 22	Little to no side pressure
Squeezing rock, moderate depth, swelling rock	42	Heavy side pressure

The magnitude of the measured loads compared to Terzaghi's predicted loads confirm that the behavior was structurally controlled. Much larger rock loads and heavy side pressure would have developed in squeezing or swelling ground.

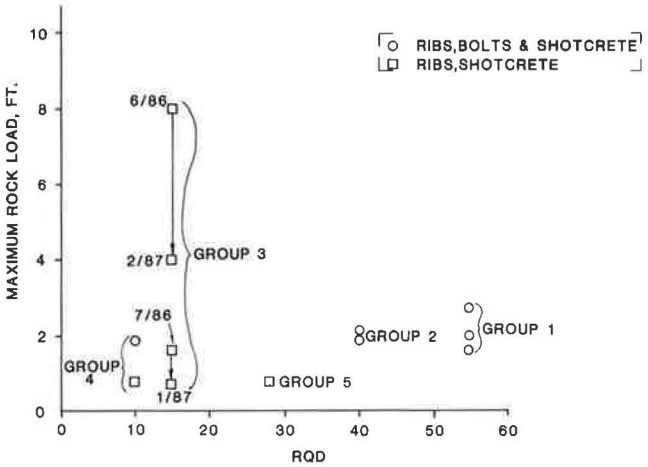

FIGURE 5 Summary of loads on steel ribs.

The loads shown in Figure 5 typically developed over a period of months, indicating structurally controlled blocks in the crown loosened over time and were supported by the ribs. The behavior of Group 3 was different from the other groups. The loads there increased to a peak in June and July 1986 and then decreased. Both the maximum and final measurements are shown in Figure 5. The anomalous behavior suggests the data for this particular group may not be reliable.

DISPLACEMENT MEASUREMENTS

Pilot tunnel convergence was monitored at selected locations using short resin-anchored eyebolts and Sinco Model 518115E/M tape extensometer. A laboratory calibration station was used to verify the accuracy of this measurement device. The attainable precision level of convergence measurements with this equipment in a tunnel construction environment was found to be only about ± 0.03 in.

Crown extensometers, installed from within the pilot tunnel, were used at only two locations. These instruments, Sinco Model 91800127, consisting of stainless steel rods connected to anchors of expandable copper bladders, were installed as close as possible to the heading in a 3 in. cored hole. As discussed previously, the first of these was installed early in the excavation in a relatively massive sandstone unit. The second was installed later in the Chattanooga shale, a highly fractured and sheared fissile shale unit, in an attempt to discern the depth of loosening beyond the excavation limit. Convergence points and extensometers installed from inside the tunnel were all installed less than 4 ft behind the heading.

At both portals, crown extensometers were installed from the surface prior to pilot tunnel excavation using groutable stainless steel rod extensometers (Sinco Model 518118). All extensometers were read from a reference head with a micrometer. Precision levels of ± 0.002 in. were generally attainable with these instruments, even with the physical difficulties of accessing the tunnel crown extensometers. As previously described, the portal extensometer results were useful in supporting the decision to eliminate many of the proposed tunnel crown extensometers. Figure 6 summarizes crown displacement at the Kentucky portal.

An attempt was made to measure both horizontal and vertical movement alongside the pilot tunnel using an inclinometer casing with telescoping couplings and a settlement probe developed by the U.S. Bureau of Reclamation. The precision of the settlement portion of this combined instrument was not high enough to reliably measure the small vertical movements that occurred. The telescoping couplings decreased the precision of the horizontal measurements somewhat, although useful horizontal movement data was obtained.

Displacement data from the pilot tunnel convergence stations and crown extensometers are summarized in Figure 7. For reference, theoretical elastic displacements are also shown in Figure 7. The elastic displacements were computed for a 10 ft diameter tunnel, plane strain conditions, Poisson's ratio of 0.3, and a ratio of horizontal to vertical stress of 1 (*8*). The rock mass modulus of 100,000 psi is estimated to represent a lower bound value for rock in the tunnel; the 1 million psi value is considered representative of the thin-bedded jointed sandstone units encountered. With the exception of the two portals, the reported displacements and convergences were measured after the heading passed the instrumented station. These instruments were installed as soon as possible after excavation and within about 2 ft of the heading. Thus, the reported displacements and convergences do not include movements that occurred prior to the installation (as the heading approached the instrumented section). Consequently, they are, by definition, not directly comparable to the theoretical elastic displacements.

Figure 7 indicates actual tunnel displacements were on the same order as the estimated elastic displacements, except for

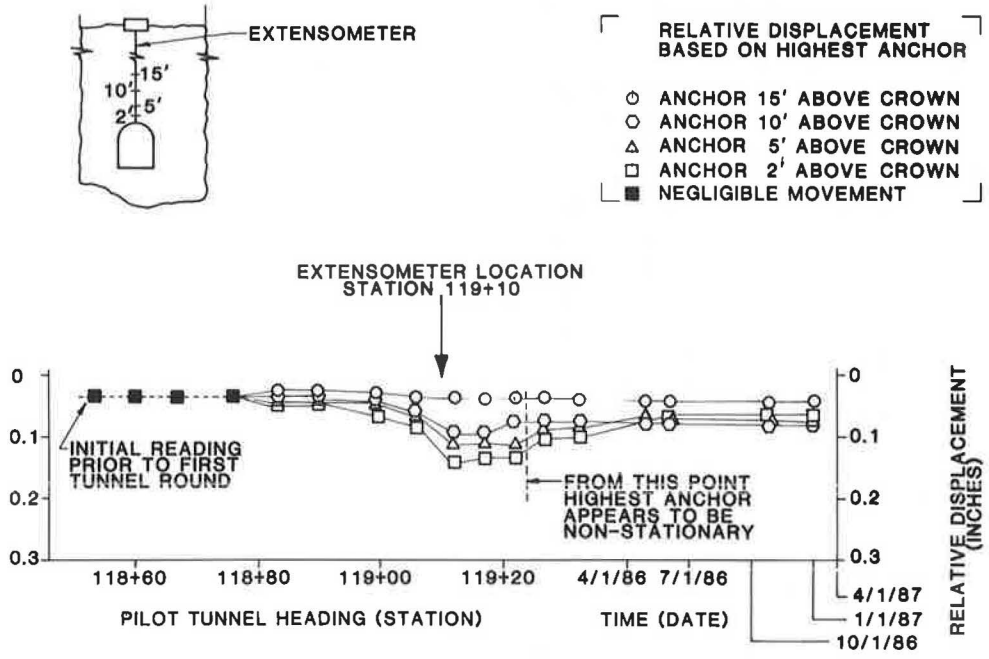

FIGURE 6 Crown displacement at Kentucky portal.

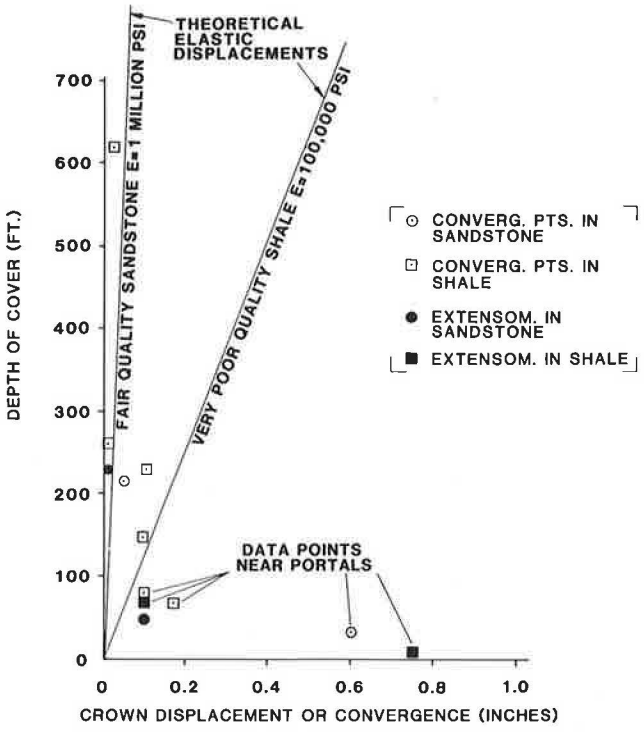

FIGURE 7 Summary of theoretical and measured displacement data for sandstone and shale.

two points at the portals. At the portals, structurally controlled loosening apparently occurred above the rockbolts. With all the data, displacements essentially ceased by the time the heading advanced 30 ft beyond the instrument. Examples of the displacements as the heading advanced are shown in the plot of extensometer data in Figure 6 and an example of the convergence data is shown in Figure 8. The very small measured displacements indicate that little or no loosening occurred in the rock mass surrounding the tunnel. This, coupled with the observation that the displacements stabilized rapidly, further confirms that the ground behavior was structurally controlled.

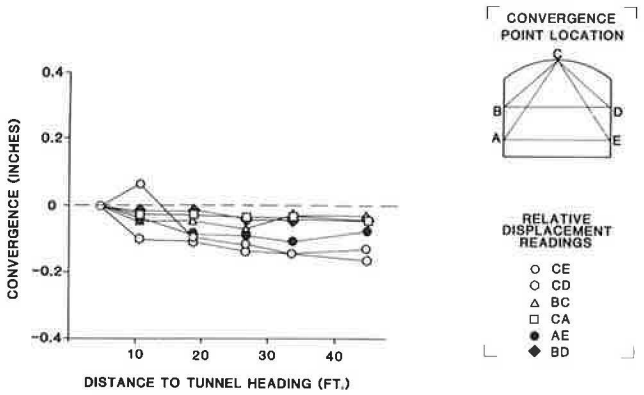

FIGURE 8 Tunnel convergence data for Instrument Station 142+88.5.

GROUNDWATER FLOW AND PRESSURE MEASUREMENTS

Environmental considerations within the National Historical Park did not allow surface access above the tunnel for any significant distance beyond the portal excavations. Yet some assurance was required that drainage into the tunnel would not dramatically affect the overall groundwater regime. Some of the sandstone units exhibited large secondary permeability (fracture flow) resulting in substantial inflow into the pilot tunnel. Some method of predicting the main tunnel inflow was desirable.

A series of V-notch weirs was therefore installed throughout the pilot tunnel to measure the quantity of inflow over various lengths. Data from these simple and inexpensive devices have shown that inflows vary somewhat during local rainfall events, due to direct hydraulic connections to the surface through solution cavities in the limestone. However, the overall inflow has remained surprisingly constant over the 3 years since the tunnel construction was completed. The original contract documents included another V-notch weir to measure immediate inflows relatively close to the advancing heading. This proposed installation proved to be impractical and was deleted shortly after excavation began.

Piezometers (Geokon Model 4500) were installed from the pilot tunnel in two sandstone units in an attempt to discern the pressure distribution in these units within the influence of the pilot tunnel. Relatively constant heads have been measured over the 3 year period since piezometer installation, despite considerable variation in rainfall conditions during the period.

Data from the piezometer installations were used to calibrate flow nets and estimate drawdown around the pilot tunnel. These results and the measured inflow data were used to estimate main tunnel inflows, the impacts of the main tunnels on the groundwater system, and groundwater pressures on the main tunnel lining. From these analyses, it is expected that the main tunnels will have a local effect on the groundwater system, but they will not have an adverse environmental effect.

PLANS FOR MAIN TUNNELS

Excavation of the main tunnels will start in mid-1990. The current design is shown in Figure 9. From the experience gained in the pilot tunnel, the ground behavior is expected to involve structurally controlled loosening and slaking, and the support has been designed accordingly. The instrumentation planned for the main tunnels is minimal and includes (1) extensometers at the four portals, where the cover is relatively low compared to the tunnel diameters, and (2) a few convergence points to monitor the behavior of particular structural blocks in the Chattanooga shale where the rock is highly fractured. Visual observations of shotcrete lining behavior will be used to identify sections requiring additional support.

RECOMMENDATIONS FOR INSTRUMENTATION FOR PILOT TUNNELS

As with any instrumentation program, clear objectives and an understanding of the types of ground behavior that are

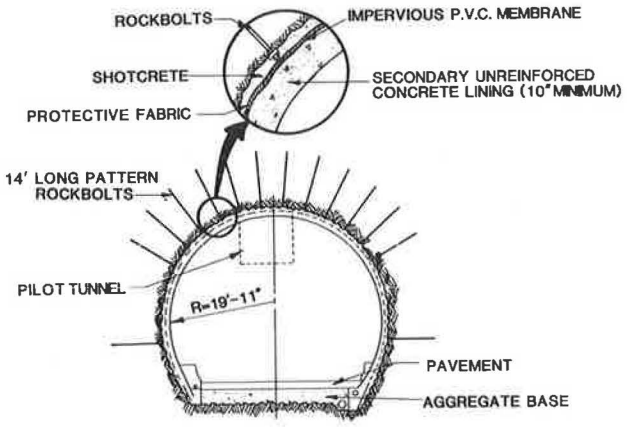

FIGURE 9 Design cross-section of southbound main tunnel.

expected should precede the development of an instrumentation program (*6*). In establishing objectives, available models for extrapolating pilot tunnel measurements to main tunnel ground behavior and support design must be considered.

In general, for the five types of ground control (*3*), the following types of instrumentation programs are considered appropriate:

- *Structural control.*—If structural control is the dominant type of ground behavior, little direct benefit can be gained from an extensive instrumentation program. The authors are unaware of models that would allow displacements and load measurements in a pilot tunnel to be used to quantitatively estimate main tunnel displacements and support requirements. Instrumentation should be limited to providing sufficient data to verify that the ground behavior is structurally controlled and to provide the monitoring needed for construction safety.
- *Stress slabbing, squeezing, and swelling.*—Significant design data can be obtained from instrumenting pilot tunnels where the ground behavior involves stress slabbing, squeezing, or swelling. The distribution of movement in the rock mass and the rates of movement with respect to time and the excavation process are useful in evaluating which type of behavior is dominant. Models are available for translating displacement and load measurements in the pilot tunnel into estimates for the main tunnel (*9*,*10*) and, therefore, for designing appropriate rock support.
- *Slaking.*—Visual observations of behavior are more appropriate than a tunnel instrumentation program for evaluating slaking.

REFERENCES

1. W. R. Sullivan and R. M. Leary. Benefits of the Pilot Tunnel on the Cumberland Gap Highway Project. *Proc., Rapid Excavation and Tunneling Conference*, New Orleans, La., 1987, pp. 3–20.
2. R. C. Hopper, T. A. Lang, and A. A. Mathews. Construction of Straight Creek Tunnel, Colorado. *Proc., First North American Rapid Excavation and Tunneling Conference*, Chicago, Vol. 1, Society of Mining Engineers, 1972, pp. 501–538.
3. E. J. Cording. State-of-the-Art: Rock Tunneling. *Proc., GEOTECH '84*, Atlanta, ASCE, New York, 1984, pp. 77–106.
4. E. J. Cording and J. W. Mahar. Index Properties and Observations for Design of Chambers in Rock. *Engineering Geology*, No. 12, 1978, pp. 113–142.
5. Shannon & Wilson, Inc. *Geotechnical Instrumentation Applications for Pilot Tunnels*. FHWA, U.S. Department of Transportation, Washington, D.C., 1982.
6. J. Dunnicliff. *Geotechnical Instrumentation for Monitoring Field Performance*. John Wiley & Sons, New York, 1988.
7. R. V. Proctor and T. L. White. *Rock Tunneling with Steel Supports* rev. ed. Commercial Shearing Inc., Youngstown, Ohio, 1977.
8. E. Hoek and E. T. Brown. *Underground Excavations in Rock*. Institute of Mining and Metallurgy, London, 1980.
9. E. T. Brown, J. W. Bray, B. Ladanyi, and E. Hoek. Ground Response Curves for Rock Tunnels. *Journal of Geotechnical Engineering*, Vol. 109, No. 1, 1983, pp. 15–39.
10. R. M. Semple, A. J. Hendron, and G. Mesri. *The Effect of Time-Dependent Properties of Altered Rock on Tunnel Support Requirements*. Federal Railway Administration U.S. Department of Transportation, 1973.

Publication of this paper sponsored by Committee on Soils and Rock Instrumentation.

Monitoring of Surcharge-Induced Settlement at the MARTA Chamblee Station

W. Tom Buchanan, John R. Wolosick, Tony Simmonds, and Rodney K. Morrison

A portion of the proposed location of the Metropolitan Atlanta Rapid Transit Authority (MARTA) Chamblee Station was underlain by uncontrolled fill and soft sandy alluvial soils atop residual Piedmont soils. Due to high groundwater conditions and adjacent railroad tracks, it was not considered viable to excavate and replace these soils. Since this area was to support a Reinforced Earth (TM) wall and the station platform, deep foundations were considered unacceptable due to concerns over differential settlements between the wall, trackway, and platform. The original design called for dewatering, placement of fill, and a surcharge load to preconsolidate the soils. The area was to be monitored with settlement platforms and observation wells that were to be extended as fill was placed. The authors jointly devised a plan to utilize vibrating wire settlement transducers and piezometers to monitor pore pressure dissipation and consolidation. These instruments were used in conjunction with consolidation tests to evaluate the rate of consolidation. Predicted magnitudes and rates of settlement are presented and compared to field measurements.

The Metropolitan Atlanta Rapid Transit Authority (MARTA) has completed 29 rapid rail stations and 32 miles of heavy rail dual trackway. The transit system currently consists of four branches emanating from a central hub in the center of Atlanta. The branches currently extend to the northeast, south, east, and west. The MARTA northeast rail line passes through the suburban city of Chamblee, Georgia. For several miles the rapid rail line parallels the Norfolk Southern Railway, which generally follows a northeast-southwest trending topographic ridge. In the vicinity of the Chamblee Station, the northeast MARTA rail line lies immediately southeast of the railroad.

SURFACE AND SUBSURFACE CONDITIONS AT CHAMBLEE STATION

Chamblee is located within the Piedmont physiographic province. The Piedmont is known for its residual soils weathered from underlying metamorphic and igneous rocks consisting of gneisses, schists, and granites. The residual soils consist mainly of sandy silts and silty sands, with clays near the surface. The Chamblee Station platform area is located in a previously existing low area that drained toward the northwest. The ground surface elevation before construction was approximately 1,021 ft.

A subsurface investigation revealed fill overlying most of the site. This fill was apparently placed for the railroad in about 1870, before the availability of heavy compaction equipment. Thus, the fill was not compacted to a significant degree and typically consisted of very loose to loose sand or soft silt, with standard penetration resistances ranging from 3 to 10.

Alluvial soils were discovered underlying the fill. These soils ranged in thickness up to 9 ft and were highly variable in composition. The alluvium consisted of clayey and silty sands, silts and clays, with occasional inclusions of fine organic matter. The deepest fill and alluvial soils were encountered down to approximately elevation 998 ft.

Loose residual soils were found directly beneath the fill and alluvium. A consolidated undrained triaxial test performed on a residual soil sample from Boring NCH-287 indicated an angle of shearing resistance of 33 degrees and a cohesion of 250 lb/ft^2. Atterberg limit testing indicated that the sample was nonplastic. Table 1 presents a summary of laboratory data for the soils tested at the site.

Partially weathered rock marked the transition from the residual soils to solid rock. The underlying rock was generally biotite gneiss. The groundwater level measured during the subsurface investigation was near elevation 1,015 ft at the site.

DESIGN CONSIDERATIONS FOR PLATFORM FOUNDATION

The station platform was 600 ft long, with the "north" end of the station actually pointing toward the northeast (see Figure 1). The entire station platform was originally intended to be part of an aerial structure supported on deep foundations. However, estimates indicated that at-grade track on embankment was less costly. The at-grade trackway on embankment required a retaining wall to separate the elevated platform from the east parking lot, access road, and east busway. This wall was designed as a Reinforced Earth (TM) wall to extend from the abutment at the south end of the platform to the north concourse. The height of the wall ranged from about 20 ft to 30 ft.

W. T. Buchanan, Parsons Brinckerhoff/Tudor, P.O. Box 469, Atlanta, Ga. 30301. Current affiliation: Metropolitan Atlanta Rapid Transit Authority, 2424 Piedmont Road, Atlanta, Ga. 30324. J. R. Wolosick, Chattahoochee Geotechnical Consultants, 6001 Live Oak Parkway, Norcross, Ga. 30093. Current affiliation: Nicholoson Construction, Inc., 4070 Nine/McFarland Drive, Alpharetta, Ga. 30201. Tony Simmonds, Geokon, Inc., 48 Spencer Street, Lebanon, N.H. 03766. R. K. Morrison, Chattahoochee Geotechnical Consultants, 6001 Live Oak Parkway, Norcross, Ga. 30093. Current affiliation: OHM Corporation, 518 Northwest 77th Street, Boca Raton, Fla. 33487.

TABLE 1 SUMMARY OF LABORATORY DATA

BORING NUMBER	SAMPLE ELEVATION (FEET)	SAMPLE CLASSIF.	MOISTURE CONTENT (%)	PERCENT FINER NO. 200 SIEVE	COMPR. INDEX	INIT. VOID RATIO
NCH-287	1008	RESIDUAL-SILTY SAND	35	39	N/A	0.95
NCH-290	1015	ALLUVIUM-SILTY SAND	16	48	N/A	N/A
NCH-291	1001	FILL-SANDY SILT	33	50	N/A	N/A
NCH-292	1018	FILL-SILTY CLAYEY SAND	28	39	0.19	0.90
NCH-292	1008	FILL-SILTY CLAYEY SAND	31	34	0.20	0.91
NCH-292	1002	FILL-SILTY CLAYEY SAND	22	38	0.11	0.65
NCH-294	1002	RESIDUAL-SILTY SAND	52	45	N/A	N/A

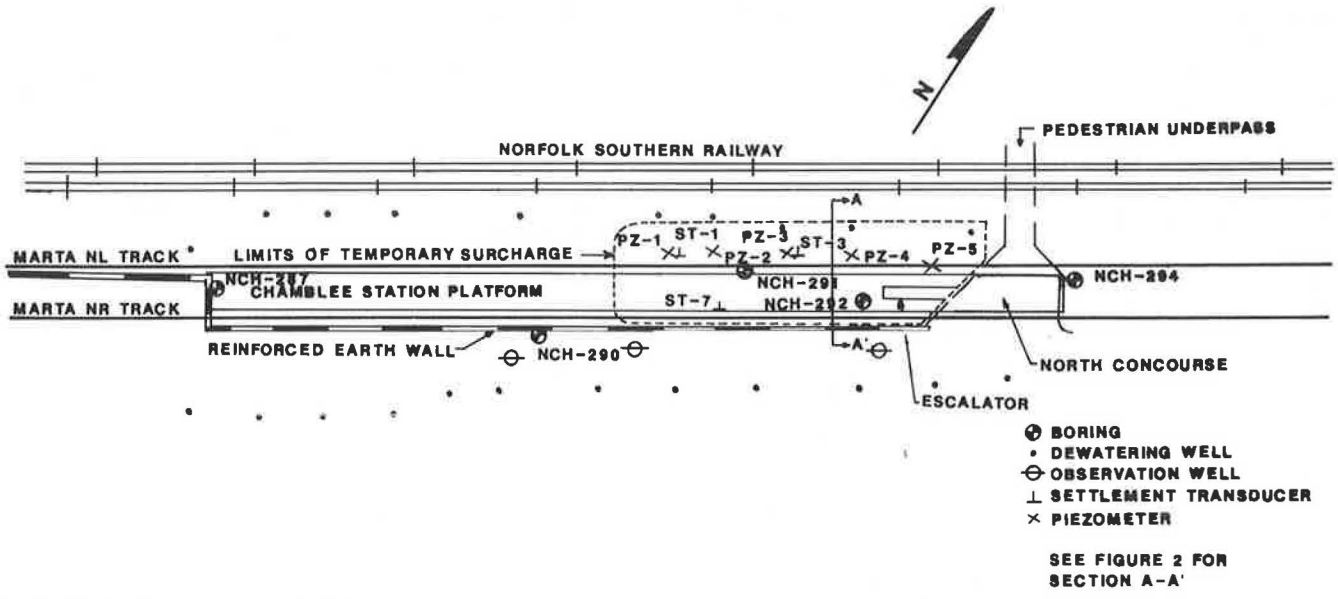

FIGURE 1 Plan of surcharge area.

The presence of the soft fill and alluvium under the proposed platform caused concern about differential settlement between the platform and trackway. Structural requirements dictated that any differential settlement be held to ¼ in. A ballasted trackway would have allowed readjustments of the track for differential settlement. However, a direct fixation trackway on a concrete slab was selected to prevent shifting of the track, which can occur with ballasted trackway. A direct fixation trackway is difficult to repair if excessive settlement occurs. Therefore, for a direct fixation trackway to be a viable solution, careful geotechnical analysis and design were required to limit differential settlement.

A temporary surcharge was chosen as the least expensive and most effective solution for preparing the subgrade to support the embankment and trackway. A temporary surcharge was initially considered for the entire length of the platform. However, within the southern section of the platform it was possible to excavate almost all of the 5 ft thickness of existing loose fill without penetrating the railroad influence line (Figure 2), below which excavation supports would have been required. Figure 1 shows the area encompassed by the temporary surcharge. Figures 3 and 4 show placement and the final configuration of the surcharge.

FIGURE 3 Placement of surcharge.

DETAILS OF CHAMBLEE STATION TRACKWAY SUPPORT

The MARTA northbound track was located immediately behind the Reinforced Earth wall, bearing on the zone of internal reinforcing and select backfill. The Chamblee Station contained a center platform, supported mainly by two low walls bearing on compacted embankment. The northern end of the platform was supported on a structure bridging the north concourse. Each track slab was composed of concrete 9 in. thick and 11 ft wide. A canopy was supported by the platform which was founded on spread foundations bearing on underlying compacted structure embankment (see Figure 2).

Near the south abutment of the north concourse (which was supported by piles), the surcharge could not be placed to full height. Removal and replacement of the existing compressible fill and alluvium was required to minimize anticipated differential settlement in this transition area from embankment support to pile support.

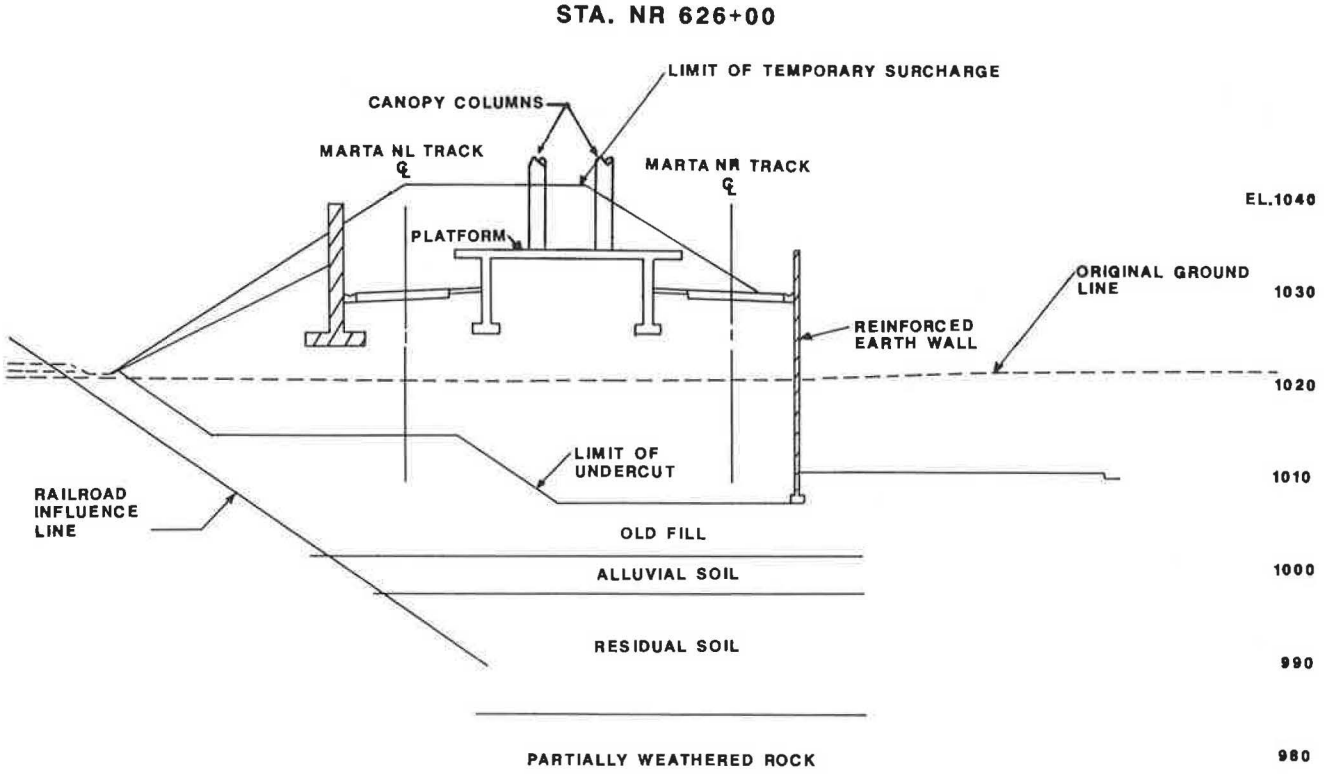

FIGURE 2 Cross-section of station area (section A-A′).

FIGURE 4 Final configuration of surcharge.

DEWATERING SYSTEM

Specifications required lowering the groundwater to at least 3 ft below the bottom of excavation, and keeping the groundwater lowered at least 3 ft below the excavation bottom at any given time. This specification was established to limit loosening of the soil due to upward seepage pressures.

The general contractor hired a specialty contractor to design and install the dewatering system. The system included about 50 deep wells in two rows. The rows were 85 to 130 ft apart. One row of wells was located on each side of the platform area and extended to the north and south. Wells within each row ranged from 44 to 58 ft apart. The system also included 6 observation wells, which were cut off as the excavation proceeded (see Figures 1 and 5). Estimated single well flows were 3.5 gal/min, and 3 to 4 weeks of pumping were anticipated to dewater the site.

All dewatering wells were drilled 10 to 30 ft into rock, terminating at depths varying from 53 to 94 ft. The wells were completed and pumping began in late February 1986. Initial flows varied from less than 1 gal/min to 18 gal/min. Wells with yields less than 1 gal/min were abandoned. The entire system pumped about 250,000 gal of water per day. Water levels were lowered significantly within 10 days, which was much faster than anticipated. Pumping rates were reduced to maintain the drawndown water level to just below subgrade elevation (989 ft).

ESTIMATES OF SURCHARGE REQUIREMENTS

The Reinforced Earth wall and compacted embankment imposed calculated loads of about 1,000 lb/ft^2 on the subgrade materials. Anticipated final loads on the trackway subgrade, including track slab, train, platform, and canopy, totaled about 560 lb/ft^2. The surcharge height of 8 ft was of limited width and was calculated to impose a pressure of 800 lb/ft^2. Assumed dewatering to a shallow depth was calculated to impose an effective pressure of 470 lb/ft^2. These total pressures were calculated to induce approximately the same settlements in 8 weeks that the final loads would have induced at the end of primary consolidation.

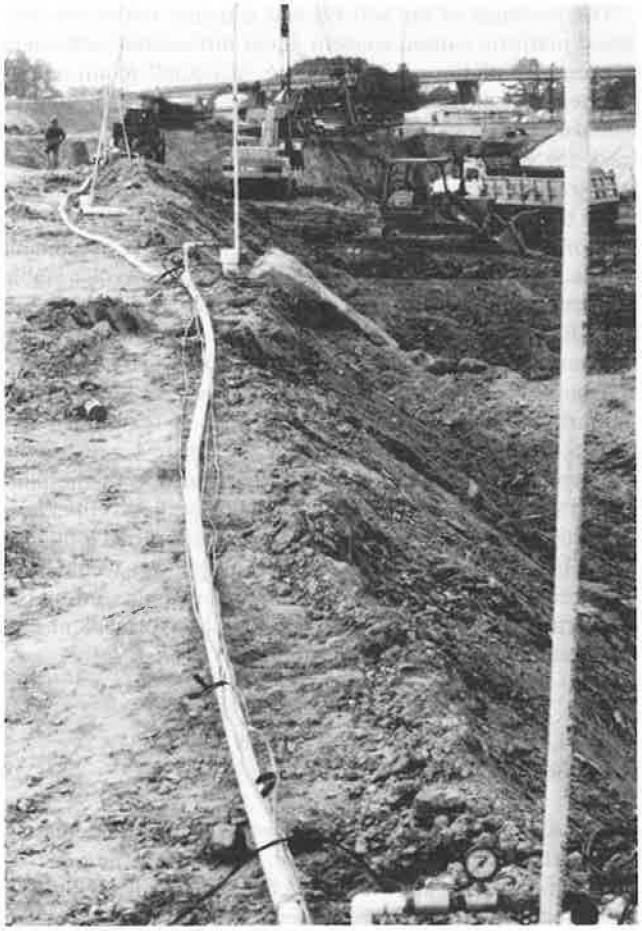

FIGURE 5 Dewatering system.

No vertical drains were planned for hastening the consolidation of the compressible materials. Settlements of the compressible materials left in place were calculated based on consolidation testing data to be between 3 and 4 in. for primary consolidation. Total compression of the material left in place and of the new embankment was expected to be 5 to 6 in., some of which would occur as the embankment was constructed. No values of pore pressure changes were predicted, since the soils were mostly unsaturated.

Estimates of the time required for the consolidation to occur were performed using consolidation test data. The depth of compressible material was highly variable across the site. Estimates for the time required for 90 percent of primary consolidation varied from 2 to 5 months. The contract time allowed for the consolidation was set at 3 months, based mainly on experience.

The contractor proposed a deep dewatering system as opposed to the shallow system assumed in the initial settlement estimates. Deep dewatering lowered the groundwater level below the compressible material, increasing the settlements of the compressible materials and reducing the required time of surcharge. The effective surcharge due to deep dewatering was calculated to be 940 lb/ft^2. For the deep dewatered condition, the time span required for 90 percent of primary consolidation was calculated to be 8 weeks. Therefore, install-

ing the deep well system reduced the estimated time for the surcharge to remain in place from 3 months to 2 months. Based on the added effect of the deep dewatering, the contractor requested that the surcharge be deleted. The request was denied, but the required surcharge time was reduced to 8 weeks.

Even with the surcharge, some long-term consolidation of the soils was expected to occur due to secondary consolidation. In general, settlements from secondary consolidation were expected to be broadly distributed and not to result in significant differential settlement between the platform and trackway.

REQUIREMENTS FOR INSTRUMENTATION

Monitoring the progress of settlement and pore pressure dissipation under the temporary surcharge was an integral part of the design of the MARTA station. The instrumentation data was used to decide whether the planned duration of the surcharge was sufficient or not. If the data indicated that the surcharge had its desired effect earlier than anticipated, then the surcharge could be removed, allowing the contractor access to the area before the scheduled date. MARTA intended for the surcharge to remain in place until both a zero rate of settlement was attained and the pore pressures recovered to their presurcharge levels.

CHOICE OF INSTRUMENTATION

The original instrumentation plan called for the use of horizontal and vertical inclinometers installed within the select backfill of the Reinforced Earth wall. Vertical inclinometer casings were to be installed just behind the Reinforced Earth wall and were to extend upward as the select backfill was placed. Horizontal inclinometer casings were to be installed in trenches in the existing fill and alluvium under the Reinforced Earth backfill and were to extend under the Reinforced Earth wall footing. The inclinometers were to be supplemented by placing settlement plates on the subgrade, welding pipe risers to the plates and extending the risers upward to the top of the select backfill as fill was placed. The risers were to be monitored by optical survey. Groundwater levels were to be monitored via open standpipe piezometers installed in the fill and likewise extended as select backfill placement continued. However, when the bids were opened, the lowest bid for constructing the station was found to be considerably over MARTA's estimate. Many items, including all of the vertical inclinometers, were eliminated from the contract to reduce costs.

The area of Reinforced Earth backfill presented a very confined work area. It was recognized that the settlement risers and open pipe piezometers would have a very high potential for damage during fill placement. The project specifications required the contractor to replace any damaged units at no additional fee and to pay a fine of $1,000.00 per unit per damage incident. These factors led to the consideration of alternate approaches to the monitoring program.

For settlement readings, consideration was given to the specified horizontal inclinometer system, along with alternate profiling systems utilizing pneumatic and vibrating wire probes. However, due to the small size of the study area, it was decided that settlement profiles were not particularly cost effective, and that discrete measurements at three or four locations within the work area would provide the necessary information. The instruments finally chosen for monitoring settlement were the Model 4600 vibrating wire settlement sensors manufactured by Geokon, Inc. These instruments were supplemented at a later stage by four standard settlement risers, which were installed from the surface of the completed surcharge down into the compacted trackway subgrade and subsequently monitored by optical survey.

The vibrating wire settlement system consisted of a vibrating wire pressure transducer connected via a fluid-filled tube to a reservoir. The transducer sensed the pressure created by the head of the fluid within the tube. Changes in head (pressure) provided a measure of the difference in elevation between the reservoir and the sensor. The pressure transducer was located in stable ground, and the reservoir was attached to a plate located at the top of the borehole, which settled along with the material around it. The transducers used were capable of discerning settlement changes with an average resolution of 0.047 in. An electrical cable extended from the sensor to a remote readout location (Figure 6). This arrangement called for the drilling of a borehole, but it avoided the need to run fluid-filled tubes laterally through the fill. The instrument is supplied filled and ready for installation, so there was little concern about performance of the system with respect to a discontinuous fluid column. Simple electrical continuity checks made on site prior to installation confirmed a continuous fluid column.

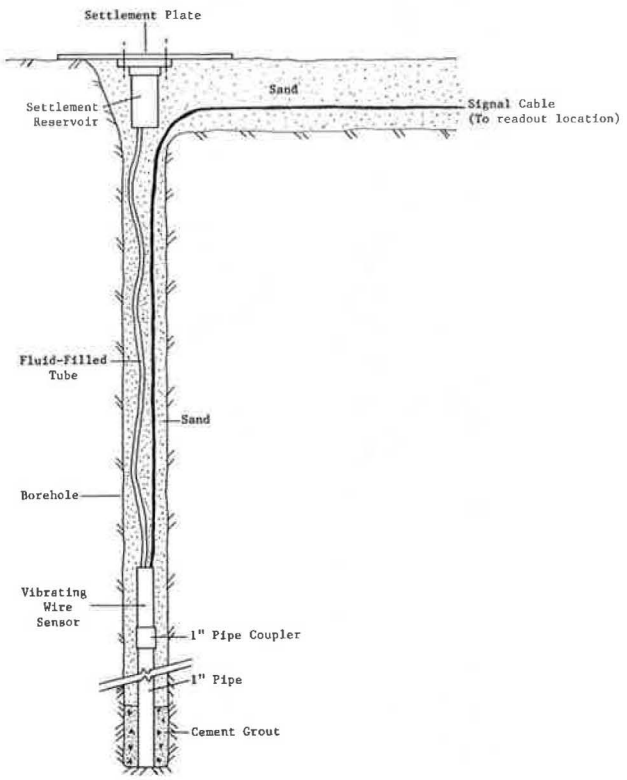

FIGURE 6 Vibrating wire settlement system.

For groundwater monitoring, pneumatic and vibrating wire piezometers were considered. The final decision was to use the vibrating wire units so that the same switching terminal and readout required for the settlement monitoring system could be used for groundwater monitoring. The instruments chosen were the Geokon Model 4500DP drive point piezometers. These piezometers utilized a vibrating wire pressure transducer, mounted to an EW drill coupling with a pointed nose cone attached (Figure 7). The average sensitivity of the piezometers was 0.023 pounds per square inch (psi). The alternate instrument selections were all submitted to MARTA and accepted.

INSTALLATION OF INSTRUMENTATION

The project specifications required the general contractor to procure the services of a specialty contractor or consultant to install all instruments. The general contractor chose to expand the duties of the consultant to include additional laboratory testing, settlement magnitude, and time frame prediction, in addition to instrument monitoring and interpretation. The installation of the settlement sensors required drilling a borehole through the alluvial soils and underlying soft residual soils into firm rock using hollow stem augers. The sensor was attached to a 1 in. diameter steel pipe and lowered through the hollow auger to the bottom of the hole. The length of steel pipe was selected to keep the elevation difference between the reservoir and transducer small, thus allowing the use of a low pressure range transducer, which resulted in greater sensitivity. A 2 to 3 ft grout plug was placed in the bottom of the hole as the augers were retracted. The hole was then backfilled with sand and the reservoir attached to a 2 ft square, ⅜ in. thick plywood settlement plate. The reservoir-plate assembly was placed over the top of the borehole and the area around the borehole (a 2 ft square by 1 ft deep excavation) backfilled with sand.

The piezometers were placed either by advancing a borehole to the planned elevation and pushing the piezometer into place with drill rods, or by excavating via backhoe to the planned elevation and driving the piezometer into place with a hand penetrometer. In both cases, the hole above the piezometer was sealed with a bentonite plug. Prior to placement, the piezometer filters (1 bar, high air entry ceramics) were saturated and the cavity between piezometer diaphragm and filter purged of air. Cables from all units were buried in trenches and connected to the readout switch panel (Figure 8).

The vibrating wire piezometer and settlement monitoring systems were installed during the week of April 21, 1986. Sixteen optical settlement reference points were also cast into the leveling footing of the Reinforced Earth wall.

INSTRUMENTATION RESULTS

The settlement transducers and pore pressure transducers were read independently by both the general contractor's instrumentation consultant and by MARTA's general engineering consultant. All data were shared by both parties to assure full coverage and consistency. Important dates in the construction sequence of the project are shown on Table 2. The results of the piezometer and settlement transducer data are shown on Figures 9 and 10.

Although the location (elevation) of the piezometers was not changed when the deep dewatering scheme was accepted

FIGURE 7 Vibrating wire piezometer.

FIGURE 8 Rotary switch panel and readout box.

TABLE 2 CALENDAR DATES VERSUS CONSTRUCTION DAYS AND EVENTS

PHASE	CALENDAR DATES	CONSTRUCTION DAYS	CONSTRUCTION EVENT
N/A	April 25-May 9	0	Initial instrument readings
1	May 9	1	Beginning of select backfill placement for Reinforced Earth wall
2	May 9-July 30	1-81	Placement of Reinforced Earth backfill
3	July 30-Aug 7	81-89	Placement of temporary surcharge
4	Aug 7-Sep 16	89-129	Approximate date of pore pressure maximum to removal of temporary surcharge
N/A	Sep 16	129	Final instrument readings

(the piezometers were installed above the drawndown groundwater level), the majority of the piezometers indicated changes in pressure to the applied surcharge loading (Figure 9). The response of piezometer PZ-4 was not as pronounced as the four other units. The reason for the poor response of this piezometer was not clear, but smearing of the ceramic filter was suspected. Since pumping for the dewatering was continuous, the pore pressure measurements indicated a general decreasing trend throughout the life of the project.

The settlement transducers indicated similar settlement patterns and magnitudes. The measured settlements shown in Figure 10 were much greater than originally anticipated. The early start and the depth of the dewatering accomplished by the contractor increased the settlements.

The time period of interest in the surcharge area can be divided into four phases (Table 2), as follows:

1. Phase 1 (April 25–May 9, 1986) began with the first instrumentation readings and ended at the beginning of select backfill placement for the Reinforced Earth wall.
2. Phase 2 (May 9–July 30, 1986) began with the initial placement of the select backfill, continued through the completion of the Reinforced Earth wall, and ended at the beginning of the placement of the temporary surcharge.
3. Phase 3 (July 30–Aug. 7, 1986) began with the initial placement of the temporary surcharge and ended when the pore pressures reached their maximum. Placement of the temporary surcharge began on July 30 and was completed on August 4.
4. Phase 4 (Aug. 7–Sept. 16, 1986) began when the pore pressures reached their maximum and ended when the surcharge was removed.

Typical data from the piezometers and settlement transducers are presented in Figures 9 and 10. Figure 9 represents the change in settlement measured at the site versus time. The data are presented by phase, as described above, so that increments of loading and its effects can be examined. During the course of the project, the settlement and pore pressure data were analyzed versus time using semilogarithmic plots. Discussion of each phase is presented below.

During Phase 1, measured settlements ranged from 1.9 to 3.0 in. Pore pressures measurements were all below atmospheric and decreased by 0.3 to 0.8 psi (Tables 3 and 4).

During Phase 2, settlements increased to accumulations varying from 9.3 to 11.9 in. The rate of settlement varied from about 4 to 7 in. per logarithmic cycle. The pore pressures continued to decline, and initial rates varied from −0.5 to −0.9 psi per logarithmic cycle. The settlements and pore pressures varied more or less logarithmically during this time period. Settlement transducer ST-1 and piezometers PZ-1, PZ-3, and PZ-4 displayed breaks in their curves about June 13. Settlement transducer ST-1 began settling at a slower rate, while piezometers PZ-1 and PZ-3 began showing higher rates of decreasing pore pressures. Instruments ST-1 and PZ-1 were located close to each other, but the cause of these changes in rates is unknown.

During Phase 3, four piezometers showed an increase of pressure, with increments ranging from +0.75 to +1.25 psi. At this time piezometer PZ-3 displayed the only algebraically positive pressure of the entire series of readings. Settlement transducers ST-1 and ST-3 began showing a higher rate of settlement than before the surcharge was applied. However, transducer ST-7 did not accelerate, probably because it was near the wall and not directly under the high portion of the surcharge. During this phase, settlement transducers ST-1 and ST-3 settled 1.1 and 1.3 in. per logarithmic cycle.

During Phase 4, all three settlement transducers continued settling initially, reaching cumulative settlements ranging from 10.9 to 12.5 in. The transducers did not indicate any significant settlements after August 25. On August 25, the contractor installed four risers in the surcharge to confirm that the majority of settlement had ceased. The piezometers showed rates of pore pressure change varying from −0.7 to −1.1 psi per logarithmic cycle. The pore pressure returned to their respective presurcharge pressures on dates ranging from August 20 to September 4. The similarity of these time spans further confirmed that the data were reliable.

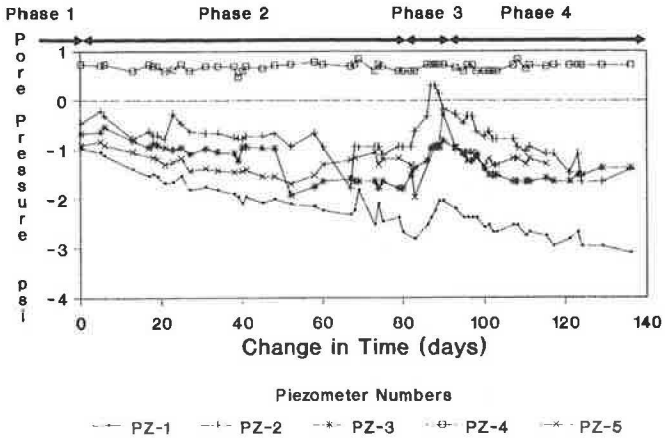

FIGURE 9 Pore pressure versus time.

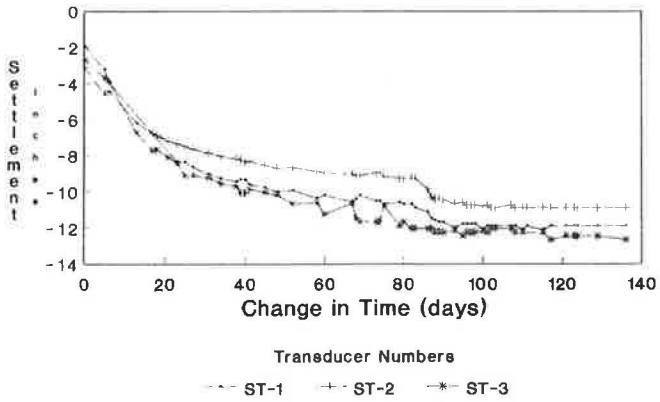

FIGURE 10 Settlement versus time.

TABLE 3 SETTLEMENT UNDER SURCHARGE AREA

DATE INTERVAL (1986)	CUMULATIVE SETTLEMENT (INCHES)			RATE OF SETTLEMENT (INCHES/LOG CYCLE)		
	ST-1	ST-3	ST-7	ST-1	ST-3	ST-7
PHASE 1						
April 25-May 9	1.9	3.0	2.5			
PHASE 2						
May 9-June 13	9.2			7.3		
June 13-July 30	10.7			3.9		
May 9-July 30		9.3	11.9		4.0	6.8
PHASES 3 and 4						
July 30-Aug 25(1)	12.0			1.1		
July 30-Aug 28(1)		10.9			1.3	
July 30-Sep 4(1)			12.5			

(1) - Date of settlement cessation.

TABLE 4 PORE PRESSURES UNDER SURCHARGE AREA

DATE INTERVAL (1986)	INCREMENT OF PRESSURE CHANGE (PSI)				RATE OF PRESSURE CHANGE (PSI/LOG CYCLE)			
	PZ-1	PZ-2	PZ-3	PZ-5	PZ-1	PZ-2	PZ-3	PZ-5
INITIAL READINGS								
April 25	-0.5	-0.1	-0.1	-0.1				
PHASE 1								
April 25-May 9	-0.5	-0.3	-0.5	-0.8				
PHASE 2								
May 9-June 13	-0.8		-0.4		-0.9		-0.5	
June 13-July 30	-1.0		-0.8		-1.9		-1.9	
May 9-July 30		-0.6				-0.5		
May 9-July 7				-0.7				-0.7
July 7-July 30				+0.3				
PHASE 3								
July 30-Aug 7	+0.8	+1.3	+0.9	+1.1				
PHASE 4								
Aug 7-Sep 4(1)	-0.8				-0.7			
Aug 7-Aug 26(1)		-1.3				-1.1		
Aug 7-Aug 26(2)			-0.8				-0.7	
Aug 7-Aug 20(1)				-1.1				-0.9
FINAL READINGS								
Sep 16	-3.0	-1.5	-1.6	-1.3				

(1) - Date that pore pressure declined to pre-surcharge value.
(2) - Date that pore pressure almost declined to pre-surcharge value.

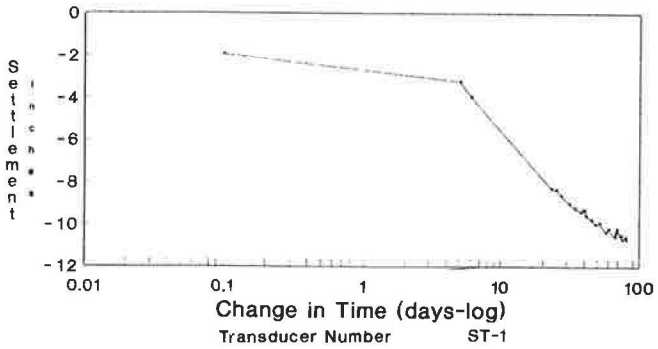

FIGURE 11 Phase 2 settlement (instrument ST-1).

On September 2, 1986, based on the instrumentation data, MARTA concluded that the settlement of the compressible soils under the temporary surcharge was complete, and allowed the contractor to remove the surcharge. By September 15, the southern end of the surcharge had been removed and excavation proceeded northward. Between July 25 and September 8, the entire length of the leveling footing of the Reinforced Earth wall settled about 1 in. (0.08 ft). All 16 of the optical settlement monitoring reference points showed similar values, within the precision of the survey. These measurements compared well with settlement measurements of 1.3 in., 1.6 in., and 0.6 in. from transducers ST-1, ST-3, and ST-7, respectively, during the same time frame.

CONCLUSIONS

The instrumentation provided data that were used in the decisions to stage important construction events. Instrumenting the temporary surcharge in the Chamblee Station enabled MARTA to implement a reliable design for a direct fixation trackway similar to the trackways in most of the other MARTA stations.

The deep dewatering accomplished throughout the platform area increased the magnitude of anticipated settlements of the compressible materials. The deep dewatering also provided a general improvement of the construction conditions. The dewatered soils, when exposed, were less sensitive to disturbance from construction equipment than they would have been if only shallow dewatering had been accomplished. In addition, the compressible soils apparently consolidated more rapidly under embankment and surcharge loads than they would have if they had remained saturated. Both of these factors benefited the contractor by saving time during construction.

The measured settlements were greater than predicted, even when the effect of the deep dewatering was considered. However, the data appeared reasonable, and no instrument malfunctions were determined.

The trends in pore pressure were not surprising, considering the dewatered nature of the soils that existed on the site throughout the time span of the monitoring program. Under these conditions, pore pressures increases were measured when surcharge was placed and the dissipation of the pore pressures with time was observed.

Visual observations of the Reinforced Earth wall have shown no obvious distortion or distress. The Chamblee Station opened to the public in December 1987 and has performed satisfactorily to date.

ACKNOWLEDGMENTS

The construction of the MARTA system has been financed in part through a grant from the United States Department of Transportation, Urban Mass Transportation Administration, under the Urban Mass Transportation Act of 1964, as amended, and in part by the taxes of the citizens of Fulton and DeKalb Counties of the State of Georgia. The general engineering consultant for MARTA was Parsons Brinckerhoff/Tudor. The geotechnical consultant for the engineering consultant was Law Engineering. The general contractor for the project was J. A. Jones-Mitchell (Joint Venture). The instrumentation consultant for the contractor was Chattahoochee Geotechnical Consultants. The dewatering subcontractor was Soil Engineering Services. Michael Randolph prepared the figures for the paper.

Publication of this paper sponsored by Committee on Soils and Rock Instrumentation.

Techniques of Backfiguring Consolidation Parameters from Field Data

RICHARD P. LONG

Methods of analyzing field consolidation data from areas with and without vertical drains are presented. All methods analyze field data independently of laboratory data. Settlement data from areas having vertical drains can be analyzed by three different techniques to yield values of the apparent coefficient of consolidation and the ultimate settlement for foundation clay. Analysis of piezometer data yields values of apparent coefficient of consolidation by a separate technique. Data from areas without drains can be analyzed for similar parameters. All methods involve the use of Terzaghi's theory of consolidation or Barron's equal strain theory for areas with vertical drains. These theories are appropriate for analysis of most clay deposits. The techniques are illustrated and results from their use on the consolidation of varved clay beneath the approach fills of the Putnam Bridge are presented. These techniques were used in analyzing the data from 49 settlement platforms and two piezometer groups of this project. The results show interesting phenomena that should be explored further with data from other sites.

Piezometers, settlement platforms, and settlement anchors are used to obtain data for the control of fills and preloads over soft clays. The pore pressures are monitored to insure against instability. Future settlements of the fill are a concern when deciding on the time to remove the preload and begin paving. During construction, the devices are carefully monitored and the data faithfully recorded. All documents are usually placed in a file drawer when the project is completed and are too often all but forgotten.

The data from each instrumented fill represent an opportunity to improve our understanding of consolidation behavior and design procedures. This opportunity cannot be realized until the data are properly analyzed. Not every project can be turned into the ultimate research site, but the amount of instrumentation normally used to control construction can, with a little planning, be positioned to effectively yield, upon analysis, important information on the consolidation and settlement behavior of soft soil.

Presented herein are techniques to analyze the settlement and piezometer data from fills placed over clay. There are several benefits from conducting these analyses. The most obvious is the case of the test fill. In this case the analysis of the test fill allows the most economical final design to be made for the entire fill. In general, even though the analysis of data occurs after the project is complete, the comparison of predicted to actual fill behavior gives the engineer insight into improving the design approach on future projects. Analysis is also a good method of exposing the young engineer to the behavior of local clay deposits under fills.

Department of Civil Engineering, University of Connecticut, Storrs, Conn. 06269.

Field consolidation data must be analyzed by some theory. The analytical procedures presented here are based on the small strain theory of Terzaghi (*1*). The limitations of this theory are well known, but it provides useful information because, for most soft soils capable of supporting a fill, Terzaghi's theory is a good approximation. For the case of vertical drains, Barron's modification using equal strain consolidation is used (*2*), rather than the direct extension of Terzaghi's theory by free strain.

Although the analysis process may be considered an autopsy (*3*), progress in geotechnical engineering, as in medicine, advances by the judicious use of the autopsy. It is important to approach the data with as little bias as possible. Previous observers have noted the ability of some to use field data to prove just about anything (*3*). To avoid this, the techniques presented here analyze the field data independently of laboratory results. In this approach both the coefficient of consolidation and the ultimate settlement are treated as unknowns when analyzing field data. Using laboratory values for the coefficient of consolidation or predicted values of ultimate settlement in the analysis of the field data biases the results toward the designer's assumptions and leads to questions concerning the validity of results and the conclusions that can be drawn from them. Whatever assumptions were used in design are neutralized in the analysis techniques presented here, and better insight is developed into the entire process of investigating and testing soils and designing and monitoring foundations. These techniques are not a replacement for engineering judgment. There are soil deposits for which it is difficult to determine properties for design from laboratory tests (*4*). Analysis of test fills for these cases yields valuable design information.

The procedures are presented for areas with and without vertical drains. The field coefficient of consolidation can be determined from piezometer data and settlement data, both separately and compared to laboratory results. The total settlement for each platform can be calculated from the field data and compared to predicted values.

PLACING THE INSTRUMENTATION

The analysis can only be as good as the data available to it. One limitation of Terzaghi's theory is that it assumes a homogeneous soil. The instrumentation can often be placed to divide the deposit into reasonably homogeneous units that can be analyzed. A location having soil layers with varying properties might be broken down into reasonably homogeneous units for the analysis by gathering data with settlement anchors as

well as platforms. A few extra piezometers might be placed to determine the rate of dissipation in contiguous layers having different properties. Stratified alluvia may be the most challenging deposits because the many layers in the soil profile often yield only global average values for the deposit.

The soil conditions that nature provides cannot all be accounted for in a brief paper. Each site requires a bit of ingenuity on the part of the designer of the instrumentation and some intuition when carrying out the analysis.

SETTLEMENTS IN GENERAL

Techniques will be presented for the condition of only one filling phase. They can, however, be used in successive applications for stage construction. Typical data are shown schematically in Figure 1. Figure 1(top) shows the filling sequence for an approach fill to the Putnam Bridge in Glastonbury, Conn. Figure 1(middle) shows the settlements with time at the same location, and Figure 1(bottom) shows piezometer data from the same area.

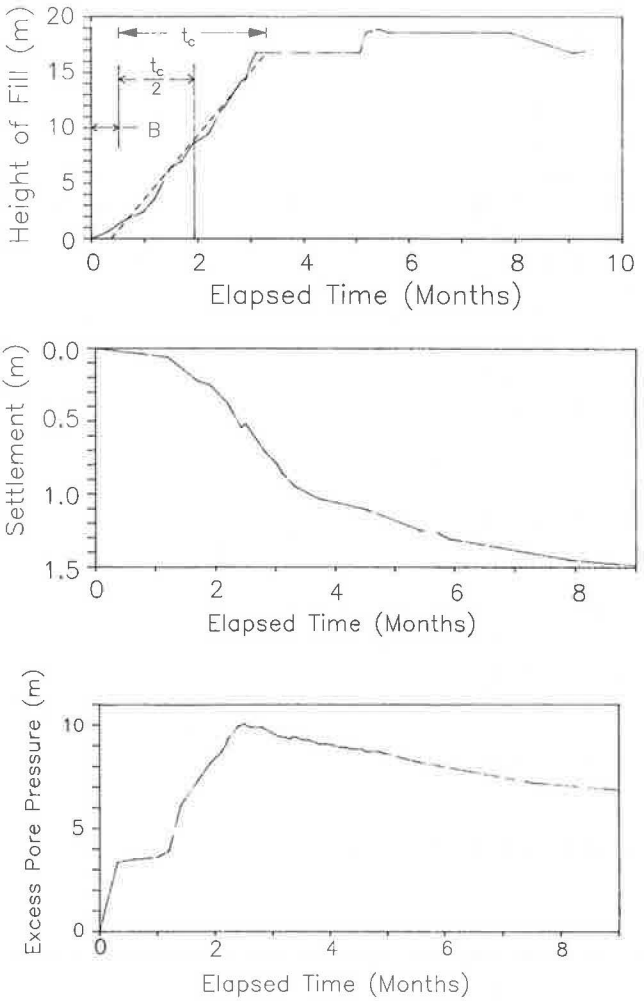

FIGURE 1 Plots of (*top*) fill height versus time, (*middle*) settlement versus time, and (*bottom*) excess pore pressure versus time for settlement platform SP-11, Putnam Bridge.

The settlement observed at any time after filling begins can be described by the equation:

$$\rho = \rho_i + U\,\rho_c \tag{1}$$

where:

ρ = observed settlement,
ρ_i = immediate settlement,
ρ_c = final consolidation settlement, and
U = average percent consolidation.

Although Equation 1 is valid for any observation of the settlement, the analysis is most easily conducted after the fill reaches final height. When plastic flow of the foundation soils can be neglected, the immediate settlement remains constant under the constant load. In cases where plastic flow is anticipated, slope indicators should be installed along the edges of the fill to measure these strains. More research is required to properly interpret the strains that accompany plastic flow, and the discussion here will be limited to cases where plastic strains can be neglected. When the load, and therefore the immediate settlement, is constant, the changes in the observed settlements are due to increases in the average percent consolidation of the layer.

AREAS WITH VERTICAL DRAINS

Vertical drains are often used to accelerate the consolidation and settlement of clays. The presence of the drains allows the pore pressures to dissipate radially. When analyzing the data, it must be recognized that the pore pressures dissipate vertically as well as radially in areas having vertical drains.

The vertical drainage affects the data from various instruments to different degrees. Piezometer data may be strongly influenced by the dissipation of pore pressures in the vertical direction if they are located near the drainage boundaries where the dissipation of pore pressures is faster than average. To insure that the analysis will yield valid results, one piezometer at each location should be placed where the dissipation of the pore pressures in the vertical direction is slowest (i.e., in the center of the layer for a double drained condition). A schematic diagram showing typical positioning of settlement platforms, and anchors, and piezometers is shown in Figure 2. The piezometer in the center of the layer can be used to determine the coefficient of consolidation in the radial direction. Piezometers such as A and C, placed closer to the upper and lower drainage boundaries, can be used in conjunction with the center piezometer to estimate the vertical coefficient of consolidation.

Settlement platforms yield the necessary data for a deposit that is reasonably homogeneous. Settlement anchors are used to isolate the settlement data from a layer. The data from a settlement platform may show a higher coefficient of consolidation than the data from a piezometer placed in the center of a double drained layer, such as piezometer B in Figure 2. This is because the settlement platform data result from the average consolidation from vertical and radial dissipation combined, while the dissipation at piezometer B is primarily the result of radial flow (*5,6*). The data from piezometers positioned similar to A and C may also show significant effects

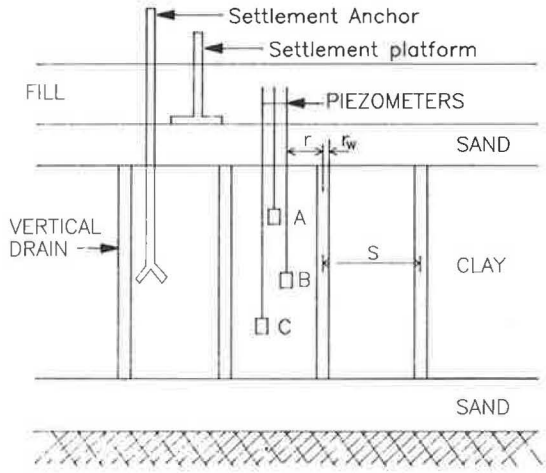

FIGURE 2 Schematic diagram showing typical instrumentation and nomenclature.

of vertical drainage, and caution must be used in the analysis and interpretation of results. An analysis of these drainage conditions has demonstrated that the average consolidation for the layer as represented by settlement with time curve for the top of the clay has approximately the same shape as average consolidation curve for the case of radial flow only and can be analyzed for an apparent coefficient of radial consolidation. The values of the backfigured coefficient of consolidation can be corrected for flow in the vertical direction (*7,8*).

Analyses Based on Settlements

There are several methods of analyzing data from areas containing vertical drains. All use the theory of equal strain consolidation. Substituting for U the expression for average percent consolidation developed by Barron (*2*) yields

$$\rho = \rho_i + \left[1 - e^{(-\lambda t)}\right]\rho_c \tag{2}$$

$$\rho = \rho_i - \rho_c\, e^{(-\lambda t)} \tag{3}$$

$$\lambda = \frac{2\,C_R}{F(n)r_e^2} \tag{4}$$

$$F(n) = \frac{n^2}{n^2 - 1}\ln(n) - \frac{3n^2}{4n^2 - 1} \approx \ln(n) - 0.75 \tag{5}$$

where

ρ_t = ultimate settlement = $\rho_i + \rho_c$,
C_R = apparent coefficient of consolidation in the radial direction,
n = r_e/r_w,
r_e = effective radius of the vertical drain, and
r_w = effective radius of the drain well.

The effective radius is related to the drain spacing, S, as shown in Figure 2, and equals $0.53S$ for a triangular pattern and $0.57S$ for a square pattern.

Rearranging Equation 3 and taking the natural logarithm of both sides,

$$\ln(\rho_t - \rho) = \ln(\rho_c) - \lambda t \tag{6}$$

Equation 6 indicates a straight line relation on a semilog plot between the natural logarithm of a settlement difference and the time. The exponential term having a base e in the basic equations often allows linearization by taking the natural logarithm of both sides of the equation. The reader is cautioned about making plots of data on graph paper having a common logarithm scale. To describe a plot on this type of paper requires the conversion $2.303\log(x) = \ln(x)$.

If the field observations are continued into the secondary compression region, estimation of the ultimate settlement can be made directly from the data. These cases are rare. For economic reasons, most observations are truncated while the clay layer is undergoing primary compression, and the ultimate settlement must be estimated from the data analysis. An example is the use of Equation 6. Values of ρ_t can be assumed. For each assumed value of ρ_t a straight line can be found to satisfy Equation 6. The goodness of fit for each straight line can be determined through the sum of the errors squared. The ultimate settlement yielding the minimum sum of the errors squared is considered the best fit. It is best to vary the size of the assumed ultimate settlement in a regular fashion. To begin with, a value for the ultimate settlement can be assumed larger than the last observed settlement and a least squares fit of the data to Equation 6 obtained (*9*). A slightly larger value of the ultimate settlement can be assumed and the data fitting and summation of the errors squared repeated. A second sum of the errors squared being smaller than the first indicates a better fit. If the process is repeated a number of times, a pattern as shown in Figure 3 usually develops (*5*). As successively larger values of the ultimate settlement are assumed, the sum of the errors squared first decreases then increases. The value of the ultimate settlement for the lowest value of the sum of the errors squared represents the best fit ρ_t. The best fit ρ_t is used in computing the best fit apparent coefficient of consolidation from the slope and Equation 5. A small computer program can be written to speed up this process.

Taking the first derivative of Equation 3 yields

$$\ln\left(\frac{d\rho}{dt}\right) = \ln(\lambda\rho_c) - \lambda t \tag{7}$$

Equation 7 indicates that if the logarithm of the slope of the settlement curve is plotted against time a straight line will

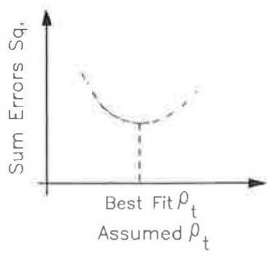

FIGURE 3 Typical plot of data as analyzed by Equation 6 for SP-11, Putnam Bridge.

result. The slope of the straight line, λ, is proportional to the coefficient of consolidation. The theory assumes that the coefficient of consolidation is constant. The slope of the settlement vs. time curve can be determined graphically or from a fitted polynomial (*7,10*). When the coefficient of consolidation decreases with increasing effective stress, the resulting plot is concave upward. To analyze data showing this trend requires an expression for the percent average consolidation that accounts for a decreasing coefficient of consolidation with increasing effective stress (*6*). The use of this approach is beyond the scope of this paper.

Each of these techniques has certain disadvantages. The search routine for Equation 6 occasionally does not converge. The graphical procedure may be considered cumbersome by some. Another method of addressing the data is to consider Equation 3 for successive settlements:

$$\rho_{n-1} = \rho_t - \rho_c\, e^{(-\lambda t_{n-1})} \tag{8}$$

$$\rho_n = \rho_t - \rho_c\, e^{(-\lambda t_{n-1})}\, e^{(-\lambda \Delta t)} \tag{9}$$

Subtracting Equation 8 from Equation 9 yields

$$\rho_n = m\rho_{n-1} + B \tag{10}$$

To use Equation 10, plot successive settlements observed at equal time increments as ρ_{n-1} vs ρ_n. Figure 4 shows a plot of the data for settlement platform SP-11 of the Putnam Bridge east approach fill. The plot results in a straight line, the slope m of which is related to the coefficient of consolidation:

$$m = \exp\left[-\frac{2\,C_r \times \Delta t}{r_e^2\, F(n)}\right] \tag{11}$$

The intercept is related to the ultimate settlement through:

$$\rho_t = \frac{B}{(1 - m)} \tag{12}$$

The results, using several of these techniques on the same data, are shown in Table 1. Settlement data from the east approach fill to the Putnam Bridge were analyzed using Equations 6, 7, and 10. As can be seen from Table 1, the three methods yield comparable results.

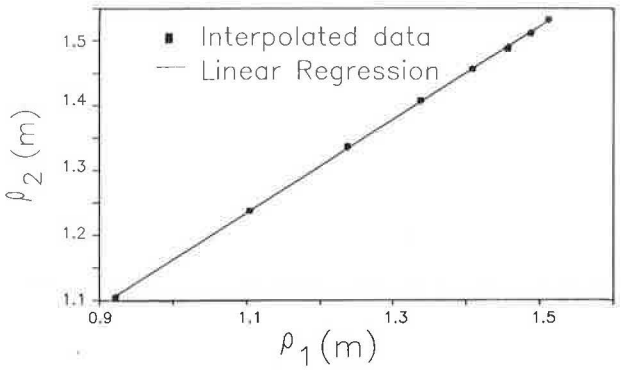

FIGURE 4 Typical plot of data as analyzed by Equation 11 for SP-11, Putnam Bridge.

TABLE 1 COMPARISON OF BACKFIGURED VALUES FROM FIELD DATA AT SP = 11

Coefficient of Consolidation (mm²/sec)	Ultimate Settlement (m)	Method
0.19	1.58	Equation 6
0.18	1.59	Equation 10
0.15	1.62	Equation 7
0.16	—	Equation 16

The data from SP-11 were not observed after equal time increments. The available data was interpolated at the required time intervals after fitting with a smooth curve using a personal computer version of POLYMATH (*10*), which runs on MS-DOS and requires a graphics card. The interpolated values of settlement were then used to complete the analysis. It would be better, when beginning a new project, to observe the settlements after equal time intervals.

Coefficient of Consolidation from Piezometer Readings

Data from piezometers reflecting dissipation in the radial direction, such as piezometer B in Figure 2, can be analyzed according to the equal strain theory of Barron (*2*) as:

$$\frac{u}{u_o} = A\; e^{(-\lambda t)} \tag{13}$$

$$A = \frac{1}{r_e^2 F(n)}\left[r_e^2 \times \ln\left(\frac{r}{r_w}\right) - \frac{r^2 - r_w^2}{2}\right] \tag{14}$$

where

u = excess pore pressure,
u_o = initial excess pore pressure, and
r = radius at which the piezometer is installed (see Figure 2).

Equation 14 indicates that, in cases where the coefficient of consolidation is constant, a plot of ln(u) against t yields a straight line, the slope of which can be used to compute the coefficient of consolidation thus:

$$\ln(u) = \ln(u_o A) - \lambda t \tag{15}$$

Piezometer data near SP-11 of the Putnam Bridge were analyzed by Equation 15 and also appear in Table 1. As can be seen from Table 1, the value of the coefficient of consolidation backfigured from the piezometer data agrees with the values backfigured from the settlement data. In this example the 28 m vertical thickness of clay, compared to the 3 m spacing of the drains, prevented the vertical dissipation of pore pressure from affecting the data significantly.

A plot of ln(u) against t for a piezometer may be concave upward for two reasons: (1) a coefficient of consolidation that is decreasing with the increase of effective stress; or (2) a piezometer that is strongly influenced by the vertical dissipation of pore pressures. In the former case, an instantaneous coefficient of consolidation can be obtained from a derivative of Equation 15 thus (*11*):

$$\frac{du}{dt} = -\lambda u \tag{16}$$

where du/dt is the derivative of the pore pressure with time.

The basic piezometer observations with time can be analyzed by several methods to satisfy Equation 16. The derivative can be approximated with the finite difference $\Delta u/\Delta t$ computed for successive observations, but more consistent results are obtained by using all of the data to develop a curve. The slope and values of the pore pressure can be determined graphically from this curve (*12*). Another method is to use POLYMATH to fit a polynomial smooth curve of best fit to the data points (*10*). A derivative of the resulting polynomial can be made by hand or with POLYMATH and the necessary values for Equation 16 computed. At each value of u, λ is computed from Equation 16 and the coefficient of consolidation estimated from Equation 5.

REDUCTION OF THE RESULTS

The apparent coefficient of consolidation and the ultimate settlement are the only two parameters that can be directly estimated from the field data. These results can be reduced into components only if additional assumptions are made. The apparent coefficient of consolidation analyzed from the settlement data can be split into true radial and vertical components with the aid of the approximation (*13*)

$$\frac{\bar{u}_R}{\bar{u}_o} = \frac{\bar{u}_r}{\bar{u}_o} \times \frac{\bar{u}_v}{\bar{u}_o} \tag{17}$$

where

$\bar{u}_o$ = average initial excess pore pressure,
$\bar{u}_R$ = average pore pressure indicated by the C_R backfigured from settlement data,
$\bar{u}_r$ = average pore pressure where the dissipation is only radial, and
$\bar{u}_v$ = average pore pressure where the dissipation is only vertical.

The values in Equation 18 can be approximated (*13*):

$$\exp\left[-\frac{2\,C_R \times t}{F(n)r_e^2}\right] = \frac{8}{\pi^2}\exp\left[-\frac{2\,C_r \times t}{F(n)r_e^2} - \frac{\pi^2\,C_v \times t}{4\,H^2}\right] \tag{18}$$

and further reduced to:

$$C_R = C_r + \frac{\pi^2}{4}\frac{F(n)}{2}\frac{r_e^2}{H^2}C_v \tag{19}$$

Equation 19 can be solved if the value of C_v or the ratio C_r/C_v is known. The best estimate of C_v would come from a value backfigured from field data collected close to the location at which you wish to apply Equation 19. If a laboratory value of C_v or an approximate ratio of C_r/C_v is used, the values computed with Equation 19 begin to be influenced by speculation rather than fact.

Similarly, the initial settlements can be extracted after a few additional approximations. The theory of consolidation was derived for instantaneous loading, but the sequence of filling in the field requires a number of days or months. Taylor developed a method of adjusting the time of filling to allow the theory to be used to compute settlements for field conditions (*14*). To use this approximation, the load vs. time curve must be able to be approximated by a straight line during the filling stage. An example is shown in Figure 1(a). The dotted line is an approximation of the filling stage. According to Taylor's approximation, the time of consolidation after the fill is complete is computed from the time middle of the filling stage. In this example, average consolidation after about 3.3 months from the beginning of filling are calculated:

$$U = 1 - e^{[-\lambda(t-\frac{t_c}{2}-B)]} \tag{20}$$

where $t_c/2$ equals one-half the estimated construction time and B equals a time adjustment to match the actual beginning of filling.

Equation 20 can now be used with settlement observations at various times after filling is complete to satisfy Equation 1 with the unknowns of ρ_i and ρ_c. Applying Equation 20 to Equation 1 at two well-spaced times allows an estimate of ρ_i and ρ_c, but the additional assumptions required to get to this point must be recognized.

AREA WITHOUT VERTICAL DRAINS

Piezometer Analysis

In areas without vertical drains, sufficient piezometers in each group should be spaced vertically between the drainage boundaries so that the readings can be used to estimate the isochrones within the layer as consolidation progresses. Normally three or more per line are required. These vertical lines of piezometers are usually placed near the centerline of the fill. The dissipation of pore pressures may be controlled predominately by vertical drainage or by a combination of vertical and horizontal drainage. In this technique, one dimensional consolidation in the vertical direction is assumed and the analyzed parameter is called the apparent coefficient of consolidation in the vertical direction, C_{va}. Piezometer groups placed at some distance laterally from the centerline may indicate a slightly different C_{va}, but an analysis to determine horizontal as well as vertical consolidation is beyond the scope of this paper.

In addition to the pore pressure readings, an estimate of the initial excess pore pressure isochrone must be made. This isochrone represents the pore pressures that would be present in the soil were the load applied instantaneously. This isochrone is normally found by calculating, according to some elastic solution, the increased stresses in the vertical direction from the applied load. Other approaches to computing pore pressures are of course possible.

An example of a pore pressure plot is shown in Figure 5. The initial excess pore pressure curve in Figure 5 was assumed equal to the increase in vertical stress. The percent average consolidation is found from Figure 5 by comparing the area under an isochrone to the area under the initial excess pore pressure isochrone with the equation:

$$U = 1 - \frac{A}{A_o} \tag{21}$$

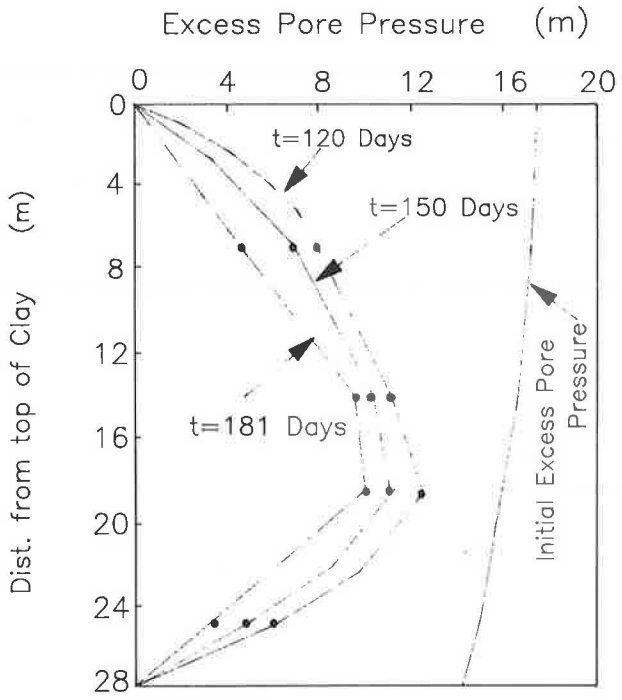

FIGURE 5 Plot of piezometer data for group near SP-66, Putnam Bridge.

where A equals the area under the isochrone at the time of interest and A_o equals the area under the initial pore pressure isochrone.

The area under the isochrones can be measured with a planimeter. Having an estimate of the average percent consolidation at several times allows the apparent coefficient of consolidation to be calculated from Terzaghi's one dimensional theory. For each percent average consolidation, the time factor T has a unique value (*1*). The isochrones occur at different times t. The change between isochrones is therefore represented by

$$\Delta T = \frac{C_{va}\Delta t}{H^2} \tag{22}$$

where H equals the maximum drainage path and Δt equals the change in time. The estimated values of the average percent consolidation can also be used in Equation 1 to determine the settlements.

Analysis Using Settlement Data

A derivation similar to that yielding Equation 11 can be made for areas without vertical drains (*15*). The resulting equation is

$$\rho_n = C\rho_{n-1} + D \tag{23}$$

Equation 23 is applied in the same manner as Equation 10, plotting successive observations of the settlement after equal time increments. The slope c of the resulting straight line can be used to estimate the apparent coefficient of consolidation thus:

$$\ln(C) = -\frac{G\,C_{va}}{H^2} \times \Delta t \tag{24}$$

where G equals a constant. The values of G suggested by Asaoka (*15*) were found by laboratory test to yield values of C_v for one dimensional consolidation that are too low. A derivation similar to Equations 8, 9, and 10 using Terzaghi's theory for average percent consolidation for the one dimensional case of vertical flow yielded a value of $G = 2.47$. This value of G appears appropriate, based on initial experimental results. The ultimate settlement is calculated from:

$$\rho_t = \frac{D}{1 - C} \tag{25}$$

An example of the results of these two analytical approaches is shown in Table 2. Of the two approaches, the one involving Equation 23 requires fewer assumptions and approximations. Settlement platforms are subject to fewer problems than piezometers, and analysis of settlement data often develops results that elicit more confidence.

FILLS AT THE PUTNAM BRIDGE

General Information

The Putnam Bridge crosses the Connecticut River south of Hartford between the towns of Glastonbury and Wethersfield, Conn. To attain the proper navigational clearance over the river, the approach fills on the Glastonbury side required a height of 17 m. The soil profile on which this fill was placed is shown in Figure 6. As can be seen from Figure 6 the site is underlain by about 28 m of varved clay. The bridge was designed and constructed for the Greater Hartford Bridge Authority in 1958. The consultants were Gookind and O'Dea of Hamden, Conn. The analysis reported here resulted from a research project for the Connecticut Department of Transportation at the time that a second crossing of the river was being planned several hundred feet south of the bridge approach described here. The purpose of the research was to reduce the amount of required laboratory testing by analyzing the available field data.

TABLE 2 COMPARISON OF BACKFIGURED VALUES FROM FIELD DATA AT SP = 66

Coefficient of Consolidation (mm²/sec)	Ultimate Settlement (m)	Method
5.8	0.57	Equations 1 and 21
7.0	0.40	Equations 23, 24, and 26

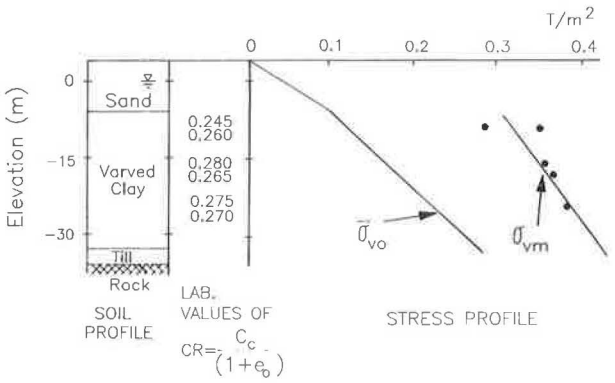

FIGURE 6 Soil profile at the Putnam Bridge.

It was desirable to open the bridge as soon as possible for economic reasons. Berms were used beside the high fill of the east approach to insure stability while allowing the filling to proceed as quickly as possible. Figure 7 shows the locations of the settlement platforms and piezometer groups in the area containing vertical drains. The sand drains were 0.46 m in diameter and spaced at 3.0 m centers in the western end, where the fill was highest. The spacing of the drains was increased to 4.6 m centers as the required fill height decreased toward the east. The sand drains were installed with hollow stem augers (*16*). The settlement platforms were placed on the original ground surface. It was important to monitor the progress of consolidation and settlement to insure that the bridge could open at an early date. However, premature paving of the approach would lead to increased maintenance costs in the future due to excessive post-construction settlements. As a result, careful monitoring of the consolidation process was necessary.

A plan of the portion of fills in which no vertical drains were used is shown in Figure 8. This figure also shows the locations of the settlement platforms and piezometer groups. The piezometers were the Casagrande hydraulic type. The contractor was responsible for the installation. The instruments were monitored by the consultant. It is not known what type of data analysis, if any, was planned at the time of construction.

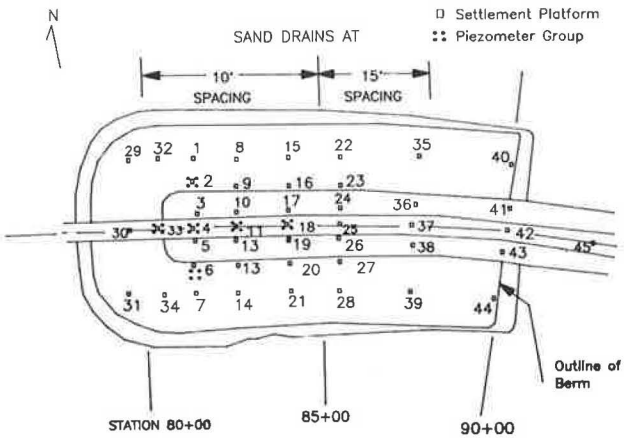

FIGURE 7 Layout of instrumentation at the area with vertical drains at Putnam Bridge (note location of SP-11 piezometer group).

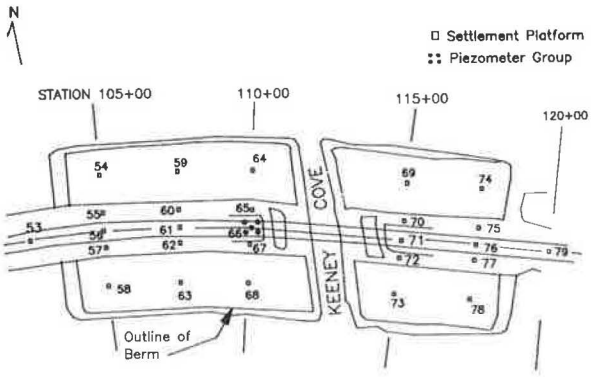

FIGURE 8 Layout of instrumentation at the area without vertical drains at Putnam Bridge (note location of SP-66 and piezometer group).

Varved clay of the Connecticut River Valley in the vicinity of Hartford often shows a laboratory coefficient of consolidation of about 1.1 mm²/s in the overconsolidated range. Larger values often observed in the field have been attributed to the dissipation of pore pressures along the horizontal varves and occasional sand seams (*17*). Horizontal dissipation can account for the values of C_{va} shown in Table 2.

Analysis of Data

The mortality of piezometers was great in the vicinity of the high fills due to the large settlements. Some piezometers showed little dissipation after filling, indicating that they had been pinched off. Only the piezometers showing regular behavior were selected for analysis. Review of the piezometer data found only two sets of piezometers showing the regular dissipation expected in consolidation. Fortunately, one set near settlement platform SP-11 was in the area with vertical drains, and one set near settlement platform SP-66 was in the area having no vertical drains. Settlement platforms are less susceptible to problems. Most of the platforms shown in Figure 7 and Figure 8 survived the construction process and their data could be analyzed.

The appropriate piezometer readings and all settlement platform data readings were analyzed by the techniques described here. Settlement analyses in the sand-drained area were made with the graphical technique and Equation 7, as well as Equation 6 and Equation 11. The three approaches gave comparable results. The analyzed values for the coefficients of consolidation are shown in Figure 9. There was no attempt to correct the backfigured coefficient of consolidation for vertical flow because of the thickness of the clay deposit.

As can be seen from Figure 9, there appears to be a relation between the spacing of drains and the coefficient of consolidation backfigured from the field data. The values are essentially below 10 m²/year for the drains on 3.0 m spacing, regardless of fill height, and 10 to 30 m²/year for the drains at 4.6 m spacing. Similar phenomena have been observed previously (*18*). The differences have been attributed to disturbance that has more effect at the smaller spacing.

The ultimate settlements are plotted against fill height in Figure 10. The data in Figure 10 show that the area having drains with 3.0 m spacing experienced more settlement under

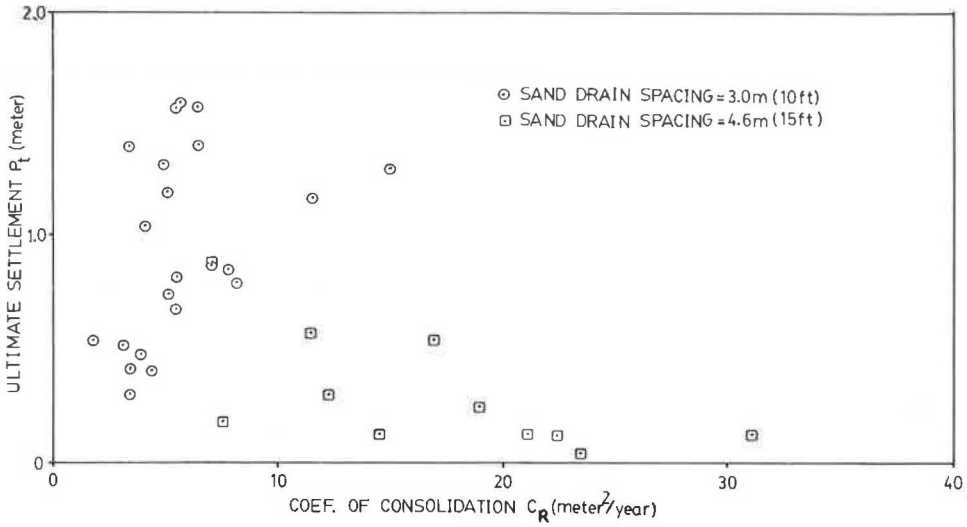

FIGURE 9 Plot of the backfigured coefficient of consolidation versus the ultimate settlement from the settlement platforms in the vertically drained area.

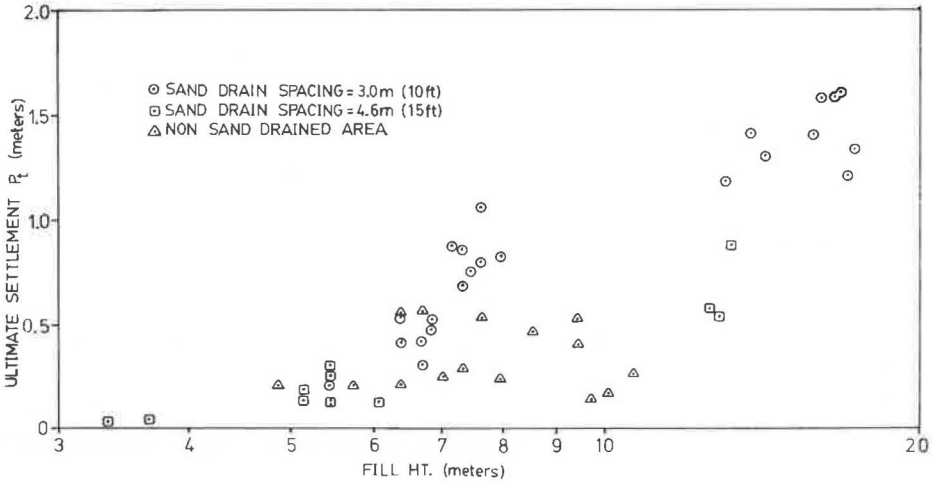

FIGURE 10 Plot of backfigured ultimate settlement versus the fill height over the settlement platforms.

a given fill height than either the area with drains at 4.6 m spacing or the undrained area. This might also be the result of disturbance. The settlement contours are plotted in Figure 11 and Figure 12. As can be seen from these two figures, use of these techniques gave a complete picture of the field behavior. The backfigured settlements are regular with the greatest settlement occurring under the highest part of the fill.

CONCLUSIONS

1. Field consolidation data can be analyzed independently of laboratory data.
2. Small strain theory for areas with and without vertical drains is a valid approximation to the field behavior.
3. Field settlement data can be analyzed for both apparent coefficient of consolidation and ultimate settlement.
4. Piezometer data can be analyzed for the case of constant and decreasing apparent coefficient of consolidation.
5. Vertical drains at 3.0 m spacing at the Putnam Bridge showed a smaller apparent coefficient of consolidation than the drains spaced at 4.6 m.
6. The closer-spaced drains also showed higher settlements than the wider-spaced drains under equal heights of fill.

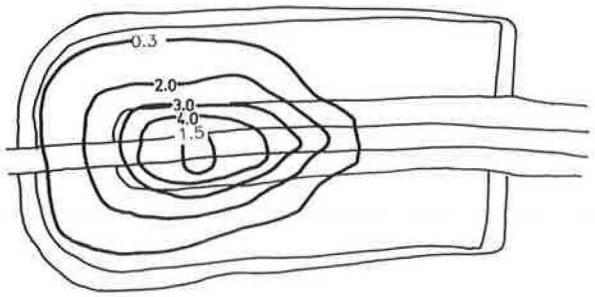

FIGURE 11 Ultimate settlement contours, in meters, for the area with vertical drains.

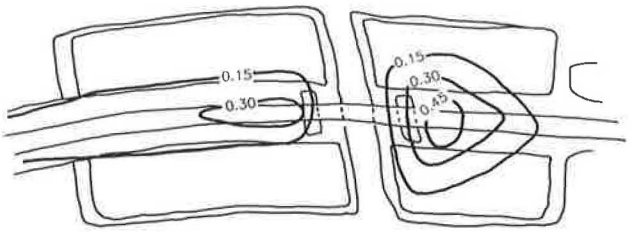

FIGURE 12 Ultimate settlement contours, in meters, for the area without vertical drains.

ACKNOWLEDGMENT

The fundamental techniques described here were developed on a research project sponsored by the Joint Highway Research Advisory Council of the Connecticut Department of Transportation (ConnDOT) and the Civil Engineering Department of the University of Connecticut. The assistance of the Soils Division of ConnDOT in supplying the data is gratefully acknowledged.

REFERENCES

1. K. Terzaghi. *Theoretical Soil Mechanics*. John Wiley and Sons, New York, 1943.
2. R. A. Barron. Consolidation of Fine-Grained Soils by Drain Wells. *ASCE Trans.*, Vol. 113, 1948, pp. 718–742.
3. T. W. Lambe. Predictions in Soil Engineering. *Geotechnique*, Vol. 23, No. 2, 1973, pp. 149–202.
4. Z. Kyfor, J. Masi, and R. Gemme. Performance of a Prefabricated Vertical Drain Installation Beneath an Embankment. In *Transportation Research Record 1159*, TRB, National Research Council, Washington, D.C., 1988, pp. 47–57.
5. R. P. Long and W. H. Hover. *Statistical Data Analysis for Sand Drained Areas*. Report No. C.E. 80-137. Department of Civil Engineering, University of Connecticut, Storrs, Conn., 1980.
6. R. P. Long and W. H. Hover. Performance of Sand Drains in a Tidal Marsh. *Proc., International Conference on Case Histories in Geotechnical Engineering*, Vol. III, St. Louis, 1984.
7. R. P. Long and P. J. Carey. Analysis of Settlement Data from Sand-Drained Areas. In *Transportation Research Record 678*, TRB, National Research Council, Washington, D.C., 1978, pp. 36–40.
8. L. Erikson and A. Ekstrom. The Efficiency of Three Different Types of Vertical Drain—Results from a Full-Scale Test. *Proc., 8th European Conference on Soil Mechanics and Foundations Engineering*, Vol. 2, Helsinki, 1983, pp. 605–610.
9. J. B. Kennedy and A. M. Neville. *Basic Statistical Methods for Engineers and Scientists*, 2nd ed. Thomas Y. Crowell Company, New York, 1976.
10. *POLYMATH (TM) Curve Fitting Program*, prelease version 2.0. Control Data Corporation, Minneapolis, Minn., 1986.
11. D. P. Nicholson and R. J. Jardine. Performance of Vertical Drains at Queenborough Pass. In *Vertical Drains* (I.R. Wood, ed.), Thomas Telford Ltd., London, 1982, pp. 67–90.
12. R. P. Long. Discussion of Performance of Vertical Drains at Queenbrough Pass. In *Vertical Drains* (I.R. Wood, ed.), Thomas Telford Ltd., London, 1892, pp. 146–7.
13. R. F. Scott. *Principles of Soil Mechanics*. Addison Wesley, Reading, Mass., 1963.
14. D. W. Taylor. *Fundamentals of Soil Mechanics*. John Wiley and Sons, New York, 1948.
15. A. Asaoka. Observational Procedure of Settlement Prediction. *Soils and Foundations*, Vol. 18, No. 4, 1978.
16. R. E. Landau. Method of Installation as a Factor in Sand Drain Stabilization Design. In *Highway Research Record 133*, TRB, National Research Council, Washington, D.C., 1966, pp. 75–97.
17. L. Casagrande and S. Poulos. On the Effectiveness of Sand Drains. *Canadian Geotechnical Journal*, Vol. 6, 1969, pp. 287–326.
18. Moran, Proctor, Mueser, and Rutledge. *Study of Deep Soil Stabilization of Vertical Drains*. Bureau of Yards and Docks, U.S. Department of the Navy, Washington, D.C., 1958.

Publication of this paper sponsored by Committee on Transportation Earthworks.

Field Performance of a Geogrid-Reinforced Embankment

TARIK HADJ-HAMOU, REDA M. BAKEER, AND WILLIAM W. GWYN

The field performance of a geogrid-reinforced levee test section built in Marrero, Louisiana, is discussed. The section was a full-scale model for a 1-mi-long levee built to protect a subdivision in Marrero from hurricane tidal waves. The section was built and monitored to assess the behavior of reinforced embankments on the extremely soft clays found in the Lower Mississippi Valley. The section was fully instrumented with inclinometers, settlement plates, and piezometers. Two rolls of geogrids were instrumented with strain gauges. Measurements were taken during and for a long period of time after construction. Field measurements included horizontal movements, vertical settlements, pore pressures, and strains in geogrids. Analyses of the data from the test section indicate that the geogrids allowed the use of smaller stabilizing berms. This conclusion was applied to the final design, resulting in appreciable savings. In addition, such large-scale tests are useful in developing design guidelines for the use of geosynthetics in protection levees in the Lower Mississippi Valley region.

Hurricane protection levees built in Louisiana must follow the guidelines of the Corps of Engineers (COE). These guidelines stipulate the height of the levee and the minimum factors of safety against stability failures. When a new levee was under consideration in Marrero, Louisiana, COE recommended that the crown of the levee be at least 3 ft above the standard project hurricane (SPH) tide level and that the slopes have a factor of safety of at least 1.3. Considering the extremely soft foundation soil at the site, these guidelines produced a levee ranging from 10 to 11 ft in height with rather flat slopes and large stabilizing berms.

To minimize the total cost of the project, the West Jefferson Levee District commissioned Eustis Engineering to examine three possible designs: (1) a standard COE uncompacted fill levee constructed from borrow cast from adjacent borrow pits, (2) a standard COE semicompacted fill levee constructed of hauled clay fill from an outside borrow source, and (3) a semicompacted reinforced fill. The three proposed cross sections are shown in Figure 1. The advantages of using as narrow a levee as possible are the lesser quantity of fill, the smaller base width of the levee, and the smaller amount of wetland destroyed by construction. The last two advantages stem from the location of the proposed levee with respect to an existing drainage canal (Figure 1), which will force the construction of the embankment in the marsh. The subdivision is situated to the east of the drainage canal and is to be protected from hurricane tidal wave coming from the marsh. The minimum distance between the centerline of the levee and the edge of the canal, the quantity of fill material per foot of levee, and base widths for each design are summarized in Table 1.

In this particular case, the distance between the swamp and the subdivision is such that Design 1 would require reclaiming some swampland, at a considerable financial and ecological cost. It was felt that even with the additional expense of the reinforcement, the third option would be more economical and protect the environment. To assess the validity of the solution, it was decided to build a test section and monitor its behavior with a full array of instrumentation.

DESIGN OF THE TEST SECTION

The test section is now part of the north-south reach of the finished levee and was constructed in a marsh. It is located in the town of Marrero in Jefferson Parish (county) on the west bank of the Mississippi River. COE recommended using a SPH tide level of 7 ft National Geodetic Vertical Datum (NGVD) for that particular reach, yielding a crown elevation of 10 ft after all settlements have taken place.

Soil Conditions

The area of interest is located in the southeastern part of the State of Louisiana. It is on the central Gulf coastal plain on the modern delta of the Mississippi River, which projects into the Gulf of Mexico. The depositional history of interest for engineering application is from the Pleistocene to present time, since most of the sediments at the site were deposited during that period. The sediments are typically divided into natural levees, point bar, and backswamp deposits. The natural levees are the slightly elevated ridges that occur on both sides of the river. Point bar deposits are the direct results of the lateral migrations of the river. Over the past 5,000 years, seven major deltas are discernible in coastal Louisiana (*1*). During the migration process, erosion occurs from the banks and the coarsest materials are redeposited immediately downstream at the convex side of the river banks. Backswamp deposits are formed by the deposition of sediments in shallow ponded areas of overbank flows. They consist primarily of thinly laminated clays and silts that sometimes have a high organic content. Initial urbanization of the New Orleans region followed the natural levees and point bar deposits. However, as the city of New Orleans has expanded, it has become more and more common to build on marginal sites such as swampy and marshy deposits. The site of interest is located in a low-lying cypress swamp area subject to inundation from tidal flows.

T. Hadj-Hamou and R. M. Bakeer, Department of Civil Engineering, Tulane University, New Orleans, La. 70118. W. W. Gwyn, Eustis Engineering, Metairie, La. 70002.

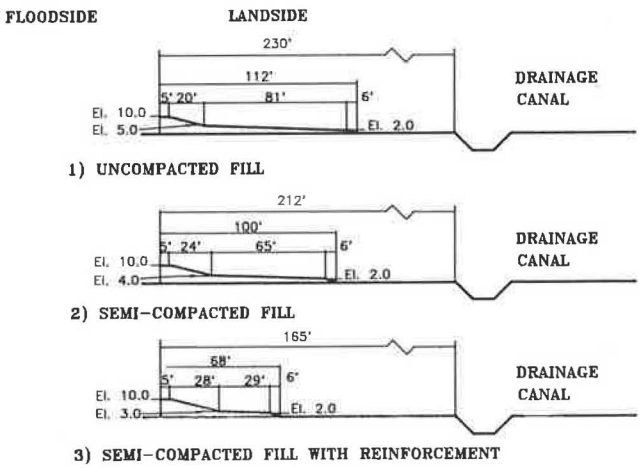

FIGURE 1 Cross sections of the alternative designs.

A total of 21 borings were drilled between January 9 and February 4, 1986, along the length of the proposed levee. The test section was constructed between Borings 12 and 13. The soil properties for the design of the test section were established from Borings 10 through 14. Boring 12 is a 5 in. diameter boring drilled to a depth of 100 ft. Borings 10, 11, 13, and 14 are 3 in. diameter holes drilled to a depth of 50 ft. Visual classification was performed at the site by a technician, and undisturbed samples were taken to the laboratory. The testing program consisted of Atterberg limits, unconfined compression tests, unconsolidated undrained triaxial tests, consolidated undrained triaxial tests, minivane tests, and consolidation tests.

The soil profile at the test section consists of 15 ft of extremely soft to very soft brown and gray clay, organic clay, and humus. This deposit is underlain by strata of very soft to soft gray clay with silt pockets to a depth of approximately 55 ft below the existing ground surface. From that depth and continuing to a depth of approximately 76 ft is a stratum of medium stiff gray clay with sand pockets and shell fragments. Pleistocene deposits are encountered at a depth of 76 ft. Pleistocene deposits are strata of stiff to very stiff overconsolidated gray and tan clays with sand lenses and clayey sand layers extending to a depth of 87 ft. These deposits form the foundations of most heavy structures in the New Orleans area. Figure 2 shows the profile along Borings 10 through 14.

When not flooded, the depth of ground water is at or very near the ground surface. The natural water content and wet unit weights are plotted versus depth in Figure 3. The large variation in water content (30 to 450 percent) and wet unit weight (67 to 115 pcf) are typical of such organic and humus layers. These extremely soft soils are responsible for most of the settlement in the area. The water content in the clay

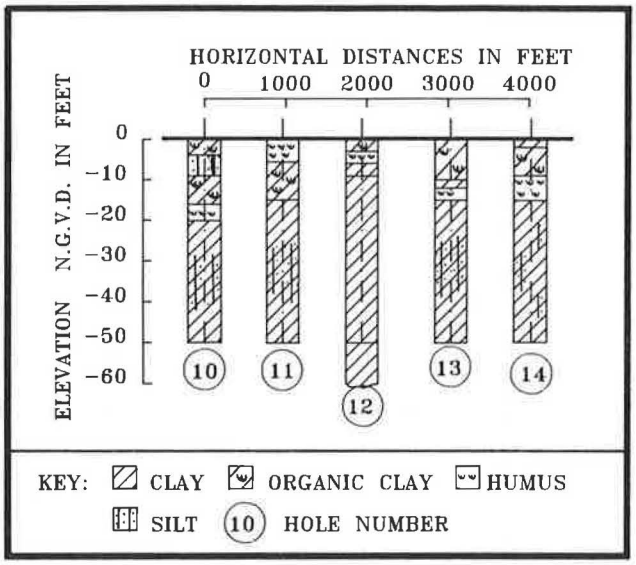

FIGURE 2 Soil profiles along Borings 10 through 14.

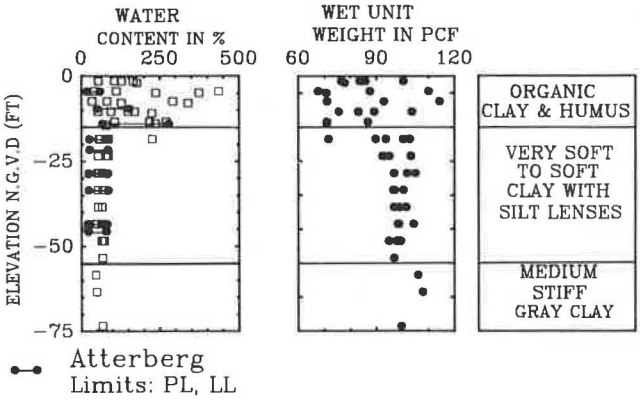

FIGURE 3 Natural water content and saturated unit weights.

stratum varies from about 40 to 80 percent. The Atterberg limits obtained on a few samples are also reported in Figure 3. Results from all shear strength tests are plotted in Figure 4. For design purposes, the 55 ft of soft material beneath the levee were divided into three sublayers:

1. a 15 ft thick layer of organic clay and humus with constant strength equal to 150 psf;
2. a 5 ft layer of very soft clay with constant undrained shear strength of 150 psf; and
3. a 35 ft soft to medium stiff clay with undrained shear strength increasing from 150 psf at elevation −20 ft to 400 psf at elevation −55 ft.

TABLE 1 CHARACTERISTICS OF THE THREE CROSS SECTIONS

Option Number	Levee Type	Distance from Drainage Canal (ft)	Quantity of Fill (yd^3/ft)	Base Width (ft)
1	Uncompacted	230	36.7	224
2	Semicompacted	212	31.7	200
3	Reinforced	165	22.8	136

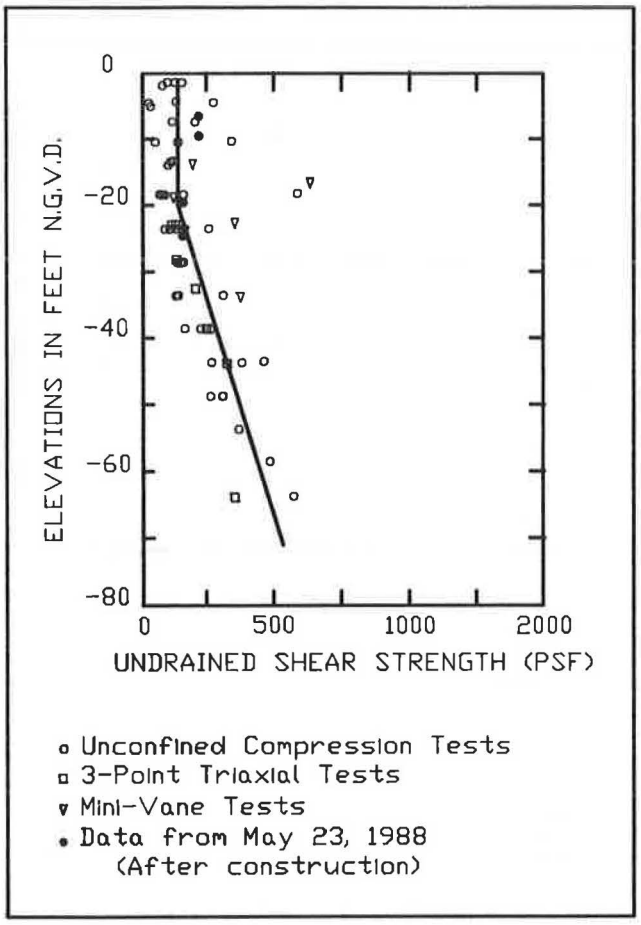

FIGURE 4 Shear strength profile.

Design and Stability Analyses

The test section is 350 ft long, 10 ft high, 10 ft wide at the crown, and 136 ft wide at the base, including the two stabilizing berms. The levee is constructed with a central core of hauled semicompacted clay fill placed on a working pad of hauled sand fill. The stabilizing berms are constructed of hauled uncompacted clay fill placed from the sand pad. The slopes of the core are 1 vertical to 4 horizontal and that of the berms are about 1 vertical to 3 horizontal, as shown in Figures 5 and 6. Figure 5 is a cross section of the test section and shows the location of the reinforcement, the type of fill material used, and the stratification beneath it. Figure 6 is a plan view of the test section. The reinforcement consists of two layers of high-density polyethylene Tensar SR2 (UX1500) geogrids located at elevation +1.5 and +3.0 NGVD. The design parameters of the three fills used to build the test embankment, the foundation soils, and the reinforcements are summarized in Table 2.

The stability of the levee was analyzed using the COE Lower Mississippi Valley Division Method of Planes Analysis, also commonly known as the Wedge Method (*2*). The levee was designed for the end of construction case utilizing a factor of safety of 1.3 for the levee itself and a factor of safety of 1.5 for analyses extending to the adjacent canal. The method is a limit equilibrium analysis and expresses the factor of safety as the ratio of the sum of the resisting forces, R, over the sum of the driving forces, D. The reinforcement is included as a tensile force, T, added to the resisting forces to bring the factor of safety to the target value. Initial analyses were performed on the unreinforced section to determine the required tensile strength of the geogrids. The critical sections are shown on Figure 7 and the factors of safety listed in Table 3. The tensile

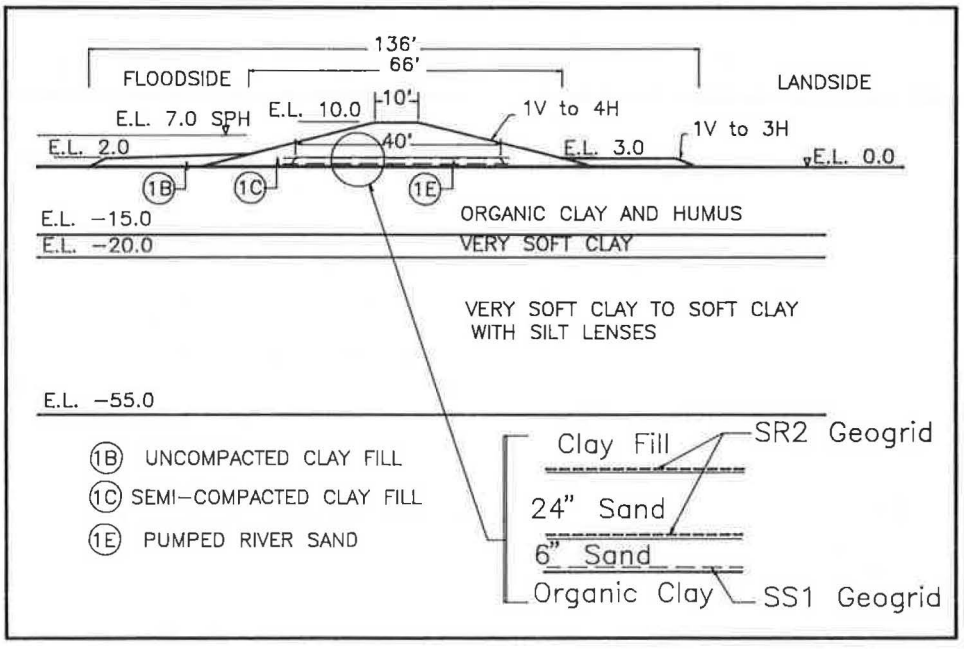

FIGURE 5 Cross section of test section.

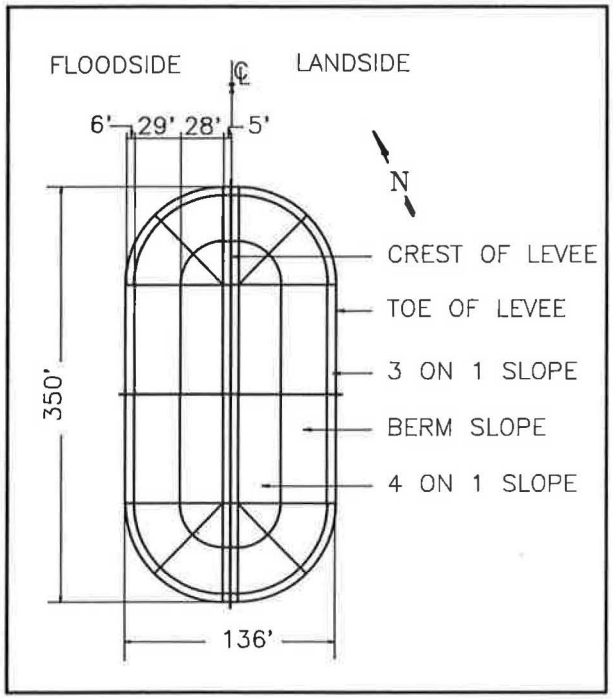

FIGURE 6 Plan view of the test section.

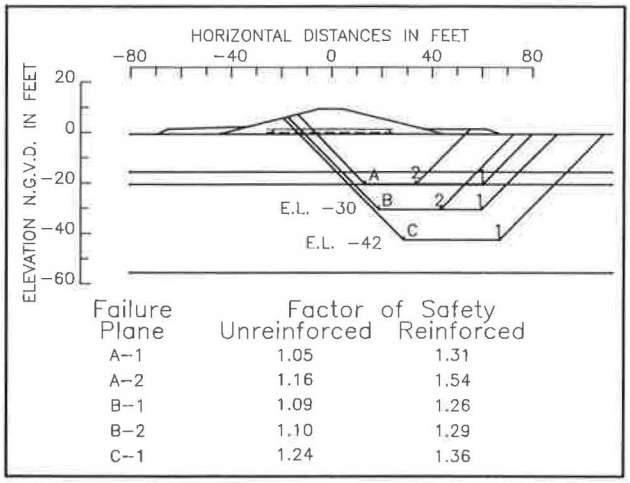

FIGURE 7 Critical failure surfaces.

strength, T, needed to raise the factor of safety to 1.3 is calculated as follows:

$$T = 1.3\,D - R \quad (1)$$

The length of embedment of the geogrids was computed to ensure adequate factor of safety against pullout. The factors of safety of the previous section computed with the reinforcement are listed in Table 3.

Because the failure masses are expected to move towards the landside (east) of the levee, both layers of geogrid were placed asymmetrically to ensure proper anchoring. The bottom layer is 49.2 ft long and starts 25 ft left of the section centerline, whereas the top layer is 32.8 ft long and starts 18.4 ft left of the centerline.

TABLE 3 FACTOR OF SAFETY OF TEST SECTION

Failure Plane	Factor of Safety	
	Unreinforced	Reinforced
A-1	1.05	1.31
A-2	1.16	1.54
B-1	1.09	1.26
B-2	1.10	1.29
C-1	1.24	1.36

TABLE 2 MATERIAL DESIGN PARAMETERS

Stratum Number	Material	Saturated Unit Weight (pcf)	Cohesion (psf)		Friction Angle (degrees)
			Center	Bottom	
1B	Clay Fill A-6 or A-7 Hauled Uncompacted	100	200	200	0
1C	Clay Fill A-6 or A-7 Hauled Semicompacted	105	400	400	0
1E	Sand Fill A-3 Trucked Pumped River Sand	120	0	0	30
2	Humus/Organic Clay	74	150	150	0
3	Clay	95	150	150	0
4	Clay	98	275	400	0
—	Geogrid Tensar SR2 (UX1500)	Ultimate strength (at 15 percent strain):			6500 lbs/ft
		Tensile strength at 2 percent strain:			2055 lbs/ft
		Tensile strength at 5 percent strain:			3900 lbs/ft
		Long-term design load:			2350 lbs/ft
		Extension at 40 percent of maximal load:			3 percent
		Tensile modulus at 2 percent:			102,7506 lbs/ft
—	Geogrid Tensar SS1 (BX1100)	Ultimate strength (at 14 percent strain):			840 lbs/ft
		Ultimate strength at 2 percent strain:			280 lbs/ft
		Ultimate strength at 5 percent strain:			570 lbs/ft

Construction

Construction began on October 26, 1987. With the water table at ground surface elevation, the layer of organic clay and humus was extremely soft and workmen would sink to their knees while walking around. A base reinforcement of Tensar SS1 (BX1100) geogrid was laid on the ground surface to improve working conditions. The SS1 was rolled parallel to the test section centerline under the core and the access road centerline. The base reinforcement was rolled perpendicular to the levee centerline beneath the uncompacted stability berms. A 3 ft overlap was used for adjacent panels of SS1. The SS1 geogrids were not included in the stability analyses of the levee section.

A layer of sand about 6 in. thick was laid on top of the SS1 grid to form a base for the first layer of SR2 geogrid. The sand was trucked to the site, dumped and dozed initially with a small track dozer (John Deere 450). However, this dozer tended to sink and create a large mud wave; it was eventually replaced by a larger dozer (Case 850C). An additional 2 ft of sand was then hauled over the geogrid layer to form the access road for construction of the berms and slopes of the levee.

The second layer of SR2 was laid on the sand, and construction proceeded with hauling of the clay fill. The SR2 grids were rolled perpendicular to the centerline of the levee in the main part of the section and parallel to the centerline at both ends. Adjacent strips of SR2 were rolled butt to butt and not overlapped. The clay was hauled from the stockpile using five dump trucks and pushed in place using two dozers (Case 1150C and 450C). The only compaction effort applied to the clay fill was that of the earthmoving equipment. This is common practice for the levees built under COE supervision. Experience has shown that adequate compaction is obtained. The construction history of the test section is summarized in Table 4.

TABLE 4 CONSTRUCTION STAGES

Date (1987)	Construction Activity
10-26	Access road graded
10-27	SS1 Roll placed at elevation 0.0 ft
10-28	Sand hauled on top of SS1
10-29 to 10-30	1.5 ft sand blanket built
10-31	First layer of SR2 installed at elevation +1.5 ft LADOTD installs the two settlement plates
11-1 to 11-2	Sand hauled to elevation +2.0 ft Clay hauled to build sides of levee
11-3 to 11-4	Sand blanket at elevation +3.0 ft
11-5 to 11-7	Clay hauled for construction of levee and berms
11-8 to 11-11	No construction work
11-12 to 11-13	Construction of berms
11-14 to 11-18	No construction work
11-16	COE installs the four piezometers
11-17	COE installs the three inclinometers
11-19	Second layer of SR2 installed at elevation +3.0 ft
11-20	Clay hauled to build levee
11-21 to 11-22	No construction work
11-23	Levee brought up to elevation +5.0 ft
11-24 to 11-25	Levee brought up to elevation +7.0 ft
11-26 to 11-29	No construction work
11-30	Levee brought up to elevation +9.5 ft
12-1	No construction work
12-2	Levee brought up to grade and shaped (end of construction)

Settlement Analyses

Most of the settlement of the test section will be caused by compression of the soft foundation soils. Three consolidation tests were performed by Eustis Engineering on samples recovered from depths of 14, 23.5, and 43.5 ft in Boring 14. The first sample was from the highly organic clay layer with initial water content of 258 percent, void ratio of 6.43, and saturated unit weight of 74 pcf, and which showed tremendous compressibility. The other two samples were from the underlying soft clay and exhibited less compressibility. A fourth consolidation test was performed by COE on a sample recovered from the hole drilled for inclinometer I-1 (see Figure 8 for location).

Settlement of the levee was estimated using Terzaghi's one dimensional consolidation theory and the results of the consolidation tests. It was computed that about 6 ft of settlement would take place under the crown of the levee and about 1.6 ft at the toe of the berms. About 4.5 ft of the total crown settlement is expected to occur in the organic layer. Further, given the extreme softness of the organic layer, it was anticipated that up to 2 ft of settlement will occur very rapidly, some of it during construction. Consequently, a new lift of fill will have to be added to bring the levee up to the required 10 ft. This aspect of the project is discussed further in a later section of this paper. The coefficient of consolidation of the soft clay was computed to be 10.1 ft^2/yr.

INSTRUMENTATION

Rationale

The purpose of the test section was to investigate the feasibility of using geogrids for the Louisiana Department of Transportation and Development (LADOTD) and the West Jefferson Levee District. An ancillary purpose was to demonstrate compliance with applicable COE design criteria. The concern of these agencies is the stability of the constructed levee and its ability to perform adequately if a hurricane hits the area. Stability means that no failure mechanism such as those examined above should develop below ground surface and that the geogrids should not be stressed near their ultimate capacities. Consequently, it was decided to monitor the lateral movement below ground surface and the strains in the geogrids. Ability to perform adequately means that the crown of the levee should be at the prescribed SPH tide level. Consequently, it was decided to monitor vertical movements of the levee and pore pressure throughout the foundation to predict future settlement and estimate gain in shear strength with time.

Layout

The instrumentation package consists of 3 inclinometers, 2 settlement plates, 4 piezometers, and 34 strain gauges installed on the geogrids. Figure 8 shows the layout of the geotechnical

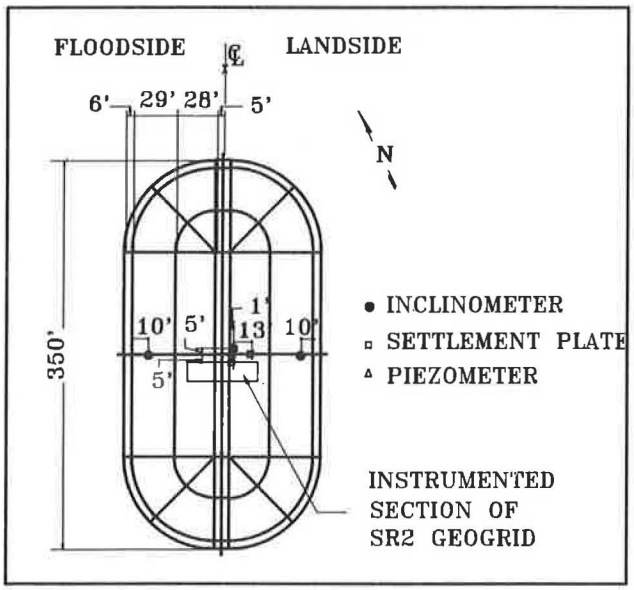

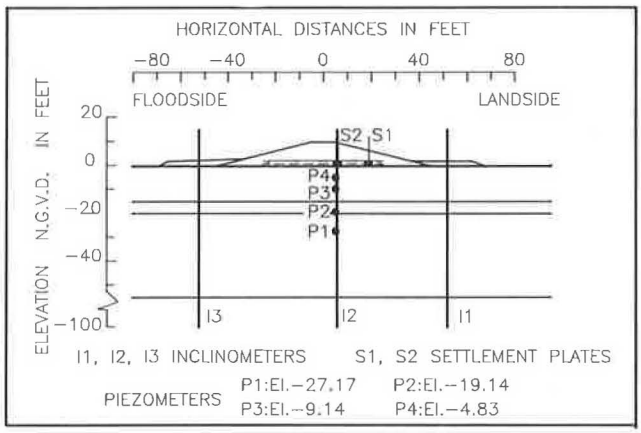

FIGURE 8 Layout of the instrumentation: (*top*) plane view, (*bottom*) cross section.

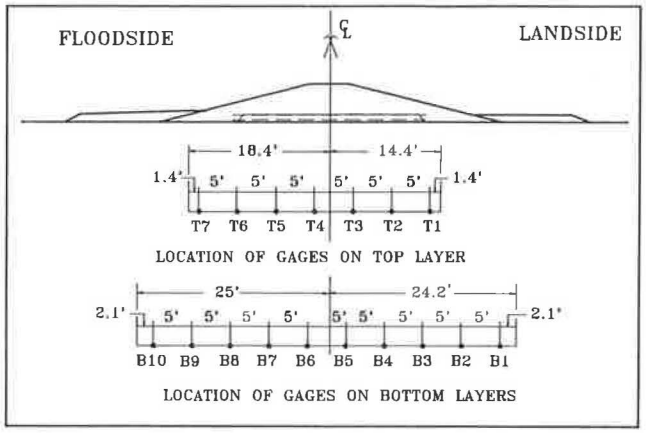

FIGURE 9 Location of the strain gauges on the geogrid.

TABLE 5 SUMMARY OF INSTRUMENTATION INSTALLATION AND MONITORING

Instrument	Installed by	Monitored by
Inclinometers	COE	EE
Piezometers	COE	LTRC
Strain gauges	LTRC	LTRC
Settlement plates	LADODT	LTRC

instrumentation installed at the test section. Figure 9 shows the position of the strain gauges on the two layers of Tensar SR2 geogrid. The installation and monitoring of the instruments was a collaborative effort of four agencies: COE, the Louisiana Transportation Research Center (LTRC), LADOTD, and Eustis Engineering (EE), as summarized in Table 5.

Inclinometers

The inclinometers (SINCO Model 50320 probes) were installed by COE at the locations shown on Figure 8. EE monitored and reduced the data from the inclinometers using a magnetic tape recorder and reduction program. The three 3.14 in. tubes are located on a line across the test section and extend 100 ft below the original ground surface. Inclinometer I-1 is located on the landside (east side) 52 ft away from the centerline of the levee; inclinometer I-3 is placed symmetrically on the floodside (west side) of the levee; and inclinometer I-2 is located 6 ft east of the centerline of the levee and 5 ft north of the center of the test section.

The specifications called for the grooves in tubes to be oriented parallel and perpendicular to the long axis of the levee. However, the tubes for inclinometers I-1 and I-2 were not installed properly, and the direction of the grooves are at angles of 12 and 20 degrees counterclockwise, respectively. Inclinometer I-2 was hit during construction and the deflections recorded in the first 10 ft may not be representative of actual displacements.

Piezometers

The four piezometers were 18 in. long, with 2 in. diameter slotted (0.01 in.) screens and 0.75 in. diameter risers. They were installed by COE and monitored by LTRC. They are set 6 ft east of the crown centerline on the middle section of the levee at elevations −27.17 (P-1), −19.14 (P-2), −9.64 (P-3), and −4.83 (P-4) ft NGVD. The piezometers tips were placed in a 6 in. diameter hole and backfilled with 4 ft of concrete sand.

Settlement Plates

The settlement plates consisted of 2 ft by 2 ft by 0.25 in. wrought iron plates with 2.5 in. riser pipes. Two plates were installed on a sand blanket at elevation +1 ft NGVD by the LDOTD and monitored by LTRC. Plate S-1 is set 19 ft east of the levee crown along the short axis. Plate S-2 is located 5 ft south of the short axis and 6 ft east of the levee crown centerline.

Strain Gauges

The Louisiana Transportation Research Center installed and monitored the strain gauges on the geogrids. The gauges (Micro Measurement Model No. CEA-13-250UM-350, using M-Bond GA-7 adhesive and 326-D-SV wire leads) were installed on panels of primary reinforcement (SR2). The exact locations of the gauges are shown in Figure 9. Note that there is a top gauge and a bottom gauge at each location.

OBSERVED PERFORMANCE

In the following discussion the reader is referred to Figure 8 for the direction of the readings. It is assumed that the levee runs north-south, and consequently the floodside is located on the west side of the levee and the protected or landside is on the east side of the levee.

Lateral Movement

The observed lateral displacements for the three inclinometers are given in Figures 10 to 12. The first measurements were taken on the morning of November 23, 1987, when there was already about 4.5 ft of fill placed at the site. At this time there was a small but measurable lateral displacement away from vertical. The second measurements, except inclinometer I-3, were taken on the afternoon of November 23, when an additional foot of fill had been hauled into place. There is a very small increase in lateral movement in inclinometers I-1 and I-2. The next measurements were taken on November 26, 1987, when the impact of the 7.5 ft of fill was being felt. The recorded displacements show a logical movement pattern within the foundation. Inclinometer I-1, located on the east side of the levee, shows eastward (landside) movement, and I-3, located on the west side of the levee, shows westward (floodside) movement. Note that due to the improper orientation of I-1 and I-2, a rather large deflection is reported in the north-south direction. I-3, which was correctly placed, shows very little deflection along the north-south axis. This expresses the near-plane strain behavior of the central section of the embankment.

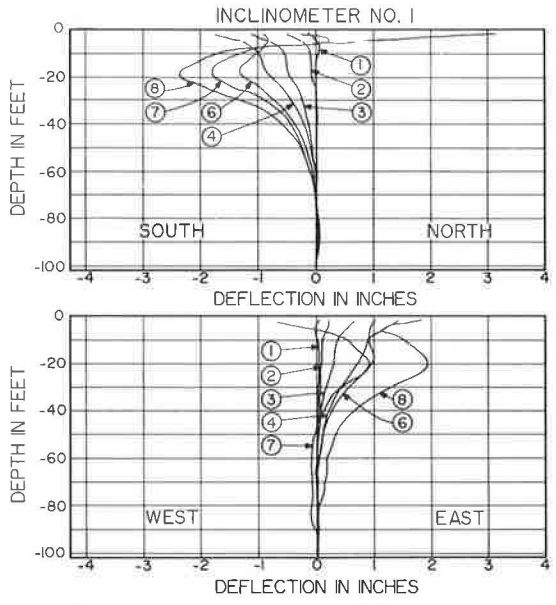

FIGURE 10 Lateral movement at inclinometer I-1. 1, November 23, 1987; 2, November 23, 1987; 3, November 24, 1987; 4, November 25, 1987; 5, January 4, 1988; 6, February 23, 1988; 7, February 24, 1989; 8, April 28, 1989.

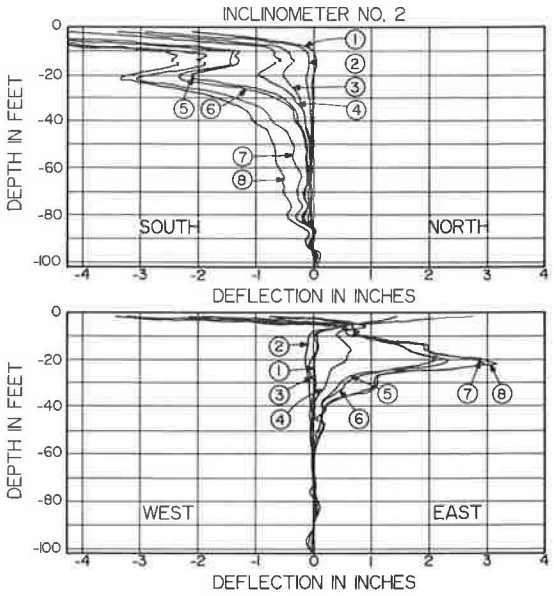

FIGURE 11 Lateral movement at inclinometer I-2. 1, November 23, 1987; 2, November 23, 1987; 3, November 24, 1987; 4, November 25, 1987; 5, January 4, 1988; 6, February 23, 1988; 7, February 24, 1989; 8, April 28, 1989.

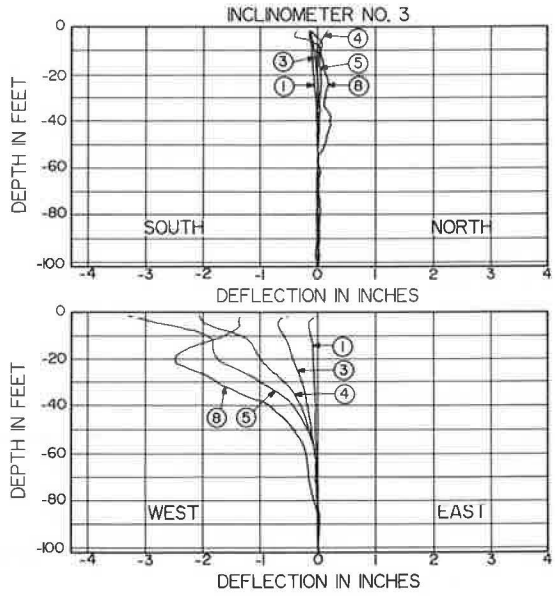

FIGURE 12 Lateral movement at inclinometer I-3. 1, November 23, 1987; 2, November 23, 1987; 3, November 24, 1987; 4, November 25, 1987; 5, January 4, 1988; 6, February 23, 1988; 7, February 24, 1989; 8, April 28, 1989.

The fourth set of readings were taken when the levee was completed. At that time maximum deflections reached 0.33 in. towards the landside at I-1, 0.6 in. towards the landside at I-2, and 1.15 in. towards the floodside at I-3. However, I-1 and I-2 also show 0.9 in. and 1.0 in. of southward deflection, mainly because of the misplacement of the tubes. The movements in the direction perpendicular to the levee (east-west or landside-floodside) should be slightly greater than indicated and can be computed from simple vector analysis. Corrected readings are 0.51 in. landside at I-1 and 0.9 in. landside at I-2.

The fifth set of measurements shown for the inclinometers were taken 40 days after completion of the test section. Maximum deflection in the east-west direction occurred at depth 20 ft and are 1 in. landside at I-1, 2.2 in. landside at I-2, and 1.9 in. floodside at I-3. Landside movement at I-1 and I-2 should be larger, considering the twisted position mentioned previously and the large deflection picked up in the north-south direction. The deflections recorded 60 days after construction are nearly equal to those measured at 40 days and follow the same pattern.

The seventh set of readings were taken 435 days after completion of the test section, just before the final lift was hauled into place to bring the crown of the test section back to 10 ft. This means that the whole levee was completed and tied to the test section, which at that time, because of settlement, was about 2.5 ft lower than the required 10 ft. The last set of deflection curves, shown in Figures 10–12, was recorded on April 28, 1989, or 2 months after construction of the final lift. Appreciable additional horizontal movement occurred near elevation −20 ft, which corresponds to the anticipated most critical failure surface A-1 shown in Figure 7. The deflections corrected for skewness of the tubes are 2.41 in. landside at I-1, 4.05 in. landside at I-2, and 2.47 in. floodside at I-3.

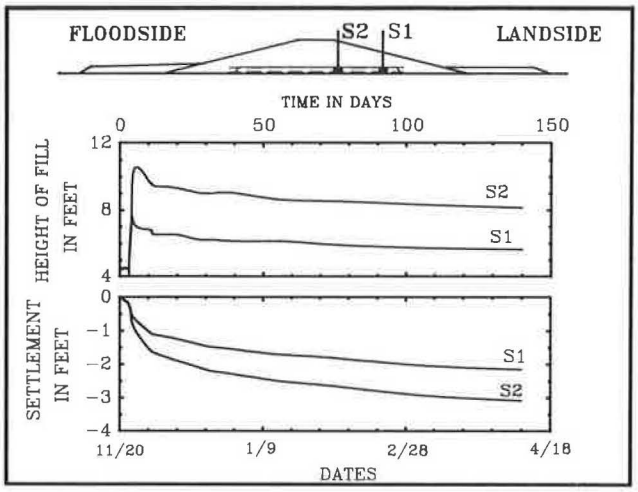

FIGURE 13 Settlement versus time at plates S-1 and S-2.

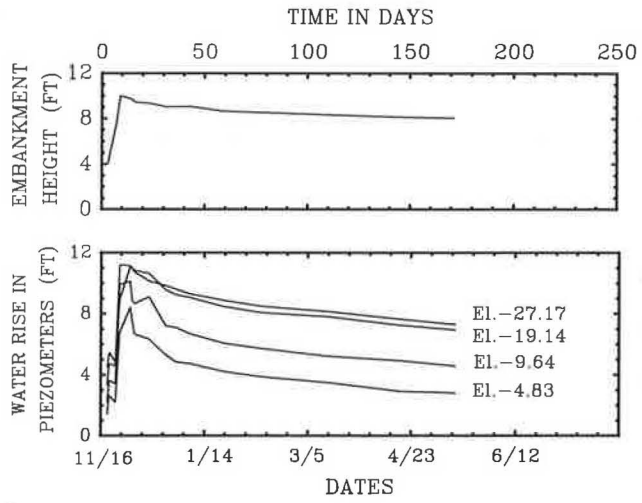

FIGURE 14 Piezometer readings versus time.

Settlement

The settlement plates were not monitored until 20 days after their installation. At that time about 4.5 ft of fill had been hauled into place, and it is reasonable to assume that some settlement has already taken place. Settlement and height of fill at the location of the plate are plotted versus time on Figure 13 for plates S-1 and S-2. At 140 days after the initial readings, the recorded settlements were 2.17 ft at S-1 and 3.1 ft at S-2. It is noteworthy that about half of the total settlement occurred during the construction period of about 15 days.

Pore Pressure

Water elevation in the piezometers was monitored during construction of the embankment and for 5 months following completion of the test section. The data are reported on Figure 14 as the water rise in each of the tubes plotted versus time. To facilitate the discussion, the height of the embankment at the location of the piezometers is also reported in Figure 14. The direct relationship between embankment height and excess pore pressure is easily seen: first, a rapid rise in pore pressure with construction; and then a time-dependent dissipation due to horizontal and vertical seepage as the soft layers consolidate. Figure 15 presents the same data for the first 20 days following installation of the piezometers (November 16 through December 6, 1987). The initial readings were taken on November 19 and the excess pore pressure reported represents the 4 ft of material already in place. The graphs in Figure 16 show clearly the effect of the interruption in construction from November 20 to November 22 and the rapid rate of construction from November 23 to November 26. Piezometers P-3 and P-4, which are the shallowest and are located in the organic layer, show the most sensitive response to construction activities. They show drops of 1.6 ft and 1.8 ft between November 30 and December 2, when the levee was shaped to grade. This normally requires the scraping of excess fill that was hauled and compacted into place. It is noteworthy that after 30 days the rates of dissipation are fairly similar for all piezometers.

The pore pressure dissipation curves were used to compute the coefficients of consolidation in the two layers using the procedure described in Navy Manual DM-7.1 (*3*). In the organic

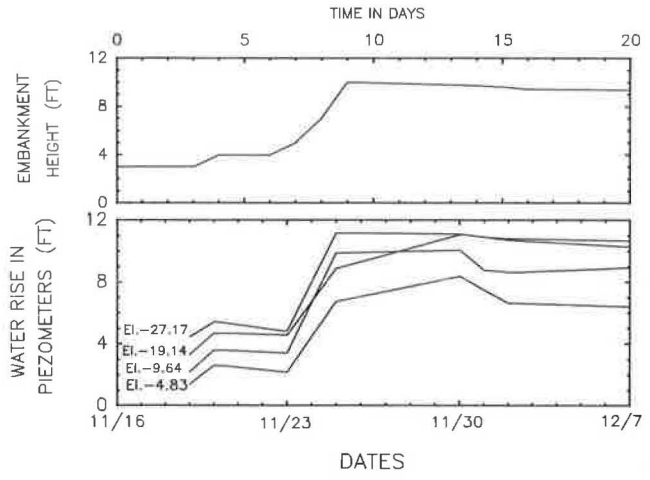

FIGURE 15 Piezometer readings versus time (reduced scale).

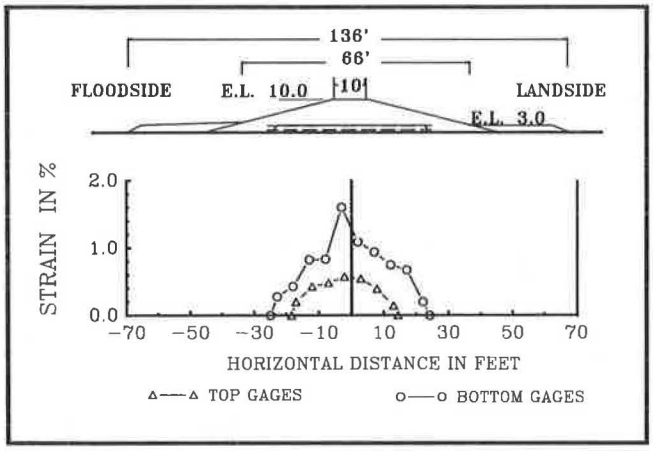

FIGURE 16 Strain in top and bottom layers of geogrids.

clay, C_v was calculated to be about 263 ft²/year. In the soft clay layer, C_v was computed to be about 58 ft²/year.

Strain Gauges

The initial readings were taken on November 19, 1987, and followed the same schedule as the piezometers. The strains recorded on April 29, 1988, in the top and bottom layers are plotted on Figure 16. The maximum strains were recorded at the gauges located near the centerline of the levee. The maximal total elongation of the bottom layer can be estimated to be about 5.0 in. and that of the top layer to be about 1.6 in. Strain gauge B-5 on the bottom layer recorded 1.669 percent and gauge T-4 on the top layer recorded 0.574 percent. The deformation with time of the geogrid follows closely the construction sequence. Figure 17 shows the increase in strain versus time for gauges B-5 and T-4. The gauges performed very well and were still operating at time of writing (November 1989). Note that each reading plotted is the average of the top and bottom reading at each location.

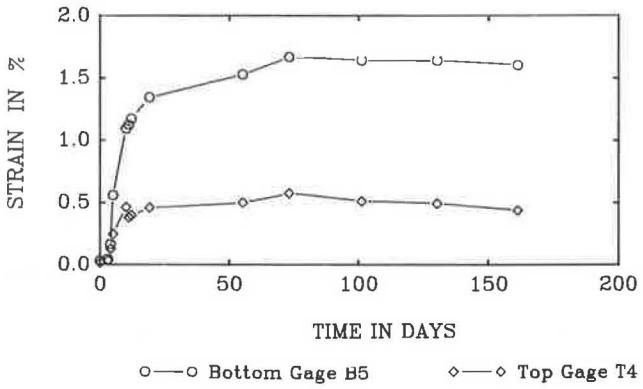

FIGURE 17 Strain in geogrids versus time.

DISCUSSION OF RESULTS

The stability analyses pointed out a potential critical sliding zone between elevation −20.0 and −30.0 ft. The inclinometer readings corroborated the prediction by indicating the largest horizontal movement at elevation −20.0 ft. The total movement of 2 in. eastward at I-1 and 2.5 in. westward at I-3 are not surprising in the type of soils underlying the levee. In addition, the total extension of about 5 in. measured in the bottom layer of geogrid agrees with the inclinometers, indicating a spreading of the base of the embankment.

The settlement analyses predicted a total compression of 5.6 ft under plate S-1, with about 4.2 ft to occur in the organic. At the end of the monitoring program (140 days), the maximum settlement under plate S-1 was 3.17 ft. Based on the laboratory C_v value, 140 days correspond to about 6 percent consolidation in the clay layer or 0.072 ft. Based on the field values of C_v, the 140 days correspond to 16 percent consolidation in the clay and 45 percent in the organic, for a total settlement of about 2.1 ft. It is important to note that the field values of C_v do not account for the effect of pore pressure dissipation during the construction stages and work stoppage. The measured 3.17 ft do not account for the 20 days of construction or for the settlement that occurred under the 4 ft of fill in place at the time the first readings were taken. The very soft organic deposit will start to experience compression as soon as earthmoving equipment rolls over the site and will compress as construction proceeds. This is further illustrated by the maximum pore pressure measured at the piezometer, which is lower than the applied overburden pressure of 10 ft of fill. In view of the working conditions at the Westminster levee, it is very likely that more than 4 ft of fill were placed to reach elevation 4.0 ft. The factor of five between the laboratory and field value of C_v for the clay is probably caused by three dimensional dissipation and by the presence of the silt lenses and seams within the layer, which increases permeability.

The average strains measured in the Tensar SR2 grids convert to about 1,700 lbs/ft in the lower layer and 600 lbs/ft in the top layer, for a total of 2,300 lbs/ft. This total tensile force is approximately the same as the allowable long-term stress in a single layer of SR2 geogrid (Table 2).

On May 23, 1988, or close to 6 months after the end of construction, two borings were drilled along the centerline of

the test section; the first boring 20 ft north of the central section and the second boring 30 ft south. The results of the shear strength tests are plotted in Figure 4 and clearly indicate a gain of strength in the organic layer due to consolidation. The logs of the borings also indicate that the bottom of the sand blanket is now around elevation −3.0 ft, further evidence of the total settlement measured by the plates. The gain of strength is on the order of 75 percent and was combined with the findings about the stresses in the geogrid to come up with a design for the full levee. Since the top layer of geogrid was only slightly stressed and the bottom layer stressed to a level less than the allowable long-term stress, the final specifications called for the use of the same section shown in Figure 7 but with only the bottom layer of geogrid. It was felt that the time-dependent strength gain of soil would not produce any load above the long-term limit of the geogrid.

CONCLUSIONS

The test section discussed in this paper was a full-scale model for the proposed one mile long Westminster hurricane protection levee. The section was fully instrumented with strain gauges, inclinometers, settlement plates, and piezometers.

The main benefits of the instrumentation program conducted at the test section of the Westminster levee are of economical and environmental nature. Results of the instrumentation program indicated that the design was stable. The movements measured are compatible with what is expected in similar soil in southwest Louisiana. The mile long levee was built using the semicompacted fill with one layer of geogrid. The time dependent gain of strength was accounted for in the analyses. The use of smaller than usual stabilizing berms resulted in appreciable savings, despite the additional cost of the reinforcement. The design selected resulted in less destruction of ecologically important marshland.

ACKNOWLEDGMENTS

The authors would like to acknowledge the help of Geneva Grille and Michael Celestine of the New Orleans office of the Louisiana Department of Transportation and Development in providing some of the data.

REFERENCES

1. C. R. Kolb and J. R. Van Lopic. *Geology of the Mississippi River Deltaic Plain, Southern Louisiana*. Technical Report No. 3-483. U.S. Army Engineer Waterways Experiment Station, Vicksburg, Miss., 1958.
2. W. W. Caver. *Slope Stability in Soft Layered Soil Systems*. M.S. thesis, Oklahoma State University, Stillwater, 1973.
3. *Soil Mechanics—Design Manual 7.1*. Naval Facilities Engineering Command, U.S. Department of the Navy, Alexandria, Va., 1982.

Publication of this paper sponsored by Committee on Geosynthetics.

Field Test of a Geotextile-Reinforced Levee

REDA M. BAKEER, TARIK A. HADJ-HAMOU, FRANK M. DUARTE, AND GERARD S. SATTERLEE

The field performance of a full-scale test section of a geotextile-reinforced embankment founded on a soil deposit of mostly soft clays is discussed. The test section was constructed in 1986 under the supervision of the U.S. Army Corps of Engineers as an enlargement prototype of an existing hurricane protection levee. The section was built to test the performance of the proposed design prior to commencing work on the entire 13-mi (20.8-km) span. The soil investigation conducted by the Corps included undisturbed and disturbed borings, soil sampling, and laboratory testing. The test section was fully instrumented with inclinometers, settlement plates, and piezometers. Displacement transducers were used to measure the deformations in the fabric. Field measurements consisted of horizontal movements, vertical settlements, pore pressures, and strains in the fabric. Measurements were taken during construction and continued for 2 years.

Soft and highly organic soils are common in Louisiana, where thousands of miles of embankments are built along highways or as levees for protection against river floods and hurricanes. Conventional construction of an embankment on soft soil may require using piles or replacing some of the soft material with sand or shells. In addition, excessive loss of marsh and dry land results from the use of very flat side slopes to assure the stability of an embankment. Recently, an alternative design was made possible by the introduction of geosynthetics. The inclusion of geogrids or geotextiles reinforces the embankment, reduces its size, controls its deformation, and increases its overall stability. The use of geosynthetics reduces the overall cost and destruction of marsh, as well as accelerating the construction process.

At present, the design of reinforced embankments is based on the classical concepts of earth pressure and slope stability, with minor modifications to account for the effect of the geosynthetics. The designer considers several potential failure wedges in the slope at the state of limit equilibrium and calculates their factor of safety. This approach is easy to apply, but it does not model the interaction of the fabric with the soil or the effect of the method of construction. It ignores the large deformations in the fabric required to develop a significant effect on the reinforced soil mass. Neither the stresses nor the strains at various parts of the embankment or the fabric could be determined by this approach. The finite element method is also used to model fabric-reinforced soils. Different models have been developed to account for nonlinearity, plastic failure, or creep, and various types of elements have been used to model the soil and fabric. However, since no reliable closed form solution is available, the results of a finite element analysis must be verified experimentally. The results of full-scale field models are the most reliable source for examining the performance of fabric-reinforced embankments, because scaling may affect small laboratory models. On the other hand, the number of field studies available in the literature is small due to the associated elaborate work, high cost, and long duration.

This paper presents the results of a field test on a full-scale fabric-reinforced embankment. The embankment under investigation is the Reach "A" test section of the hurricane levee at Tropical Bend in Louisiana. The levee was constructed and instrumented by the New Orleans District of the U.S. Army Corps of Engineers (COE) in association with Plaquemines Parish (county) of Louisiana in the period between October and December of 1986.

DESCRIPTION OF THE TEST SECTION

The levee under consideration is located near the Gulf of Mexico in Lower Plaquemines Parish in southeastern Louisiana. From a geological standpoint, the site is in the central Gulf coastal plain at the modern delta of the Mississippi River, where several other major deltas were also formed over the past 5,000 years (*1*). The main sediments of engineering interest in this area were deposited from the Pleistocene epoch to present time. These sediments are divided into three main categories: natural levee, point bar, and backswamp deposits. Slightly elevated ridges of natural levees extend along the banks of the Mississippi River. The constant migration of the river in the past resulted in the formation of point bar deposits, where the coarse materials are deposited downstream on the convex side of the river banks. On the other hand, backswamp deposits were formed by the deposition of fine sediments in the shallow ponded areas during bank overflows. These backswamp deposits contain thin laminated clays and silts of high organic nature.

The test section is a prototype for a proposed enlargement of the existing levee located between the Gulf of Mexico and a drainage canal, with its centerline 160 ft (48.8 m) off the centerline of the canal, as shown in Figure 1. The crown of the existing levee along this 13-mi (20.8-km) reach is approximately at elevation 7.5 ft (2.29 m) National Geodetic Vertical Datum (NGVD) and its centerline is 20 ft (6.1 m) off the centerline of the enlarged levee on the canal side. It is to be raised to elevation 14.5 ft NGVD (4.42 m) to protect the

R. M. Bakeer and T. A. Hadj-Hamou, Department of Civil Engineering, Tulane University, New Orleans, La. 70118. F.M. Duarte and G. S. Satterlee, U.S. Army Corps of Engineers, New Orleans District, New Orleans, La. 70160.

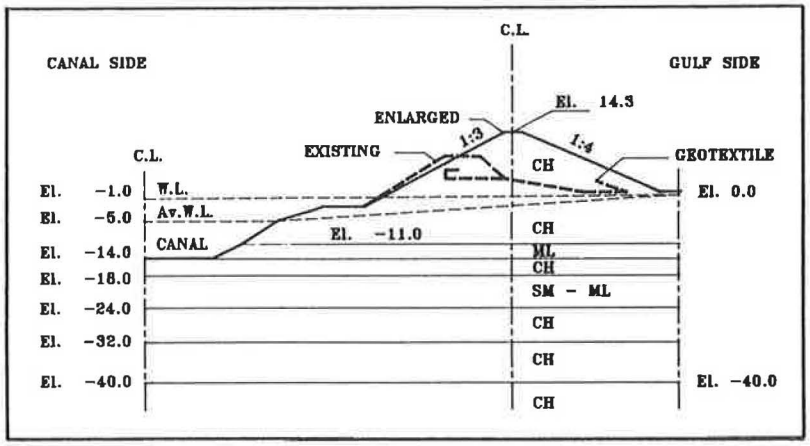

FIGURE 1 Cross section of test levee.

canal side of the levee against a 100-year storm after compensating for consolidation settlement. The 500 ft (152.4 m) long test section is reinforced with high-strength polyester geotextile. The water table is at elevation −1.0 ft (−0.305 m), NGVD, whereas the average water level in the canal is at elevation −5.0 ft (−1.52 m). The crown of the levee is 8 ft (2.13 m) wide and its base is 122 ft (37.19 m) wide. The levee has side slopes of 1V (vertical) on 4H (horizontal) on the Gulf side and 1V on 3H on the canal side.

Soil samples, laboratory tests, and a thorough soil investigation were conducted by the COE New Orleans District. The simplified soil profile in Figure 2 shows that the top layer between the ground surface [elevation 0.0 and elevation −11.0 ft NGVD (−3.35 m)] is mostly highly organic clay (CH). Two thin layers of silt of low plasticity (ML) extend between elevations −11.0 and −14.0 ft (3.35 and 4.27 m) and elevations −21.0 and −24.0 ft NGVD (6.4 and 7.32 m). A thin layer of silty-sand 3 ft (0.91 m) thick exists between the bottom ML layer and a second 4 ft thick (1.22 m) CH layer. The soil deposit below elevation −24.0 ft (7.3 m) consists of layers of highly organic clay (CH). The borrow materials used in the levee construction consist of poorly graded river sand for the core and silty clay for the impermeable cover.

Soil samples were collected from two soil borings on the Gulf side at 4.2 and 5.5 ft (1.28 and 1.68 m) on the centerline

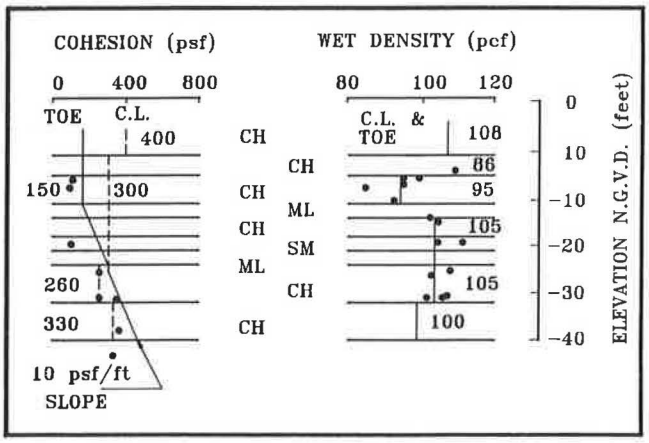

FIGURE 2 Shear strength and densities in subsoils.

of the new levee and one soil boring 69.0 ft (21 m) off its centerline on the canal side. Properties of the CH clay layers were obtained from the results of consolidated undrained (R) and unconsolidated undrained (Q) triaxial tests at different confining pressures. Settlement calculations were based on the results of consolidation tests performed on clay samples (CH) from different depths. A summary of the average soil properties accumulated from the different tests is shown in Table 1. Examination of the consolidation curves, water content, and Atterberg limits indicated that the CH layers were all normally consolidated except for the top layer, which was slightly overconsolidated under the weight of the existing levee. Variation of the shear strength and wet density of the subsoils with depth are also plotted in Figure 2.

Analysis of the existing levee was performed by COE using conventional slope stability analysis (*2–4*). Their study indicated that the existing levee has a safety factor of 1.1. Raising the crown to the new elevation with the same side slopes would induce failure in the levee, because the factor of safety would decline to 0.8 for a slide toward the canal and 0.85 for a slide toward the Gulf. Stabilizing the levee with symmetrical berms was not feasible because of its closeness to the canal. Enlargement of the existing levee using conventional methods implied that the centerline of the levee had to be relocated about 120 ft (36.6 m) toward the Gulf into the marsh, in order to accommodate the required flat slopes and berms. The top 10 ft (3.05 m) of highly compressible soil would have to be excavated and replaced with sand using hydraulic dredging. Clay would have to be hauled to form the levee cover and bring the section to its design grade.

An alternative design using geotextiles and showing significant advantages over the conventional solution was proposed and analyzed by COE (*3*). Stability analysis was performed using the wedge method of analysis (*2*) to determine the tensile strength of the fabric required to provide a safety factor of 1.3. A woven polyester fabric with a tensile strength of 1,700 lb/in (297.7 kN/m) at 5 percent strain was selected for the final design shown in Figure 1. Laboratory tests were performed at Drexel University on samples of different geotextile fabrics to determine which would meet the design requirements. A summary of the properties of the fabric is given in Table 2. Based on the available information, the most critical circular failure was found to be toward the canal and

TABLE 1 AVERAGE PROPERTIES OF THE SUBSOILS

SOIL LAYER[1]	1	2	3	4	5	6
THICKNESS (ft)	11	3	4	3	3	>16
TYPE USCS[2]	CH	ML	CH	SM	ML	CH
LL	110	NA[3]	61	NA	NA	71
PL	24	NA	22	NA	NA	22
PI	86	NA	39	NA	NA	49
ø (degrees)	22.0	25.0	22.0	30.0	25.0	0.0
c (psf)	290	200	200	0	200	300
γ_d (pcf)	51.9	NA	69.6	NA	NA	64.4
γ (pcf)	95.0	117.0	106.0	122.0	117.0	102.4
e_o	2.44	NA	1.45	NA	NA	1.65
W_c (%)	89.4	NA	52.6	NA	NA	60.1
S_r (%)	99.1	NA	98.7	NA	NA	97.7

[1] Refer to Figure 1

[2] Unified Soils Classification System

[3] Not Available

TABLE 2 PROPERTIES OF THE GEOTEXTILE FABRIC

Property	Value
Tensile warp @ 5 percent strain	1,700 lb/in.
Tensile warp @ ultimate	3,793 lb/in.
Tensile fill @ ultimate	1,188 lb/in.
Seam strength @ ultimate	486 lb/in.
Polyester thread	6 stitches/in.
Creep elongation @ 500 hours	1.22 percent
Friction angle	
Levee to levee	30 degrees
Silty-sand to marsh (organic clay)	14 degrees

passing through the bottom CH layer at elevation −40 ft (12 m).

It was decided to test a full-scale section before commencing the actual construction, in order to obtain more information on field performance and to provide guidelines for current and future designs. The test section was constructed by Plaquemines Parish under COE supervision according to the schedule given in Table 3 and Figure 3. The existing levee was enlarged by maintaining its landward toe on the canal side and backfilling into the marsh toward the Gulf (see Figures 1 and 3). The top 3 ft (0.9 m) of the existing levee (Region 2 in Figure 3), were degraded to elevation +5.0 ft NGVD (1.52 m) to provide a wide working platform and additional anchorage for the fabric.

Four rolls of fabric, each weighing 1.5 tons (1,360 kg) were used to cover Region 1 in Figure 3. The geotextile had an unseamed length of approximately 70 ft (21.34 m) in the warp direction. The fabric was rolled in place by a crawler-mounted hoe and stretched by hand over the degraded levee surface, its Gulf side slope, and the marsh grass on the Gulf side, and submerged in the ponded areas. Sand was placed over the fabric in Region 3 to a maximum height of 4 ft (1.22 m) to form the core of the new levee. Both ends of the fabric were folded back over the sand to increase the anchorage and pullout resistance. The clay cover was placed over the sand to the specified design grade in Regions 2 and 4-8 according to the sequence shown in Figure 3 and Table 3. Borrow material was hauled to the site by dump trucks and spread using bulldozer and a crawler-mounted hoe. All soils were placed in their natural state, and compaction was provided by the repeated motion of the construction equipment.

FIELD INSTRUMENTATION

The instruments were installed at similar locations along two stations (659+00 and 660 + 00) 100 ft (30.5 m) apart. The instruments were installed prior to the placement of the sand layer. Construction was halted for a week to install the instruments and for another 5 days after the levee reached elevation

TABLE 3 CONSTRUCTION SCHEDULE OF THE TEST SECTION

DATE[1]	ACTIVITY	REGION
10-17	Started degrading levee to El.[2] +5.0	2
10-20	Finished degrading levee to El. +5.0	2
10-21	Started installing fabric	
10-22	Finished installing fabric	
10-22	Replace clay over fabric on levee	2
10-22	Hauled sand cover on fabric (1908 yd^3)	3
10-23	Hauled sand cover on fabric (840 yd^3)	3
10-24		
TO	Shutdown for soil borings and instrumentation	
11-02		
11-03	Hauled clay cover (1368 yd^3)	4
11-04	Hauled clay cover (1908 yd^3)	4
11-07	Hauled clay cover (696 yd^3)	5
11-10	Hauled clay cover (1416 yd^3) El. +10.0	5
11-11		
TO	Shutdown for instruments readings & evaluation	
11-16		
11-17	Hauled clay cover (1536 yd^3)	6
11-18	Hauled clay cover (2208 yd^3)	7
11-19	Hauled clay cover (1602 yd^3)	8
11-20	Hauled clay cover (816 yd^3)	8
11-21	Dressed out levee	
11-24	Dressed out levee	
12-08	Fertilized levee	
12-09	Seeded levee	

[1] Calendar year 1986

[2] Elevation in feet N.G.V.D.

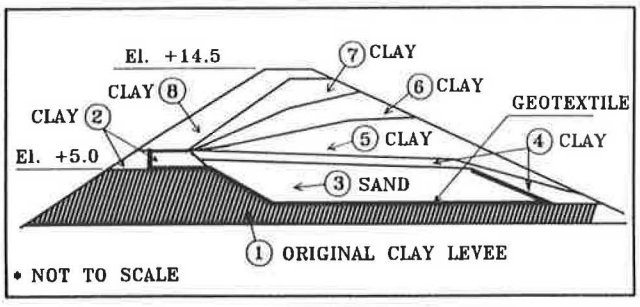

FIGURE 3 Construction procedure of test section.

+10 ft NGVD (3.05 m) to check the instruments and evaluate the performance of the section. Readings of the instruments were recorded using an electronic recording device and backed up by hand-written forms during construction and for the next two years after completion.

Six inclinometers were installed by COE at the two stations. At each station, one inclinometer was installed near the canal (11 or 12), at the crown of the levee on the Gulf side (13 or 14), and on the side slope of the levee on the Gulf side (15 or 16). At station 660+00, shown in Figure 4, inclinometers 11, 13, and 15 were located at distances of 83.0, 5.5, and 30.0 ft (25.30, 1.68, and 9.14 m) off the centerline of the new levee, respectively. The inclinometer's tips above the ground surface were at elevations 3.8, 19.8, and 13.6 ft NGVD (1.16, 6.04, and 4.15 m), whereas their bottom tips were at elevations −101.2, −95.5, and −96.8 ft (−30.85, −29.11, and −29.50 m), respectively.

Four settlement plates, 4 ft by 4 ft (1.22 m) each, were installed by Plaquemines Parish on the surface of the fabric below the sand core at the same two stations. At station 660+00, shown in Figure 5, settlement plates S-1 and S-3 were located 5 and 25 ft (1.52 and 7.62 m) off the centerline of the new levee. The original elevations of the settlement plates after installation were 3.53 and 1.82 ft (1.08 and 0.56 m), respectively.

A total of eight piezometers were installed by COE at stations 659+00 and 660+00. The piezometers at station 660+00

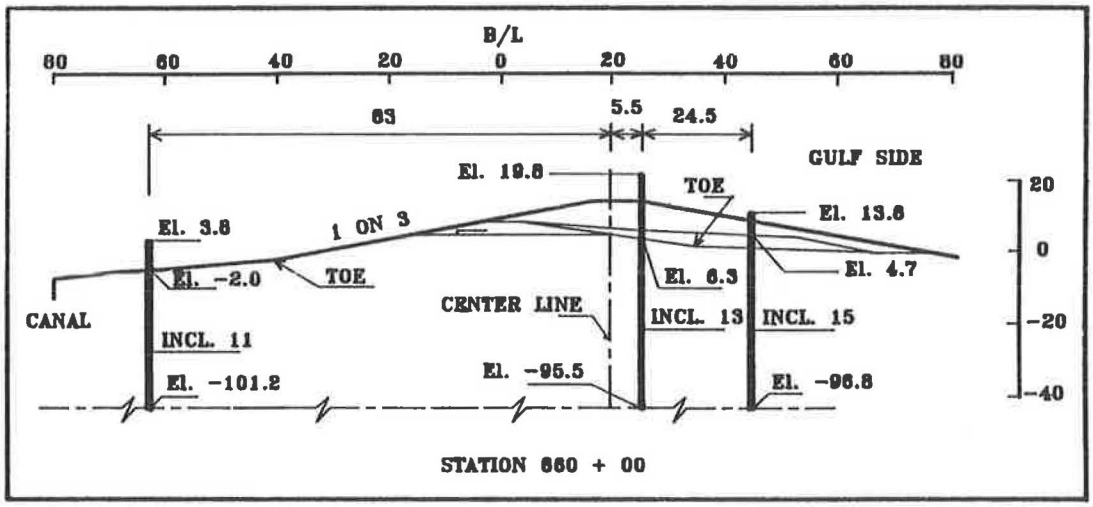

FIGURE 4 Layout of inclinometers.

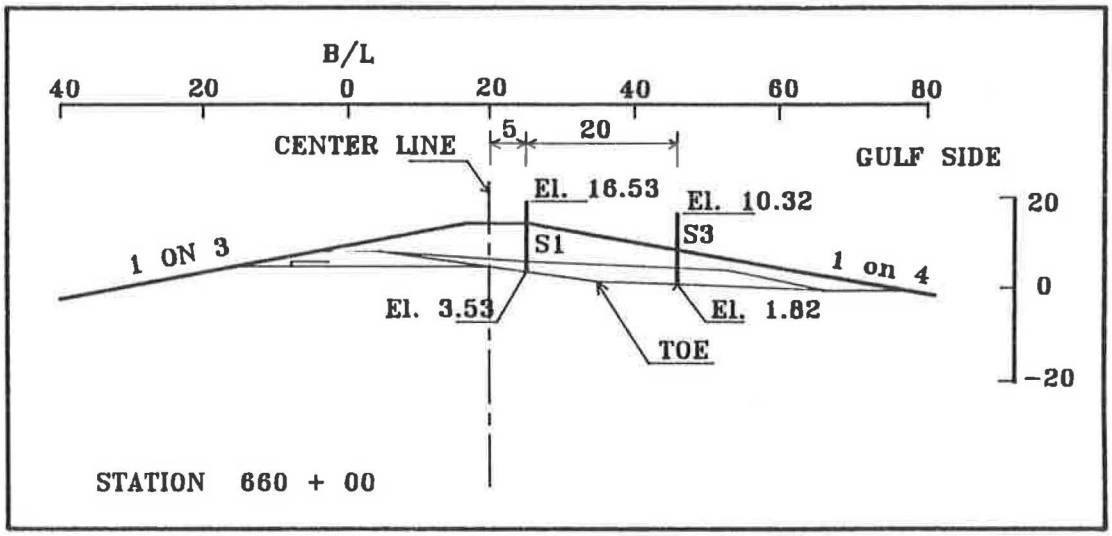

FIGURE 5 Layout of settlement plates.

were placed along an axis 5.5 ft (1.68 m) off the centerline of the new levee on the Gulf side, as shown in Figure 6. The tips of piezometers 1A, 1B, 1C, and 1D were at elevations −4.8, −10.8, −20.8, and −30.3 ft NGVD (−7.02, −3.29, −6.34, and 9.24 m), whereas their riser pipe elevations were 17.61, 17.34, 17.45, and 17.36 ft NGVD (5.37, 5.29, 5.32, and 5.29 m), respectively. The tips of the A piezometers were at the top clay layer (CH), whereas the tips of the B piezometers were at the bottom of the second CH layer, just above the silt layer (ML). The tips of the C piezometers were in the center of the silty sand layer (SM) between a CH layer and the second ML layer. The tips of the D piezometers were 6 ft (1.83 m) deep into the bottom CH layer located below the second ML layers.

Two types of strain gauges were installed on the fabric during construction along three profiles. Two of these profiles, at stations 659+00 and 660+00, contained mechanical displacement transducers manufactured and installed by U.S. Army Waterways Experiment Station (WES). The third profile was equipped with foil gauges (linear voltage displacement transducers or LVDTs). The mechanical strain gauges were attached to plates previously installed on the fabric at WES, whereas the foil gauges were glued to the fabric at the factory. A sketch of the layout of the foil gauges used in this study is shown in Figure 7. The foil gauges were placed along three rows spaced 4 ft (1.22 m) apart with each row containing five gauges spaced equally at 8 ft (2.44 m). The center row consisted of the CT gauges (CT-1 through CT-5). The left row contained LT gauges, whereas the right row included RT gauges. These gauges were used to measure the lateral strains in the fabric, perpendicular to the test section. A fourth group of longitudinal foil gauges (CL-1 through CL-5) was installed adjacent to the center row of lateral foil gauges to measure the longitudinal strains along the test section, as shown in Figure 7. All foil gauges were calibrated after installation and normalized to an initial reading of 0.9 percent strain. This

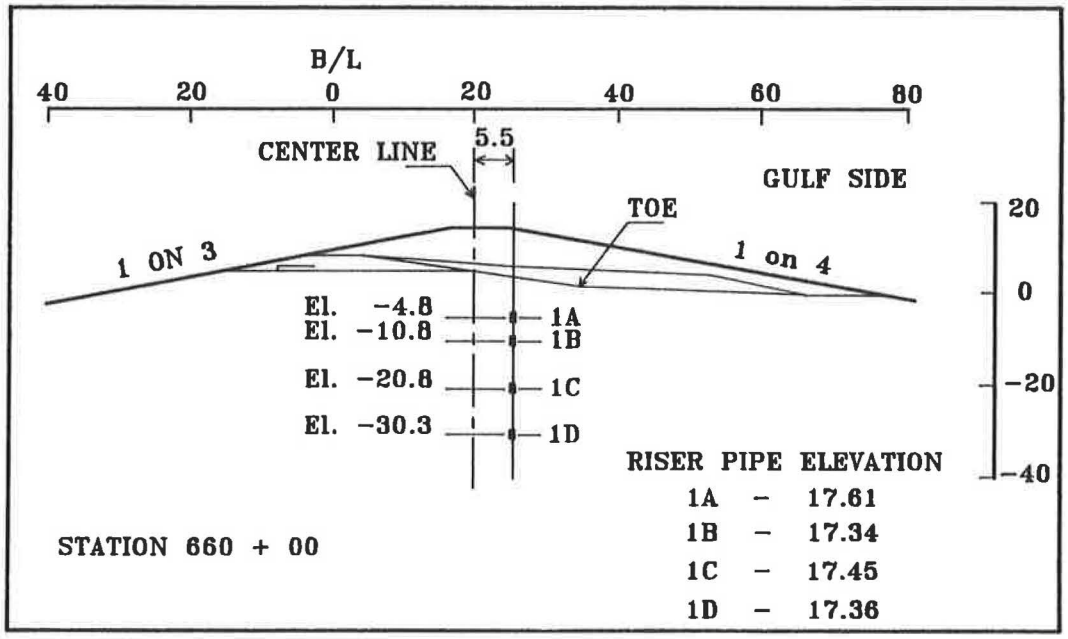

FIGURE 6 Layout of piezometers.

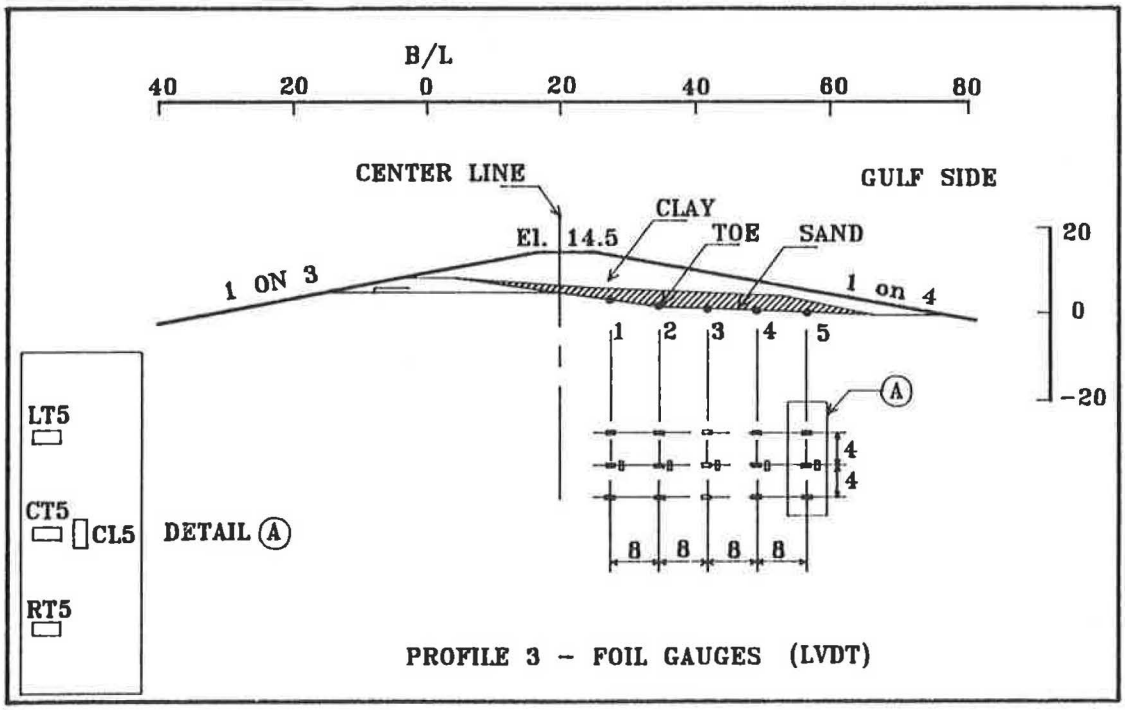

FIGURE 7 Layout of foil gauges.

offset value is approximately equal to that obtained in the laboratory tests conducted at Drexel University (5) on the fabric used in this study.

RESULTS OF THE FIELD TEST

The data obtained from the displacement transducers (WES gauges) were inconclusive; some of them jammed and the readings of others were inconsistent. The readings from the foil gauges were reasonably coherent but, unfortunately, no foil gauges were placed on the canal side or along the folds. The foil gauges measured a noticeable increase in strain with the progress of construction. The strains continued to increase slowly with time after the completion of construction for up to 400 days. However, no measurable increase was recorded by most of the gauges after 300 days. Table 4 shows a summary

TABLE 4 NET STRAINS IN THE FABRIC AFTER 300 DAYS

FOIL GAUGE GROUP	STRAIN READINGS OF FOIL GAUGES (%) CT	LT	RT	MAX DIFF	AVERAGE	CL
1	1.40	0.80	1.20	0.60	1.133	0.40
2	1.60	0.80	1.00	0.80	1.133	1.10
3	1.50	1.30	1.40	0.20	1.400	0.50
4	1.00	1.60	0.30	1.30	0.967	1.40
5	2.30	2.00	2.60	0.60	2.300	1.90
AVERAGE						1.06

of the strains in the fabric measured by the foil gauges after 300 days.

Typical lateral strains measured in the fabric by the foil gauges during the first 300 days are shown on Figure 8 for Group 5 (CT-5, LT-5, and RT-5). The readings of other groups of gauges followed similar patterns. The lowest strain of 0.8 percent was measured by gauges LT-1 and LT-2, and the maximum lateral strain was 2.6 percent at gauge RT-5. On average, a maximum strain of 2.3 percent was measured by Group 5 of lateral gauges, located near the fold on the Gulf side, and a minimum strain of 0.97 percent at Group 4. A gradual decrease in strain was observed toward the slope on the canal side, except for an inconsistent reading of Group 4. The 300 days readings of RT-4 and CT-4 were small (0.3 and 1.0 percent) in comparison with the reading of 1.6 percent at LT-4 (maximum difference of 1.5 percent) and the average readings of Groups 3 and 5 of 1.4 and 2.3 percent, respectively. In addition, lower strains were observed at Group 2 of gauges, located at the toe of the existing embankment (bend in the fabric), than in Groups 1 and 3, located before and after the toe.

The longitudinal strains in the geotextile did not follow a particular pattern and ranged from a minimum of 0.4 percent at CL-1 to a maximum of 1.9 percent at CL-5, as shown in Table 4. The variation in the readings could be attributed to the different amount of fabric stretching during construction or to the different soil conditions along the 500 ft (152.5 m) span. An average of 1.06 percent strain was observed along the longitudinal axis of the levee, which represents 46 percent of the maximum lateral strain measured by Group 5 and 94 percent of the minimum lateral strain measured by Group 1.

No appreciable movement was detected by inclinometers 11 and 12, installed near the canal. Consistent patterns of progressive lateral deformation toward the Gulf were observed

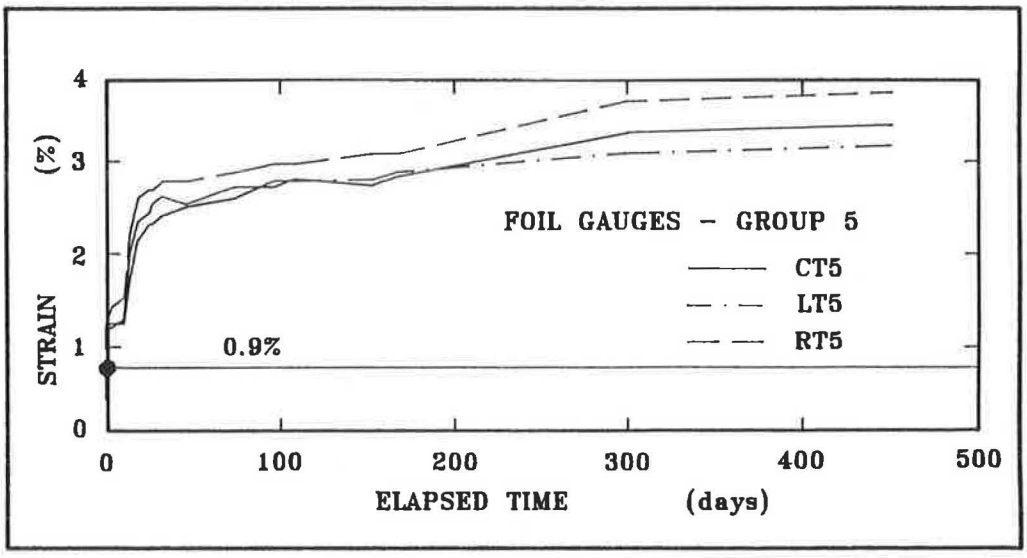

FIGURE 8 Strains in the fabric.

in all inclinometers with time, as shown in Figures 9 and 10. The horizontal movement measured by the inclinometers after 400 days is also shown in Table 5 at four selected elevations. Inclinometers 13 and 14, near the center of the embankment, experienced a horizontal movement toward the Gulf of 13 and 8.5 in. (330 and 216 mm), respectively. The average movement of 10.75 in. (273 mm) detected by these inclinometers is equivalent to 12.8 percent of the 7 ft (2.13 m) wide crown. The horizontal movement at the surface of the slope on the Gulf side was measured by inclinometers 15 and 16 as 14.3 and 10.5 in. (363 and 267 mm) toward the Gulf, respectively, for an average value of 12.4 in. (315 mm). This average reading represents 1.35 percent of the levee width of 76.4 ft (23.3 m) at that elevation (8.9 ft, 2.72 m). The horizontal movement at the fabric level was also toward the Gulf and ranged from 6.8 in. (173 mm) at inclinometer 14 to 14.4 in. (366 mm) at inclinometer 15. The average horizontal movement of 10.6 in. (0.27 m) corresponds to a 1.26 percent lateral strain in the 70 ft (24.4 m) long fabric. This value is consistent with the average reading of all foil gauges of 1.4 percent.

A plane of relatively large horizontal movement and potential failure surface was detected along the interface between the top CH clay layer and the first ML silt layer at approximately elevation −11 ft (−3.4 m). No appreciable horizontal movement, more than 0.5 in. (12 mm), was measured in the subsoils below elevation −30 ft (−9.1 m) by inclinometers 13 and 14, or below elevation −60 ft (−18.2 m) by inclinometers 15 and 16. All inclinometers showed movements in the subsoils toward the Gulf except for inclinometer 14, which

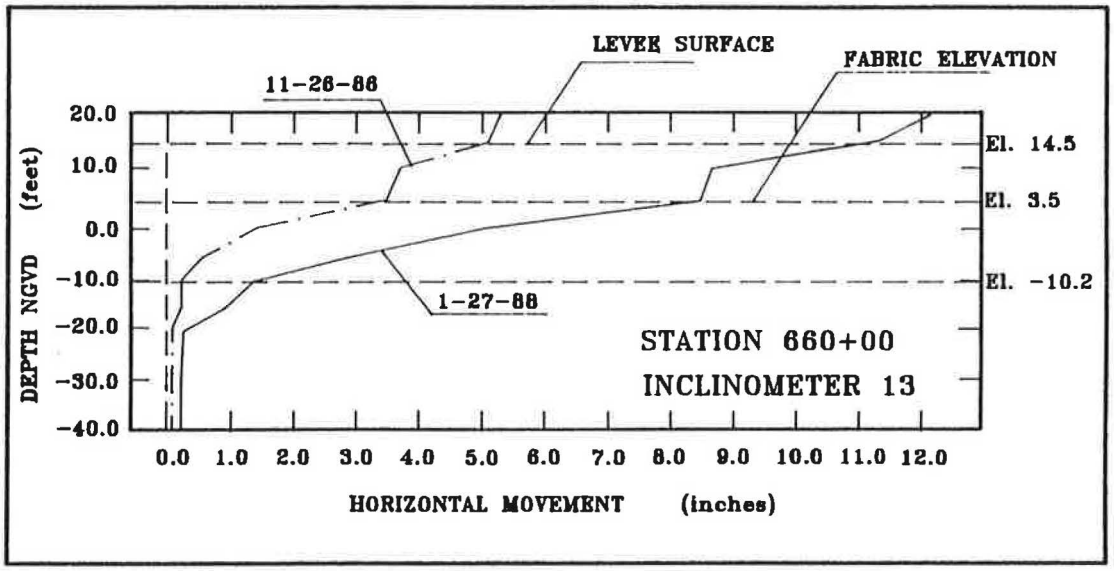

FIGURE 9 Horizontal movements below crown.

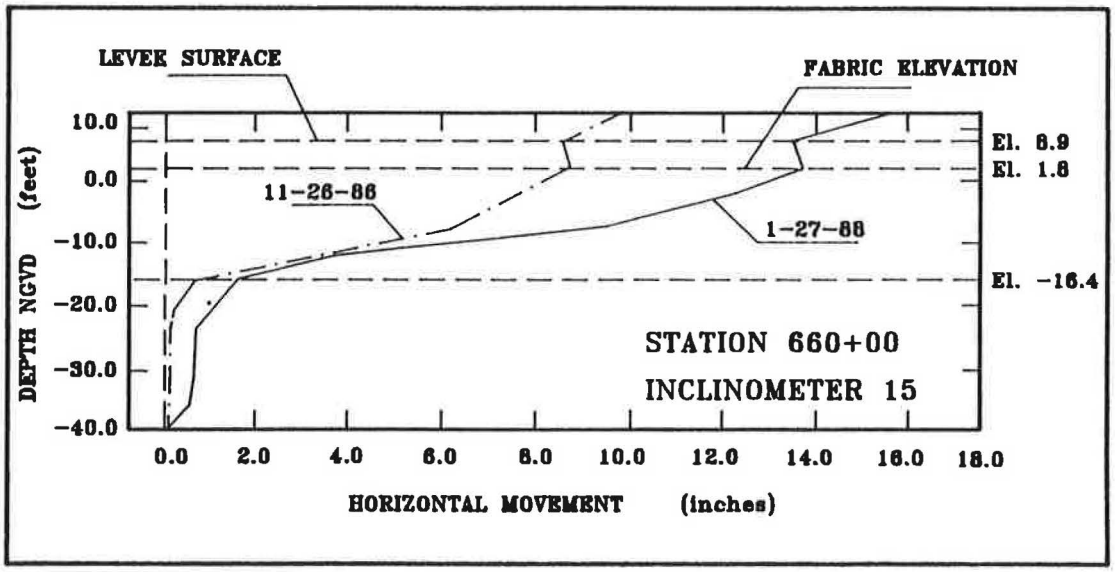

FIGURE 10 Horizontal movements at Gulf slope.

TABLE 5 HORIZONTAL MOVEMENTS IN THE SECTION

	HORIZONTAL MOVEMENT (inches)			
	LEVEE SURFACE	FABRIC	GROUND	SUBSOIL
Incl 13 CROWN	13.00 (El 14.5)[1]	7.30 (El 3.5)	5.1 (El 0.0)	1.30 (El -10.0)
Incl 14 CROWN	8.50 (El 14.5)	6.80 (El 3.5)	4.0 (El 0.0)	0.250 (El -10.0)
AVERAGE (CROWN)	10.75	7.90	5.0	0.525
Incl 15 GULF SLOPE	14.30 (El 8.9)	14.40 (El 1.8)	13.0 (El 0.0)	4.00 (El -11.0)
Incl 16 GULF SLOPE	10.50 (El 8.9)	9.50 (El 3.5)	8.0 (El 0.0)	1.00 (El -11.0)
AVERAGE (SLOPE)	12.40	11.95	10.5	2.50

[1] El. elevation in feet N.G.V.D.

showed movement toward the canal below elevation −30 ft NGVD (−9.1 m).

Fill hauling was completed on November 20, 1986, and design grade was reached one day later. No piezometer readings were taken until November 26 because of the extremely wet conditions at the site due to heavy rainfall. Table 6 shows the initial, peak, 300 days, and 400 days readings of the piezometers at the two stations. Figure 11 shows plots of the pore pressure distribution at station 660+00. Pore pressure increased gradually with the progress of filling and peaked when the height of the fill reached elevation 13.5 ft (4.1 m), then dissipated rapidly to small residual values above the initial readings. There was very slow change in the pore pressure after 80 days from the completion of construction, which reflects the low permeability of the subsoils.

The maximum average increases in the pore pressure at piezometers A, B, C, and D were 4.1, 9.03, 3.68, and 7.1 ft (1.25, 2.75, 1.12, and 2.17 m), respectively. A reduction in the pore pressure of 28 percent occurred in the four days after reaching the design grade of the levee. This rapid reduction is indicative of the quick process of consolidation in these clays. The maximum average increase in pore pressure of 9.03 ft (2.77 m) is equivalent to about 64 percent of the added fill of 8.5 ft (2.9 m) between elevations 5 and 13.5 ft (1.53 to 4.11 m) when the last reading was taken during construction. It should be noted that removal of the top soil of the existing levee may have resulted in negative initial pressures, and no readings were taken just after completion, which allowed pore pressures to dissipate somewhat. The highest residual pressure of 5 ft (1.53 m) was measured by the deepest piezometers, D, located in the bottom thick clay layer of very low permeability and poor drainage conditions. On the other hand, the quick dissipation of the pressure in piezometers B and C is due to their location between relatively highly permeable lay-

TABLE 6 PORE PRESSURES IN SUBSOIL

PIEZ No.	SOIL TYPE	TIP ELEVATION (ft)	PIEZOMETER READING (ft) INITIAL	13.5' FILL	300 DAYS	400 DAYS
1A	CH	-4.8	0.91	5.11	2.31	1.74
2A	CH	-5.0	0.91	4.91	2.21	2.38
1B	CH/ML[1]	-10.8	0.49	9.84	0.84	0.69
2B	CH/ML	-11.0	0.55	9.25	1.15	1.01
1C	ML	-20.8	-1.70	2.45	-0.45	-0.26
2C	ML	-20.0	-1.75	1.45	-0.75	-0.66
1D	CH	-30.3	0.06	7.36	3.26	2.43
2D	CH	-31.3	0.73	7.63	4.53	3.66

[1] Tip at interface of two layers

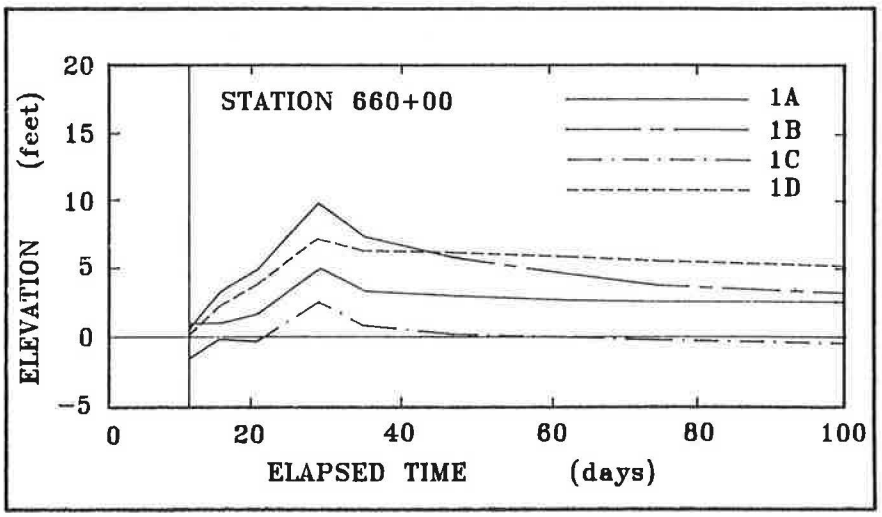

FIGURE 11 Pore pressures in subsoils.

ers of sand or silt. Piezometers A, by contrast, are located in the middle of the top CH layer, just below the clay levee, and accordingly measured much slower decays.

As expected, the pattern of settlement at the fabric level followed that of the pore pressures, with measurable increase in settlement recorded during the construction phase of lifts 2 through 8 (refer to Figures 2, 11, and 12). The rate of settlement decreased considerably after 150 days, and no measurable increase in the settlement was recorded after 300 days. The two settlement plates on the side slope, S-3 and S-4, showed identical readings, but an average difference of about 2 in. (50 mm) was observed between the readings of plates S-1 and S-2, located below the crown. The difference may be attributed to the variation in the thickness of the clay layers at the two stations or their drainage conditions. The maximum average settlement was 2.56 ft (0.78 m) under the slope on the Gulf side and 2.04 ft (0.62 m) below the crown. The settlement at the crown and the slope of the levee is equivalent to a loss of 18 and 38 percent of the added height of fill above each settlement plate, respectively. The net loss due to settlement at the crown as a ratio of the total height of the levee is 14 percent.

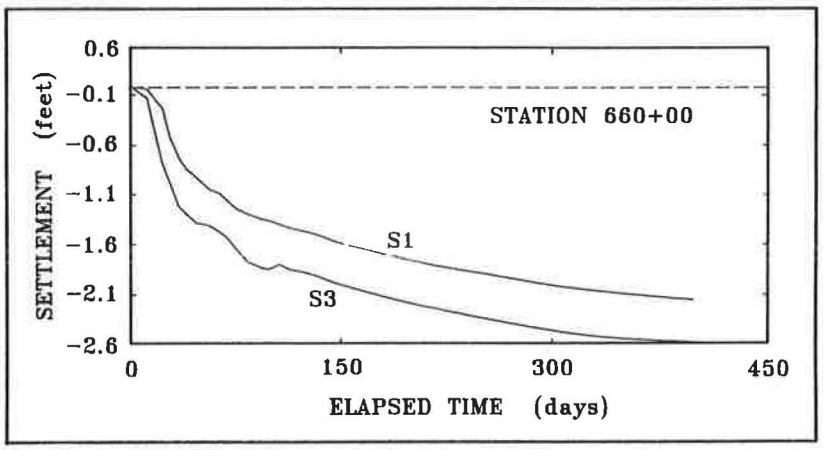

FIGURE 12 Measured settlement in the test section.

DISCUSSION OF THE RESULTS

The performance of most of the equipment was satisfactory. Readings were consistent and agreed well with the design and expected theoretical response. Further examination of the results yields the following remarks:

1. The goals of the project were achieved, considering the limited budget of $200,000 available for the field test. This budget represents a small fraction of the overall construction cost of the actual levee. The results of the test showed the feasibility of the design and construction, and accordingly it was decided to use geotextiles along the 13 mile stretch of levee. Use of geotextiles reduced the overall cost by 35 percent, required less than half the time to complete, and reduced the loss of marsh by 90 percent compared with a conventional levee. The reduction in the required construction materials for the levee is estimated to be about 60 percent.
2. The banks of the canal experienced very small movement due to the enlargement activities, which was originally a major concern for COE during the design phase. The data obtained from the test section were used to evaluate the design and to set guidelines for future designs. It is currently used in a research project to verify a new finite element computer program for the analysis of reinforced embankments.
3. Performance of the fabric was satisfactory, because the measured strains were much smaller than the long term design value of 5 percent. The other positive contribution of the fabric, besides providing a tensile resistance to the soil mass, was the reduction in size of the levee and accordingly the driving forces and settlements. The longitudinal strains in the fabric were relatively high for a plain strain type problem, as usually assumed in conventional or finite element analysis.
4. A fabric may stabilize an embankment, but the possibility of a deep-seated or shallow failure in the subsoil may still exist. The field test indicated a possible block failure along the interface surface between the relatively soft top CH layer and the much stiffer ML layer. This failure surface was examined to reassess the tensile requirements of the fabric computed by the wedge and circular arc analysis (*1-3*). Slope stability analysis was performed on the unreinforced and reinforced embankments using the wedge method and program UTEXAS-2 (*3*) based on the Spencer and Simplified Bishop methods. It was found that, to maintain a safety factor of unity, a fabric would require a tensile strength of 670 lb/in. (117 kN/m), based on the results of the wedge analysis, or 550 lb/in. (96.3 kN/m), based on the arc analysis. The required tensile strengths determined by the wedge and circular arc analyses were much larger than the actual stresses in the fabric, computed from the measured strains in the field. Hence, it was concluded that the fabric used in the field test was adequate.
5. Existing field conditions affected, to some extent, the movement pattern and performance of the test section. The subsoils under the canal slope and the crown of the enlarged levee were preconsolidated under the weight of the existing levee, whereas the Gulf slope was situated in the marsh over relatively virgin soils. Accordingly, smaller horizontal and vertical movements were recorded at the crown of the enlarged levee than were recorded at the slope on the Gulf side. This pattern of deformation indicated a possible general movement of the enlarged levee toward the Gulf over the degraded stiff surface of the existing levee.
6. The results of the project demonstrated the necessity of installing a backup system of measurement in a field test. In spite of the malfunction and erratic readings recorded by the WES strain gauges, sufficient measurements of the strains in the fabric were obtained from the backup system of foil gauges. Considering the high price tag and the elaborate work associated with such a massive project, the cost of a backup system becomes trivial.
7. The wide scatter in the data obtained from the soil investigation is evidence of the need for an extensive soil investigation in any major project. Laboratory tests on the clay samples from the top layer showed cohesion values (c) ranging from 90 to 490 psf (4.31 to 23.46 kN/m^2), with an average value of 290 psf (13.88 kN/m^2). A design based on an average value of a soil parameter may be a dangerous practice. For example, underestimating a strength parameter and overestimating a unit weight in a slope stability analysis may result in an overly conservative design, whereas the opposite may produce an unsafe design.
8. The recorded change in pore pressure and settlement with time were consistent with the sequence of construction. Pore pressure and settlement increased with the increase of the fill height up to the design grade. The residual values

measured by the piezometers after 400 days were indicative of the low permeability of the bottom thick clay layers. Faster dissipation was observed in the thin clay layers surrounded by more permeable layers of sand or silt. The measured settlements agreed reasonably well with the values calculated from consolidation theory.

9. Creep deformation should be accounted for in the design of earth structures founded on highly organic soils. Large time-dependent or creep deformation, accompanied by little or no dissipation of pore pressures, was observed in the test section. Pore pressure dissipated rapidly after completion of the section, then continued to dissipate at a much slower rate. Meanwhile, the horizontal and vertical deformations of the levee continued to increase with time at a higher rate than the dissipation of the pore pressure, as shown in Figures 10 through 13. Between 10 and 20 percent of the total settlement and 8 percent of the horizontal displacement of the levee occurred without any measurable change in the pore pressure.

10. Even though it was possible to obtain all necessary information from the field test, it is advisable for future tests to lay out the instruments in a symmetrical arrangement about the centerline of the embankment. Using more settlement plates distributed on both sides of an embankment would allow for plotting the displacement profiles under the embankment. Using inclinometers on both sides of an embankment would also provide a complete view of the overall deformed shape of the section. Using additional instruments in this project was not feasible due to budget constraints.

CONCLUSIONS

The results of the field test indicated the feasibility and benefits of using geotextiles in the construction of levees on soft soils. Using a fabric reinforcement reduced the estimated construction cost of the 13 miles of levee from $85 million to $54.2 million. The expected construction time was reduced from 13 years to 6 years, and only 100 acres of marshes will be used instead of 4,000 acres. Most of the instruments performed well throughout the duration of the project in spite of the harsh field conditions. Readings of the instruments indicated that the section has performed according to design. Displacements and settlements were within the expected range for this size levee and soil conditions. The strains in the geotextile were much smaller than the design value of 5 percent that was assumed in the limit equilibrium analysis. The results of the test will be used in the future to calibrate finite element analysis of geotextile reinforced embankments. Parametric studies will be performed using the finite element method to develop new guidelines for future designs.

REFERENCES

1. C. R. Kolb and J. R. Van Lopic. *Geology of the Mississippi River Deltaic Plain, Southern Louisiana*. Technical Report 3-483. U.S. Army Engineer Waterways Experiment Station, Vicksburg, Miss., 1958.
2. W. W. Caver. *Slope Stability in Soft Layered Soil Systems*. M.S. thesis. Oklahoma State University, Stillwater, 1973.
3. F. M. Duarte and G. S. Satterlee. Case Study of a Geotextile Reinforced Levee on a Soft Clay Foundation. *Proc., Geosynthetics '89 Conference*, San Diego, Calif., 1989, pp. 160–171.
4. E. V. Edris, Jr. *User Manual, UTEXAS-2 Slope Stability Package*, Vol. 1. Report I.R.GL.-87-1. U.S. Army Engineer Waterways Experiment Station, Vicksburg, Miss., 1987.
5. R. M. Koerner. *Comparative Strain Evaluation of the Nicolon O-2 Geotextile Using LVDT and Foil Strain Gauges*. Drexel University, Philadelphia, Pa., 1987.

Publication of this paper sponsored by Committee on Geosynthetics.

Instrumentation of Geogrid-Reinforced Soil Walls

RICHARD J. BATHURST

An experimental program involving the construction and monitoring of large-scale geosynthetic-reinforced soil walls has been under way at the Royal Military College (RMC) of Canada for several years. Several 3-m-high model walls have been built within the RMC Retaining Wall Test Facility and these walls taken to failure under uniform surcharge loading. The instrumentation, calibration of equipment, data acquisition, and monitoring strategies that have been developed over the course of this program are described. Examples of qualitative features of model wall behavior during construction, under working load conditions, and at incipient collapse are given. These examples highlight the success of the instrumentation program to date.

A research program conducted by the Civil Engineering Department at the Royal Military College (RMC) of Canada has been under way for several years. The program is directed at acquiring detailed measurements of the mechanical behavior of soil retaining walls constructed with polymeric reinforcement (i.e., geosynthetics). The experimental program involves the construction and testing to failure of carefully monitored full-scale models of geogrid-reinforced soil walls constructed within the RMC Retaining Wall Test Facility. The data collected can then guide the development of physically correct models that are needed to design geosynthetic reinforced retaining walls and predict their performance in the field.

A total of 10 reinforced soil walls constructed with a variety of facing treatments have been tested to date. The results of these tests have been reported by the author and coworkers in other publications (*1-5*).

This paper is focused on a description of the instrumentation that has been developed and employed in recent wall tests to allow researchers to measure the load-deformation response of these composite structures during construction, under working load conditions, and at collapse of the structures during surcharging.

RMC RETAINING WALL TEST FACILITY

The RMC Retaining Wall Test Facility was constructed to provide a general purpose, large-scale apparatus to test a variety of reinforced soil wall systems (Figures 1 and 2). The principal structural components of the facility are six rigid heavily reinforced concrete counterfort cantilever wall modules that are used to confine a block of soil 6.0 m long by 3.6 m high by 2.4 m wide. The facility sidewalls are composed of a composite plywood-plexiglas-polyethylene sheeting that assists to reduce sidewall friction. Shear box tests have shown that the sand-sidewall interface has a fully mobilized friction angle of 15 degrees. Three dimensional stability analyses have shown that the friction-reducing sidewall construction reduces the contribution of the test facility boundaries to less than 15 percent of the total active earth force that would be resisted by the facings in a true plane strain condition (*6*).

In a typical test the soil surface is surcharged by inflating airbags that are confined between the concrete modules and structural steel sections at the top of the facility. The current surcharging arrangement allows a vertical pressure of up to 100 kPa to be applied to the upper soil surface.

Typical Test Configurations

Typical test configurations are shown in Figure 3. Figure 3(a) represents an incremental wall construction technique in which rows of panels were placed sequentially as the height of the retained soil was increased. Each row was temporarily supported until the soil behind the wall had reached the top of the panels. In this way a portion of the load-carrying capacity of the grid reinforcement layers was mobilized as construction proceeded. The wall facings were constructed with 0.75 m high articulated panels. Each panel was connected to a separate strip of geogrid reinforcement extending 3 m into the soil backfill. In some tests the facings comprised single full-height (propped) panels (*1,2,5*) and in others a wraparound fascia (*3*). For the propped wall construction illustrated in Figure 3(b), single full-height panels were used and the external support to these panels was only released after the retained soil had been placed and compacted to the full height of the model wall.

The panels in the incremental and propped wall tests were constructed in three columns in order to decouple as much as possible the central instrumented panels from the influence of the test facility sidewalls. Four central panels, 0.75 m by 1 m by 400 mm thick, were manufactured out of aluminum and designed to support a variety of instrumentation. The panels were mounted independently to form an articulated incremental wall or bolted together to form a full-height (propped) panel wall. The base of each panel column was supported by a pinned connection. The pinned connection was in turn supported by an instrumented levelling pad, which corresponds to the footing that provides support and alignment for similar fascia in the field.

All tests carried out to date have used SR2 and SS1 Tensar geogrids as the geosynthetic reinforcement (Figure 4 and Table 1). The choice of Tensar geogrids has been largely dictated by the convenience of being able to mount strain gauges directly

Civil Engineering Department, Royal Military College of Canada, Kingston, Ontario, Canada K7K 5L0.

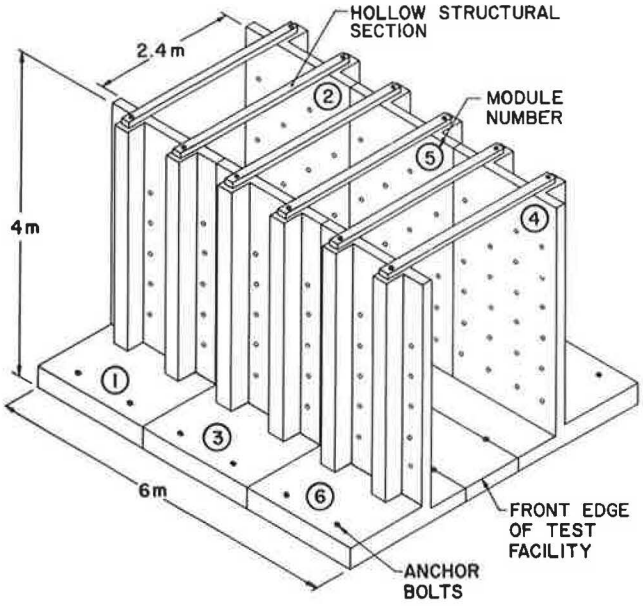

FIGURE 1 RMC Retaining Wall Test Facility.

to the reinforcement ribs. However, initial experience with the relatively high-strength, high-modulus SR2 material resulted in wall models that were very stiff and could not be failed with the surcharge capacity at hand (*1*,*2*). Consequently, a relatively weak and extensible Tensar geogrid (SS1) has been used in more recent RMC trial walls, and these structures have exhibited excessive deformations and grid rupture leading to wall collapse. Finally, it should be noted that a coarse sand material has been used in all RMC model tests carried out to date.

General Test Procedure

The performance of test walls was carefully monitored, commencing at construction and ending at failure under uniform surcharging. The standard procedure following construction was to stage load the test configuration by applying a series of uniform surcharge pressures up to a maximum of 100 kPa. The composite systems exhibited time-dependent deformations under constant surcharge loading, which is largely the result of the properties of the constituent polymer in the geo-

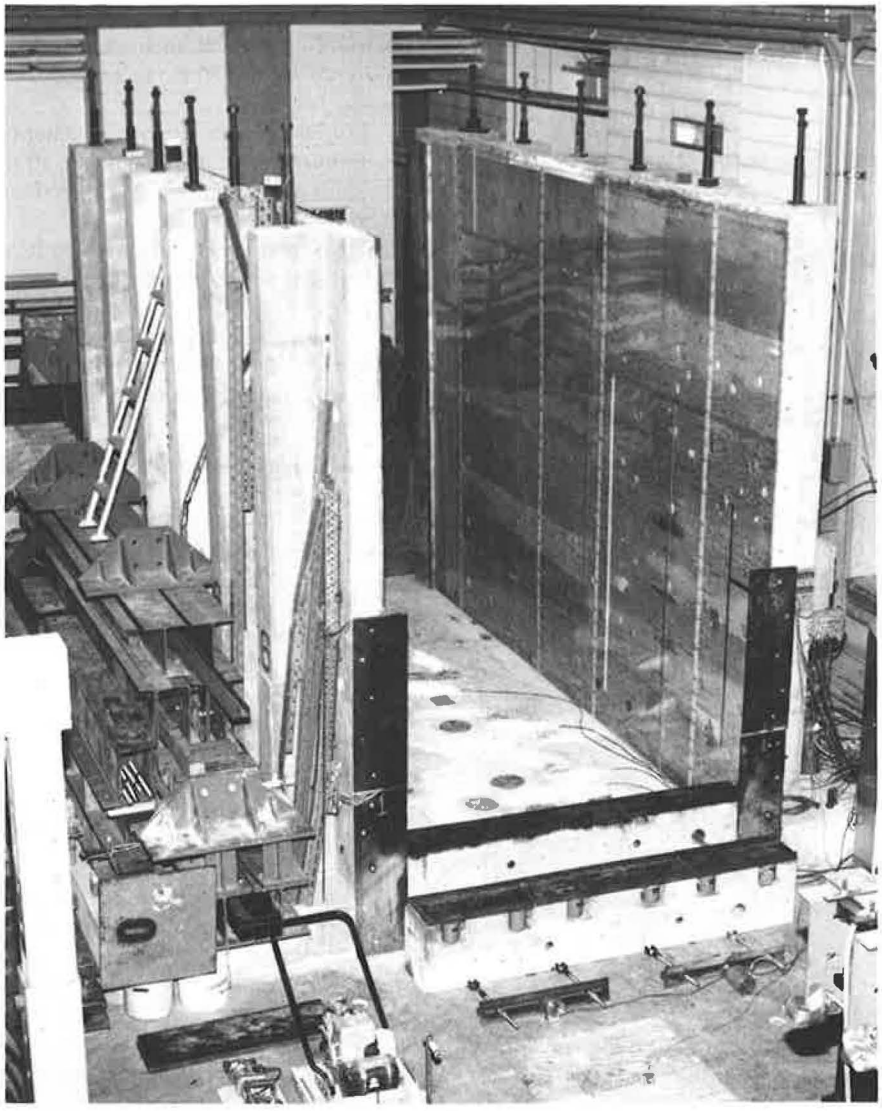

FIGURE 2 Overview of RMC Retaining Wall Test Facility.

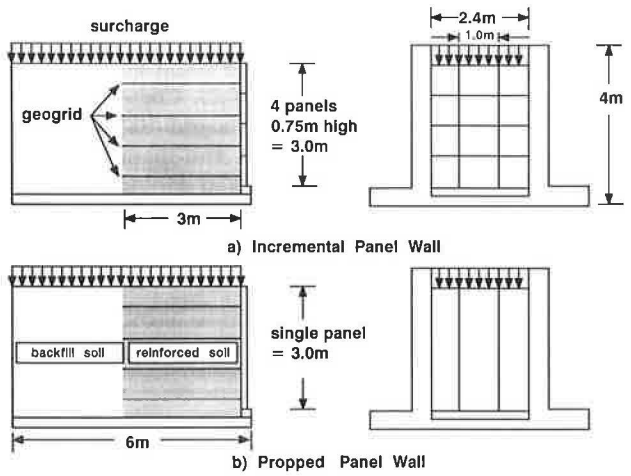

FIGURE 3 Typical test configurations: (a) incremental panel wall; (b) propped panel wall.

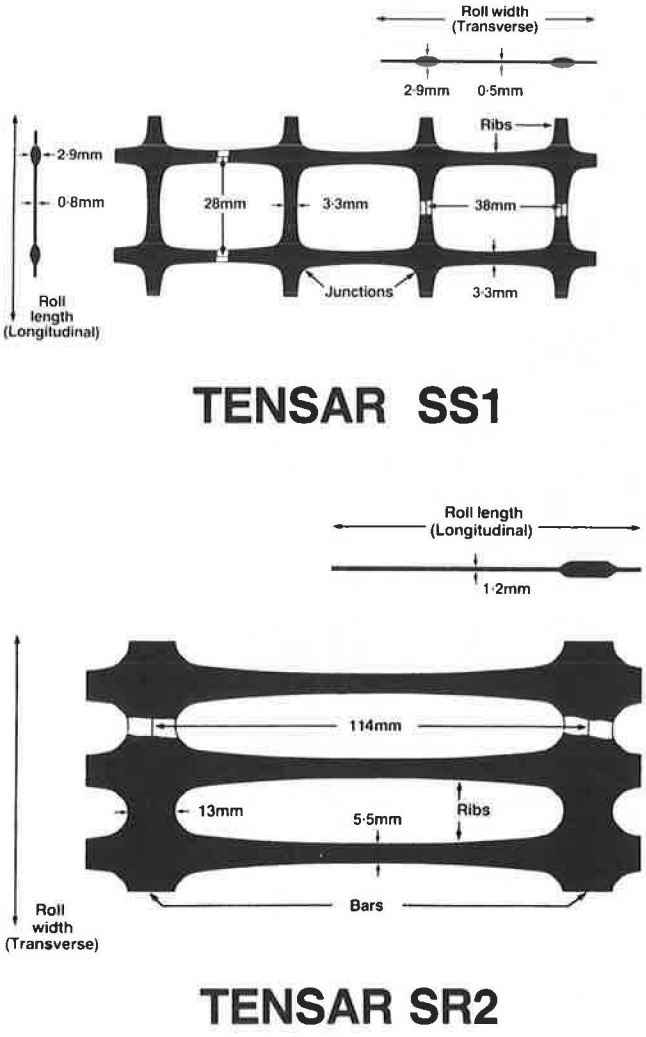

FIGURE 4 Tensar geogrids: (*bottom*) Tensar SR2; (*top*) Tensar SS1.

TABLE 1 MECHANICAL PROPERTIES OF GEOGRID REINFORCEMENT MATERIALS (ASTM D4595 WIDE WIDTH STRIP TENSILE/ELONGATION TEST)

Material	Stiffness @ 2% strain (kN/m)	Peak Load (kN/m)	Strain @ Peak Load (%)
Tensar SR2[a]	1,096	79	17
Tensar SS1[b]			
transverse (strong)	292	20	14
longitudinal (weak)[c]	204	12	14

[a]High-density polyethylene uniaxial grid.
[b]Polypropylene biaxial grid.
[c]SS1 oriented in weak direction for RMC trial walls.

SOURCE: Manufacturer's literature.

grid. Consequently, each load was left on for a minimum of 100 hours to observe time-dependent deformations in the wall and, in particular, creep in the grid reinforcement.

INSTRUMENTATION

General

The following measurements were considered to be of primary importance in the RMC wall tests:

1. horizontal and vertical movements of the facing units;
2. reinforcement displacements, strains, and forces;
3. loads at the panel-grid connections;
4. vertical earth pressures;
5. horizontal and vertical toe loads; and
6. internal soil displacements.

The instrumentation used to make these measurements is described in the following sections, and an instrumentation layout used in a typical test is shown in Figure 5.

Horizontal and Vertical Movements of Facing Panels

The pattern and magnitude of horizontal facing movements is a primary set of data, because facing geometry is an important and obvious indicator of wall performance. Spring-loaded hybrid track rectilinear (HTR) potentiometer displacement devices manufactured by Penny and Giles Potentiometers Limited were used to measure wall deformations. These devices operate on a potentiometer principal and were powered by 10 volt DC excitation. The devices gave an accuracy of ± 0.5 mm and were relatively cheap and extremely robust. In some instances, devices that were in pieces due to wall collapse were reconstructed and used again with no performance deterioration. Figures 6(a) and 6(b) show typical panel deformation profiles recorded at the end of construction, at the end of the 50 kPa surcharge increment, and just prior to wall failure in two recent tests that used a very extensible reinforcement (Tensar SS1). Figure 6(b) shows that the largest panel movements in the incremental wall occurred in Panel 3. However, subsequent tests have shown that the relative movement in incremental panel movement profiles is critically dependent on the details of panel placement and alignment during the construction phase.

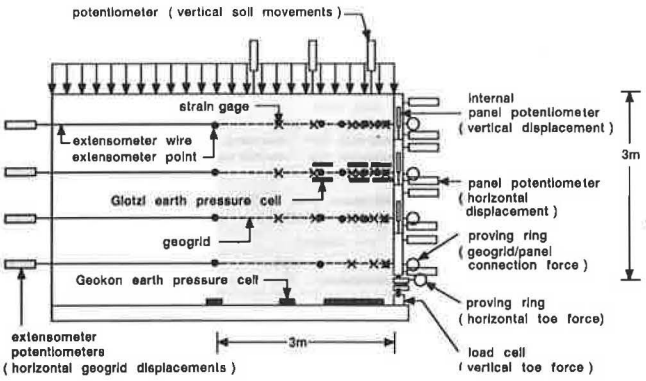

FIGURE 5 Typical layout of principal instrumentation for incremental panel wall test.

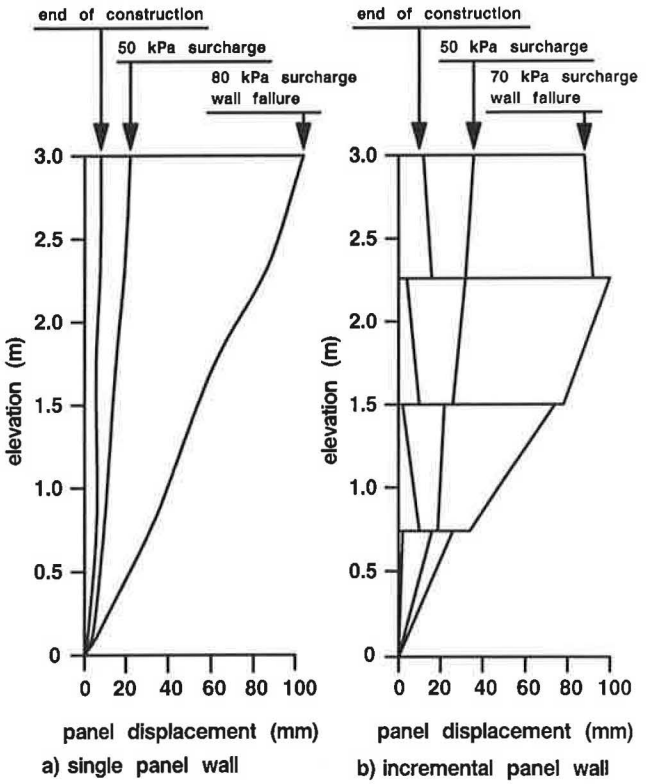

FIGURE 6 Panel displacements using SS1 geogrid: (a) single panel wall; (b) incremental panel wall.

Reinforcement Displacements, Strains, and Forces

Displacements and strains in the reinforcement inclusions were measured because these parameters allow conclusions to be drawn concerning grid-soil load transfer mechanisms and creep behavior in polymeric grids. In addition, if the mechanical properties of the grid material are known, grid forces can be estimated and the grid forces used to examine stability of the retaining walls at limiting equilibrium.

Total horizontal displacements at selected grid locations were monitored by extensometers attached to grid junctions. These devices were constructed in-house and comprised a thin galvanized steel line attached to a miniature bolt and eye attachment passing through the grid junction. The extensometer wire was protected and isolated from the soil by passing it through a stiff plastic brakeline tubing. The wires were attached to HTR potentiometers mounted on a rack at the back of the test facility (Figure 5). The horizontal displacement response of extensometers mounted on grid layer 3 of an incremental wall test is shown in Figure 7. The data show that abrupt changes in grid displacement matched surcharge loading steps and that, as the magnitude of surcharging increased, there was increased creep deformation in the reinforcement layer. Similar qualitative features were observed in all layers. In this particular test there was a soil-to-soil failure through the reinforced mass of soil after the final load increment had been applied for 93 hours. Approximately 400 hours after soil failure, grid rupture occurred and the wall collapsed. Figure 8 plots displacement profiles in grid layers as recorded by the extensometer devices from several tests at wall failure. The data shows that all significant grid deformations were restricted to less than 1.5 m behind the panel facings. An implication from these results is that the reinforcement lengths are unnecessarily long even though conventional limit equilibrium-based methods of design for these systems would typically result in grid lengths greater than 2-m, assuming a design surcharge of 50 kPa.

Strains in the grid reinforcement up to 2 or 3 percent strain were measured by bonding high-deformation gauges directly to mid-rib locations on the reinforcement. The combination of grid type, grid surface preparation technique, and type of glue was developed at RMC after much experimentation (*7*). A high-strain foil-type gauge manufactured by Showa Measuring Instruments Co. Ltd. (Type Y11-FA-5-120) has proved successful with both polypropylene and high-density polyethylene Tensar geogrids. Grid surface preparation involved abrading the surface of the rib with a fine grit sand paper, surface cleaning, surface neutralization followed by bonding of the gauge to the grid using a RTC two-part epoxy resin cement. The gauges and lead wires were protected by a waterproof bubble of silicon and the silicon wrapped with flexible plastic tubing. The strain gauging technique has proved very reliable, and a 100 percent success rate following placement in soil is routine. The same gauge and bonding technique has

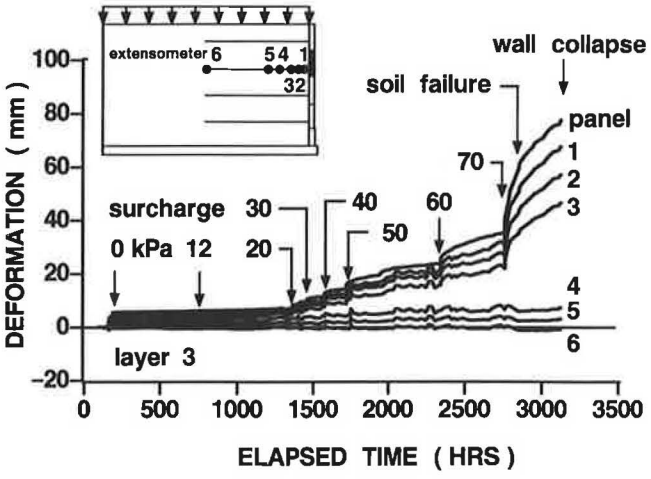

FIGURE 7 Horizontal grid deformations measured by extensometers (incremental panel wall test).

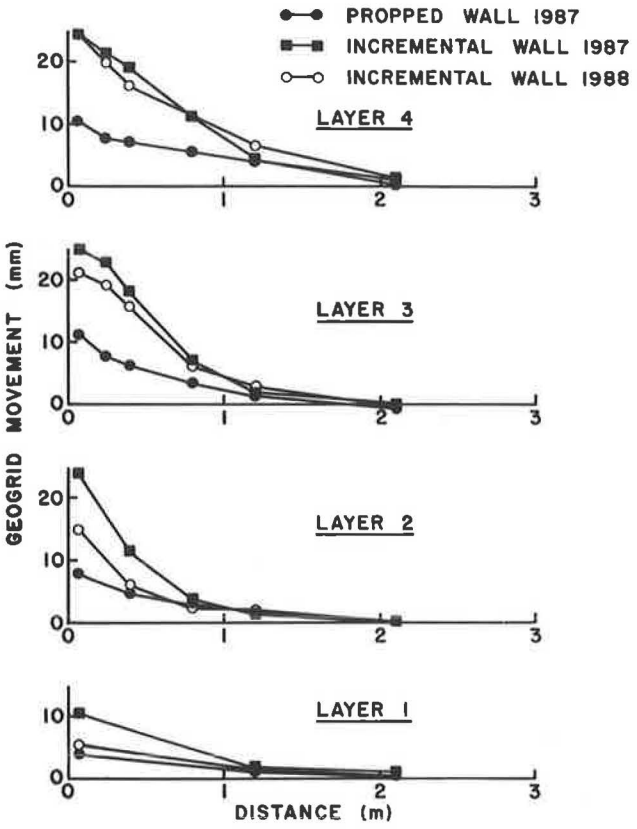

FIGURE 8 Distribution of grid displacements (incremental and propped panel wall tests).

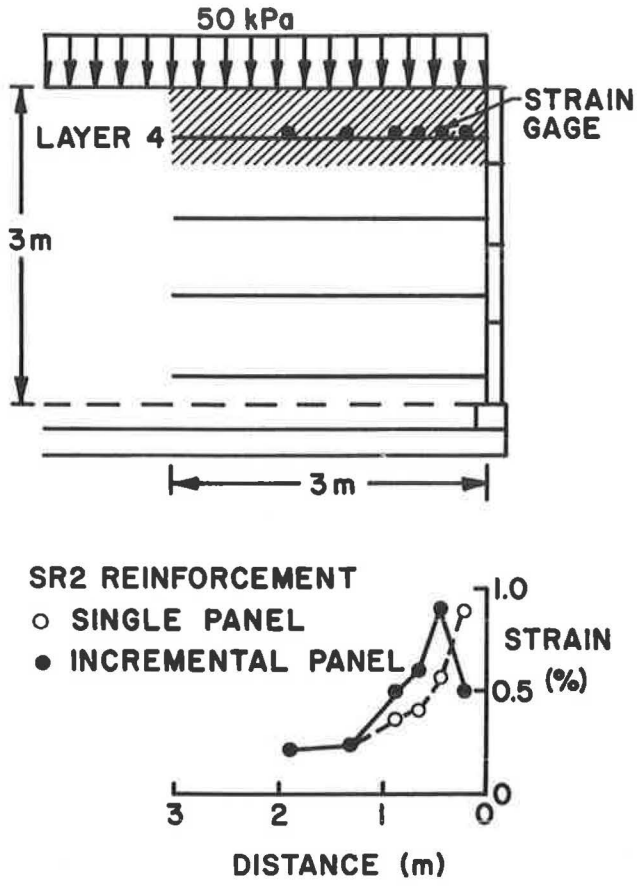

FIGURE 9 Influence of wall type on grid strains.

been successful in more aggressive environments, including strain-gauged grids placed at the interface between granular bases and peat subgrades (*8*) and in hot mix asphalt pavements (*9*).

Experience with full-scale geogrid-reinforced soil walls constructed with Tensar SR2 geogrid showed that the strains in the grid did not exceed 1 percent strain even under surcharging to 50 kPa (*1*). At this level of strain the gauges were adequate. However, when trial walls with a very weak grid were constructed, these grids exhibited prerupture strains as high as 10 percent, by which time the strain gauges had debonded (*2*,*4*,*5*). Nevertheless, at large strains the extensometer movements were such that, after about 3 percent strain in the grid, extensometer movements were great enough that large-strain measurements could be calculated with confidence from the array of extensometers attached to each grid layer. An example of strains measured along the length of the topmost grid layer in incremental and propped walls reinforced with Tensar SR2 is shown in Figure 9. The profiles indicate that significant grid strains only extend to about 1 m into the soil when a 50 kPa surcharge pressure was applied to the models. The maximum strain is less than about 1 percent strain.

Also of importance is the difference in the pattern of strain between these two tests. The propped panel wall showed maximum strain close to the connection, while the grid with the incremental panel showed a peak strain at working load conditions that was located back from the wall. The trend toward peak strains in the vicinity of the connections in the propped wall case is thought to be due to the relative downward movement of the retained soil with respect to the panels, which are restrained in the vertical direction. The incremental panels, on the other hand, were constructed with a compressible foam layer between panels that reduced the magnitude of relative movement. An important implication to the design of propped wall systems is that, at working load levels, the largest grid strains are likely to occur at the connections rather than at locations within the reinforced soil mass as predicted by tie-back wedge methods of analysis. This is particularly true in the field, where voids in the soil directly below the connections are inevitable. Consequently, tensile loads due to a membrane effect can be anticipated for these grids immediately behind the wall, in addition to the tensile loading associated with grid anchorage. Details of connection arrangements to minimize connection strains have been reported by Jones (*10*).

Figure 10 shows grid strain profiles at different times during surcharging of an incremental panel wall constructed with a weak grid (*4*). The data for Figure 11 show that grid strains were largest at locations on the reinforcement layers corresponding to the internal failure wedge observed during excavation of the reinforced wall and during excavation of an unreinforced wall that was carried out for comparison purposes (*6*). Superimposed on the figure is an approximation of the failure line based on Rankine theory. It appears that at incipient collapse the volume of failed soil is reasonably well represented by a Rankine failure wedge. However, as Figure

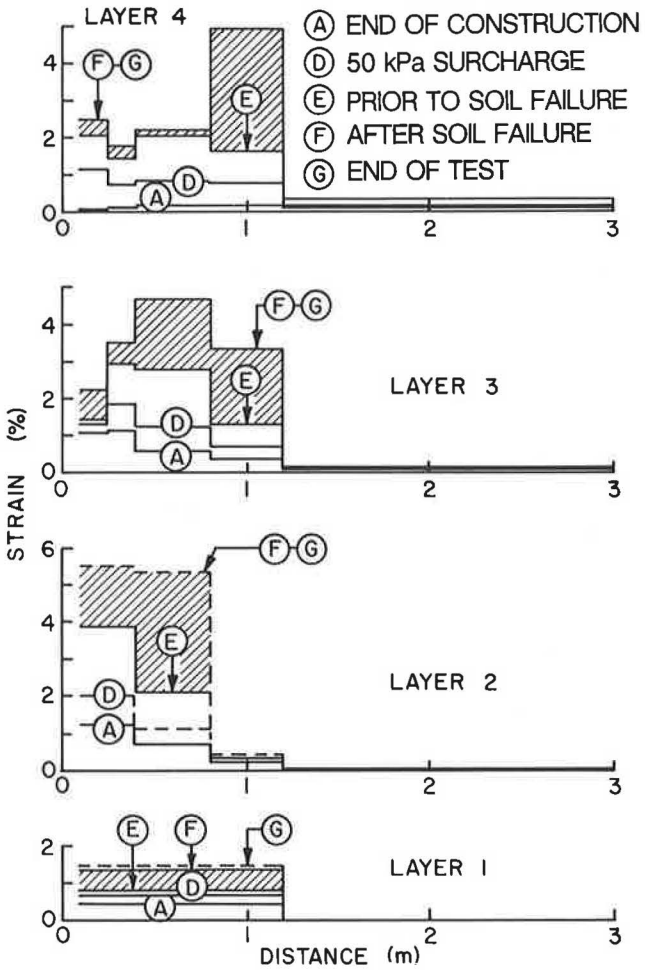

FIGURE 10 Distribution of grid strains (incremental panel wall test).

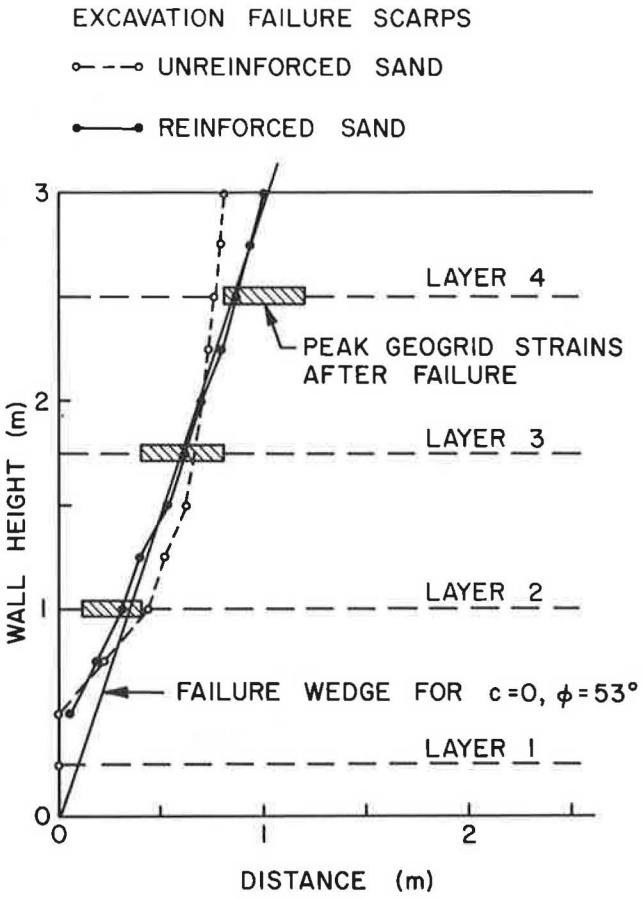

FIGURE 11 Excavated failure surfaces.

10 demonstrates, the pattern of grid strain distribution at working load levels (say 50 kPa) does not reflect the trend observed at the end of the test at 100 kPa surcharge, when the wall was close to collapse. This discrepancy highlights the problem of using design methods that attempt to scale conditions at limiting equilibrium to working load conditions.

The results of in-isolation calibration tests with uniaxial SR2 and biaxial SS1 grids loaded in the longitudinal (weak) direction has shown that gauges mounted at mid-rib location record strains that are sensibly equivalent to the gross strain in the sample measured over several grid apertures. However, this is not necessarily true of all grid materials. The location of the gauge, the geometry of the rib, and the modulus of the highly oriented polymer all influence gauge registration.

The strain gauges in the RMC walls were placed in rows such that there were three gauges at nominally identical locations from the back of the facings. This procedure ensured a representative average strain at nominally identical locations, since the strain gauge response can be influenced by small variations in the location of the gauges on the rib and the local effects of soil in contact with the gauge-grid assembly. In addition, it has been noted that grid tensile strains may not be attenuated uniformly along rib lengths, owing to (1) inherent warps during attachment and laying out of the grid, and (2) skewness in the grid as manufactured.

The calculation of grid forces at locations within the soil mass is difficult, owing to the complex load-strain-time-temperature behavior of the polymeric grids. The mechanical properties of grids in this context have been the topic of investigation by others (*11*,*12*). Based on this earlier work, in-isolation tensile testing was carried out on virgin samples of grid taken from the same rolls of material supplied by the manufacturer. Each sample was subjected to a constant load and temperature for periods up to 1,000 hours. The in-isolation testing temperature of 20°C corresponds to the ambient temperature of the RMC test facility. The results of testing of this type on Tensar SR2 are presented in Figure 12 in the form of isochronous load-strain curves and a Sherby-Dorn plot (*1*). These data were used to estimate the tensile grid forces at any time during the loading program, based on the assumption that the cumulative strain during a surcharge load increment is equivalent to the strain that would have occurred had the surcharge load been applied in a single load step. The results of stage-loaded in-isolation tensile testing of Tensar geogrids suggest that this is a reasonable assumption (*11*). A similar tensile testing program was carried out with samples of SS1 Tensar geogrid and the data used to estimate grid forces in the RMC trial walls constructed with a weak reinforcement. The results of grid force calculations confirmed that the early trial wall tests with SR2 were stable and that grid forces and

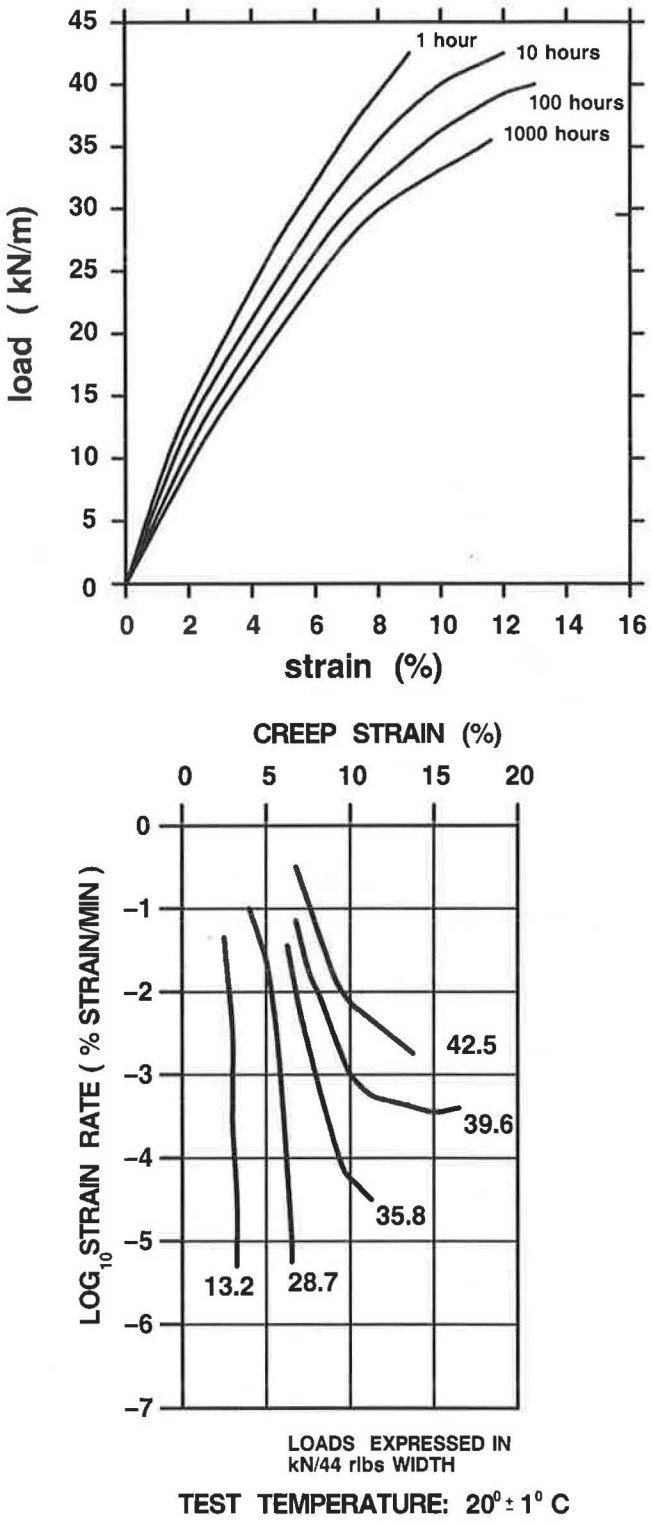

FIGURE 12 Load-strain-time properties of Tensar SR2 geogrid: (top) isochronous load-strain curves; (bottom) Sherby-Dorn plot.

strains were well below levels associated with long-term rupture. Similarly, walls that have failed using SS1 grid material showed that inferred tensile forces were consistent with the restraining forces required to maintain a wedge-shaped zone of reinforced soil at the point of incipient failure (*4*) and that measured connection forces were consistent with inferred grid tensile forces in the vicinity of the connections when incremental facings were used.

Connection Forces

Loads generated at the connection between the panel and the grid reinforcement can be used to estimate the distribution of lateral earth pressure acting at the facings. The calculation of lateral earth pressures is a routine step in many current methods of reinforced soil wall design.

Connection loads have been measured using a series of proving rings connected to the grid layers. The essential features of these devices are shown in Figure 13. Five proving rings per layer were used. The grids were clamped to a plate using a bolt and angle arrangement, and the clamp was connected in turn to the proving rings by high-strength stainless steel rods passing through a series of bushings to the proving rings.

An example of the response measured in a recent reinforced wall taken to failure is illustrated in Figure 14. The forces measured at the connections show that they are sensitive to surcharge load level and that there is time-dependent load shedding to the facing units. An interesting feature is that prior to the final 70 kPa load increment there was a nonuniform distribution of connection loads. However, at incipient failure the connection loads appear to have become uniform, suggesting that as the collapse condition is approached there is a tendency of load redistribution in the vicinity of the connections.

Vertical Earth Pressures

The distribution of vertical earth pressures at the base of the wall was measured using a total of six Geokon EP-3500 pressure cells. Each cell is constructed from two circular stainless steel plates welded together along their perimeter to create a narrow cavity, which is filled with an incompressible fluid (Figure 15). The cells are 230 mm in diameter and have an aspect ratio of 18 (diameter/thickness ratio). A length of stainless steel tubing connects the pressurized cavity to a housing that contains a semiconductor strain gauge pressure transducer. The pressure cells were modified by the manufacturer with low-pressure transducers to ensure adequate sensitivity to the relatively low vertical earth pressures anticipated for these walls (i.e., maximum of 160 kPa).

Two problems routinely present themselves when using earth pressure cells for the purpose described here: the difficulties associated with seating the instrument so that the pressures at the point of measurement are not altered by the installation; and accurate calibration of the device. The installation problem was overcome by placing the cells in a plaster of paris layer so that the face of the cell was flush with the surface of the plaster. The plaster of paris was extended over a wide area so that arching of the soil in the vicinity of the active face was prevented, and the connecting tube and housing were also rigidly seated.

A number of calibration techniques were considered. Calibration in air was not attempted, since general experience with a number of earlier cells has shown that calibration in air does not necessarily give the in situ response despite nominally identical pressures. Instead, as a first attempt, the cells

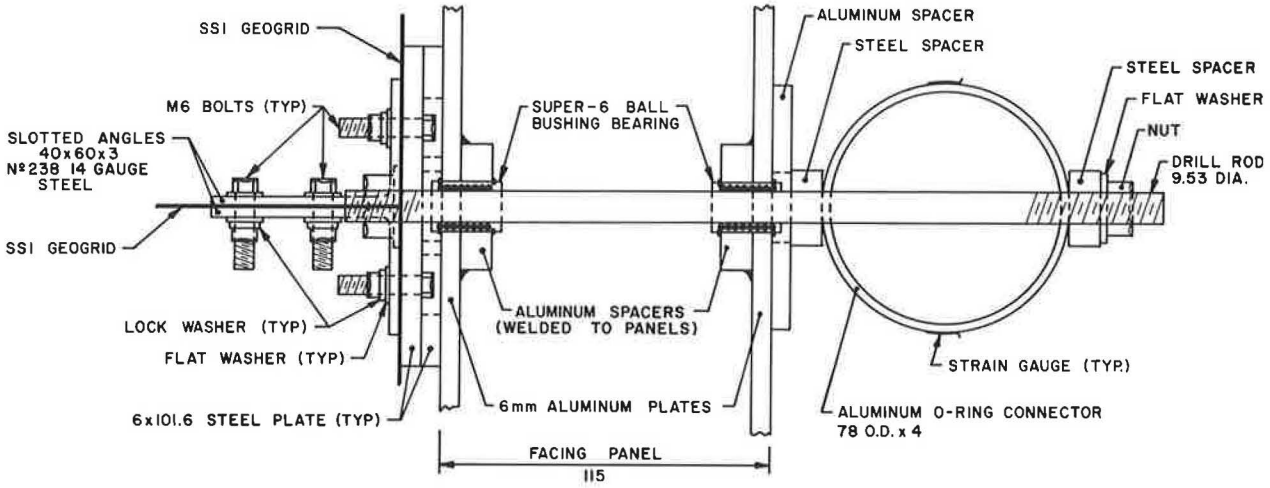

FIGURE 13 Proving ring arrangement for connection load measurement (all dimensions in mm).

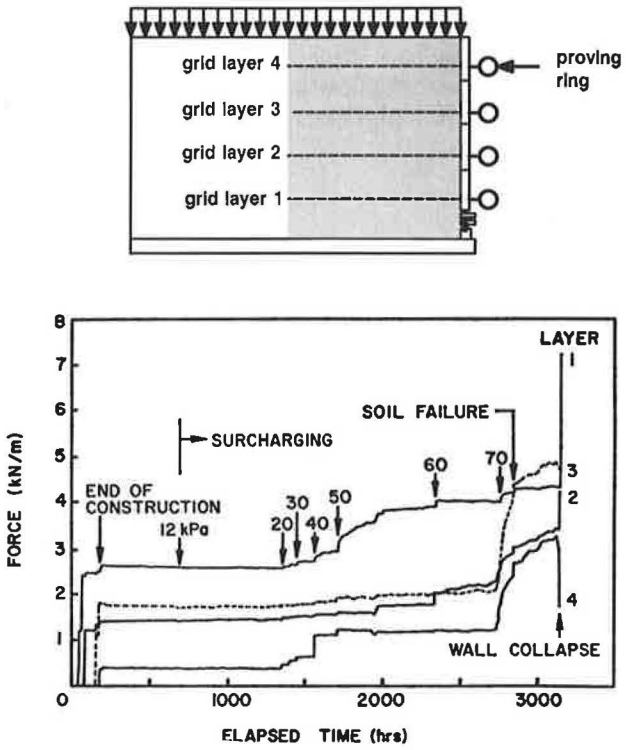

FIGURE 14 Connection forces (incremental panel wall with SS1 geogrid reinforcement).

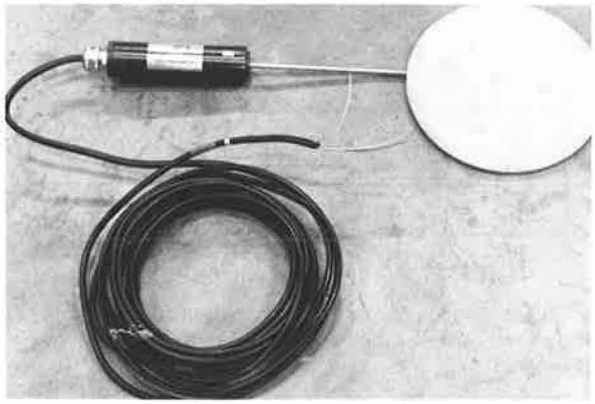

FIGURE 15 Geokon EP 3500 earth pressure cell (diameter = 230 mm).

were placed in a modified 250 mm diameter Rowe oedometer. However, the response of the cells was found to be sensitive to details of placement and compaction of the sand soil and oedometer edge effects. The most successful method was to calibrate the Geokon pressure cells in situ. In this approach the cell response was determined based on the unit weight of the soil placed to a depth of 1 m over the cell during the initial stages of wall construction. Once this calibration was established, it was used to determine the response of the cell at all subsequent stages in the loading program. This method avoided the difficult problem of replicating in situ placement conditions within a calibrating device.

The Geokon cells proved very successful in identifying the distribution of earth pressures at the base of the reinforced soil mass. Typical data for an incremental panel wall test are summarized in Figure 16. In general, the vertical earth pressure distribution was observed to be roughly equivalent to the value predicted from the combined weight of the applied surcharge and soil self-weight, with the exception of the cell closest to the wall. These data, together with similar measurements from other tests, indicate that under surcharging a significant portion of vertical soil pressures in the immediate vicinity of the facing panels is carried by the wall.

Horizontal and Vertical Toe Forces

Geosynthetic-reinforced walls constructed from incremental or rigid facing units are built with a concrete footing that serves to support and maintain grade for the facing units. If the stability of the reinforced wall at limiting equilibrium is based on a tie-back wedge analysis, then it is possible to view the free-body diagram defining the failure wedge as having a restraining force acting at the wall toe. This additional restraint is not considered in any current methods of analysis known to the author. Of particular interest has been the magnitude

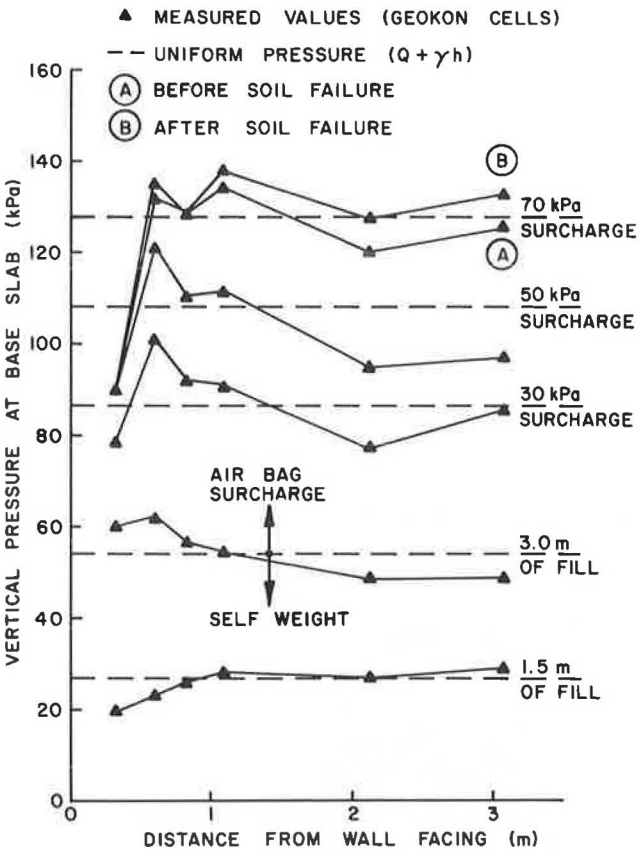

FIGURE 16 Distribution of vertical earth pressures at base of reinforced soil (incremental panel wall with SS1 geogrid reinforcement).

of the vertical and horizontal forces carried by the levelling pad in walls having a generic construction similar to the RMC trial walls.

In order to monitor these forces, a series of load cells were used to support the pin connection at the base of the facing units (Figure 5). The base of the wall was restrained in the horizontal direction by a series of proving rings manufactured in-house. The results of horizontal load measurements were consistent with the results of earth pressure measurements at the base of the reinforced soil mass. In other words, the integrated vertical earth pressure distribution plus the vertical component of wall force was equivalent to the soil self-weight and surcharge force. The results of horizontal force measurements showed that the magnitude of vertical toe force was roughly equivalent to the connection forces at wall failure. This observation has important implications for the design of these structures, since this additional stabilizing force is not routinely included in reinforced wall design but can, as these results have shown, contribute a resistance equal to 20 percent of the total active force measured at the facings.

Additional Instrumentation

An array of instrumentation of secondary importance was deployed in recent RMC trial wall tests and is described briefly here for the purpose of completeness.

A number of 30 mm Bison inductance coils were placed in coaxial pairs at selected locations within the reinforced soil mass to record horizontal soil movements. These devices have been used by other investigators to measure "strains" in soil (*13*). Experience with these devices showed them to be difficult to install and align, and soil "strains" could not be inferred from the response. Nevertheless, the devices did prove useful in confirming the location of soil volumes that were disturbed and the exact times at which events such as soil failure occurred.

HTR potentiometers were mounted inside the panels to record the compression of foam layers between incremental wall panels and to record vertical soil movements at the surface of the reinforced soil mass (Figure 5).

In selected tests a number of Glotzl cells (*13*), 200 mm by 300 mm in plan with electrical pressure transducer readouts, were placed above and below grid layer 3 (Figure 5). These cells were also calibrated in situ using the same approach as that described for the Geokon cells. The results of vertical earth pressures measured in the vicinity of grid layer 3 were consistent with qualitative features in Figure 16, indicating that there is a membrane effect whereby vertical stresses are relieved by the reinforcement inclusion in the area of the connection and transferred to the wall panels.

Data Acquisition

Up to 300 electronic devices have been installed in the RMC test walls. Necessarily, the devices can only be effectively monitored using automatic data acquisition. The primary piece of equipment to meet this need was a 300-channel Hewlett Packard HP 3497A/3498A data acquisition system. All electrical devices gave an analog DC voltage signal or were connected to external electrical circuitry that could convert output signals to a DC voltage that could be read by the data acquisition system (e.g., Bison inductance coils).

The data acquisition system was controlled by a PC-DOS microcomputer with its own 20 minute power backup supply. The data acquisition system was programmed to record the response of all instruments at a selected time interval (typically 8 hours). However, several of the potentiometers on the panel facing units and air pressure supply transducers were monitored continuously and were programmed to trigger full-channel acquisition if significant changes in device output were sensed. In this way, significant events in the testing program were captured, such as tertiary creep in the grids just prior to wall collapse.

At least as important as data acquisition was data post-processing. A tremendous amount of data was routinely generated because some tests lasted as long as 7 months. Commercially available software was used to write post-processing packages for the accumulated data after conversion to LOTUS format. The raw data from the PC controller was analyzed for changes in signal output and the optimized data set converted to useful units and then plotted. The post-processing software allowed a full history of all test instrumentation to be available within minutes. This ability to digest a large amount of data rapidly is important when quick decisions have to be made concerning the magnitude and duration of surcharge loading to be applied as wall failure is approached.

CONCLUDING REMARKS

The development of the RMC Retaining Wall Test Facility and ancillary instrumentation has provided the author and coworkers with the capability to carry out carefully monitored tests of full-scale geosynthetic-reinforced walls. The comprehensive monitoring of model walls and the quality of the data has allowed the author to identify important mechanisms in the behavior of these complex systems during construction, under working load conditions, and at failure. The data are also proving useful in the development and calibration of analytical models, which are proceeding concurrently with the experimental program.

ACKNOWLEDGMENTS

The program of experimentation reported in this paper has taken place over a period of 5 years. During this time many people have contributed to the success of the program, and it is not possible to identify them all. However, the author would like to acknowledge the important contribution of P. M. Jarrett of the Civil Engineering Department at RMC; graduate students S. R. Lescoutre, W. F. Wawrychuk, D. S. Benjamin, A. W. Wisniowski; and research assistants J. Bell and J. DiPietrantonio. The author is also indebted to The Tensar Corp. and Netlon Ltd. for provision of reinforcement materials, and to Dr. A. McGown of the University of Strathclyde, Glasgow, Scotland, for the laboratory testing of the Tensar materials. The funding for the work reported in the paper was provided by the Department of National Defence (Canada).

REFERENCES

1. R. J. Bathurst, W. Wawrychuk, and P. M. Jarrett. Laboratory Investigation of Two Large-scale Geogrid Reinforced Soil Walls. In *The Application of Polymeric Reinforcement in Soil Retaining Structures* (ed. P. M. Jarrett and A. McGown), Kluwer Academic Publishers, Dordrecht, Netherlands, 1987, pp. 71–125.
2. R. J. Bathurst, D. J. Benjamin, and P. M. Jarrett. Laboratory Study of Geogrid Reinforced Soil Walls. In *Geosynthetics for Soil Improvement*, (ed. R. D. Holtz), ASCE, New York, 1988, pp. 178–192.
3. R. J. Bathurst, P. M. Jarrett, and S. R. Lescoutre. An Instrumented Wrap-around Geogrid Reinforced Soil Wall. *Proc., 3rd Canadian Symposium on Geosynthetics*, Waterloo, Ontario, 1988.
4. R. J. Bathurst, D. J. Benjamin, and P. M. Jarrett. An Instrumented Geogrid Reinforced Soil Wall. *Proc., XII International Conference on Soil Mechanics and Foundation Engineering*, Rio de Janerio, Brazil, 1989.
5. R. J. Bathurst and D. J. Benjamin. Failure of a Geogrid Reinforced Soil Wall. Presented at 69th Annual Meeting of the Transportation Research Board, Washington, D.C., 1990.
6. R. J. Bathurst and D. J. Benjamin. Preliminary Assessment of Sidewall Friction of Large-Scale Models in the RMC Test Facility. In *The Application of Polymeric Reinforcement in Soil Retaining Structures* (eds. P. M. Jarrett and A. McGown), Kluwer Academic Publishers, Dordrecht, Netherlands, 1987, pp. 181–192.
7. *Strain Gauge Preparation Notes for Tensar Geogrids*. Civil Engineering Department, Royal Military College of Canada (unpublished).
8. P. M. Jarrett and R. J. Bathurst. Strain Development in Anchorage Zones, *Proc., Geosynthetics '87 Conference*, New Orleans, 1987.
9. O. A. Abdelhalim, R. C. G. Haas, J. Walls, R. J. Bathurst, and W. A. Wang. A New Method for Effective Reinforcement of Asphalt Pavements. *Transportation Forum*, Vol. 2, No. 1, 1985, pp. 29–41.
10. C. J. F. P. Jones. *Earth Reinforcement and Soil Structures*. Butterworths, London, 1985.
11. K. C. Yeo. *The Behaviour of Polymeric Grids used for Soil Reinforcement*. Ph.D. Thesis, Department of Civil Engineering, University of Strathclyde, Glasgow, Scotland, 1985.
12. A. McGown, K. Andrawes, K. Yeo, and D. Dubois. The Load-Strain-Time Behaviour of Tensar Geogrids. *Proc., Symposium on Polymer Grid Reinforcement in Civil Engineering*, London, 1984.
13. T. H. Hanna. Field Instrumentation in Geotechnical Engineering. Trans Tech Publications, Cleveland, Ohio, 1985.

Publication of this paper sponsored by Committee on Mechanics of Earth Masses and Layered Systems.

Evaluation of Bearing Capacity of Vibro-Driven Piles from Laboratory Experiments

MICHAEL W. O'NEILL, CUMARASWAMY VIPULANANDAN, AND DANIEL O. WONG

Representative methods for predicting the bearing capacity of piles driven by vibration are described briefly, and a need to establish pile resistance prediction procedures that are based on soil properties is established. In order to investigate the influence of soil properties on piles installed by vibration, a large-scale model study was conducted in which piles were driven into a pressure chamber, to simulate in situ stress conditions, and subjected to loading tests. The soil, vibrator, and pile properties were closely controlled. Methods were developed from pile mechanics considerations and the test data (a) to predict pile capacity and (b) to select vibrator characteristics to drive piles of known target capacities. These methods are expressed in the form of simple equations that can be applied by designers having appropriate knowledge of soil, pile, and vibrator conditions. Whereas every attempt was made in the laboratory study to simulate field conditions, field verification and calibration of the capacity prediction methods are necessary before they can be applied in practice.

The driving of piles by vibration is favored by many contractors, since the installation process generally requires less time than installation by impact driving, especially in cohesionless soils. It is not uncommon for a 60- to 70-ft-long pile to be installed in less than 5 min with vibration, whereas a similar pile driven by impact may require 15 to 30 min to install.

A schematic of a typical pile-driving vibrator, or "vibrodriver," is shown in Figure 1. The vibrator employs counterrotating masses, or an equivalent mechanism, to produce dynamic forces. In some systems, a bias mass that is isolated from the mass of the vibrator by soft springs is used to provide additional static bias load to assist in penetration. The vibrodriver forces are transmitted to the head of the pile through some type of connection, usually a chuck or hydraulic clamp, which affords an opportunity for energy loss, much as cushioning systems produce energy losses during impact driving. The pile, in turn, resists the applied forces by a combination of shaft and toe resistance that may deviate from the patterns of resistance developed during impact driving.

An impediment to the use of vibratory drivers has been the inability of designers to verify the bearing capacity of installed piles in the manner afforded by wave equation analysis of impact-driven piles. Consequently, current accepted practice consists of restriking of vibro-driven piles with an impact hammer to verify static capacity calculations by means of wave equation analysis or by direct dynamic monitoring. This field procedure is counterproductive to the contractor's progress.

M. W. O'Neill and C. Vipulanandan, Department of Civil and Environmental Engineering, University of Houston, Houston, Tex. 77204-4791. D. O. Wong, McBride-Ratcliff and Associates, 7220 Langtry, Houston, Tex. 77040.

PREDICTIVE FORMULAE

In the past, some notable attempts have been made to develop driving formulae to predict the capacity of vibro-driven piles without restriking the piles. Several representative examples are described briefly below.

Snip Formula

This empirical formula is used in Soviet practice and is predicated on observed behavior of full-sized piles in the Soviet Union (*1*):

$$Q_t = \lambda \left(\frac{25.5\ P}{A_o f} + W_t \right) \tag{1}$$

where

Q_t = ultimate, static, compressional bearing capacity of pile, in kN;
P = power used by vibrator to drive pile, in kilowatts;
A_o = displacement amplitude of vibrator, in cm;
f = frequency of vibrator, in Hz;
W_t = total weight (force) of vibrator and pile, in kN; and
λ = empirical coefficient reflecting the influence of driving on soil properties (e.g., in Soviet practice λ is taken to be equal to 5 in cohesionless soils).

Davisson's Energy Balance Formula

Davisson's formula (*2*) is the vibratory equivalent of the modified Engineering News formula for impact-driven piles, in that it is based on an energy balance (energy supplied = energy used + losses). It was specifically developed for piles driven with resonant drivers and may be expressed in the form

$$Q_t = \frac{550\ P\ (\text{horsepower})}{(r_p + f\, s_l)} \tag{2}$$

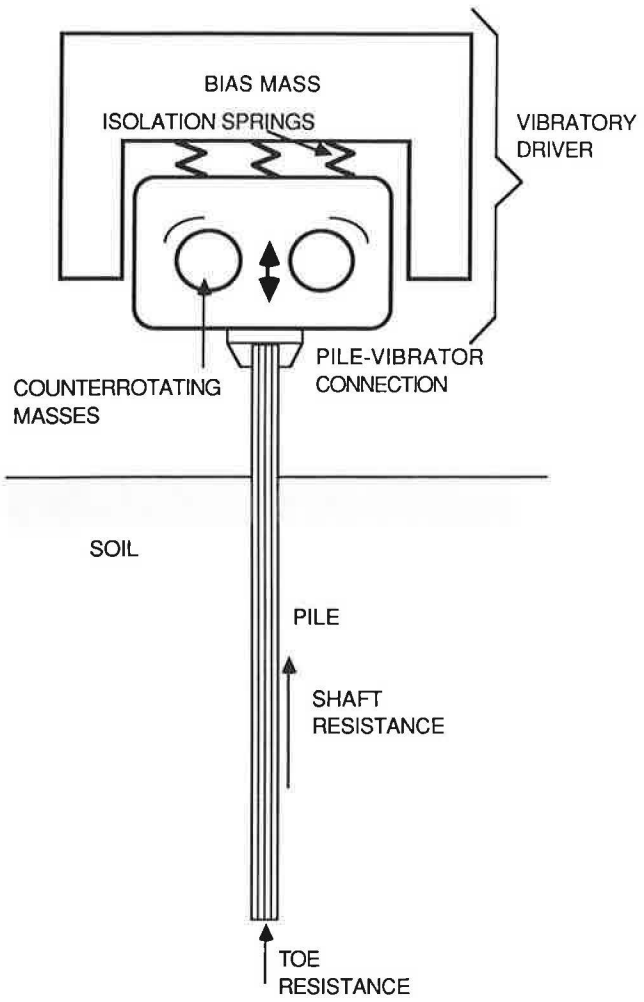

FIGURE 1 Schematic of typical vibro-driver and pile.

where

r_p = rate of pile penetration, in ft/sec; and
s_t = loss factor (equivalent set), in ft/cycle.

If the rate of penetration is high (pile capacity low), it is necessary to add another term to the numerator of Equation 2 to account for the kinetic energy of the driver. This term is evaluated as 22,000 r_p. It is necessary at present to calibrate Equation 2 to specific site conditions in order to evaluate s_t. Typical values that have been used for resonant drivers (specifically, the Bodine BRD 1000) are 0.0008 to 0.008 for loose to dense cohesionless soil, respectively, with closed-ended pipe piles. Corresponding values for s_t for H piles are -0.0007 to $+0.007$.

Schmid's Impulse Formula

This equation (*3*), appropriate in principle for low-frequency, nonresonant drivers, focuses on the impulse at the pile toe during driving. Considering the pile and vibrator as a free body, the impulse equation for one cycle of vibration, after cancellation of the impulse from the unbalanced forces from the vibrator, becomes

$$\frac{W_b + W_v + W_p}{f} = \int_0^{T_c} Q_t \, dt = \alpha Q_t \, T_c \tag{3a}$$

where

W_b = weight of bias mass (mass separated from vibrator by springs to prevent its vibrating in phase with the vibrator);
W_v = weight of vibrator and
W_p = weight of pile;
α = a coefficient, generally taken to be 0.67; and
T_c = time of contact between toe and underlying soil on one cycle.

In order to evaluate T_c, one must find the minimum pile acceleration amplitude to affect penetration by means of driving tests. Acceleration amplitude in excess of this minimum acceleration (acceleration corresponding to impending refusal) is termed excess acceleration, a_e, and T_c is computed as follows:

$$T_c = \left(\frac{2\, r_p}{f\, a_e}\right)^{0.5} \tag{3b}$$

From Equations 3a and 3b it follows that

$$Q_t = \frac{\alpha\,(W_b + W_v + W_p)}{f\,(2\, r_p / f\, a_e)^{0.5}} \tag{3c}$$

Wave Equation Methods

The one-dimensional wave equation may logically be extended from impact driving to vibratory driving; however, very few published studies exist relative to this point. Chua et al. (*4*) describe replacing the ram, cushion, and capblock with a forcing function from a simple oscillator to model the rate of penetration of a full-scale pipe pile in a sand deposit. They indicate generally good agreement between calculated and measured penetration rates and force time histories, which suggests that, with suitable studies to calibrate the soil parameters, a wave equation approach to capacity prediction, based on vibrator properties and rate of pile penetration, may be successful in the future.

While the methods reported above and other similar methods are potentially useful, they do not explicitly incorporate fundamental soil properties, such as relative density, effective stress, and grain size. Since such properties are known to have significant effects on the capacity of impact-driven piles, it is logical that formulae that include them for the evaluation of bearing capacity of vibro-driven piles should produce more accurate predictions than formulae that do not explicitly contain their effects. The remainder of this paper describes a set of such formulae derived from large-scale laboratory tests in clean, submerged sands, in which the test piles were full-displacement, closed-ended steel pipe piles. The formula are presented in such a way as to be useful in practice, and a discussion of their applicability to field conditions follows their presentation.

TESTING SYSTEM

Details of the laboratory testing system and observed behavior of the test piles, including their performance relative to piles driven by impact, are described elsewhere (*5,6*); however, a brief description of the testing system is provided here for clarity. A reusable, instrumented, closed-ended steel pipe, approximately 95 in. long and 4.00 in. in diameter, was driven with a vibrator 78 in. (or to refusal) into a pressurized sand column 30 in. in diameter, contained within a chamber. Coarse and fine uniformly graded clean sands were placed in the chamber at relative densities ranging from 65 to 90 percent. For the lower relative density, both sands were very slightly contractive and possessed angles of internal friction of 38.5 and 39.6 degrees (coarse and fine sand, respectively). For the higher relative density, both sands were dilative and possessed angles of internal friction of 42.2 and 43.6 degrees, respectively. Angles of wall friction on the steel of the test pile were 25 to 27.5 degrees for the coarse sand and 27 to 30 degrees for the fine sand, with the lower ends of the range corresponding to the lower values of relative density. Lateral effective pressures in the range of 10 to 20 psi were applied to the submerged sand column to represent mean lateral effective pressures that would be encountered in situ along the lengths of prototype piles in slightly overconsolidated, submerged sands that penetrate 50 to 100 ft. Vertical effective stresses equal to the lateral stresses and equal to twice the lateral stresses were applied to investigate the effect of K_0, the coefficient of earth pressure at rest. Drainage was provided at the lateral and upper horizontal boundaries of the sand. Controlled effective stresses were maintained at the chamber boundaries during driving and subsequent static loading tests. A schematic of the sand column is given in Figure 2.

The test pile was made of cold drawn steel tubing and had a wall thickness of 0.188 in. It was closed at the toe with a flush plate containing both a load cell and an accelerometer to measure toe performance.

The vibratory driver, which was designed and constructed specifically for this research, operated on the counterrotating mass principle. A schematic of the vibratory driver is shown in Figure 3. The rotating parts were impelled by hydraulic motors, which were in turn driven by an electrical hydraulic pump. The vibrator, which weighed 780 lb, could be configured to operate at frequencies ranging from 5 to 50 Hz (well below the resonance frequency of the test pile) with unbalanced moments of 35 to 300 in-lb and with bias mass weights ranging from 380 to 2,000 lb.

Preliminary driving tests were performed to investigate the combination of driver parameters that would produce the peak rate of penetration for the laboratory testing system. Thereafter, for all of the tests that were used in the development of the predictor equations in this paper, the vibrodriver parameters were held constant at those values: W_v = 780 lb, W_b = 2,000 lb, f = 20 Hz (18-22), and unbalanced moment = 100 in-lb. The theoretical peak free force amplitude at the axis of the motors for these conditions was 4.1 kips.

TEST RESULTS

The testing program was detailed. It involved investigation of power transmitted from pile head to toe, pore pressure generation and dissipation, mode of pile penetration (e.g., rapid impulses at the toe, as suggested by Schmid), and measurement of load transfer both during driving and statically. These fundamental aspects of behavior are covered elsewhere (*7,8*); overall results relevant to the development of static capacity relations are given in Table 1. In that table, r_{pt} is the observed average terminal rate of penetration in the final one-pile-diameter of penetration; σ'_h is the horizontal effective stress maintained at the boundary of the sand column; d_{10} is the 10-percent soil particle size; and D_r is the relative density of the sand.

BEARING CAPACITY PREDICTION AND HAMMER CHARACTERISTIC SELECTION FROM LABORATORY TESTS

The experimental data in Table 1 have been developed into analytical expressions that permit the prediction of pile capacity. These expressions are described briefly below, and procedures are described in which these expressions can be used both to predict pile capacity and to select hammer characteristics.

Power Transfer Expressions

The bearing capacity Q_t of the vibro-driven piles correlates to several variables, including r_p, absolute peak acceleration of the pile head (denoted a_h), σ'_h, D_r, and d_{10} for the driving system used in the study. Whether the pile is restruck after vibro-driving did not correlate to capacity; therefore, that effect is not included in the equation for bearing capacity. The following relationship, predicated on the power actually transferred by the vibrator to the pile head and derived from a nondimensional combination of the most significant system parameters, incorporates these variables:

$$Q_t = \frac{0.050\,P_h}{r_{pt}\,[\beta_1(\sigma'_h)\,\beta_2(D_r)\,\beta_3(d_{10})]} \tag{4a}$$

in which P_h is the average power delivered to the pile head during the final one-diameter of penetration; r_{pt} is the average rate of penetration during the final one-diameter of penetration; and the β functions are empirical parameters that relate measured capacity independently to the variables indicated in the parentheses. Units for P_h, r_{pt}, and Q_t can be any consistent set.

Equation 4a presumes rigid body behavior of the pile (i.e., zero or very small phase angle between head and toe), which is generally appropriate for prototype piles driven at low frequency (20 to 25 Hz) with lengths less than 50 ft. The dimensionless β factors have been determined by regression analysis of the data to be as follows:

$$\beta_1(\sigma'_h) = -0.486 + 0.0743\,\sigma'_h \qquad 10\,\text{psi} \le \sigma'_h \le 20\,\text{psi} \tag{4b}$$

$$\beta_2(D_r) = 1.96\,D_r - 1.11 \qquad 0.65 \le D_r \le 0.90 \tag{4c}$$

$$\beta_3(d_{10}) = 1.228 - 0.19\,d_{10} \qquad 0.2\,\text{mm} \le d_{10} \le 1.2\,\text{mm} \tag{4d}$$

Equation 4a, with parameters defined in Equations 4b to 4d, was found to compute the mean measured static compres-

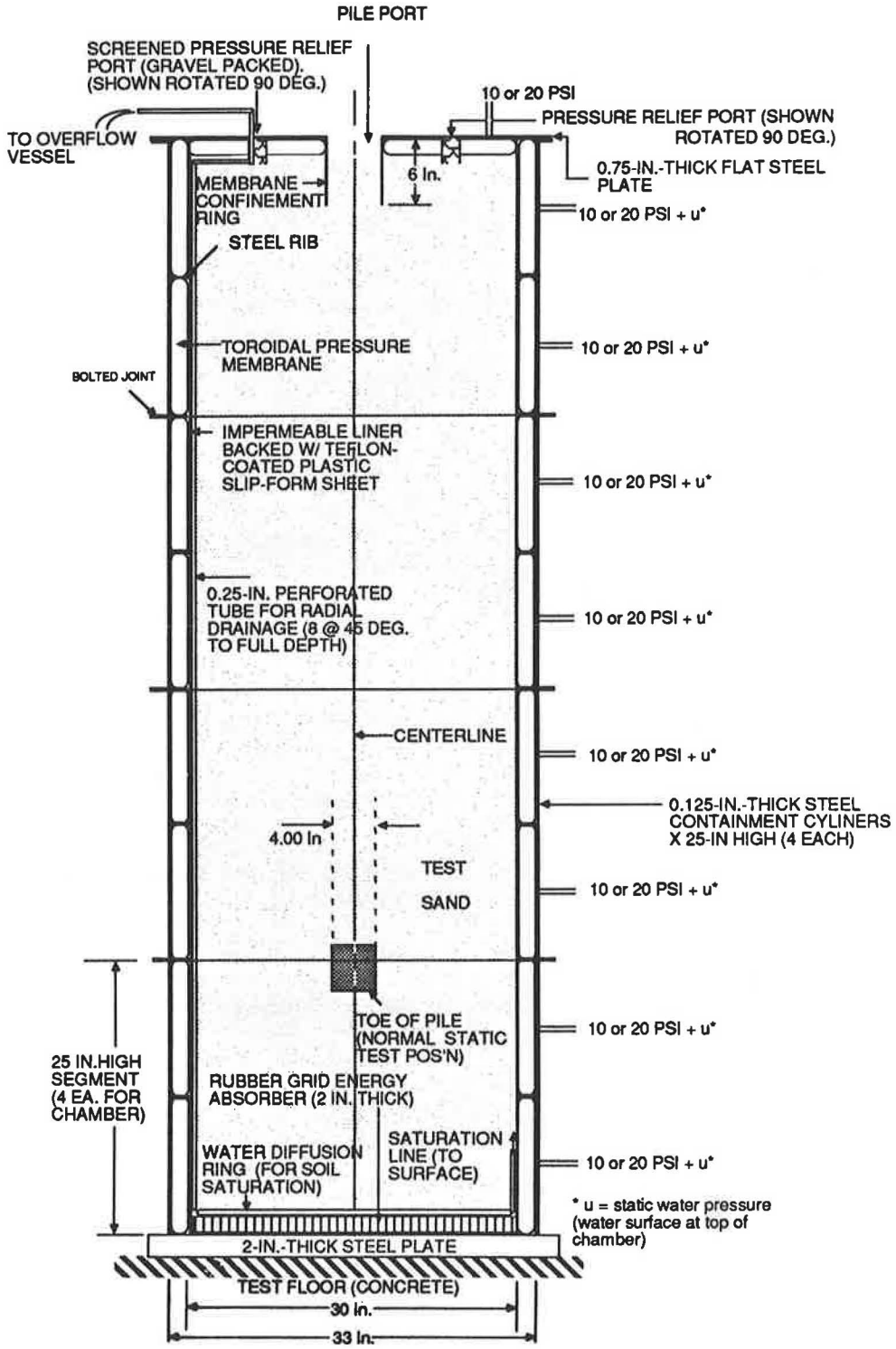

FIGURE 2 Detailed schematic of the pressure chamber, showing lateral and vertical pressure membrane system.

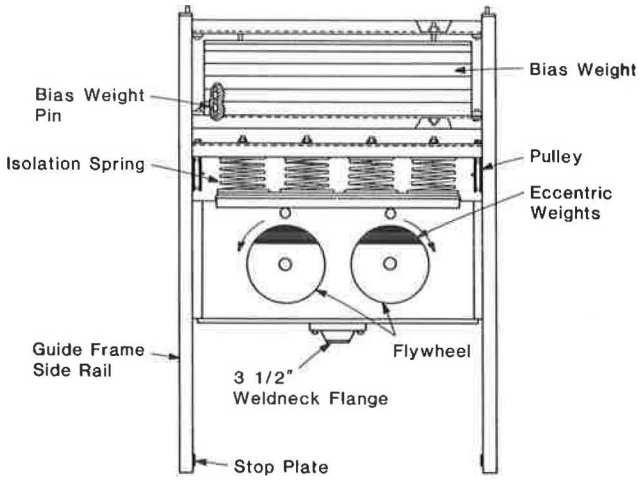

FIGURE 3 Schematic diagram of vibro-driver used in laboratory tests.

sional capacity of the vibro-driven test piles to within 1 percent, with a coefficient of variation of 12 percent.

A key parameter in Equation 4a is P_h, the power actually transmitted to the pile head during terminal penetration. The laboratory experiments revealed a strong correlation between P_h, the theoretical power of the hammer, P_t, and the absolute peak acceleration of the pile head, a_h, as follows:

$$P_h = P_t\,[0.25 + 0.063\,a_h\,(g)] \tag{5}$$

It can be shown from a dynamic equilibrium analysis of the vibrator that the theoretical power P_t for a rotating-mass vibrator operating at frequency f can be obtained as

$$P_t = f\left(4W_b + \frac{8\pi^2 f^2 f_n^2 me}{(f_n^2 - f^2)}\right)\frac{mef^2}{M(f_n^2 - f^2}} \tag{6}$$

where

m = combined mass of all rotating, unbalanced weights;
M = mass of the vibrator, excluding bias mass;
e = eccentricity of the rotating weights;
f_n = natural frequency of the vibrator mass-isolation spring system = $(k/M)^{0.5}$; and
k = combined spring constant of the isolation springs.

Absolute peak acceleration a_h was found to correlate to soil properties and r_{pt} in the laboratory tests as indicated below:

$$a_h(g) = \alpha_1(D_r)\,\alpha_2(d_{10})\left(r_{pt}^{\alpha_3(\sigma'_h)}\right), \tag{7a}$$

where r_{pt} is expressed in in./sec.

The dimensionless α factors, which correlate independently the soil properties given in the parentheses to a_h, were found by regression analysis to be as follows:

$$\alpha_1(D_r) = -2.186 + 3.54\,D_r, \quad 0.65 \le D_r \le 0.90 \tag{7b}$$

$$\alpha_2(d_{10}) = 8.99 + 2.76\,d_{10}, \quad 0.2\,\text{mm} \le d_{10} \le 1.2\,\text{mm} \tag{7c}$$

$$\alpha_3(\sigma'_h) = 1.71 - 0.081\,\sigma'_h, \quad 10\,\text{psi} \le \sigma'_h \le 20\,\text{psi} \tag{7d}$$

Comparison of Capacity Prediction Methods for Chamber Tests

In order to provide some comparison of the results yielded by various predictive methods, the three methods described in this paper that employ rate of penetration as an index to capacity were used to predict the static capacity, Q_t, as a function of terminal rate of penetration, r_{pt}, in the large-scale model pile tests reported in this paper. The results are summarized in Figure 4. The intent of Figure 4 is not to suggest that the new method proposed in Equation 4a is superior to the other two methods. Equation 4a is biased to give more accurate results, since the parameters were evaluated from the reported model study. However, it is clear that the new method predicts lower rates of penetration for a given static capacity than the other two for the conditions that were studied experimentally.

Application of Power Transfer Expressions to Bearing Capacity Prediction

Equations 4a through 7d contain implicitly the effects of the interaction of the pile, driver, and soil through the power, velocity, and acceleration terms and the soil coefficients and exponents. As with all empirical relationships, they must be considered to be valid only for the ranges of conditions modelled in the tests. The soil parameter ranges are given in Equations

TABLE 1 TEST DATA RELEVANT TO DEVELOPMENT OF STATIC CAPACITY RELATIONS

Terminal rate of penetration (r_{pt}) (in./sec)	Horizontal effective stress (σ'_h) (psi)	Ratio of horizontal to vertical effective stress (K_0)	10-percent soil particle size (d_{10}) (mm)	Relative density of sand (D_r) (percent)	Total penetration (diameters)	Mean static compressional capacity of pile (Q_t) (kips)
2.1	10	1	0.2	65	19.5	13.5
3.7	10	1	1.2	65	19.5	12.0
5.5	10	1	1.2	65	19.5	12.5
0.1	20	1	0.2	90	13.8	23.5
0.1	20	1	1.2	90	18.8	38.4
0.2	10	1	0.2	90	19.5	21.0
0.4	10	1	0.2	90	19.5	25.0
0.4	10	0.5	0.2	90	19.5	17.5
0.4	10	1	1.2	90	19.5	27.0
0.7	10	1	1.2	90	19.5	24.0

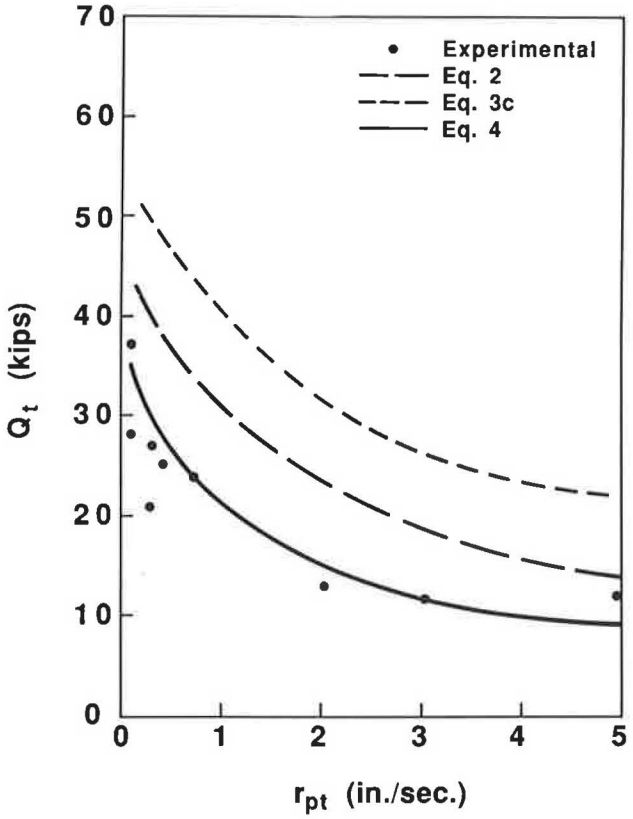

FIGURE 4 Comparison of capacity prediction methods for laboratory tests.

4a and 7a. The ranges of vibrator and pile conditions covered by the study are (1) peak single-amplitude unbalanced force developed by the vibrator was between 0.1 and 0.3 Q_t; (2) vibrator weight (excluding bias masses) was 0.15 to 0.25 times the peak single-amplitude unbalanced driver force; (3) bias weight was 0.05 to 0.10 Q_t; (4) f was the optimum frequency for driving (20 Hz in this study); and (5) the pile was closed-ended (displacement-type pile) and was driven without stopping.

It must also be considered that the power transfer equations are based on model tests in a large-sized pressure chamber and not on field tests, since field tests with appropriate measurements (acceleration time history, rate of penetration, vibrator properties, meaningful soil properties) have not heretofore been generally unavailable. The only parameter that was scaled in the pressure chamber was mean effective stress in the soil. This consideration leads to three important points:

1. Scaling of mean effective soil stress allows the relatively small model pile to represent prototypes that penetrate to depths at which the mean effective stress between the ground surface and the toe is 10 to 20 psi; that is, slightly overconsolidated, submerged sands ($0.5 \leq K_0 \leq 1$) of typical unit weights to depths of 50 to 100 ft. Scaling of effective stress also reproduces the elastic and plastic properties of the soil that exist in the prototype system and that control the displacements in the pile-soil system as the pile is being driven. Vertical gradients of horizontal stress were not scaled because such scaling induces shear stresses in the soil in the chamber that do not exist in the prototype. Therefore, some judgment must be applied when selecting a single value of σ_h' or d_{10} in a variable soil profile for use in Equations 4a and 7a, if these equations are to be applied to field conditions. It is tentatively suggested that, based on observations of relative resistances developed along the shaft and toe in the static loading tests in this study, single values be estimated as follows:

$$\mu = 0.67\,\mu_{toe} + 0.33\,\mu_{middepth\ of\ pile} \quad D_r = 65\,\text{percent} \tag{8}$$

$$\mu = 0.61\,\mu_{toe} + 0.39\,\mu_{middepth\ of\ pile} \quad D_r = 90\,\text{percent} \tag{9}$$

where μ is either σ_h' or d_{10}. A condition not studied in the chamber tests, yet which is relatively common in the field, is that in which there is a significant change in D_r along the length of the pile, as when the pile is driven through loose soil into very dense soil. While further studies are necessary to determine the relative contributions of the toe and shaft during vibro-driving under these conditions, it is tentatively suggested that Equation 8 (in which μ becomes relative density) be used to approximate the single value of relative density to be used in Equations 4c and 7b.

2. Since time was not scaled in the tests, the ratio of operating frequency applied to the model pile to its resonance frequency was much lower than would occur in a field prototype (approximately 0.02 in the short model and approximately 0.2 in a 75-ft-long steel pile in the field for 20 Hz excitation). This creates a model pile that behaved more rigidly than a typical prototype, although the effect is perceived to be minor, since both the model and prototype are driven at a small fraction of their resonance frequency, unless the prototype pile is either very long (>75 ft) or consists of a material that has a lower unit weight and a lower p-wave velocity than those of the steel in the model pile (e.g., timber).

3. Size also was not scaled. Thus, the laboratory test results are valid for the actual relative ratios of soil particle size to pile diameter employed in the laboratory tests, which are realistic for full-scale prototypes in medium to coarse sands. The length of the drainage path in the chamber, which scales directly to prototype drainage path length, is approximately 13 in., the distance from the pile wall to the lateral drains in the sand column. The extent to which this value is representative of field conditions and the influence of the drainage path length on prototype behavior have not been established, although the relationship of length of drainage path times soil permeability is known to affect rates of pore water pressure dissipation and, presumably, rates of penetration of piles driven by vibration.

Future field verification of the power transfer equations is therefore necessary before they can be applied to practice. Once this verification, with modification if necessary, is accomplished, it may be possible to apply the method in practice by following the step-by-step procedure outlined below:

1. Determine or estimate the relative density, average effective grain size, and mean lateral effective stress in the soil to the anticipated depth of penetration.
2. As the pile is driven, measure r_{pt}, the average velocity of penetration in the last one-diameter of penetration (or equivalent for noncircular pile).
3. Either measure a_h, the absolute peak acceleration of the pile head during the final diameter of penetration, or compute a_h from r_{pt} and the soil parameters using Equations 7a through 7d. (If power at the pile head, P_h, is actually measured during

the last one-diameter of penetration, as with a pile-driving analyzer or similar device, Steps 3 through 5 can be skipped, and the compressional capacity can be computed directly from Step 6).

4. Determine f, the frequency of operation of the hammer, and the theoretical power of the vibratory hammer at the operating frequency, P_t, either from the hammer manufacturer or from Equation 6, if the hammer is of the counterrotating mass type.

5. Determine the power actually transmitted to the pile head, P_h, either through direct measurements or by the use of Equation 5, together with the computed value of a_h (Step 3) and the relevant soil properties (Step 1).

6. Finally, compute the compressional capacity of the pile from Equations 4a through 4d.

It is presumed that any site investigation would include the recovery of samples of cohesionless soils for grain-size analysis. However, if σ'_h and D_r are not measured directly, appropriate correlations may be employed. For example, if the overconsolidation ratio (OCR) versus depth profile of the soil can be deduced from past geologic events, D_r can be obtained from cone tip resistances from electronic cone penetrometer soundings using correlations developed by Schmertmann (*9*), which can be approximated in ratio (not percentage) form, for the range of relative densities and effective stresses covered by this test program, by

$$D_r = 0.007 \frac{(q_{cnc})0.5}{\sigma'_v 0.33} \tag{10}$$

in which q_{cnc} is the cone tip resistance in kgf/cm^2 for a normally consolidated sand at the depth at which the vertical effective stress is equal to σ'_v expressed in kgf/cm^2. Thus, q_{cnc} can be estimated from q_c, the measured cone tip resistance in an overconsolidated sand, from Equation 11, also proposed by Schmertmann (*9*).

$$q_{cnc} = q_c/\{1 + 0.75\,[(\mathrm{OCR})^{0.42} - 1]\} \tag{11}$$

In order to estimate σ'_h along the depth profile, one can simply compute σ'_v from the known position of the piezometric surface, unit weight of the soil and depth, and use a simplification of a relation proposed by Mayne and Kulhawy (*10*) to compute K_o as follows:

$$K_o = 0.43\,(\mathrm{OCR}^{0.57}) \tag{12}$$

Equation 12 is valid where past geologic events have not produced lower effective stresses in the ground than exist presently and for granular soils of medium to high density. Finally, σ'_h is computed from Equation 13 for any depth (e.g., toe or mid depth of pile).

$$\sigma'_h = K_o \sigma'_v \tag{13}$$

Application of Power Transfer Expressions to Selection of Hammer Characteristics

The power transfer expressions can also be used to aid in the selection of a driver. Before this can be done a target static pile capacity must be estimated. Results of the static compressional loading tests on the piles driven by vibration in the test chamber indicated the following expression for ultimate static compressional capacity:

$$Q_t = N_\sigma \sigma'_o A_t + \sum_{i=1}^{N} \beta'\, i\sigma'_{hi} A_{si} \tag{14}$$

where

σ'_o = the mean effective stress in the soil at the pile toe,
A_t = the area of the toe,
i = an index for pile segments (e.g., top half and bottom half) for shaft resistance computations,
A_{si} = the peripheral area of segment i,
σ'_{hi} = the lateral effective stress in the soil in situ at the elevation of the middepth of segment i (obtained, for example, from Equation 13),
N_σ = a bearing capacity parameter, and
β' = a shaft resistance parameter.

These latter parameters were determined from the tests in the present study to be as follows:

$$N_\sigma = 181.1\, D_r + 11.36\, d_{10}(\mathrm{mm}) - 76.1 \tag{15}$$

$$\beta' = 2.50\, D_r - 0.076\, d_{10}(\mathrm{mm}) - 0.85 \tag{16}$$

Other appropriate methods for estimating static capacity can be substituted for the method described above, if such is desired.

Once the static capacity of the pile has been established, the following steps are employed:

1. A target value of terminal penetration velocity r_{pt} is selected. It is suggested that a value of 0.1 in./sec represents refusal.
2. The power required at the pile head, P_h, to produce the selected value of terminal penetration velocity is then computed from Equation 4a.
3. The peak absolute value of pile head acceleration, a_h, that would result from the above choices is estimated from Equation 7a.
4. Finally, the power required for the vibrator is computed from Equation 5.

The application of the procedure for selection of a vibrator is subject to the same constraints (ranges of variables and scaling considerations) described for estimation of static capacity. For example, once the required power is determined for a displacement-type pile, the bias weight is then set at 0.05 to 0.10 Q_t, the amplitude of the unbalanced force is set at 0.1 to 0.3 Q_t, and the vibrator is operated at approximately 20 Hz.

CONCLUSIONS

Consistent bearing capacity prediction equations were developed from a series of large-scale model tests in which displacement piles were installed in submerged sand by vibration. Constants in the model tests were vibrator and bias weight, amplitude of unbalanced force, operating frequency,

and pile characteristics (rigid, closed-ended steel pipe). Variables were focused on soil properties and included relative density, effective grain size (d_{10}) and mean effective stress. Equations 4a through 4d were found to provide predictions of ultimate bearing capacity in varied modelled soil conditions with a coefficient of variation of 12 percent. A procedure is suggested for applying these equations to the estimation of bearing capacity of installed piles in cohesionless soils from rate-of-penetration data that involves the calculation (or direct measurement) of power transferred to the pile head. A complementary procedure is also suggested for the selection of hammer properties for piles of given design ultimate capacity. Potential users of the method are strongly cautioned that the method has not yet been verified in the field.

ACKNOWLEDGMENT

The study reported in this paper was supported by the National Cooperative Highway Research Program, to which the authors are indebted for permission to publish this paper.

REFERENCES

1. G. Steffanof and B. Boshinov. Bearing Capacity of Hollow Piles Driven by Vibration. *Proc., Ninth International Conference on Soil Mechanics and Foundation Engineering*, Vol. 2, ISSMFE, Tokyo, 1977, pp. 753–758.
2. M. T. Davisson. BRD Vibratory Driving Formula. *Foundation Facts*, Vol. 6, No. 1, 1970, pp. 9–11.
3. W. E. Schmid. *Driving Resistance and Bearing Capacity of Vibro-Driven Model Piles*. ASTM STP 444. American Society of Testing and Materials, New York, 1968, pp. 362–375.
4. K. M. Chua, S. Gardner, and L. L. Lowery, Jr. Wave-Equation Analysis of a Vibratory Hammer-Driven Pile. *Proc., Offshore Technology Conference*, Houston, Tex., Vol. 4, 1987, pp. 339–345.
5. C. Vipulanandan, D. Wong, M. Ochoa, and M. O'Neill. Modelling of Displacement Piles in Sand Using a Pressure Chamber. In *Foundation Engineering: Current Principles and Practices*, Vol. 1 (ed. F.H. Kulhawy), ASCE, New York, 1989, pp. 526–541.
6. D. O. Wong. *Driveability and Load Transfer Characteristics of Vibro-Driven Piles*. Ph.D. dissertation, Department of Civil and Environmental Engineering, University of Houston, 1988.
7. M. W. O'Neill, C. Vipulanandan, and D. Wong. Laboratory Modelling of Vibro-Driven Piles. Submitted for publication to *Journal of Geotechnical Engineering*, ASCE.
8. C. Vipulanandan, D. Wong, and M. W. O'Neill. Behavior of Vibro-Driven Piles in Sand. Submitted for publication to *Journal of Geotechnical Engineering*, ASCE.
9. J. H. Schmertmann. *Guidelines for Cone Penetration Test: Performance and Design*. Report FHWA-TS-78-209. FHWA, U.S. Department of Transportation, Washington, D.C., 1978, pp. 13–14.
10. P. W. Mayne and F. H. Kulhawy. *K_o-OCR Relationships in Soil. Journal of the Geotechnical Engineering Division*, ASCE, Vol. 108, No. GT-6, 1982, pp. 851–872.

Publication of this paper sponsored by Committee on Foundations of Bridges and Other Structures.

Bearing Capacity Prediction from Pile Dynamics

M. A. SATTER

A new method of predicting static bearing capacity of a pile foundation is presented. The method utilizes the dynamic behavior of the pile. In particular, the pile velocity, the displacement, and the driving force records are the necessary parameters. The analysis is conducted through a nonlinear differential equation that originates from the assumption that the soil reaction to the pile is a nonlinear function of the pile displacement. Examples based on data of four impact-driven field piles are presented. In these cases, since the driving forcing functions are not regular, it was necessary to resort to numerical solution of the governing equation by using the "continuous analytic continuation" method. The predicted static bearing capacity results of the piles have good agreement with those obtained from the field tests.

Prediction of static bearing capacity of an embedded pile is of great importance in pile foundation engineering. The conventional method of estimating static bearing capacity through static load tests is often difficult and expensive. It is therefore highly desirable to look for an easy and cheap alternative method of estimating pile bearing capacity. There have been several attempts (*1–11*) over the recent past to determine bearing capacity through dynamic tests, which are considered to be relatively easy and cheap. The dynamic response of a pile can be obtained by suitable instrumentation while the pile is being installed by vibrations or impacts, thereby eliminating separate test arrangement as is the case with static load tests.

Dynamic response of an embedded pile depends on the driving force, the physical properties of the pile, and the characteristics of the soil resistance. By measuring the pile response it is possible to obtain information about soil reaction, which then leads to determination of pile bearing capacity. Since soil remolding can occur during and after pile driving, soil reaction (resistance) will vary depending on the stage at which the pile is being tested. Dynamic tests can take into account the soil characteristics prevailing at the time of the tests. The level of complexity of the dynamic response analysis and the accuracy of the predicted results depends, among others, on the assumed pile-soil model. Scanlan and Tomko (*1*) in their study on impact-driven piles employed a rigid-elastic pile model with soil resistance (reaction) acting along the sides of the piles, the tip resistance being negligible. In computing the results from the governing equations, four parameters were chosen and adjusted to obtain a best match between the predicted and measured results. It was stated that the soil resistance was negligible or small until the pile velocity reached about the maximum. Here it had a constant value, which in principle was the static bearing capacity of the pile just after driving. The study also indicated that a long pile "compresses up" initially and then "descends into the soil more or less like a rigid body". For a short pile, "the rigid body action is the principal one, with only a relatively small elastic effect exhibiting oscillations about a mean much nearer to zero".

Rauche, Moses, and Goble (*2*) undertook a study to predict pile static bearing capacity by using a concept of "measured delta curve" that gave a measure of pile bearing capacity. The delta curve is obtained from the following consideration. Two identical piles, one free and the other embedded, are tested for identical input forces. First, the force level at the top of the free pile is computed, which acts as the reference force. Then, the force level at the top of the embedded pile is measured. The difference between the force levels of the free pile and the embedded pile is the force due to the soil resistance and is defined as the "delta curve".

Both the aforementioned studies (*1,2*) utilize wave equations and have met with varying degrees of success in predicting pile static bearing capacity.

The present study attempts to predict pile static bearing capacity just after driving through a new concept of "dynamic soil resistance" that was developed from laboratory tests on model piles (*3*). The soil used in the laboratory tests was Shiraz brown subangular sand corresponding to No. 16/40 sieve size. According to this concept, the soil imparts an impactive resistance (reaction) at certain stages of the pile motion. By measuring the pile response, it is possible to estimate the dynamic soil resistance, from which it is possible to derive information about static bearing capacity at the time of driving or soon after. The impactive soil reaction resembles the "delta curve" (*2*) and in some respects is similar to the type of soil resistance mentioned by Scanlan and Tomko (*1*). Their field test results were obtained for silty soil with silt content varying from 56 to 82 percent, clay from 42 to 14 percent, and fine sand from 2 to 4 percent. The piles were of steel pipe construction and were impact driven. Static load capacities were determined by both ML and CRP tests (*1*).

Instruments and techniques of pile response measurement have been studied by several authors (*12,13*). Accurate measurement of pile response is essential for proper evaluation of the pile static bearing capacity from dynamic tests. A sophisticated computer program, CAPWAP, has been developed based on the stress-wave theory of the elastic pile model to predict bearing capacity from dynamic tests (*14*). Although the new concept can be applied to an elastic pile model, the present investigation is restricted to a rigid body model. The agreement between the predicted and the field test results is remarkable, and justifies the assumptions.

Department of Mechanical Engineering, Shiraz University, Shiraz, Iran. Current affiliation: Yuasa Battery Bangladesh Ltd., 60/1 Purana Palton, Dhaka, Bangladesh.

REVIEW OF SOME SIMPLE METHODS

For the purpose of comparing the existing simplified methods and the theoretical method to be presented later, it is necessary to quote the equations that are currently used to predict pile static bearing capacity. The methods have been used extensively in the past in the field. These methods are based on rigid body pile models. The equation for the static bearing capacity, R_0, is given by

$$R_0 = F(t_0) - Mf(t_0) \tag{1}$$

where

t_0 = the time of zero velocity;
M = mass of pile;
$F(t_0)$ = pile force at time t_0; and
$f(t_0)$ = acceleration at time t_0.

Equation 1 does not provide very satisfactory results. To improve this, an average value of the acceleration is added to Equation 1, which becomes

$$R_0 = F(t_0) - \frac{M}{t_1 - t_2}\int_{t_2}^{t_1} f(t)dt \tag{2}$$

where t_1 is the time of maximum force and t_2 equals t_0. Using the concept of stress wave travelling time, Equation 2 can be improved further:

$$R_0 = \frac{F(t_1) + F(t_1 + 2l/c)}{2} - \frac{Mc}{2l}\int_{t_1}^{t_1 + (2l/c)} f(t)dt \tag{3}$$

Again, t_1 is set equal to t_0, c equals stress wave propagation velocity in the pile material, and l equals pile length. It should be noted that Equations 1–3 use input force and acceleration records of the pile for evaluating the static bearing capacity.

THEORETICAL CONCEPTS

The present theoretical concept arises from an investigation of driving a low frequency vibropile, the details of which appear elsewhere (*3*). It was found during the driving of the vibropile that a pile under a certain static surcharge required a certain input power, called optimum power level, to achieve a certain maximum depth of penetration. If the input power is increased beyond the optimum level without changing the static surcharge, the pile will not penetrate the soil further, but it will undergo steady state vibration. It will also induce impactive reaction from the soil. The present theory is proposed for the postoptimum pile condition, and it assumes that the soil resistance is proportional to the cube of the pile dynamic displacement. The pile is assumed to be rigid, an assumption that is certainly valid for low-frequency vibropile driving and also valid to a large extent for impact pile driving (*1*). In order to elucidate the theory, it is first developed for a pile driven by a low-frequency vibratory force; later a more general forcing function is included in the theory.

The equation of motion of the pile during low-frequency steady state vibration is (*3*)

$$Mx'' + R[H(t - t_1) - H(t - t_2)]x^3 = S + F_0 \sin \omega t \tag{4}$$

where

S = static surcharge;
F_0, ω = amplitude and frequency, respectively, of the forcing function;
R = unknown soil constant; and
$H(t, t')$ = filter function.

The filter function (*15*) is introduced to ensure that R has a certain magnitude ($R > 0$) during pile-soil interaction; otherwise R is assumed to be zero. The pile-soil interaction takes place in the time interval, $(t_2 - t_1)$, during the downward stroke of the pile.

The solution of Equation 4 is assumed to be of the form, $x = a \sin \omega t$, where the amplitude, a, is unknown. Substituting for x, we obtain

$$x'' + \omega^2 x = \frac{S}{M} + \left\{\frac{F_0}{M} + \omega^2 a - \frac{3Ra^3}{4M}[H(t,t')]\right\}\sin \omega t + \frac{Ra^3}{4M}[H(t,t')]\sin 3\omega t \tag{5}$$

In order to avoid the secular term, we must impose the condition

$$\frac{F_0}{M} + \omega^2 a - \frac{3Ra^3}{4M}[H(t,t')] = 0 \tag{6}$$

For simplicity, the filter function may be dropped, but the fact that it is associated with R must be remembered. Equation 6 may then be written as

$$R = 4(F_0 + M\omega^2 a)/3a^3 \tag{7a}$$

or

$$Ra^3 = 4(F_0 + M\omega^2 a)/3 \tag{7b}$$

Equation 7a is very significant, because it relates the two unknown quantities, a and R. If the amplitude, a, is measured, R can be evaluated from Equation 7a.

Returning to Equation 5, deleting the secular term reduces the equation to

$$x'' + \omega^2 x = \frac{S}{M} + \frac{Ra^3}{4M}[H(t,t')]\sin 3\omega t \tag{8}$$

Assuming that, at $t = T/4$, where T is the periodic time, $x(t) = a$ and $x'(t) = 0$, the solution of Equation 8 is (*3*)

$$x(t) = \frac{S}{M\omega^2} + \left(a - \frac{S}{M\omega^2}\right)\sin \omega t - \frac{Ra^3}{32M\omega^2}(\sin \omega t + \sin 3\omega t) \tag{9}$$

Equation 4 is formulated for a rigid pile that is driven by a low-frequency vibratory force. The formulation may be generalized by introducing a general forcing function, including impacts, and a damping term. As mentioned earlier, the pile may be considered rigid even for impactive loads without great loss of accuracy (*1*). Soil damping is, of course, complicated. In several analyses (*7–10*) the damping is considered to be

viscous—an assumption that is also adapted here. Thus, Equation 4 may be reformulated as

$$Mx'' + Cx' + Rx^3 = S + F(t) \tag{10}$$

Equation 10 is evidently nonlinear; its solution depends on the complexity of $F(t)$. For Equation 4, $F(t) = F_0 \sin \omega t$ and $C = 0$, so its solution is given by Equation 9. But for a complicated $F(t)$, a reasonable analytical solution may not be obtainable. For field problems in which $F(t)$ may not be expressed analytically, Equation 10 should be solved through numerical integration.

One such numerical method is known as "continuous analytic continuation" (*16*). This method is simple to program and provides fairly good accuracy. Two equations expressing instantaneous displacement and velocity are used:

$$x(t) = x_0 + x_0'\Delta t + \frac{x_0''}{2!}(\Delta t)^2 + \frac{x_0'''}{3!}(\Delta t) + \ldots + \frac{x_0^{(n)}}{n!}(\Delta t)^n + R_n \tag{11}$$

and

$$x'(t) = x_0' + x_0'' \Delta t + \frac{x_0'''}{2!}(\Delta t)^2 + \ldots + \frac{x_0^{(n)}}{(n-1)!}(\Delta t)^{n-1} + R_n' \tag{12}$$

where

$R_n = x_p^{(n+1)}(\Delta t)^{n+1}/(n+1)!$;
$R_n' = x_p^{(n+1)}(\Delta t)^n/n!$; and
$t_p = t_0 + \theta(\Delta t)$, for $0 \le \theta \le 1$.

Using the initial conditions, the values of x and x' for the first point at $t = t_0 + \Delta t$ are computed. The computed point is considered as an initial point for computing the values of x and x' at $t = t_0 + 2\Delta t$. The procedure is repeated such that the values of x and x' obtained for each point serve as the initial conditions for the successive point.

APPLICATION OF THE THEORY

The theory is applied below to a problem taken from Scanlan and Tomko (*1*). The driving forces for four different piles have been reproduced graphically in Figure 1. The pile data and the dynamic records are shown in Figures 2–5. From the driving force records, it is clear the forces may not be represented by simple analytical functions, and thus the numerical method outlined earlier must be used. The initial condition at $t = 0$ are $x_0 = 0$ and $x_0' = 0$. Denoting the derivatives of x with respect to t by $\frac{dx}{dt} = x'$, $\frac{d^2x}{dt^2} = x''$, etc., we rewrite Equation 10 as

$$x'' + \frac{C}{M}x' + \frac{R}{M}x^3 = \frac{S}{M} + \frac{F(t)}{M}$$

or

$$x'' = [S + F(t) - Cx' - Rx^3]/M \tag{13}$$

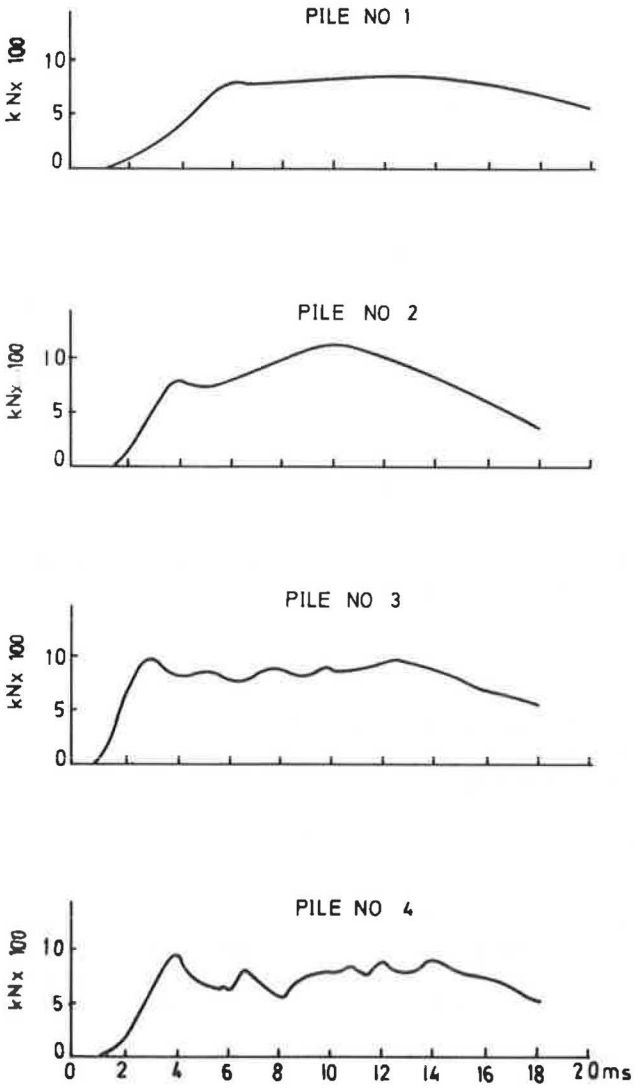

FIGURE 1 Pile input forcing records (source: ASCE).

The third, fourth, and fifth derivatives of x are

$$x''' = [F'(t) - Cx'' - 3Rx^2x']/M \tag{14}$$

$$x^{iv} = \left\{F''(t) - Cx''' - 3R[2x(x')^2 + x^2x'']\right\}/M \tag{15}$$

$$x^{v} = \left\{F'''(t) - Cx^{iv} - 3R[2(x')^3 + 6xx'x'' + x^2x'''] \right\}/M \tag{16}$$

The derivatives of the forcing functions were obtained by numerical differentiation, assuming that each derivative is a linear function of time, t. Thus,

$F'(t) = \{F(t + \Delta t) - F(t)\}/\Delta t$,
$F''(t) = \{F'(t + \Delta t) - F'(t)\}/\Delta t$, and
$F'''(t) = \{F''(t + \Delta t) - F''(t)\}/\Delta t$.

At $t = 0$, $F_0'(t) = F_0''(t) = F_0'''(t) = 0$.

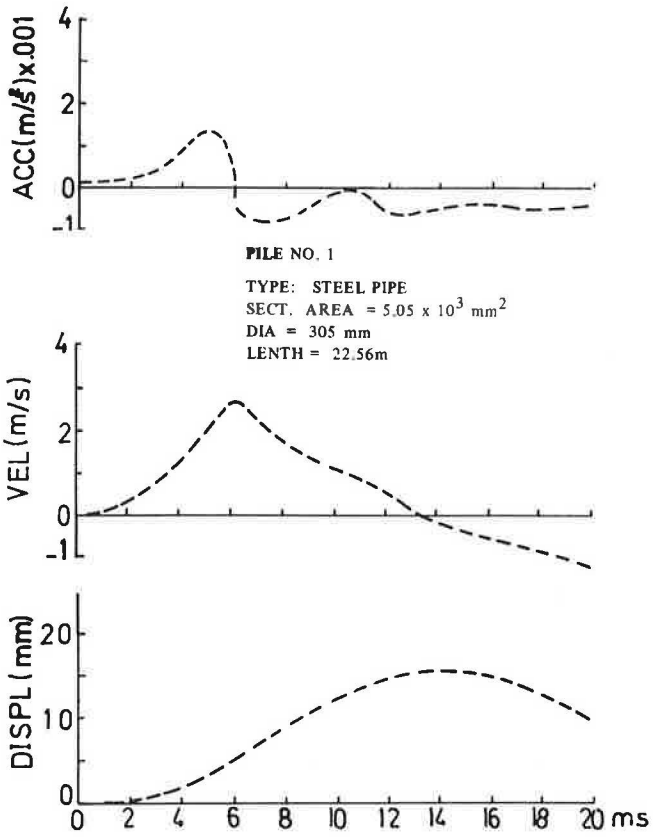

FIGURE 2 Measured dynamic response of Pile 1 (source: ASCE).

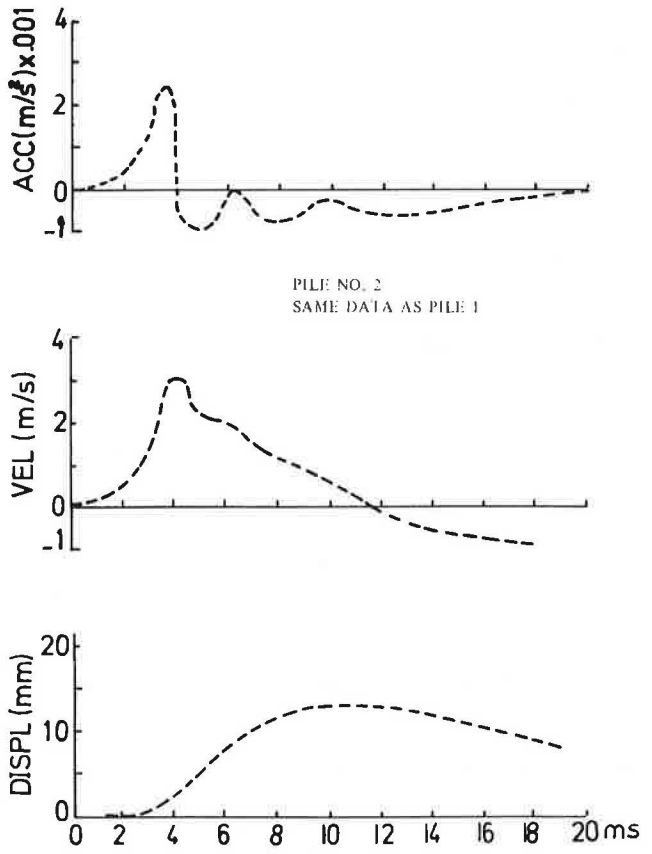

FIGURE 3 Measured dynamic response of Pile 2 (source: ASCE).

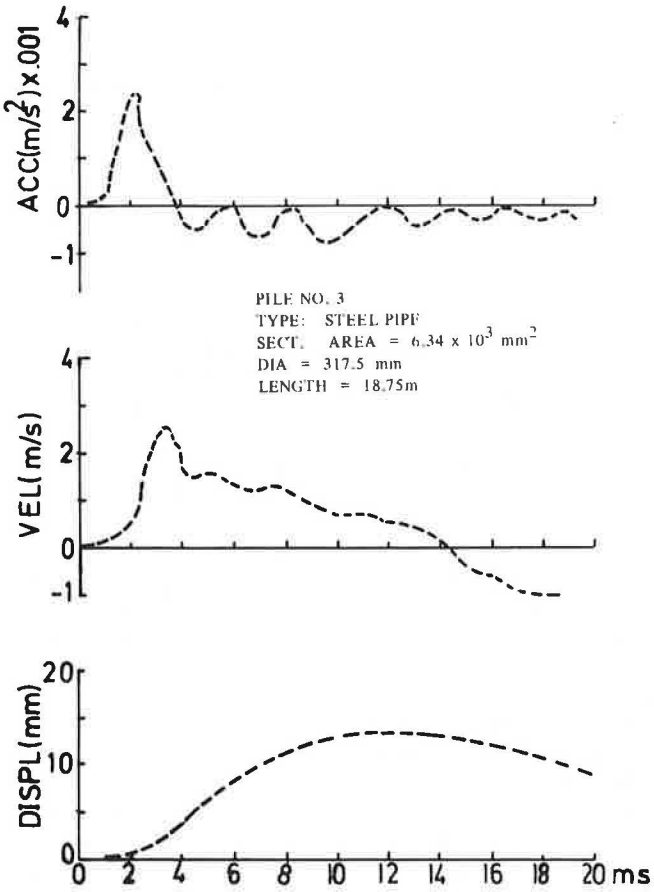

FIGURE 4 Measured dynamic response of Pile 3 (source: ASCE).

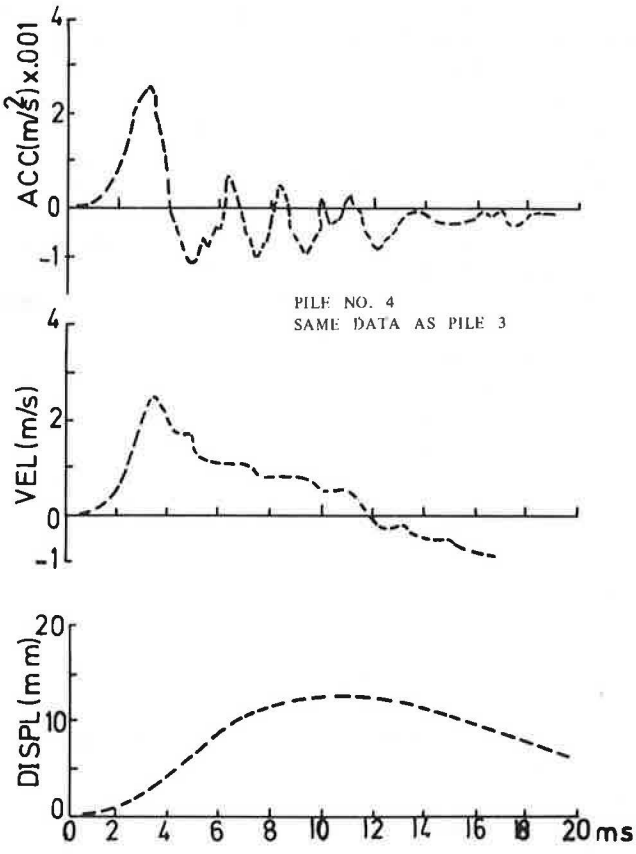

FIGURE 5 Measured dynamic response of Pile 4 (source: ASCE).

The mass of the pile may be calculated easily from the pile data. The constant, R, which is related to the soil properties, may also be evaluated from Equation 7a, provided an estimate of the dynamic displacement, a, and the level of pile acceleration are obtained from the measured records. Care must be taken in evaluating the numerical value of the dynamic displacement, a, from the pile displacement record. Its numerical value should be chosen so that x_{max} given by Equation 11 matches the experimentally obtained maximum displacement value. A good estimate for the dynamic displacement has been found to be the simple average value of the displacement record over the interval bounded by the maximum and subsequent zero velocities. This procedure ensures that x_{max} calculated from Equation 11 will match approximately and will not exceed the maximum displacement obtained experimentally.

According to Equation 7a, the mean acceleration level over the interval bounded by the maximum and the subsequent zero velocities is also required. The mean value of the acceleration must be evaluated from the acceleration records, although care should be taken to separate the acceleration due to elastic response of the pile. For a preliminary estimate of the value of R, the mean acceleration level may be considered negligible and then improved by the method explained below. The value of the forcing function, F, may be taken at the instant at which the measured instantaneous displacement equals the average value mentioned above. Hence, the constant R may be evaluated from Equation 7a and this will lead to the numerical solution of Equation 10.

In order to evaluate the pile static bearing capacity, it is necessary to plot the curves of dynamic soil resistance (Rx^3) and the pile velocity. The dynamic soil resistance at the point where the pile velocity passes through the maximum represents the static bearing capacity. Scanlan and Tomko (*1*) also evaluated the static bearing capacity at around the maximum velocity measured at the pile top. The records of displacement, velocity, and dynamic soil resistance (Rx^3) obtained from Equations 11 and 12 for the four piles are shown in Figures 6–9. The results are summarized in Table 1.

As mentioned earlier, the value of the constant, R, was calculated from Equation 7a by considering the pile deceleration to be negligible. This was because of the difficulty of distinguishing the elastic and rigid body parts of deceleration from the measured acceleration records. The calculations for approximate values of the static bearing capacity of various piles reported in Table 1 utilize the values of R calculated by considering the pile deceleration to be negligible. It has been found that the bearing capacity values may be improved significantly without resorting to the measured acceleration curve. To improve the results, it is necessary to calculate the pile maximum displacement for a range of R while keeping the average dynamic displacement constant. The value of R that yields the maximum displacement equal to that obtained from measurements on the pile concerned is to be accepted as the improved value. Then, the static bearing capacity is calculated simply by multiplying the improved value of R with the cubic power of displacement at (or just after) the instant the pile achieves the maximum velocity. The predicted improved values of static bearing capacities for various piles are also shown in Table 1.

In the absence of any reported values for piles statically surcharged and damping coefficient, these have been considered small. Depending on the method of pile driving, these factors have different roles to play. In vibropile driving static surcharge is necessary, while in impact pile driving this may not be the case. Also, damping coefficient along the pile may be small due to a small clearance that may be created between the pile and the soil during driving; but after soil settlement has taken place, the damping coefficient may not be negligible.

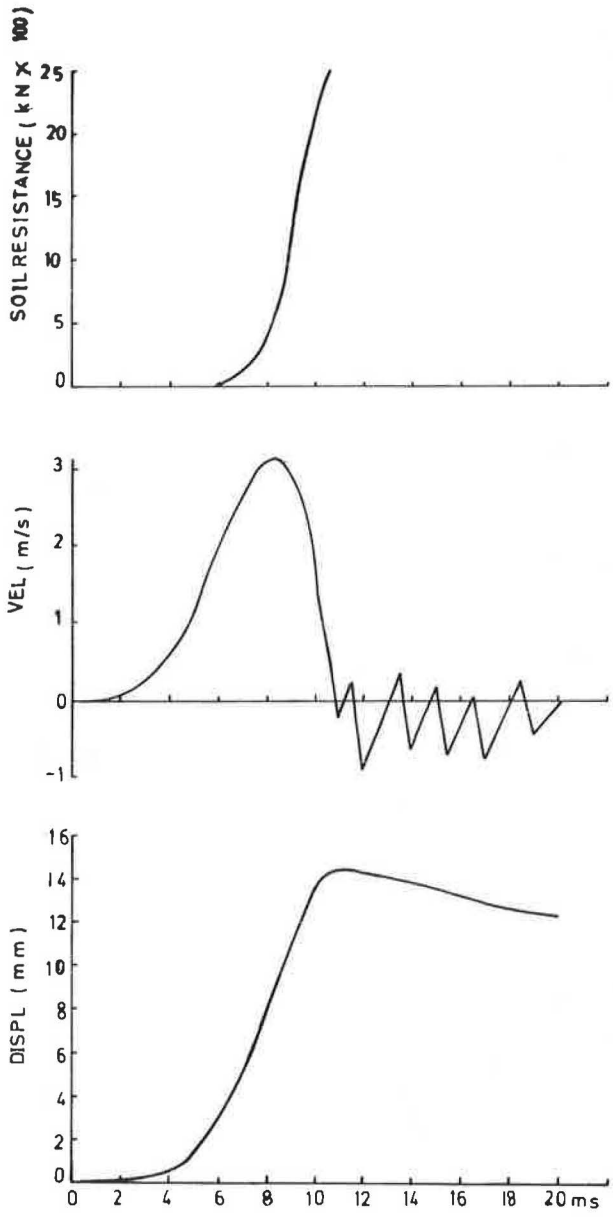

FIGURE 6 Predicted response of Pile 1.

The numerical computations for all the example piles have been carried out by taking a time increment of 0.25 ms.

DISCUSSION OF RESULTS

The dynamic soil resistance as well as the displacement and velocity responses for various piles have been plotted in Figures 6 through 9 using the approximate value of R and are

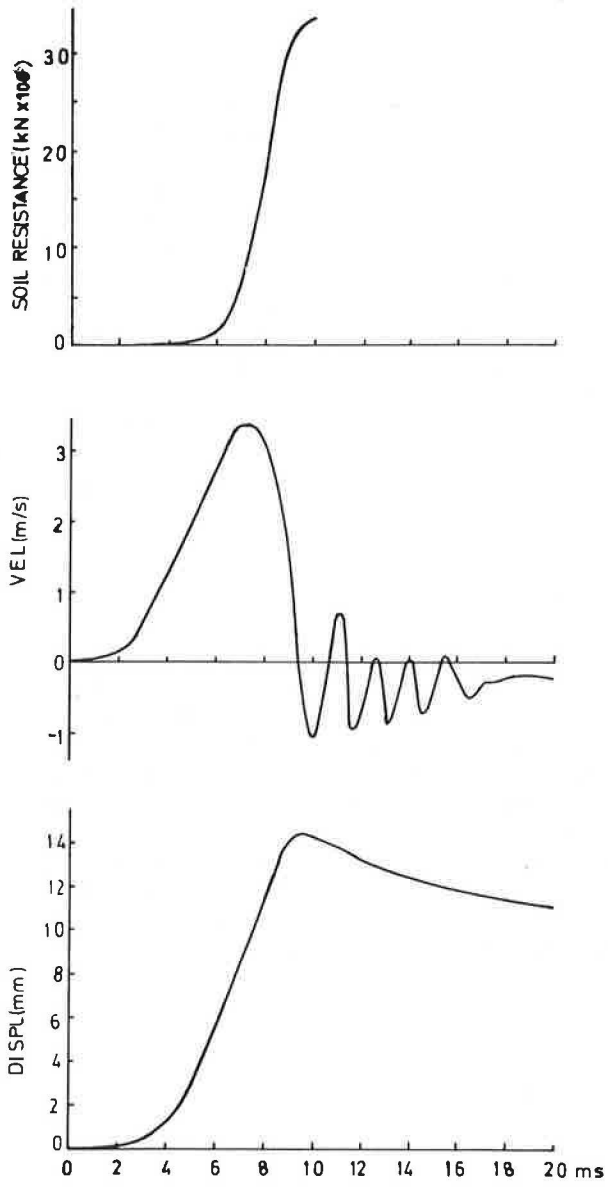

FIGURE 7 Predicted response of Pile 2.

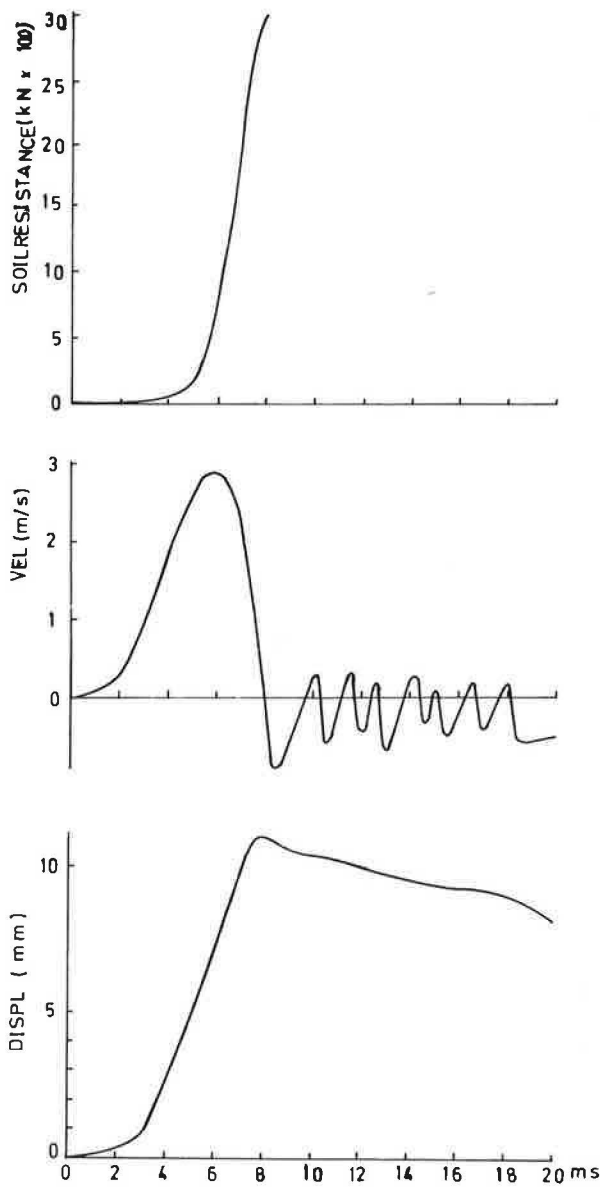

FIGURE 8 Predicted response of Pile 3.

therefore intended to show the general trend of the pile dynamic behavior. It is to be noted that the main aim of this paper is to determine the static bearing capacities from the dynamic behavior of piles. The results are summarized in Table 1.

In all cases, the displacement and the velocity curves show the same general trend as those of the corresponding experimental curves. As mentioned, it is necessary to adjust the value of R so that the computed maximum displacement corresponds to the experimentally obtained maximum displacement. The static bearing capacity of a pile is evaluated from the dynamic soil resistance curve at the instant of (or just after) the maximum velocity. The dynamic soil resistance could be much higher than the static bearing capacity.

The predicted bearing capacity for Pile 1 is 903 kN and the experimental value is 952 kN, showing a discrepancy of less than 5 percent. The discrepancy between measured and calculated maximum displacements is about 2.5 percent. Agreement between the measured and calculated static bearing capacity is excellent for Pile 2. The calculated bearing capacity is 1,115 kN as against 1,121 kN obtained from field tests; the discrepancy between these values is less than 1 percent. For Pile 3, the predicted bearing capacity is 875 kN, and the corresponding measured value is 908 kN. The discrepancy is less than 4 percent. Pile 4 is the same pile as Pile 3, but it was redriven after the ground had set. The predicted bearing capacity is 960 kN, as opposed to 1,077 kN obtained from the field tests. The discrepancy in this case is about 11 percent, which is relatively high. The cause of the discrepancy is probably ground settlement, which has a damping effect on the sides of the pile. To account for damping, further computations were carried out with an assumed value of 87.6 kN s/m for the damping coefficient in Equation 10. The new bearing

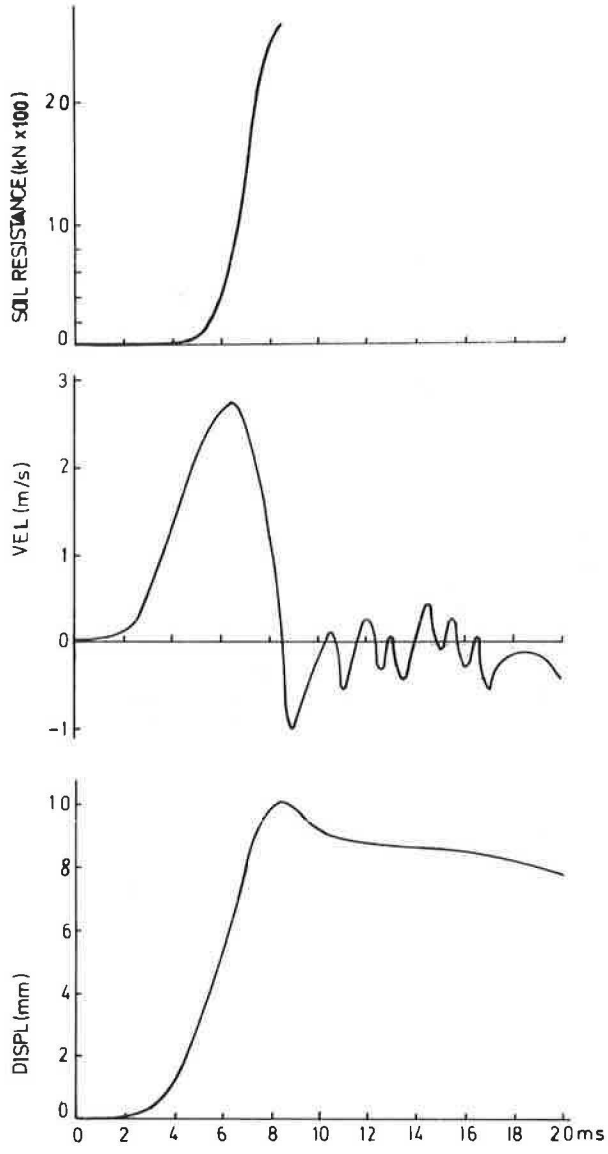

FIGURE 9 Predicted response of Pile 4.

capacity improved to 1,006 kN, narrowing the difference between the measured and predicted values to 6.5 percent (see Table 1).

In all the cases cited above, the predicted bearing capacity is slightly lower than the corresponding field test value. Some discrepancy is probably due to not accounting for the damping coefficient, which is difficult to measure. However, prediction of a slightly lower value than the actual provides more confidence in the construction of a pile foundation.

Although the present method has been applied to a limited number of cases, it appears to predict pile static bearing capacity fairly accurately and appears valid just after driving for different kinds of soils. This is because the pile acceleration response that is normally measured takes into account the individual soil characteristics. The numerical solution is straightforward, requiring very little expertise in computer programming. Actual computation time for each pile is relatively small.

CONCLUSIONS

The study has provided a new and simple technique for predicting pile bearing capacity through the use of dynamic soil resistance concept. The driving force and the acceleration response are the only quantities that must be measured. It is, however, necessary to obtain from the acceleration records the pile velocity and displacement for calculation purposes. The rigid-pile assumption for determination of static bearing capacity seems to be confirmed by the good agreement between the predicted and measured results. The test procedure could be applied to embedded piles even after soil settlement had taken place, but the effect of damping should be included in the analysis. The numerical method presented is relatively simple and accurate.

ACKNOWLEDGMENTS

The author wishes to acknowledge gratefully the facilities provided for this research by the Department of Mechanical

TABLE 1 SUMMARY OF CALCULATED AND MEASURED CHARACTERISTICS OF IMPACT-DRIVEN PILES

Pile No	Aver. AMP(mm)	R* kN/cm^3	R** kN/cm^3	Max. Displacement(mm)			Static Bearing Capacity(kN)			Discrepancy***%
				Calculated*	Calculated**	Measured	Calculated*	Calculated**	Measured	
1	10.2	870	923	14.44	14.5	14.87	903	910	952	4.5
2	10.0	1104	1153	14.48	14.6	14.63	1115	1115	1121	.50
3	7.7	2143	1357	10.54	13.00	13.00	1000	875	908	3.7
4	7.3	2578	2035	10.10	11.0	11.2	960	960 (1006)	1077	11 (6.5)

* Approximate Result

** Improved Result

*** Discrepancy Between Improved and Measured Values

Engineering and Computing Centre of Shiraz University. Thanks are due to Michael W. O'Neill, Houston University, for helpful suggestions towards improving the paper.

REFERENCES

1. R. H. Scanlan and J. J. Tomko. Dynamic Prediction of Pile Static Bearing Capacity. *Journal of the Soil Mechanics and Foundation Division*, ASCE, Vol. 95, No. SM2, 1969, pp. 583–604.
2. F. Rausche, F. Moses, and G. G. Goble. Soil Resistance Predictions from Pile Dynamics. *Journal of the Soil Mechanics and Foundations Division*, ASCE, Vol. 98, No. SM9, 1972, pp. 917–937.
3. M. A. Satter and A. Ghahramani. Prediction of Tip Resistance from Pile Dynamics. *Iranian Journal of Science and Technology*, Vol. 8, No. 2, 1979.
4. F. T. Touma and L. C. Reese. Behavior of Bored Piles in Sand. *Journal of the Geotechnical Engineering Division*, Vol. 100, No. GT7, 1974, pp. 749–761.
5. Y. Koizumi, et al. Field Tests on Piles in Sand. *Soils and Foundations*, Vol. 11, No. 2, 1971, pp. 29–49.
6. M. A. Satter. Dynamic Behavior of Partially Embedded Piles. *Journal of the Geotechnical Engineering Division*, Vol. 102, No. GT7, 1976, pp. 775–785.
7. D. D. Barkan. *Dynamics of Bases and Foundations*. Translated by L. Drashevska, McGraw-Hill, New York, 1962.
8. A. Ghahramani. *Vibratory Pile Driving—Ultimate Penetration and Bearing Capacity*. Ph.D. thesis. Princeton University, Princeton, N.J., 1966.
9. F. E. Richart, Jr., J. R. Hall, Jr., and R. D. Woods. *Vibrations of Soils and Foundations*. Prentice-Hall, Englewood Cliffs, N.J., 1970.
10. R. D. Chellis. *Pile Foundations*. McGraw-Hill, New York, 1961.
11. G. G. Goble, R. H. Scanlan, and J. J. Tomko. Dynamic Studies on the Bearing Capacity of Piles. In *Highway Research Record 167*, HRB, National Research Council, Washington, D.C., 1967.
12. R. Hooydonk, D. Pluimgrauff, and B. Broms. Non-Destructive Pile Testing in Singapore Practice. *Proc., 4th I.G.S. Conference on Field Instrumentations and In-Situ Measurements*, Singapore, 1986.
13. L. H. J. Scheap and deVos. The Sonic Pile Test Recorder and its Applications. *Proc., 2nd International Conference on Application of Stress-Wave Theory of Piles*, Stockholm, 1984.
14. F. Rauche, G. G. Goble, and G. E. Likins. Dynamic Determination of Pile Capacity. *ASCE Journal of Geotechnical Engineering*, Vol. 3, No. 3, 1985, pp. 367–387.
15. C. R. Wylie, Jr. *Advanced Engineering Mathematics*, 3rd ed. McGraw-Hill, New York, 1966.
16. H. T. Davis. *Introduction to Nonlinear Differential and Integral Equations*. Dover, New York, 1960.

Publication of this paper sponsored by Committee on Foundations of Bridges and Other Structures.

Axial Capacity of Vibratory-Driven Piles versus Impact-Driven Piles

REED L. MOSHER

In recent years, vibratory pile drivers have gained popularity with contractors due to the increased productivity that can be realized with their use. The driving time can be reduced by a factor of 10 to 20 over that of an impact-driven pile. This gain in productivity is very attractive and profitable, but questions exist as to whether vibratory driving has an effect on a pile's axial capacity when compared with an impact-driven pile. This paper will present and discuss the results of a study of three pile testing programs that make direct comparison between vibratory- and impact-driven piles. One of these testing programs has never before been reported in the literature. From the study of these testing programs, it was found that the vibratory-driven piles had a significant reduction in axial capacity when compared with the impact-driven piles. This reduction in capacity of the vibratory-driven piles was due to a lower tip resistance.

In recent years the use of vibratory pile driving hammers has gained popularity with contractors because of the increased productivity realized with their use. Driving piles with a vibratory hammer can reduce driving times by a factor of 10 to 20 over that of an impact-driven pile. This gain in productivity is very attractive and profitable when a large number of piles are being installed.

As the popularity of vibratory hammers has increased, so have the questions about the axial capacity of vibratory-driven piles as compared with impact-driven piles. Pile installation invariably results in altering the stresses in the soil surrounding the pile. Studies (*1*,*2*,*3*) have revealed that impact driving in granular soils causes compaction of the soil in the vicinity of the pile. Consequently, the stress levels are increased. Less is known about the changes that the soil undergoes in the vicinity of a vibratory-driven pile.

This paper presents the findings of an investigation that examined pile test data to determine if there were any significant differences between the axial capacity of piles driven by vibratory hammers and by impact hammers. The pile load test has long been recognized as the only true measure of axial capacity for a given site. A load test permits the direct measurement of pile capacity under the actual construction and soil conditions that prevail at the site. The investigation concentrated on test programs at sites where tests were performed on piles driven by both vibratory and impact hammers.

BACKGROUND

During the construction of Lock and Dam No. 1 for the Red River Waterway, a pile testing program was undertaken to verify the pile design for the dam. The piles at the site were driven with a vibratory hammer. The piles tested were H piles with lengths between 55 and 70 ft. The capacities of the piles tested were 40 to 70 percent less than the expected values. In an effort to discover if the reduced capacity was due to the driving of the piles with a vibratory hammer, the U.S. Army Engineer Division, Lower Mississippi Valley, initiated the investigation reported in this paper.

Information Technology Laboratory, U.S. Army Engineer Waterways Experiment Station, P.O. Box 631, Vicksburg, Miss. 39181-0631.

FIELD PILE TESTS

A search of the literature and Corps of Engineer files was conducted to find as many pile test programs as possible that had direct comparisons of vibratory- and impact-driven piles. This paper presents three of the pile test programs discovered during the investigation (*4*). These three programs were selected because they were well documented and represented the most common use of vibratory hammers for pile driving. Brief descriptions of the site conditions, the pile tested, and the test results are presented here.

Arkansas River Lock and Dam No. 4

The pile testing program for Lock and Dam No. 4 was instituted as the primary source of information for the design and construction of the four locks and dams along the lower Arkansas River. In view of the magnitude of the projects and the lack of factual information regarding the drivability and capacities of piles in the lower Arkansas River Valley, a comprehensive pile testing program was conducted by the U.S. Army Engineer District, Little Rock. The purpose of the tests was to develop criteria for the design and construction of pile foundations for future locks and dams. The general objectives of the pile test program were to establish design and construction criteria for axially and laterally loaded piles and to determine the type and size of pile-driving hammers required for economical installation. The results of the pile test program were presented in a report for the Little Rock District prepared by Fruco and Associates (*5*).

Site Description

Soil conditions in the lower Arkansas River Valley are typical of an alluvial pastoral zone. In general, they consist of alluvial deposits of loose surface silts, sandy silts, and clays of variable thickness, underlain by a zone of medium to dense silty sand

with a thickness ranging from 70 to 150 ft. This all overlies a stratum of deeply bedded Tertiary clays.

The test site was located on the east bank of the Arkansas River about 20 miles downstream from Pine Bluff, Ark., and 9 miles upstream from the future site of Lock and Dam No. 3 (Figure 1). The soil conditions at the pile testing site were determined by exploratory borings and laboratory tests made in connection with the foundation investigation for Lock and Dam No. 4, and further explorations were made specifically for the pile testing program. These explorations indicated that three major soil strata exist at the test site: a surface blanket of silts and clays, which extends about 15 ft below the ground surface; a deep stratum of relatively dense, fine to medium sand, which extends about 100 ft; and a basal stratum of Tertiary clay of undetermined thickness. Discontinuous thin seams of silt and clay were encountered in a sand stratum at depths between 30 and 50 ft.

The test area was prepared by excavating approximately 20 ft of silty surface soils, exposing the underlying stratum of sand. Post-excavation standard penetration resistances increased with depth, ranging from 20 to 40 blows/ft, with an average of about 27 blows/ft. The dry density of the sand ranged from 90 to 109 pcf, but showed no significant trend with depth. The groundwater level was held at 2 to 3 ft below the surface of the site. Figure 2 shows a generalized profile for the test site.

Description of Testing Program and Results

The basic pile investigation included field driving and load tests on a variety of pile types. Tests were performed on square prestressed concrete piles, steel pipe piles, and steel H piles that were driven with both a double-action steam and a Bodine sonic vibratory hammer. The field load tests included compression, tension, and lateral loading of single piles. Strain instruments were attached to steel piles to determine the distribution of stresses in the piles under compression, tension, and lateral loads.

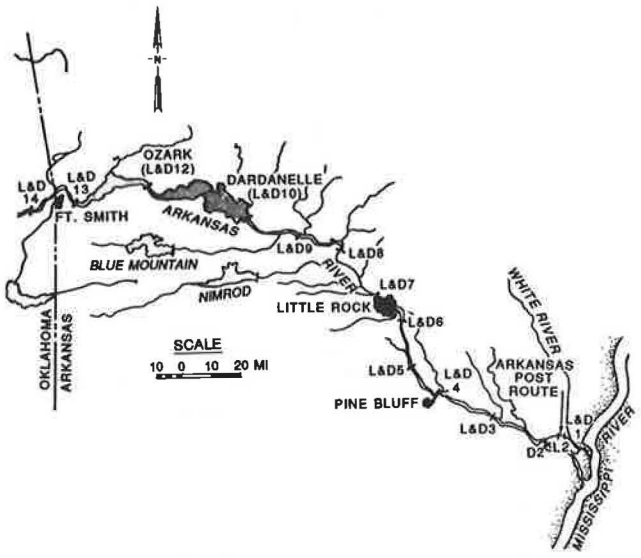

FIGURE 1 Arkansas River Navigation Project.

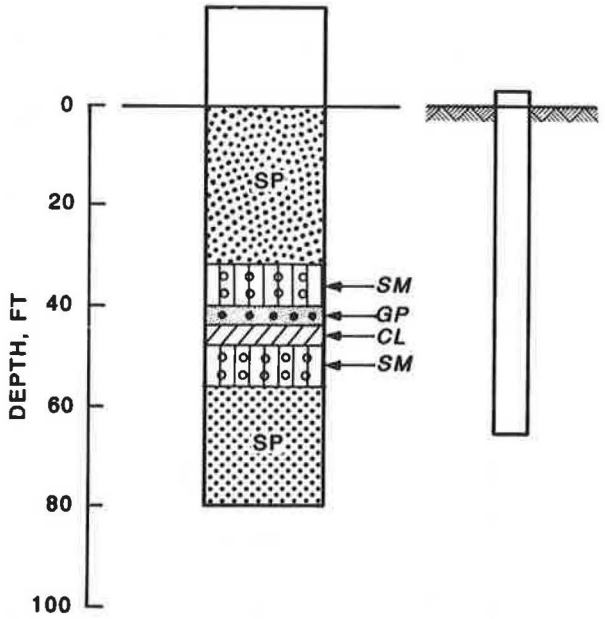

FIGURE 2 Generalized soil profile at Lock and Dam No. 4 pile test site.

Table 1 presents a summary of the axial load tests performed at the site. The table shows the type of pile tested, penetration, type of hammer used for installation, and reported average failures for compression and tension. Comparisons between impact- and vibratory-driven piles can be made with the 16 in. pipe piles, the H piles, and the 16 in. concrete piles.

In Table 2, the distribution of the load being carried by the side and the tip of the pile is given for the pipe sections. The total, tip, and side loads at failure are plotted in Figure 3 against the pile diameters for the various pipe piles tested. Piles 2 and 10, being spaced just 8 ft apart, provide a direct comparison between a pile installed by a Bodine sonic hammer (a high-frequency vibratory hammer) and a similar pile driven with a Vulcan steam impact hammer. Comparing the load carried by the tip and side for Piles 2 and 10, 16 in. pipe piles, shows that the impact-driven pile has significantly more capacity at the tip, 58 tons, than the vibratory-driven pile, 46 tons, while the side capacities differed only by 3 tons.

Table 3 presents the distribution of the load being carried by the side and tip for the H piles tested. Comparisons can be made between Piles 7 and 9. Pile 9, which was driven with the Bodine sonic hammer, had 20 tons greater capacity than Pile 7, which was impact driven. Examination of the distribution of the load in the piles reveals that the vibratory-driven pile, Pile 9, had 14 tons less tip capacity than the impact-driven pile, Pile 7, but had a substantially greater side capacity of 34 tons.

Arkansas River Lock and Dam No. 3

Exploration prior to construction showed a stratigraphy of the site typical of Arkansas River alluvial soils and comparable with that found at Lock and Dam No. 4. However, during the initial pile driving and load testing, it became apparent that the soil characteristics at the site were not as anticipated.

TABLE 1 SUMMARY OF ARKANSAS RIVER LOCK AND DAM NO. 4 PILE TESTS

TEST NO.	TYPE	PENETRATION Ft	HAMMER TYPE	AVERAGE PILE FAILURE LOAD, TONS	
				COMPRESSION	TENSION
1	12 IN. PIPE	53.1	140C	140	70
2	16 IN. PIPE	52.8	140C	195	91
2X	16 IN. PIPE	52.8	140C	210	-
3	20 IN. PIPE	53.0	140C	215	90
4	16 IN. CONCRETE	40.2	140C	170	71
5	16 IN. CONCRETE	51.0	140C	240	-
6	14 BP 73	40.0	80C	140	-
7	14 BP 73	52.1	80C	190	45
8	TIMBER	38.6	65C	80	25
9	14 BP 73	53.2	BODINE	210	-
10	16 IN. PIPE	53.1	BODINE	180	87
11	16 IN CONCRETE	38.8	BODINE	150	-

TABLE 2 LOAD DISTRIBUTION IN PIPE PILES

TEST NO.	NOMINAL DIAMETER IN.	PENETRATION Ft	AVERAGE FAILURE LOAD TONS	TIP LOAD		SKIN FRICTION	
				TONS	PERCENT	TONS	PERCENT
1	12	53.1	140	34	24	106	76
2	16	52.8	195	58	30	137	70
2X	16	52.8	210	67	32	143	68
3	20	53.0	215	77	36	138	64
10	16	53.1	180	46	26	134	74

The initial compression and tension tests indicated that the design pile lengths would not carry the required loads with appropriate safety factors. Therefore, additional soil borings and field and laboratory tests were made. The results of these tests indicated that the removal of the overburden and/or scour during the cofferdam construction had relaxed the confining stresses within the soil mass, resulting in a significant reduction in the strength of the foundation. To determine the required pile lengths for the unexpected soil conditions, and to investigate the acceptability of the contractor's proposal to drive the bearing piles with a Foster vibratory hammer, the Little Rock District initiated a pile testing program.

Site Description

Arkansas River Lock and Dam No. 3 is located at Arkansas River navigational mile 49.3, approximately 30 miles down-

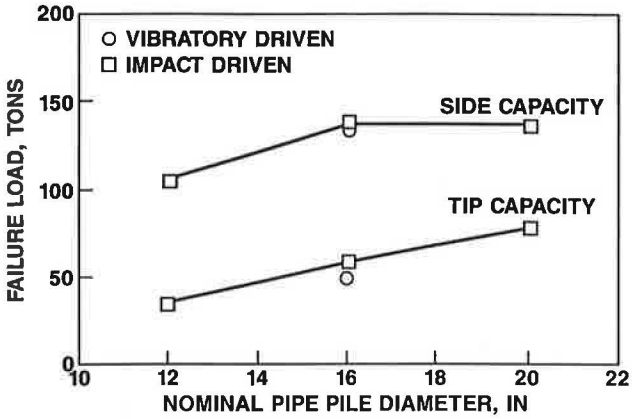

FIGURE 3 Failure load versus pipe pile diameter at Lock and Dam No. 4.

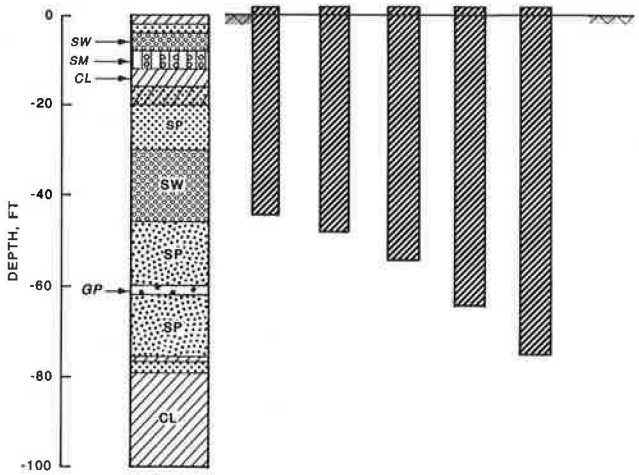

FIGURE 4 Generalized soil profile at Lock and Dam No. 3 pile test site.

stream from Pine Bluff, Ark. (Figure 1). The geological conditions and stratigraphy are similar to those previously described for Lock and Dam No. 4.

The tests of interest were performed in the vicinity of the left river bank. The top stratum varied from 0 to 30 ft in thickness and consisted of erratically stratified silt and lean clay. These surface soils are underlain by 90 to 130 ft of sand, primarily gray and brown, clean, fine to medium sand with frequent lenses of clay, silt, and silty sand mixed with gravel lenses and occasional boulders. Below the sand deposit lies a Tertiary formation of stiff to hard, overconsolidated clay of low to high plasticity. The generalized soil profiles shown in Figure 4 were derived for the test area. Prior to pile driving, the test site was excavated into the thick sand stratum. Approximately 40 to 50 ft of the surface stratum was removed.

Description of Testing Program and Results

Load tests were performed to determine the axial capacity for different driving equipment, lateral capacity of piles, load versus length curves of the site, and water table correction factors for the submerged condition. For each of the piles tested, a cluster of at least nine piles was driven, with the center pile being the designated test pile. The test program consisted of 15 compression, 7 tension, and 10 lateral load tests (*6*).

Only the pile tests relevant to the comparisons of capacities between vibratory- and impact-driven piles were examined. The piles of interest were 14 BP 73, of lengths 45, 50, 55, 65, and 75 ft. Table 4 presents a summary of pile types, lengths, penetrations, hammer types, and failure loads for the piles that were examined for the investigation. Piles 1, 3, 3A, 3B, and 9 were driven by a Foster 2-50, low-frequency, vibratory hammer, and Piles 2, 2A, 5, 6, and 7 were driven by a Vulcan 140C steam hammer.

During the driving of the piles for these tests, the sand surrounding the piles loosened, and voids 5 to 10 ft deep formed between the flanges near the surface. Attempts were made to fill the voids and to compact the sand surrounding the piles. For Piles 3A and 3B, a concrete vibrator was used to place and increase the density of the sand in the flanges around the top of the pile. For Pile 2A, the voids in the flanges were filled with sand and water without compaction. For Pile 9, the voids were filled with sand and water, and the area surrounding the pile was compacted by vibroflotation. The vibroflotation compaction resulted in a significant increase in the capacity.

The main objectives of this portion of the testing program were to obtain data for determining the pile lengths needed for this lock and dam and to make a direct comparison between piles driven with a vibratory and an impact hammer. Figure 5 shows the failure loads versus depth of penetration for the compression tests. This figure shows that the impact-driven piles have a substantially higher capacity than the vibratory-driven piles, by an average of 32 tons. Figure 6 presents the

TABLE 3 LOAD DISTRIBUTION IN H PILES

TEST NO.	PENETRATION Ft.	AVERAGE FAILURE LOAD Tons	TIP LOAD		SKIN FRICTION	
			TONS	PERCENT	TONS	PERCENT
6	40.0	140	21	15	119	85
7	52.1	190	39	21	151	79
9	53.2	210	25	12	185	88

TABLE 4 SUMMARY OF ARKANSAS RIVER LOCK AND DAM NO. 3 H PIPE TESTS

TEST NO.	HAMMER *	PENETRATION FT	COMPRESSION FAILURE LOADS TONS		TENSION FAILURE LOADS, TONS	
			TESTED	ADJUSTED **	TESTED	ADJUSTED **
1	FR 2-50	42.3	85	71	25	22
2	VC 140C	42.8	134	104	34	27
2A	VC 140C	61.8	185	145	-	-
3	FR 2-50	46.7	105	80	-	-
3A	FR 2-50	46.7	120	92	31	23
3B	FR 2-50	61.8	145	117	-	-
5	VC 140C	52.8	150	128	39	32
6	VC 140C	63.0	175	155	51	44
7	VC 140C	73.0	215	190	-	-
9	FR 2-50	42.9	127	88	-	-

* FR 2-50 = FOSTER VIBRATORY HAMMER; VC 140C = VULCAN STEAM HAMMER.
** ADJUSTED FOR WATER LEVEL.

tension failure loads versus the depth of penetration. This figure reveals that the impact-driven piles have only a slightly greater capacity, 5 tons, than the vibratory-driven piles.

Crane Rail Tracks

During the construction of pile foundations for crane rail tracks for jib and gantry cranes, it was decided to investigate the use of a vibratory hammer for the pile driving instead of a drop hammer. It was believed that, for the subsoil conditions at the sites, the vibratory-driven piles would give the same bearing capacities as the impact-driven piles and would shorten the construction time. To substantiate this assumption, a series of pile load tests were conducted to make direct comparisons between piles driven with a vibratory hammer and with an impact hammer. Mazurkiewicz (*7*) reported the results and conclusions from the pile testing program. Site and pile descriptions and test results are summarized in the following paragraphs.

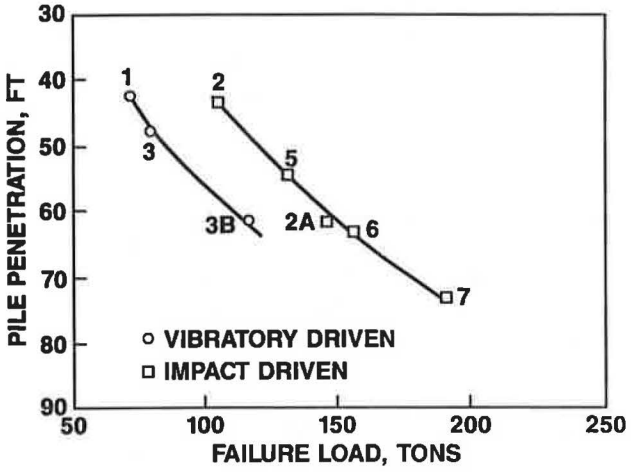

FIGURE 5 Failure load versus depth for compression tests at Lock and Dam No. 3.

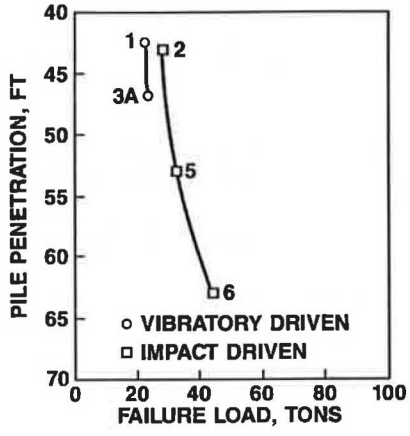

FIGURE 6 Failure load versus depth for tension tests at Lock and Dam No. 3.

In the vicinity of the construction sites and pile tests, the subsurface profile consists of a 3 to 5 ft layer of fill over a 3 to 6 ft layer of peat. The peat is underlain by layers of fine to medium sand and sandy gravels, which overlie a stratum of silty clay with silt. Penetration tests show a linear increase in resistance with depth through the sand and no trend in the clay. The stratification and representative penetration records are shown in Figure 7.

The load tests were performed on prestressed concrete piles with a diameter of 13.4 in. (34 mm) and lengths from 42.7 ft (13 m) to 88.6 ft (27 m). The comparison tests were made for 11 piles driven by a drop hammer and 11 piles driven by a vibratory pile driver. The distance between the two piles used for comparison (one impact driven and one vibratory driven) was 10 to 25 ft. Table 5 shows the failure loads obtained from the 11 sets of load tests. The ratios between the failure loads of the vibratory-driven and impact-driven piles are also given. Figure 8 is a plot of failure loads versus depth of penetrations for the 11 test sets. For each test set of piles, the impact-driven piles showed substantially higher failure load than the vibratory-driven piles.

The influence of time on the ratio of axial capacity of the vibratory- and impact-driven piles was also studied. It was found that, if the piles were tested after 4, 12, or 30 or more days, the difference in capacity between vibratory- and impact-driven piles remained unchanged. However, some increase in capacity with time did occur for both methods of installation.

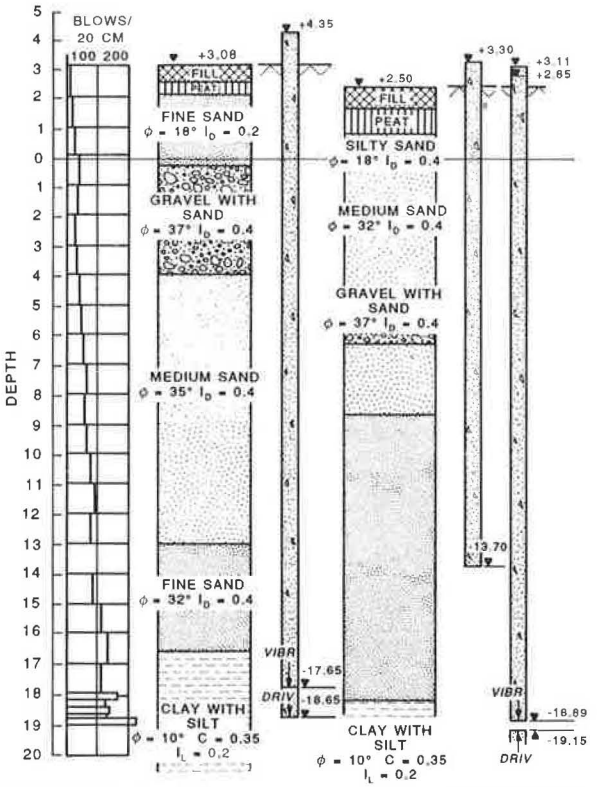

FIGURE 7 Stratification for the crane rail track test sites.

TABLE 5 SUMMARY OF CRANE RAIL TRACKS PILE TESTING PROGRAM

PILE TEST SET	LENGTH Ft (m)	FAILURE LOAD FOR VIBRATORY DRIVEN tons (mtons)	FAILURE LOAD FOR IMPACT DRIVEN tons (mtons)	RATIO
1	42.7 (13)	38.5 (35)	92.4 (84)	0.42
2	42.7 (13)	46.2 (42)	52.8 (48)	0.88
3	42.7 (13)	71.5 (65)	93.5 (85)	0.76
4	57.8 (17)	44.0 (40)	69.3 (63)	0.63
5	57.8 (17)	50.6 (46)	124.3 (113)	0.41
6	59.1 (18)	28.6 (26)	115.5 (105)	0.25
7	72.2 (22)	103.4 (94)	159.5 (145)	0.65
8	75.5 (23)	55.0 (55)	82.5 (75)	0.67
9	75.5 (23)	77.0 (70)	148.5 (135)	0.52
10	75.5 (23)	38.5 (35)	66.0 (60)	0.54
11	88.6 (27)	93.5 (85)	115.5 (105)	0.81

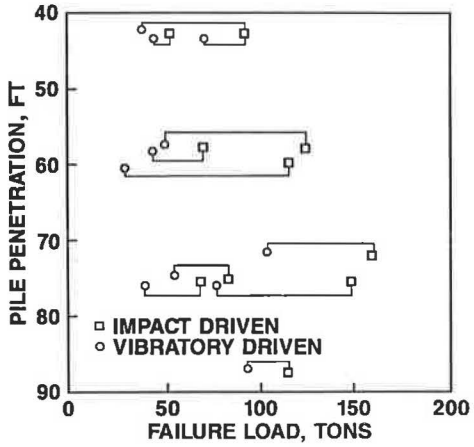

FIGURE 8 Failure load versus depth for the crane rail tracks pile testing program.

SUMMARY OF FIELD TESTS

The piles driven by the impact hammers had a significantly greater axial capacity than those driven with the vibratory hammers. In Figure 9, the failure load for the impact-driven piles is plotted versus the failure load of the vibratory-driven piles. The diagonal line in the plot represents a one-to-one correspondence between the impact and vibratory capacity; points below this line show a greater capacity for impact-driven piles, and points above this line show a greater capacity for vibratory-driven piles. This plot shows that, for the majority of the pile tests examined in this study, the vibratory-driven piles have less axial capacity than impact-driven piles.

REDUCED CAPACITY FOR VIBRATORY-DRIVEN PILES

A possible explanation for the reduced capacity for vibratory-driven piles is that the vibratory driving process results in less compaction at the pile tip, thus lowering the tip capacity. Hunter and Davisson (*8*), in their investigation of the Arkansas River Lock and Dam No. 4 pile tests, explained the difference in capacities by examining the driving process. They state that a vibratory hammer is very effective in overcoming the side resistance or skin friction along a pile in sand, but the very nature of the longitudinal pile vibration requires a small tip force. Therefore, the soil beneath the tip of a vibratory-driven pile remains relatively undisturbed compared with its state before driving. In comparison, Meyerhof (*1*) showed that impact driving in sand results in substantial compaction beneath the tip, which prestresses the surrounding soil mass.

Evidence of this can be found in the Arkansas River Lock and Dam No. 4 pile testing program. Figure 10 presents a plot of the tip load, skin friction, and total pile load at failure for impact-driven piles versus the vibratory-driven piles for Lock and Dam No. 4. The plot reveals that for each comparable set of piles the tip load at failure for the vibratory-driven piles is lower than the impact-driven piles. Even for the set of H piles, the load carried by the tip of the vibratory-driven pile was 14 tons less than the impact-driven pile, even though the vibratory-driven pile had a greater total load at failure.

RETESTS

Further supporting evidence that the tip capacity for vibratory-driven piles is less than for impact-driven piles can be found in the crane rail testing program. To investigate whether a pile previously vibrated into place and then driven a short distance by a drop hammer would achieve the same ultimate capacity as a pile completely driven with a drop hammer, some additional tests were performed in the crane rail testing program. These tests showed that vibratory driven piles with the last 9 ft of penetration driven by a drop hammer had the same failure load as purely impact-driven piles with the same penetration.

As previously mentioned, the axial capacity of the piles at Red River Lock and Dam No. 1 was significantly less than anticipated. In an attempt to investigate the reasons for the reduced capacity, several of the piles were retested. Figures 11, 12, and 13 show plots of the tip load versus displacement for three of the load tests and their retest at Red River Lock

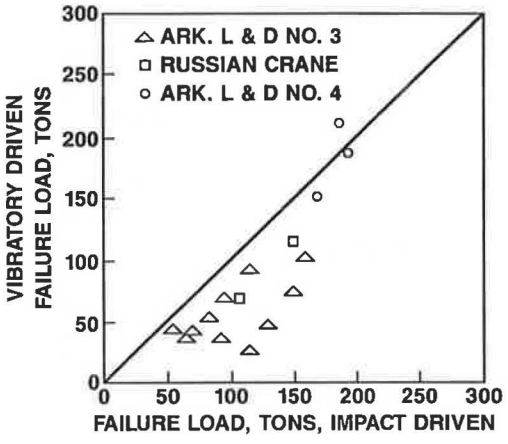

FIGURE 9 Comparison of impact- and vibratory-driven piles.

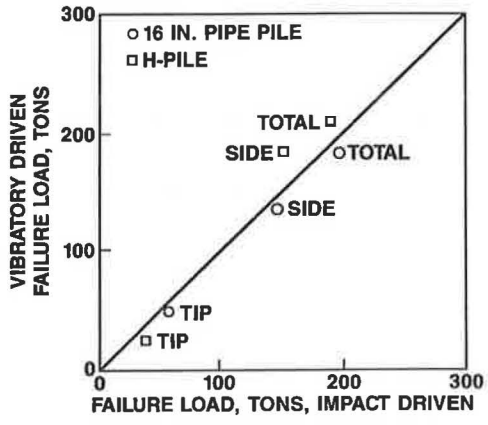

FIGURE 10 Comparison of load distribution of impact- and vibratory-driven piles for Lock and Dam No. 4.

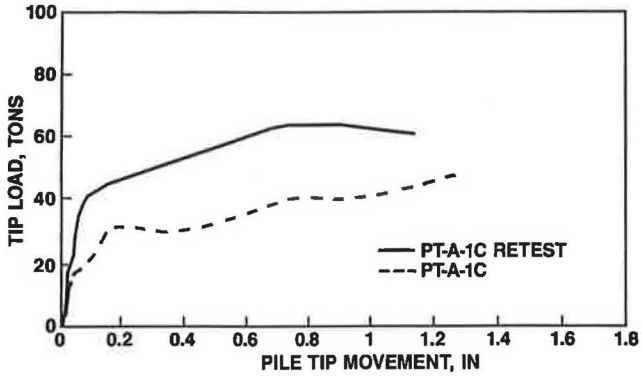

FIGURE 11 Tip load versus pile tip movement for Red River Lock and Dam No. 1 pile test PT-A-1C (*9*).

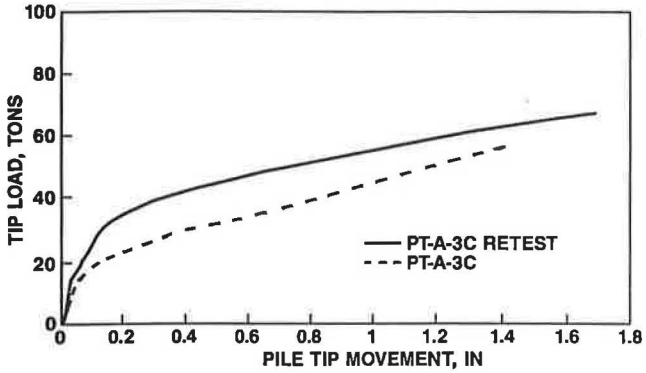

FIGURE 12 Tip load versus pile tip movement for Red River Lock and Dam No. 1 pile test PT-A-3C (*9*).

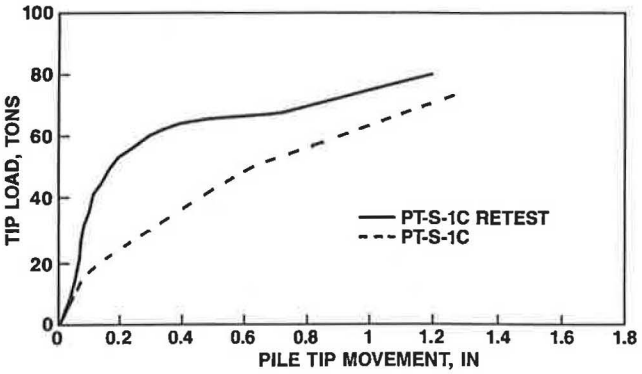

FIGURE 13 Tip load versus pile tip movement for Red River Lock and Dam No. 1 pile test PT-S-1C (*9*).

and Dam No. 1. In these plots, the retests have significantly greater load-carrying capacity than when previously tested. A large portion of the additional capacity exhibited by the retested piles resulted from the compaction of the soil surrounding the tip during the first load tests. The influence of time may also have had a small effect on the increased capacities.

CONCLUSIONS

The results of the field tests presented in this paper show that, for a significant majority of cases, the installation of piles in sand with a vibratory hammer of any type (high or low frequency) resulted in less axial capacity than impact-driven piles at the same site. Additional information was found showing that the influence of time affects piles driven by both methods equally and that additional driving by an impact hammer of a vibratory-driven pile causes an increase in its axial capacity compared with that of a pile driven totally by an impact hammer.

ACKNOWLEDGMENTS

The author would like to express his thanks to the U.S. Army Engineer Division, Lower Mississippi Valley, for the financial support provided for the original investigation. Permission was granted by the Chief of Engineers to publish this information.

REFERENCES

1. G. G. Meyerhof. Compaction of Sands and Bearing of Piles. *Journal of the Soil Mechanics and Foundations Division*, ASCE, Vol. 85, No. SM6, 1959, pp. 1–29.
2. E. I. Robinsky and C. F. Morrison. Sand Displacement and Compaction Around Model Friction Piles. *Canadian Geotechnical Journal*, Vol. 1, No. 4, 1964, pp. 189–204.
3. R. D. Ellison. *An Analytical Study of the Mechanics of Single Pile Foundations*. Ph.D. dissertation, Carnege-Mellon University, Pittsburgh, Pa., 1969.
4. R. L. Mosher. *Comparison of Axial Capacity of Vibratory-Driven Piles to Impact-Driven Piles*. Report ITL-87-7. U.S. Army Engineer Waterways Experiment Station, Vicksburg, Miss., 1987.
5. Fruco and Associates. *Pile Driving and Loading Tests*. U.S. Army Engineer District, Little Rock, Ark., 1964.
6. *Data and Recommendation for Steel Bearing Pile Foundation in Sand Based on Experience at Lock and Dam No. 3 and David D. Terry Lock and Dam (No. 6), Arkansas River Navigation Project*. U.S. Army Engineer District, Little Rock, Ark., 1967.
7. B. K. Mazurkiewicz. Influence of Vibration of Piles on their Bearing Capacity. *Proc., First Baltic Conference on Soil Mechanics and Foundation Engineering*, Gdansk, Poland, Vol. 3, Sec III, 1975, pp. 143–153.
8. A. A. Hunter and M. T. Davisson. Measurement of Pile Load Transfer. In *Performance of Deep Foundations*, Report STP 444, American Society for Standards and Testing, New York, 1969, pp. 106–117.
9. R. L. Mosher. *Load-Transfer Criteria for Numerical Analysis of Axially Loaded Piles in Sand*. Report K-84-1. U.S. Army Engineer Waterways Experiment Station, Vicksburg, Miss., 1984.

Publication of this paper sponsored by Committee on Foundations of Bridges and Other Structures.

Axial Response of Three Vibratory- and Three Impact-Driven H Piles in Sand

JEAN-LOUIS BRIAUD, HARRY M. COYLE, AND LARRY M. TUCKER

Three H piles were impact driven in a medium dense sand deposit, load tested in compression, and then extracted. The same three piles were then vibro-driven at a different location and load tested in compression. The top load-top movement curves show that the vibro-driven piles have, on the average, the same ultimate capacity as the hammer-driven piles. These curves also show that at half the ultimate load, the movement of the vibro-driven piles is 2.5 times larger than the movement of the hammer-driven piles, on average. At half the ultimate load, however, the movement of the vibro-driven piles was only 0.25 in. Some of the piles were instrumented; this allowed researchers to obtain the load transfer curves. These curves showed that the vibro-driven piles carry much more load in friction and much less load in point resistance than the hammer-driven piles.

In the spring and summer of 1986, a series of vertical load tests was carried out on instrumented piles driven in sand at Hunter's Point in San Francisco. The Federal Highway Administration (FHWA) sponsored two projects on impact-driven piles: one on the testing of five single piles, and one on the testing of a five-pile group (*1*,*2*). The U.S. Army Engineer Lower Mississippi Valley Division (LMVD), Waterways Experiment Station (WES), and FHWA then sponsored a project on the comparison of impact-driven piles and vibratory-driven piles. Subsequently, the Deep Foundation Institute drove a number of piles with various vibratory hammers to compare the hammers' efficiencies.

This article is a summary analysis of the pile load tests sponsored by LMVD, WES, and FHWA comparing impact- and vibratory-driven piles. The site is characterized, the load tests are described, the load tests results are analyzed and discussed, and conclusions are made. The details of the work can be found in Tucker and Briaud (*3*).

THE SOIL

The soil has been described in detail by Ng, Briaud, and Tucker (*1*). Below a 4 in. thick asphalt concrete pavement is a 4.5 ft thick layer of sandy gravel with particles up to 4 in. in size. From 5 ft to 40 ft depth is a hydraulic fill made of clean sand (SP). Below 40 ft, layers of medium stiff to stiff silty clay (CH) are interbedded with the sand down to the bedrock. The fractured serpentine bedrock is found between 45 ft to 50 ft depth. The water table is 8 ft deep.

Department of Civil Engineering, Texas A&M University, College Station, Tex. 77843.

Many tests have been performed at the site, including standard penetration tests (SPTs) with a donut hammer and a safety hammer, sampling with a Sprague-Henwood sampler, cone penetrometer tests (CPTs) with point, friction and pore pressure measurements, preboring and selfboring pressuremeter tests, shear wave velocity tests, dilatometer tests, and stepped-blade tests. The CPT, SPT, and stepped-blade tests were performed before and after driving and testing of the FHWA test piles. Selected profiles are shown in Figures 1 through 6. The hydraulic fill has the following average properties: friction angle 32 to 35 degrees, water content 22.6 percent, dry unit weight 100 pcf, D_{60} 0.8 mm, D_{10} 0.7 mm, SPT blow count 15 bpf, CPT tip resistance 65 tsf, PMT net limit pressure 7 tsf, and shear modulus (from shear wave velocity measurements) 400 tsf.

THE PILES AND THE LOAD TESTS

Three HP14x73 steel H piles were used in this program. They were all embedded 30 ft below the ground surface; however, a 4.5 ft deep, 14 in. diameter hole was drilled prior to pile insertion for the impact driven piles, making the true pile embedment equal to 25.5 ft. For the vibratory-driven piles a hole was drilled through the 4 in. thick asphalt layer only, making the embedment equal to 29.5 ft. Each pile had two angles (2.5 x 2.5 x 3/16 in.) welded to the sides of the pile web as protection for the instrumentation.

The first pile (Pile 1) was one of the single piles used in the FHWA program. Pile 1 was instrumented with seven levels of strain gauges and a telltale at the pile tip. This pile was calibrated before driving and the pile stiffness was measured for use in the data reduction. The measured value of pile stiffness (AE) was 614,908 kips. This value was used for all three piles. Pile driving analyzer measurements were obtained during the driving of Pile 1 with an impact hammer. Pile 1 was then load tested in compression 30 days after it was driven (FHWA program): this is load test 1I. Pile 1 was then retested at 67 days after driving: this is load test 1IR. After Pile 1 was retested, the pile was restruck with an impact hammer and pile driving analyzer measurements were obtained. Pile 1 was then extracted and vibro-driven about 30 ft from the impact test. It was load tested at 33 days after driving (load test 1V) and again at 63 days after driving (load test 1VR). After load test 1VR the pile was struck with an impact hammer and pile driving analyzer measurements were obtained.

The second pile (Pile 2) was instrumented with two levels of strain gauges: one at the point and one at mid-length. Pile 2 was impact driven and tested at 65 days after driving: this is load test 2I. Pile 2 was then extracted and vibrodriven and

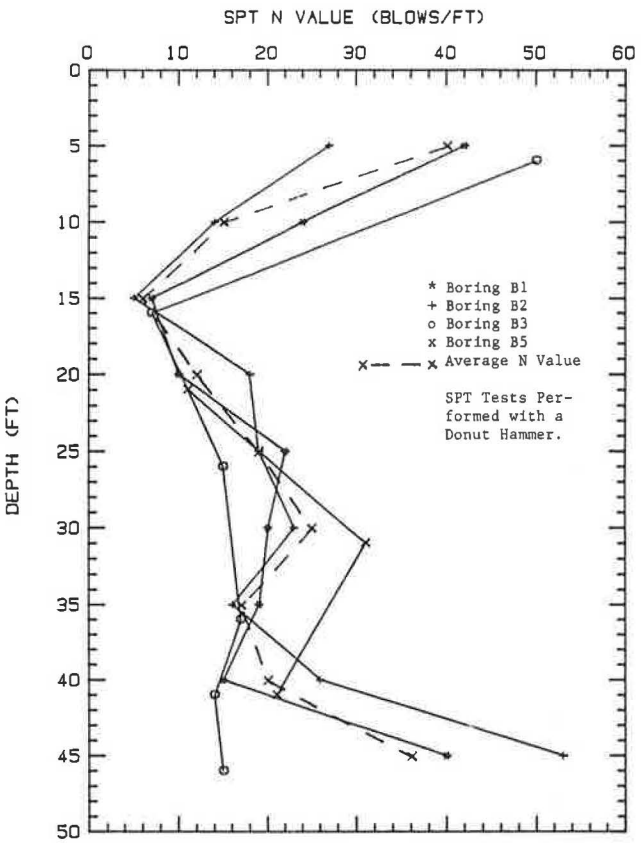

FIGURE 1 Profiles of standard penetration test blow counts.

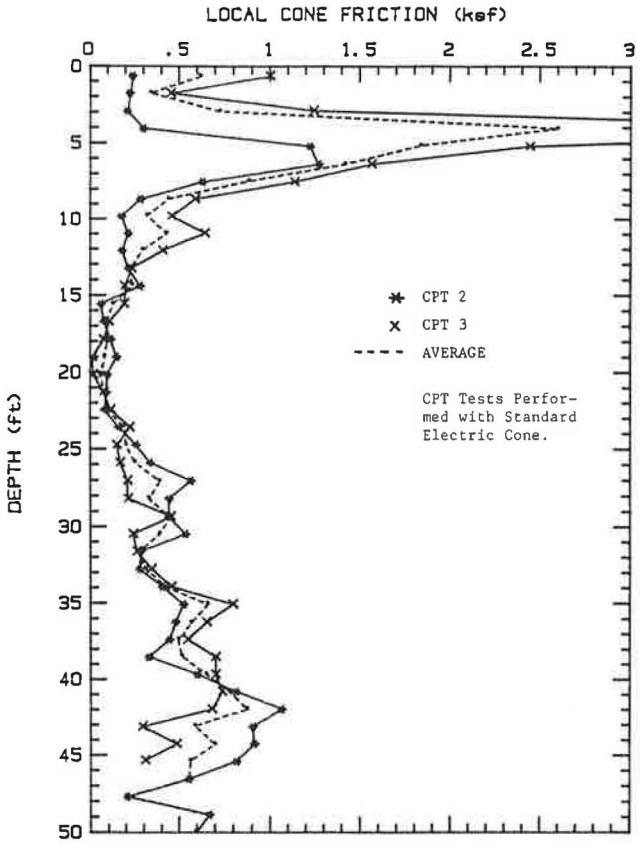

FIGURE 3 Cone tip penetration test profiles for friction resistance.

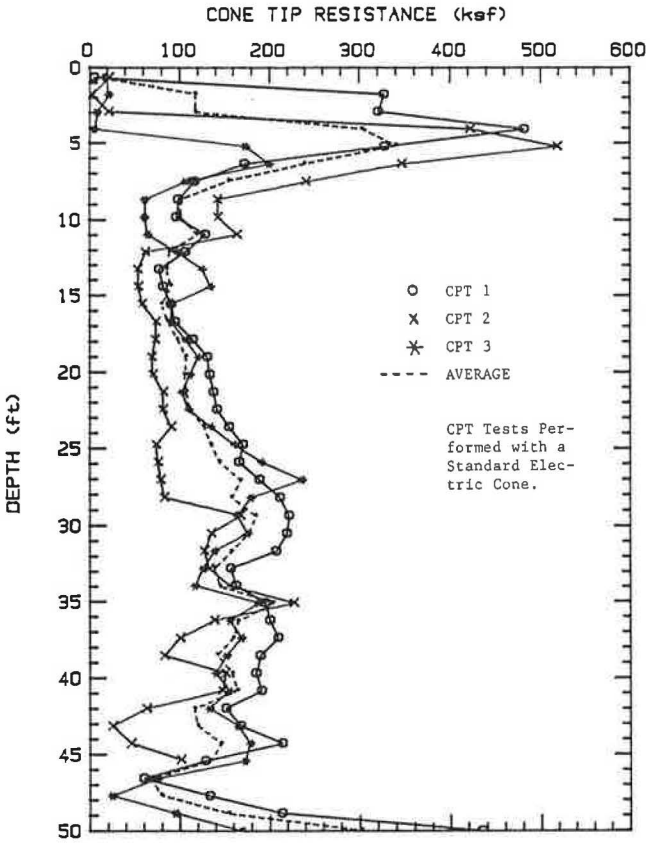

FIGURE 2 Cone tip penetration test profiles for point resistance.

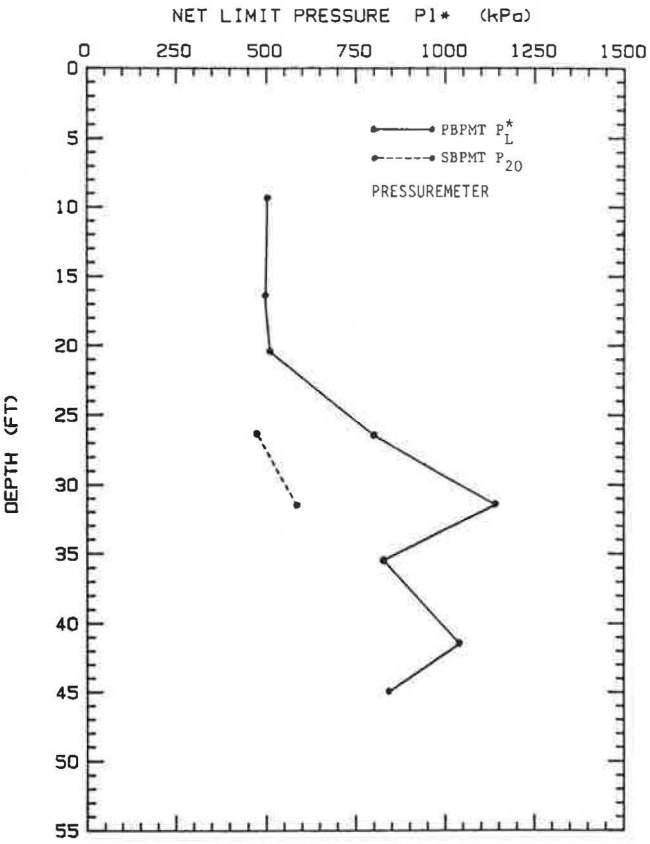

FIGURE 4 Net limit pressure profile.

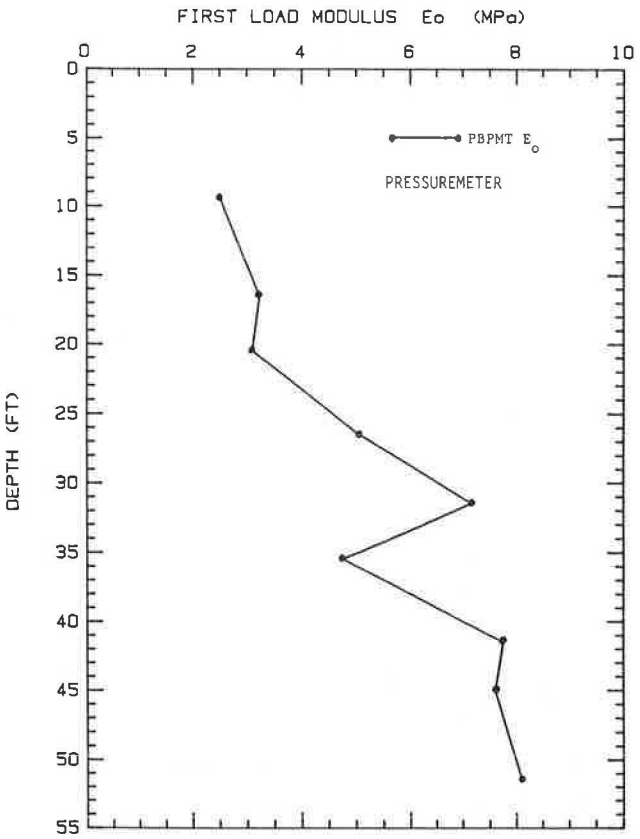

FIGURE 5 First load modulus profile.

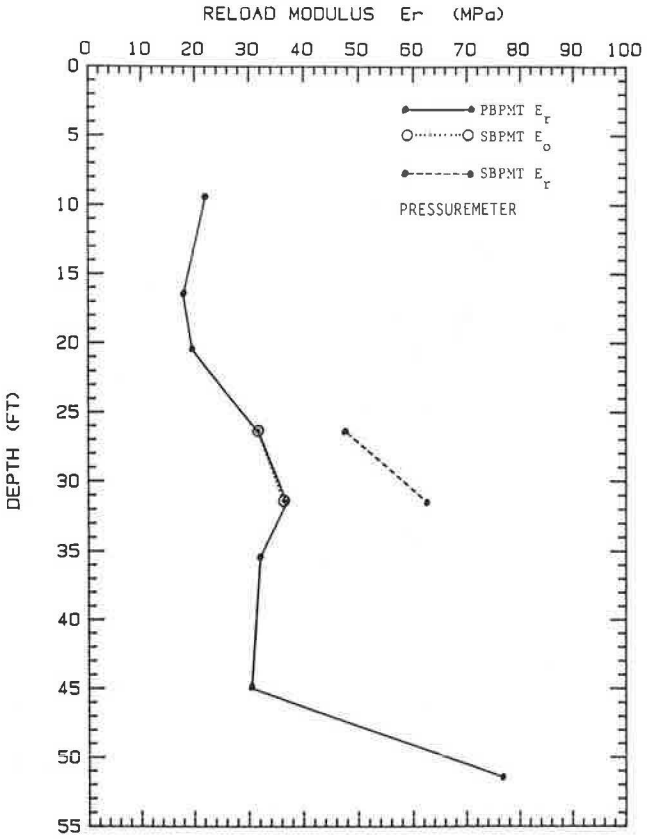

FIGURE 6 Reload modulus profile.

tested at 64 days after driving. This is load test 2V. After load test 2V, the pile was struck with an impact hammer and pile driving analyzer measurements were obtained.

The third pile (Pile 3) was not instrumented. It was impact driven and tested at 12 days after driving: this is load test 3I. Pile 3 was then extracted and vibrodriven. It was tested at 12 days after driving: this is load test 3V. Table 1 summarizes the eight load tests presented in this report.

The impact-driven piles were installed using a Delmag D22 diesel hammer at full throttle. All restrike measurements were also obtained using this hammer. The final blow count for the impact driven piles averaged 11.5 blows/ft (Table 2). The specifications for the Delmag D22 hammer are given in Table 3.

The vibratory-driven piles were installed with an ICE-216 vibratory hammer (Table 4). The penetration rate over the last 2 ft of penetration varied between 12 and 20, averaging 16 ft/min (Table 2). The impact hammer and the vibratory hammer drove the piles in approximately the same time.

The load test procedure consisted of applying the load of 10 percent of the estimated ultimate load. Each load step was held for at least 30 minutes, with the load being monitored continuously. All readings from electronically monitored instruments were recorded every 5 minutes.

RESIDUAL STRESSES

Residual driving stresses were measured for Pile 1I. The stress profile was not monitored between load test 1I and test 1IR. Therefore the same residual stress profile after driving was also used for load test 1IR. Since additional residual stresses are usually induced due to a compression test, this profile and all subsequent profiles for Pile 1R are in error by an unknown amount. The residual stress profile is the first load profile shown in Figure 7.

An attempt was made to record the residual driving stresses for Pile 2I. However, the readings obtained were judged unreliable. Therefore, the residual stress profile from Pile 1I was used in reducing the load test data for Pile 2I (Figure 7).

The vibratory-driven piles were assumed to have no residual driving stresses. No attempt was made to verify this. However, published data substantiate this assumption (*4*).

LOAD TEST RESULTS

The load movement curves for all the piles are shown on Figure 8. The point load-point movement curves backfigured from the measured data are presented on Figure 9. The load versus depth profiles for Piles 1I and 1V are presented on Figures 7 and 10, respectively. The friction transfer curves were obtained after fitting the load versus depth profiles with a second order polynomial curve. The friction transfer curves are shown for Piles 1I and 1V in Figures 11 and 12, respectively.

PILE DRIVING ANALYZER RESULTS

The pile driving analyzer (PDA) consists of the dynamic monitoring of strain gauges and accelerometers attached to the

TABLE 1 LOAD TEST PROGRAM SUMMARY

Test Piles		
1I	- FHWA Pile (Impact)	30 Day Test
1IR	- FHWA Pile (Impact)	67 Day Test
1V	- FHWA Pile (Vibratory)	33 Day Test
1VR	- FHWA Pile (Vibratory)	63 Day Test
2I	- New Pile (Impact)	65 Day Test
2V	- New Pile (Vibratory)	64 Day Test
3I	- New Pile (Impact)	12 Day Test
3V	- New Pile (Vibratory)	13 Day Test

Notes:

A. 1I, 1IR, 1V, and 1VR - Seven strain gauge levels

B. 2I and 2V - Two strain gauge levels

C. 3I and 3V - No strain gauges

TABLE 2 DRIVING RECORDS

		Pile 1	Pile 2	Pile 3
Impact Driven	- last foot	12 bl/ft	NA	11 bl/ft
	- total	96 blows	NA	131 blows
Vibro-Driven	- last foot	20 ft/min	15 ft/min	12 ft/min
	- total	85 sec.	96 sec.	85 sec.

TABLE 3 SPECIFICATIONS FOR DELMAG D22 IMPACT HAMMER

Rated energy	39,700 ft-lbs
Ram weight	4,850 lbs
Blows/minute	42-60
Maximum explosive pressure on pile	158,700 lbs
Working weight	11,275 lbs
Drive Cap weight	1,500 lbs

TABLE 4 SPECIFICATIONS FOR ICE-216 VIBRATORY HAMMER

Eccentric moment	1000 in-lbs
Frequency	400-1600 vpm
Amplitude	1/4-3/4 inches
Power	115 HP
Pile clamping force	50 tons
Line pull for extraction	30 tons
Suspended weight with clamp	4825 lbs
Length	47 inches
Width	16 inches
Throat width	12 inches
Height with clamp	78 inches
Height without clamp	68 inches

pile close to the top. The strain measurements are used to obtain force measurements as a function of time, and the accelerometer measurements are integrated to obtain velocity versus time. From these two measurements, various parameters may be calculated, including the maximum energy delivered to the pile and the static resistance of the pile by the CASE method. This static resistance represents the PDA capacity prediction.

PDA measurements were made on Pile 1I (driven with the impact hammer) for both the initial driving and the restrike sequence after the load tests were performed, and on Piles 1V and 2V (driven with the vibratory hammer) for restrike after the load tests were performed. The results are presented in Table 5.

DISCUSSION OF RESULTS

Top Load-Movement Curves

The top load-movement curves for the eight load tests are shown together in Figure 8. Two main observations can be made. First, in all cases the vibratory-driven piles have a lower initial stiffness than the impact-driven piles. Second, the impact-

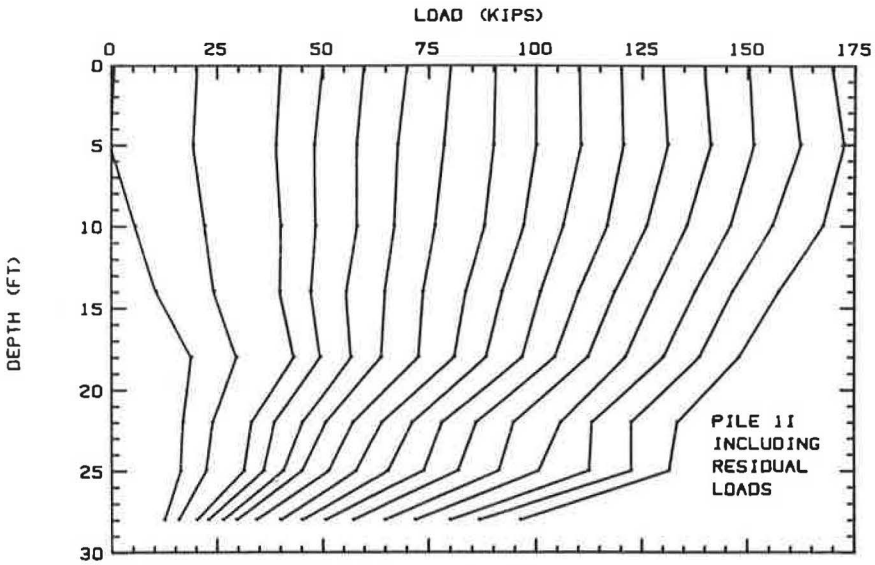

FIGURE 7 Corrected load versus depth profiles for Pile 1I.

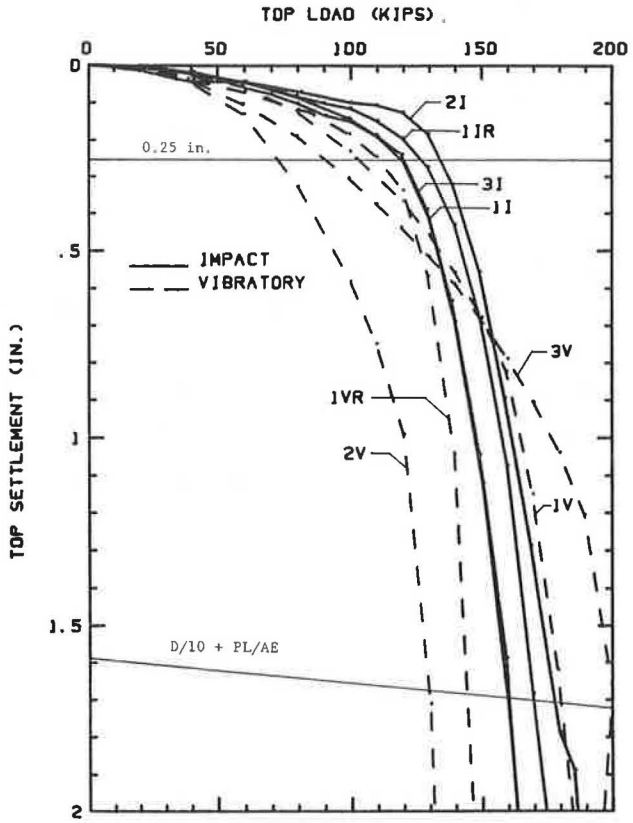

FIGURE 8 Comparison of load-settlement curves.

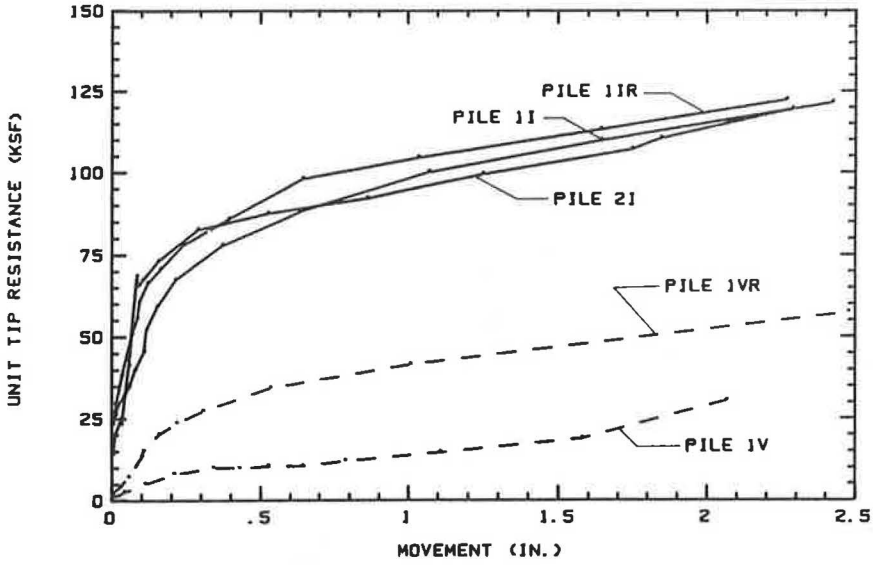

FIGURE 9 Comparison of point load transfer curves.

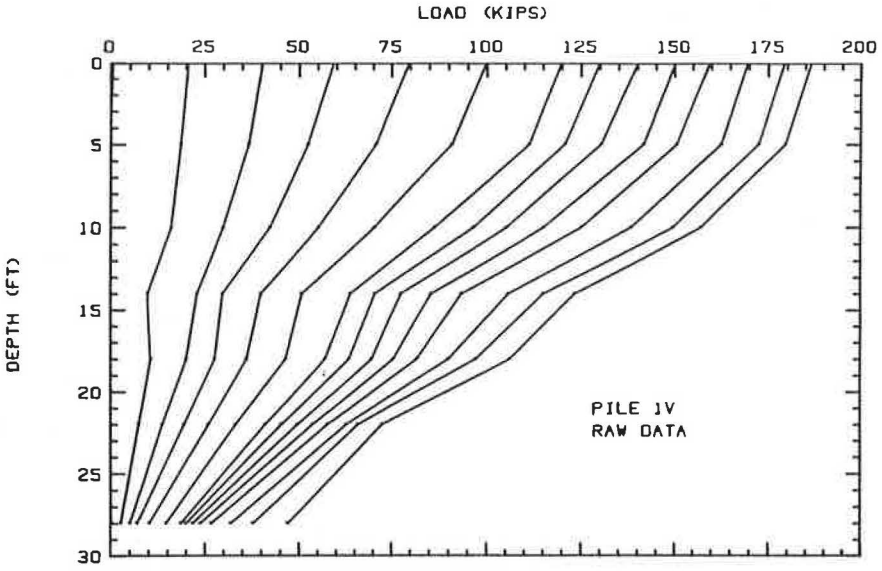

FIGURE 10 Raw load versus depth profiles for Pile 1V.

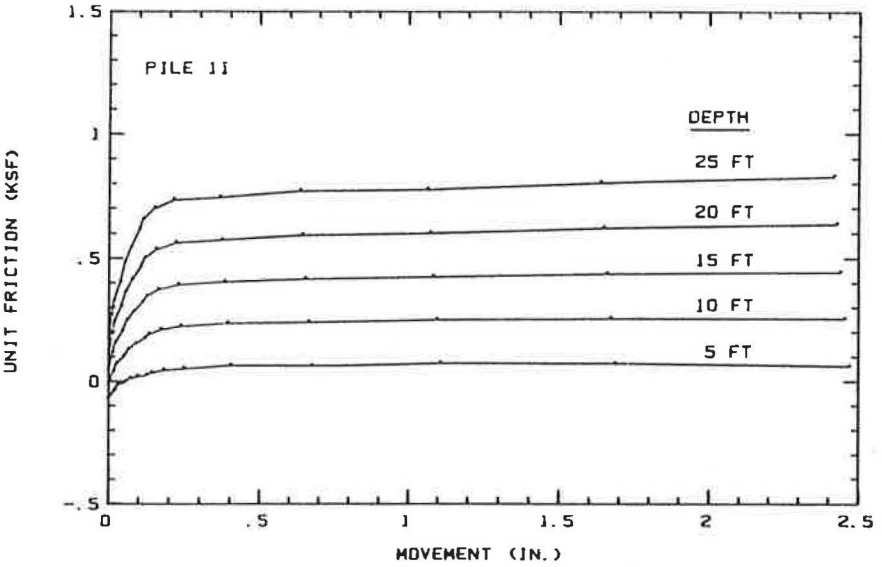

FIGURE 11 Friction versus movement curves for Pile 1I.

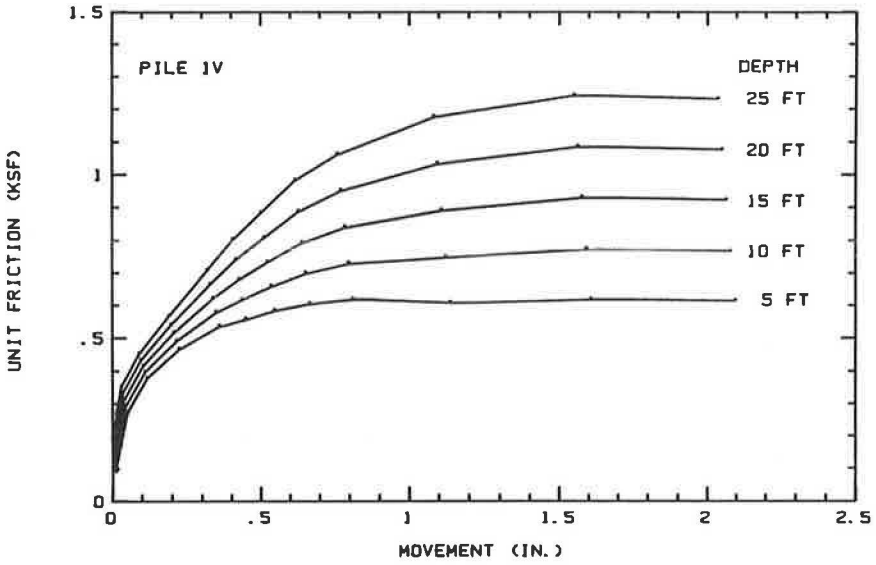

FIGURE 12 Friction versus movement curves for Pile 1V.

TABLE 5 PILE DRIVING ANALYZER RESULTS (7)

Pile	Blowcount	Maximum Force (kips)	Maximum Energy (kip-ft)	Estimated Capacity[a] (kips)
1I[b]	12/12 in.	340-510	5-15	140-165
1I[c]	6/6 in.	350-505	10-17	145-200
1V[c]	7/6 in.	300-415	4-13	120-140
2V[c]	14/12 in.	355-520	5-11	125-150

[a]Case method capacity assumes a damping constant $J = 0.25$.
[b]Initial driving.
[c]Restrike.

driven piles show more consistent response between piles than the vibratory-driven piles. Third, on the average, the ultimate load is the same for the vibro-driven and the impact-driven piles, but the ultimate load is more erratic for the vibro-driven piles.

In an effort to quantify these observations, four measurements have been made from the load-movement curves. First, the ultimate load has been defined as the load corresponding to a movement of one-tenth of the equivalent pile diameter plus the elastic compression of the pile under that load as if it acted as a free-standing column. This line has been drawn on Figure 8. Second, the load at a movement of 0.25 in. has been obtained from the load-movement curves. Third, the movement at one-half the defined ultimate load has been obtained. Fourth, the piles' stiffness response has been calculated as one-half the defined ultimate load divided by the movement occurring at that load. These four items are tabulated in Table 6 for the eight load tests.

Table 6 shows that, on the average, there is only 1 percent difference in the average ultimate load between the impact-driven piles and the vibratory-driven piles. However, the coefficient of variation of the ultimate loads for the vibratory-driven piles is 4.3 times higher than that of the impact-driven piles. The factor of safety would therefore have to be higher for the vibro-driven piles in order to obtain the same risk level as for the hammer-driven piles.

The second column of Table 6 shows that at a movement of 0.25 in. the impact-driven piles carry 33 percent more load than the vibratory-driven piles. The coefficient of variation of this load for the vibratory-driven piles is 4.2 times higher than that of the impact-driven piles.

The movement at one-half the ultimate load for the vibratory-driven piles is over two times larger than that of the impact-driven piles, and the coefficient of variation is 5.5 times larger. The movements, however, are very small even for the vibro-driven piles.

The initial stiffness response of the pile, defined as one-half the ultimate load divided by the movement at that load, is 1.91 times higher for the impact-driven piles than for the vibratory-driven piles. The coefficient of variation of this stiffness for the vibratory-driven piles is 3.6 times that of the impact-driven piles.

Load Distribution

The load distribution of the vibratory-driven piles differs greatly from that of the impact-driven piles. At the maximum load, the impact-driven piles carried approximately 51 percent of the load in point resistance, whereas the vibratory-driven piles carried only 13 percent of the load in point resistance (see for example Figures 9, 11, and 12). In the reload test on the vibratory-driven pile, the point resistance had increased to 29 percent of the total load. This indicates that the difference in the driving process causes a different soil reaction, but the difference becomes less upon repeated loading. Indeed, one compression load test can be considered as a slow blow.

The unit friction profiles at maximum loading are shown in Figure 13 for the five instrumented pile tests. Again it can be seen that there is a definite difference in soil reaction between the impact-driven and vibratory-driven piles, and that the difference becomes less pronounced upon repeated loading.

Load Transfer

The H pile presents a problem when computing unit point resistance and unit friction values. What is the failure surface?

TABLE 6 ANALYSIS OF PILE TEST RESULTS

Pile	Load at D/10 + PL/AE (kips)	Load at 0.25 in. (kips)	Movement at $Q_{ult}/2$ (in.)	Initial Stiffness (kips/in.)
1I	160	120	0.104	769
1IR	170	126	0.094	904
2I	175	131	0.088	994
3I	160	120	0.088	909
Average	166	124	0.094	894
Standard Deviation	7.5	5.3	0.0075	93
Coefficient of Variation	0.045	0.043	0.081	0.104
1V	180	102	0.181	497
1VR	145	110	0.103	704
2V	130	71	0.184	353
3V	200	90	0.313	319
Average	164	93	0.195	468
Standard Deviation	32	17	0.087	175
Coefficient of Variation	0.195	0.182	0.446	0.374
Impact / Vibratory	1.01	1.33	0.48	1.91

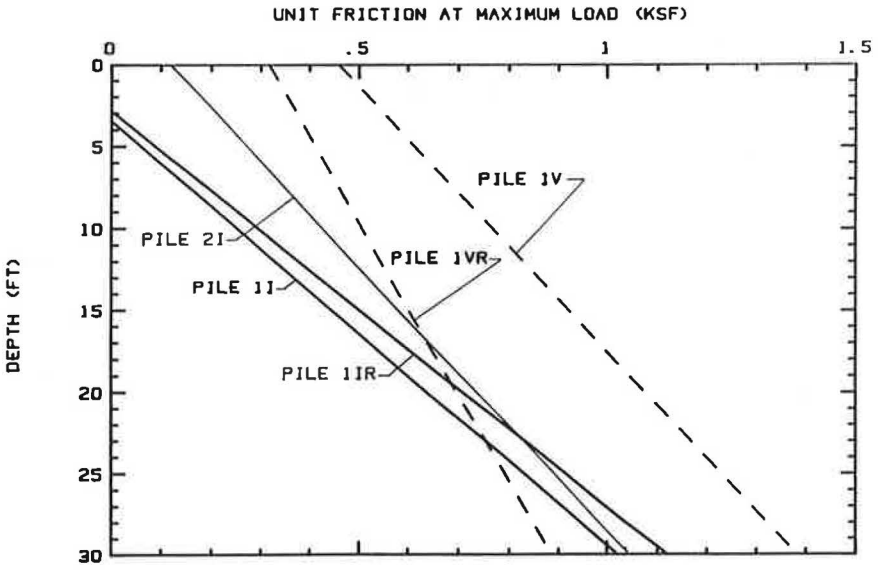

FIGURE 13 Friction versus depth profiles.

One possible assumption is that the pile fails along a rectangle which encloses the H section, with a soil plug forming between the flanges. Another possibility is that the pile fails along the soil-pile interface, with no soil plug forming. Previous research has shown that a better assumption may be that the failure surface is in between the previous two assumptions, with a soil plug filling half the area between the flanges (*1*). For the HP14x73 piles used in this study, this assumption gives the following properties: perimeter, 70.47 in.; tip area, 109.8 in.^{2}. This assumption is used for all further analyses.

Figure 9 shows the unit tip resistance versus tip movement curves for the five instrumented piles. Figure 14 shows the same curves with the tip resistance normalized by dividing by the maximum tip resistance. These two figures show a fundamentally different reaction between the vibratory-driven piles and the impact-driven piles: the tip resistance of the vibratory-driven piles is much lower than that of the impact-driven piles, and the initial slope of the curve is different. However, the difference in shape almost vanishes upon reloading.

The shape of the tip resistance curve of the initial loading of the vibratory-driven pile suggests that the sand immediately under the pile point is initially loose but densifies as the pile is loaded. Indeed, at higher loads the tip resistance begins to increase at a faster rate, rather than reaching a limiting value as the other tests show. By comparing the curves for tests 1I and 1IR, it can be seen that the impact-driven piles do not undergo such a change in behavior between initial loading and reloading.

Figures 15 and 16 show the normalized friction movement curves for the impact-driven piles and vibratory-driven piles, respectively. Figure 15 shows again that the impact-driven

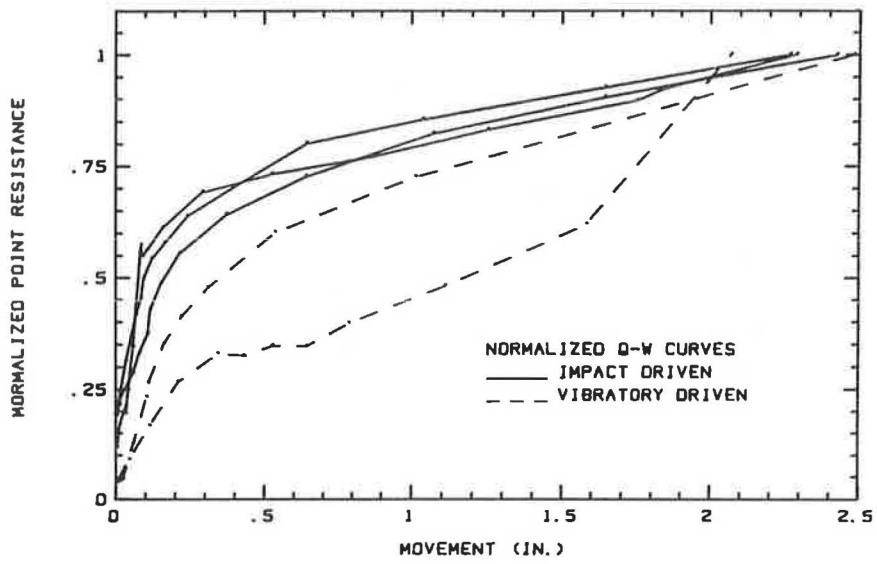

FIGURE 14 Normalized point load transfer curves.

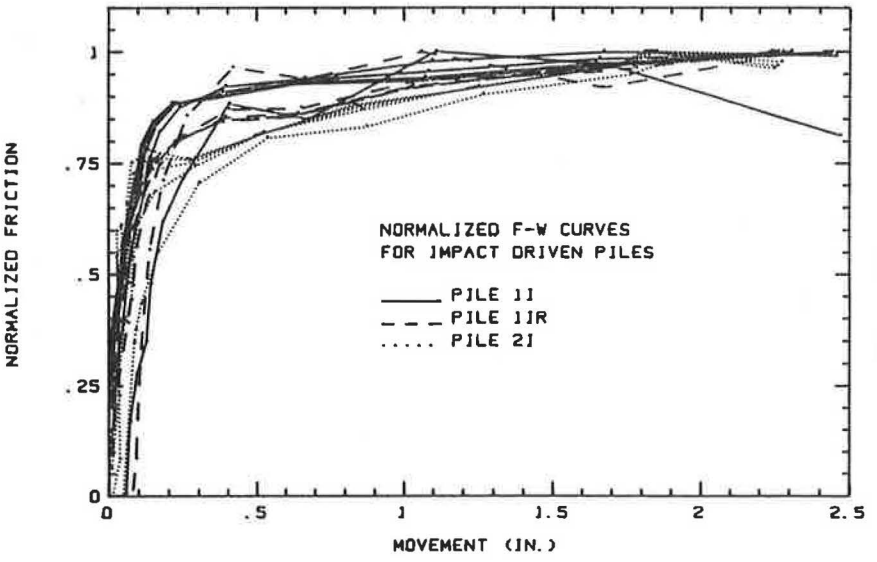

FIGURE 15 Normalized friction transfer curves for impact-driven piles.

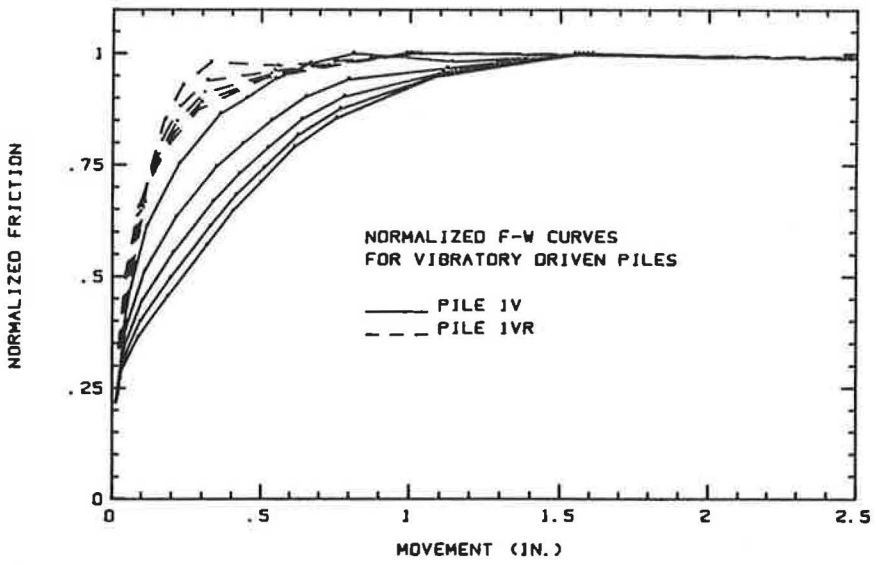

FIGURE 16 Normalized friction transfer curves for vibratory-driven piles.

piles are very consistent in their responses and that no change in behavior occurs between initial loading and reloading. However, Figure 16 shows that the vibratory-driven pile exhibits a great change in behavior between initial loading and reloading. The five curves for the initial loading have a much softer initial response than the reloading curves. The initial loading curves also become softer as the depth increases, whereas the reload curves become stiffer as the depth increases. The reloading curves exhibit a pattern that matches the impact-driven piles very well.

Effect of Time

Piles 1I and 1V were tested about 31 days after driving and then retested about 65 days after driving. The plots of ultimate load versus time for two criteria are shown in Figures 17 and 18. The trend given by those two figures does not allow us to conclude that there is an increase in capacity versus time. Indeed, Figure 17 shows an increase in stiffness, but Figure 18 shows a decrease in capacity for the vibratory-driven piles; for the impact-driven piles, Figure 17 shows an increase while Figure 18 shows a slight increase. At Lock and Dam 26, where impact-driven H piles were also load tested (*6*), the capacity obtained in the load test was 67 percent higher than the capacity predicted by the wave equation method, on average. This could have been due to a 67 percent average gain in capacity of the piles between the time of driving and the time of the load test (1 week). Note that the sand at Lock and Dam 26 had an average of 7.5 percent passing the No. 200 sieve and a blow count averaging 30 bpf, while the sand at Hunter's

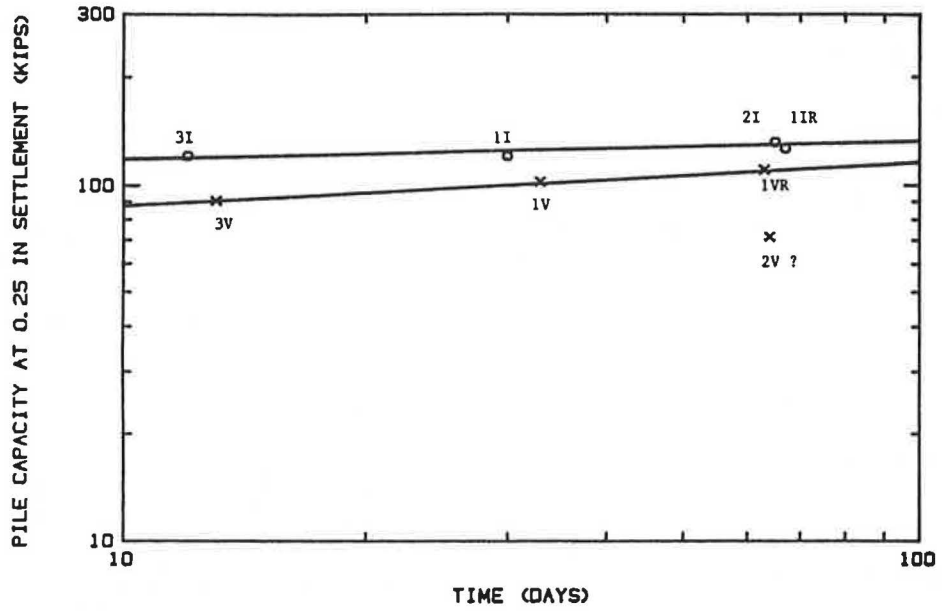

FIGURE 17 Pile capacity at 0.25 in. settlement versus time.

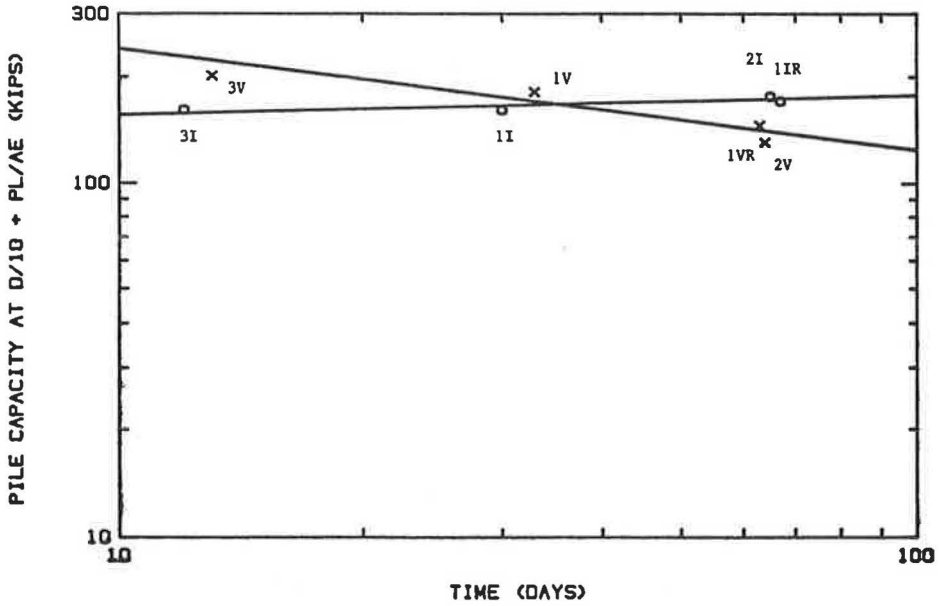

FIGURE 18 Pile ultimate capacity versus time.

Point had 0 percent passing the No. 200 sieve and a blow count averaging 15 bpf.

In the case of Hunter's Point, several factors influence the change of capacity, one of which is the effect of time. The others include the influence of soil heterogeneity and the influence of the first load test on the second load test. In order to isolate the effect of time, one solution would be to use low-strain testing to obtain the variation of stiffness versus time. Another solution would be to use a series of load tests more closely spaced in time, performed on the same pile over a longer period of time (e.g., 1 day, 4 days, 15 days, 40 days, 100 days).

CONCLUSIONS AND RECOMMENDATIONS

The main conclusions to be drawn from this study are the following:

1. Compared to impact driving, vibratory driving of piles leads to approximately the same maximum load at large movements, to a large scatter in this maximum load from one pile to the next, and to a larger movement at working loads. This larger movement was only 0.25 in. and may not require a reduction in allowable load; however, the scatter in the maximum load may require a higher factor of safety for the same risk level and therefore a lower allowable load.
2. The load distribution is influenced greatly by the driving process. For the piles in this study, impact driving led to a point resistance that was 51 percent of the total load at maximum loading, compared to 13 percent for vibratory driving. The load transfer curves are also affected by the driving process. Vibratory driving led to load transfer curves that required much larger movements to reach maximum loading.
3. The effects of vibratory driving listed above are lessened upon reloading of the pile. Upon reloading, a vibratory-driven pile carries a larger percentage of the load in point resistance, and the load transfer curves take on the same shape as the impact-driven piles. It would therefore seem desirable to have a vibratory hammer that can switch to an impact hammer and impart a few seating blows at the end of the vibro-driving sequence.
4. The data show that, in this relatively loose clean uniform sand, there is a trend for impact-driven piles towards a slight increase in capacity versus time. For vibratory-driven piles however, the data does not show any clear trend.
5. The piles encountered very easy driving, and the time required to driven the piles was the same for the impact and vibratory hammer.

ACKNOWLEDGMENTS

This project was sponsored by the U.S. Army Engineer Division, Lower Mississippi Valley, and monitored by the U.S. Army Engineer Waterways Experiment Station. Frank Weaver and Rich Jackson of LMVD and Britt Mitchell of WES are thanked for their valuable comments and support.

REFERENCES

1. E. S. Ng, J.-L. Briaud, and L. M. Tucker. *Pile Foundations: The Behavior of Piles in Cohesionless Soils*, Report FHWA-RD-88-080. FHWA, U.S. Department of Transportation, 1988.
2. E. S. Ng, J.-L.Briaud, and L. M. Tucker. *Field Study of Pile Group Action in Sand*. Report FHWA-RD-88-081. FHWA, U.S. Department of Transportation, 1988.
3. L. M. Tucker and J.-L. Briaud. *Axial Response of Three Vibratory*

and Three Impact Driven H Piles in Sand. Miscellaneous Paper GL-88-28. U.S. Army Engineer Waterways Experiment Station, Vicksburg, Miss., 1988.
4. A. H. Hunter and M. T. Davisson. Measurements of Pile Load Transfer. In *Performance of Deep Foundations*, Report STP 444, American Society for Testing and Materials, New York, 1969, pp. 106–117.
5. F. Rausche, G. G. Goble, and G. E. Likins. Dynamic Determination of Pile Capacity. *Journal of Geotechnical Engineering*, ASCE, Vol. 3, No. 3, 1985, pp. 367–387.
6. L. M. Tucker and J.-L. Briaud. *Analysis of the Pile Load Test Program at the Lock & Dam 26 Replacement Project*. Miscellaneous Paper GL-88-11. U.S. Army Engineer Waterways Experiment Station, Vicksburg, Miss., 1988.
7. D. M. Holloway. *Dynamic Monitoring Program Results, FHWA Vibratory Hammer-Pile Testing, Hunter's Point, California*. Report to Geo/Resource Consultants, 1987.

Publication of this paper sponsored by Committee on Foundations of Bridges and Other Structures.

Construction and Design of Drilled Shafts in Hard Pinnacle Limestones

DAN A. BROWN

Construction and design of drilled shaft foundations in hard pinnacle limestone requires flexibility from all parties involved due to the variability of the subsurface conditions. Strategies that have been found useful in the Birmingham, Ala., area are described. The importance of well-trained and experienced field personnel in these conditions is noted. It is also vital that engineers understand the construction challenges so as to provide both quality assurance and cost-effectiveness in design and in the specifications.

In the southeastern and eastern United States, many areas of the Valley and Ridge as well as the Cumberland Plateau physiographic regions are underlain by hard limestones and dolomites that have highly irregular surfaces due to weathering. These rocks generally weather to form clayey soils that typically fill the "slots," as shown on Figure 1 (*1*). Boulders often exist in the residual soil, and solution cavities can be present in the rock. The rock itself can be quite hard, with compressive strengths often exceeding 10,000 psi.

Foundation construction of heavy structures including highway bridges in pinnacle limestone is often accomplished using drilled shafts. Steel H piles are a common alternative to drilled shafts, but the very large load-carrying capacity of shafts founded on hard rock often serve to make drilled shafts more cost effective. Additionally, it is possible to inspect the shaft-bearing stratum, including probing beneath the bearing surface, so as to provide reasonable assurance that adequate bearing material is reached. The challenges to using drilled shaft foundations in these areas involve the erratic nature of the rock bearing surface, the difficulty in drilling the hard rock materials, and the need to make engineering decisions in the field.

GENERAL CONSTRUCTION CONSIDERATIONS

Overburden Soils

Because the residual soils tend to be cohesive, drilling through soil is typically performed in the dry with a casing set after rock is encountered. Although groundwater may be shallow in some instances, sand and/or gravels that would provide significant flows are not common. Groundwater is normally encountered in significant quantity upon reaching bedrock. Chert nodules and layers are sometimes present, and these cherts are extremely hard. Chert beds and occasional boulders may require rock excavation techniques.

Department of Civil Engineering, Harbert Engineering Center, Auburn University, Auburn, Ala. 36849.

Rock Excavation

The hard limestones are quite difficult to drill with conventional rock augers, and southeastern contractors tend toward downhole drill and shoot methods. Blasting is performed using delayed charges, in which the charges in several center holes are shot first, followed by light charges around the periphery of the hole. Generally only about 2 to 3 ft of hole is advanced at a time. The steel casings are tipped with carbide for use as a core barrel, but coring is slow and expensive. After about 2 ft of rock is drilled and blasted with light charges, the casing is advanced by coring and the rock removed with a rock auger. Air-operated "cluster drills" are effective in dry environments but are not widely used where significant seepage is expected. The large volume of air used to lift cuttings has been known to blow into nearby shaft excavations. At least one southeastern contractor has rigged a bucket catcher above the cluster drill to catch cuttings and minimize the necessary air pressure and volume in deep holes.

In general, seepage of groundwater through slots, fissures, and fractures preclude advancing the hole without advancing the casing. The hardness of the rock material itself generally does not favor slurry drilling techniques, as drilling tools that are used with slurry tend to be less efficient and very costly at drilling hard rock. Slots, seams, and other rock surface irregularities are often filled with soil; excavation of this soil into a slot can often result in sudden large inflows of water, so this type of hand "dental work" is generally avoided.

DESIGN FOR AXIAL COMPRESSION LOAD

Design of drilled shafts for axial compressive loading in hard pinnacle limestones is generally based upon end bearing resistance in the hard rock. Because of the difficulties with forming a clean socket into massive rock, designers tend either to neglect rock socket friction or to use some extremely conservative value. Early attempts to construct and inspect a rock socket into pinnacle limestone in Birmingham, Ala., met with great difficulties due to seepage from the rock below the casing. In addition, Kulhawy and Goodman (*2*) have proposed that rock-socketed drilled shafts should generally be designed on the basis of socket side friction or end bearing, but not both simultaneously.

The relatively high strength of the intact rock would feasibly allow extremely high bearing pressures at the tip, if the presence of an intact massive rock mass could be assured. In fact, designers in the Southeast tend to limit tip resistance in these rocks to the 100 to 200 ksf range; this range is only a fraction

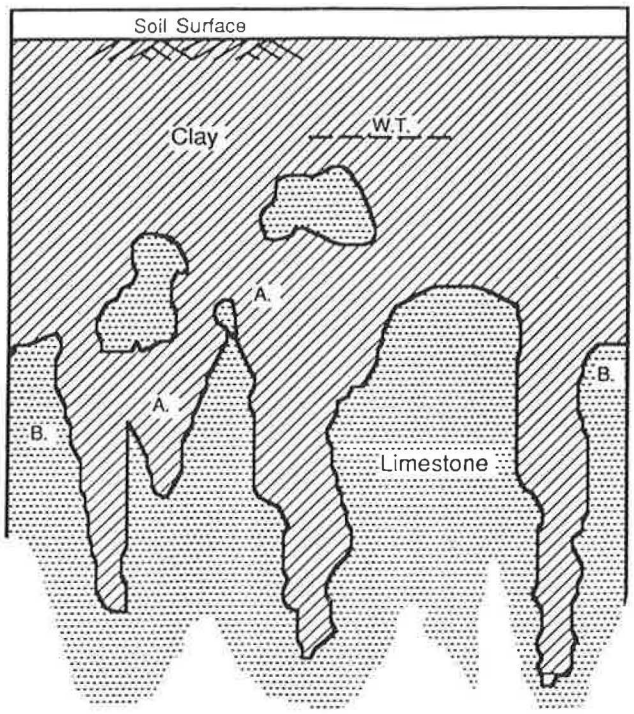

FIGURE 1 Profile of severely weathered rock (*1*).

of the rock's unconfined compressive strength. The reasoning behind these apparently conservative pressures is to allow field acceptance of a shaft on rock that provides less than full coverage of the bearing surface, as illustrated on Figure 2. In some areas of Birmingham, it has proven extremely difficult to place every shaft into intact rock even after excavating many tens of feet of rock.

Load tests of drilled shafts on hard limestone are extremely rare, and none are known to have been conducted to achieve failure. Because the compressive strength of the rock is typically greater than that of the concrete, it seems likely that geologic discontinuities that may be unknown at the time of design govern the ultimate bearing capacity of the foundation. The justification for the design bearing pressures is thus experience (lack of failures), and the emphasis is appropriately on inspection and evaluation of the bearing material at the time of construction.

Shafts in pinnacle limestone are designed for side friction in areas where fault zones or other geologic features have produced deep slots that have virtually no sound rock. The rock in these limited areas tends to be very fractured and prone to solution features, so that conventional rock bearing shafts are not feasible. Friction shafts tend to be used in groups in areas of a site where slots are present, and they are usually reinforced with a structural steel member because of the potential for concrete to flow laterally into cavities and seams. Unit side friction values used tend to be chosen as if the shafts were in soil, due to the erratic and unpredictable rock zones. At least some of the rock penetrated in these slots is likely to consist of isolated boulders.

INSPECTION OF THE BEARING STRATUM

Inspection of the bearing material is performed both by inspecting the bearing surface and by drilling one or more 2

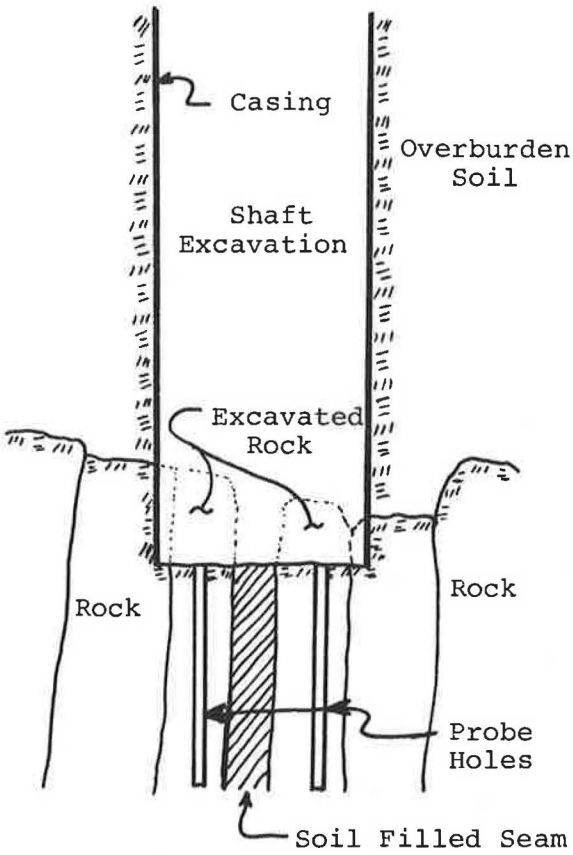

FIGURE 2 Shaft bearing over vertical soil-filled seam.

in. diameter probe holes to a depth of at least 2 shaft diameters below the bearing surface. Probe holes can be drilled expeditiously and economically down the hole using a hand-operated percussion tool. The hole is probed using a hooked rod, as illustrated in Figure 3, with which the inspector scratches the side of the probe hole in an attempt to locate discontinuities. Good communication between the inspector and the contractor's "hole man," who drills the probe hole, is important, because weak seams are easily detected during drilling.

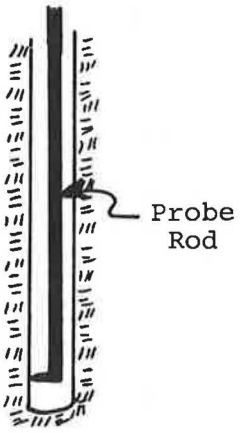

FIGURE 3 Rock probing tool.

More than one probe hole may be performed if a weak seam on the bearing surface is thought to represent a vertical feature, as shown on Figure 2.

Because of the importance of understanding the nature of the geologic discontinuities, as well as the need to make field decisions relating to the load-supporting capability of the foundation, it is vitally important that the inspector be a well-trained and experienced person. Optimum strategies and acceptance criteria may vary depending upon specific project needs, and the inspector should be a person capable of making such judgments.

STRATEGIES FOR CONSTRUCTION IN DISCONTINUOUS ROCK

Early attempts to construct drilled shafts in pinnacle limestones in Alabama involved the search for the elusive "sound rock," in which no discontinuities were present within two shaft diameters below the base. Some formations in Birmingham, such as the Ketona dolomite and areas of the Conasauga formation, are particularly prone to solution cavities and irregularities. The frequent result was removal (at great expense) of many tens of feet of rock, only to encounter limestone that was worse than that which had been drilled through. Additionally, the increasing water pressures with increasing depths make the construction work potentially more hazardous with respect to blowins. Stories abound in which a worker is chased out of a hole by a sudden spout of water or casings are floated out of the ground on the rock plug at the base. In one case a downhole worker who began to scream and shout for help was observed to be hanging onto a safety rope; the rock into which he was drilling a probe hole had dropped away into a cavern the size of a house!

Vertical Discontinuities

Where a vertical discontinuity or seam exists, as shown on Figure 2 or 4, the recommended approach is to probe the rock that is present over the base of the shaft (on both sides of the seam if the seam is within the shaft base). If sound rock exists except for a small area, it may be possible to accept the hole as adequate if the resulting bearing pressures are not excessive. Often, rock coverage over 75 percent or more of the shaft base is considered acceptable, provided that the rock that exists can be demonstrated to be sound. Some overdesign with respect to the allowable tip bearing pressures thus pays dividends during construction, in that less than a full bearing surface can be accepted. A nonvertical seam, as shown on Figure 4, should generally be detected by one of the probe holes and would necessitate additional drilling.

The tendency for shear failure of the rock into the seam can be reduced by excavating the soil into the seam and backfilling with concrete, a technique sometimes used for shallow foundations on rock. This practice is not recommended in deep shafts drilled below the groundwater table because of the possibility of large and uncontrolled seepage into the shaft through such an excavated seam. Note that it is generally necessary to keep the casing seated into the base of the shaft to minimize seepage. If there is concern about the integrity

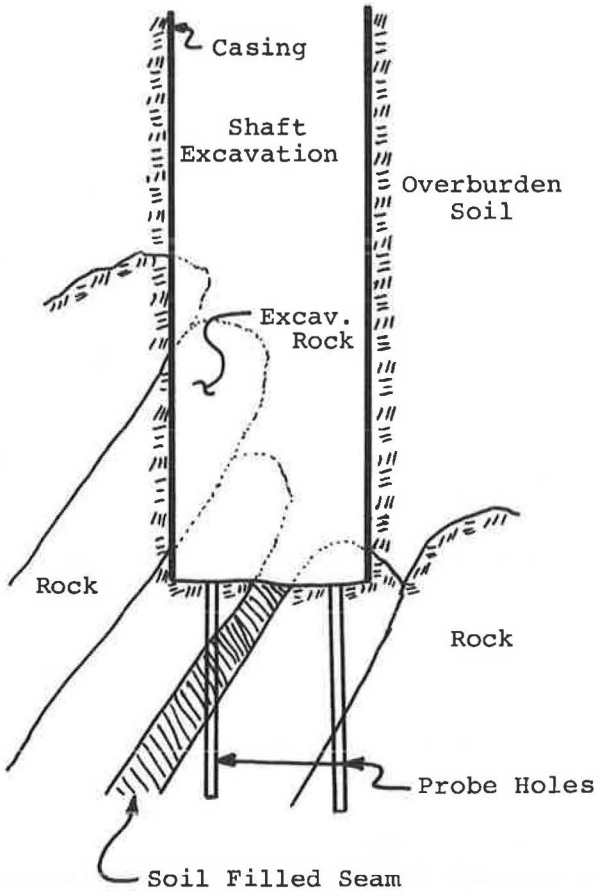

FIGURE 4 Nonvertical soil-filled seam.

of the adjacent rock, the hole should be deepened or other measures taken to provide additional support.

Once the shaft excavations exceed about 70 ft or so below the groundwater level, additional drilling becomes much more difficult due to seepage concerns, and alternative solutions should be considered. Alternatives include the use of driven piling within the shaft excavation and the use of rock anchors installed as described below. In some cases it has even been deemed necessary to place additional shafts and use grade beams to transfer load from the problem shaft to adjacent units.

Composite Piling

Deep slots are often encountered where geologic discontinuities such as fault zones have produced exceptional rock irregularities (often called "ratty rock"). Where deep slots make it impossible to attain adequate bearing material, one solution that has been used is to drive steel H piles into the slot to form a composite pile and provide support for the missing portion of the bearing surface. The difficulty with using this technique is that the piles may not achieve good bearing until a great length of piling is driven, and so this approach is not common.

Another use of composite piling where poor rock is encountered to great depth is to simply drill a shaft designed to

provide capacity by side friction. The composite shaft is formed by placing a structural steel member, such as an H pile or a wide flange section, into the fresh concrete. The structural steel is used because of the tendency for lateral loss of concrete into voids and cavities, which could potentially disrupt a rebar cage during concrete placement. Because these shafts may not have the high capacity of shafts bearing on sound rock, it may be necessary to install several composite shafts to replace one conventional shaft. Composite piling tends to be used only in those areas of a site where a large deep slot is present, with conventional shafts on rock used where possible.

On sites where the need for composite piling is anticipated, it is generally advisable to drill a pilot hole at each and every foundation location to determine in advance which type of foundation is most appropriate. The pilot hole could be a conventional soil boring, but for reasons of economy is more often a small-diameter percussion-drilled hole. If the pilot hole does not encounter sound rock at a particular location, that foundation is planned as a group of composite piles designed to carry load in side friction. Small-diameter shafts on the order of 18 in. in diameter are most common, with reinforcement provided by a single H pile placed after the concrete. These shaft groups are more expensive than conventional shafts and thus are used only where necessary.

Rock Anchors for Nonvertical Discontinuities

Where concern exists that there may be fractures or sloping bedding planes within the rock, rock anchors may be used to provide continuity and load transfer across nonvertical discontinuities, as shown on Figure 5. Rock anchors generally consist of No. 10 or 11 high-strength steel bars such as Dywidag, grouted into a hole 2 to 2¼ in. in diameter and 10 to 12 ft in length. Larger diameter holes have been used but require the use of surface drilling equipment; the 2 to 2¼ in. size holes can be more economically installed downhole using handheld air impact equipment. A specific rock anchor plan must be developed in the field after investigation of the existing geologic conditions, and thus the need for field personnel capable of designing such a plan.

Rock anchors may also be used across thin-seam horizontal discontinuities, as shown in Figure 6. However, simple horizontal fractures in flat-bedded limestone generally would not require any additional treatment and may not even be detected by simple probing operations. In general, probing is intended to detect significant soft seams or the presence of cavities within a reasonable distance of the bearing surface.

CLASSIFICATION FOR PAY PURPOSES

One of the key elements to successful use of drilled shafts in pinnacle limestone is the structure of the bid document related to drilled shaft pay items. Because of the considerable uncertainty involved in this geology, there will undoubtedly be uncertainties in the quantities of cost items. The most cost-effective approach to foundation construction is to identify these cost items and to price the job on a unit cost basis for each item. This is the approach that has evolved in the Birmingham market, and it is a key element in the acceptance

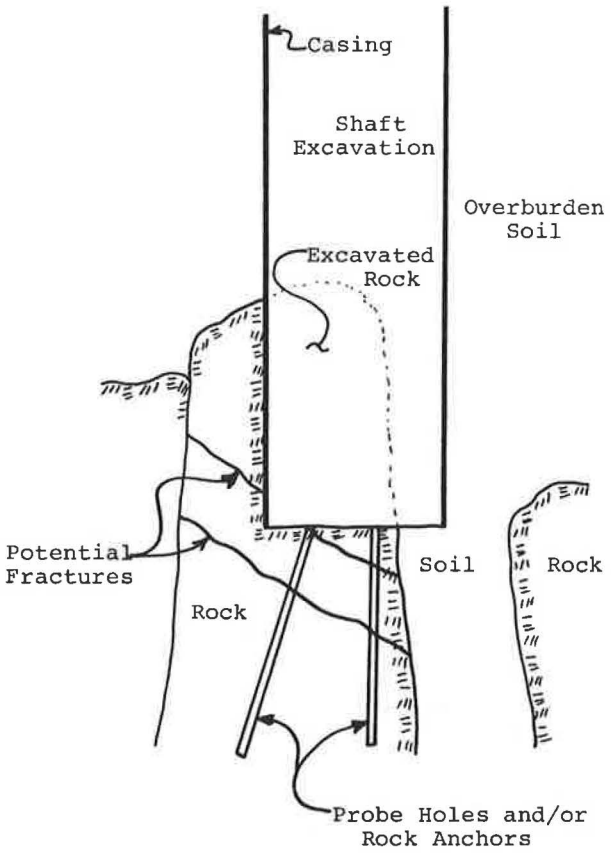

FIGURE 5 Rock anchors on fractured rock.

and use of drilled shafts on a widespread basis. The general items identified for unit costs are the following:

- Earth augering, with unit costs for each diameter anticipated.
- Rock augering, with unit costs for each diameter anticipated. Augerable rock includes shales and sandstones that can be excavated with a rock auger but not an earth auger. Sometimes this item is even listed as shale excavation.
- Hard rock drilling, with unit costs for each diameter anticipated. This rock includes most of the hard pinnacle limestones and is defined as that rock that cannot be excavated with a rock auger but requires blasting or other special drilling tools.
- Concrete, per cubic yard and based on dray tickets.
- Steel reinforcement, per pound.
- Test holes, per linear foot.
- Mobilization.
- Any other special items, such as rock anchors, composite piles, etc.

Note that the excavation items almost always include casing, shoring, and pumping, rather than listing these as a separate item.

The engineer provides an estimate of these quantities, but actual payment is based upon unit costs for the quantities used on the job. Rock excavation typically runs 4 to 5 hole diameters on average, but can vary significantly from job to

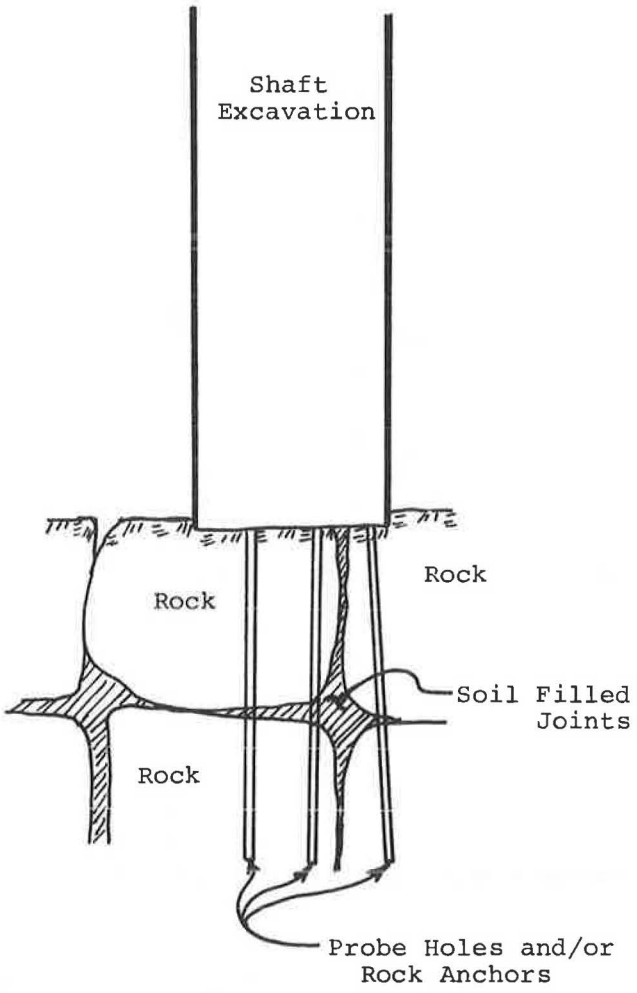

FIGURE 6 Rock anchors on flat-bedded rock with discontinuities.

job. It is particularly important to separate items such as concrete placed in the hole from the cost of excavating the hole; because of cavities and irregularities in the rock, the amount of concrete needed often ranges from 150 to 300 percent or more of the theoretical volume of the hole. In some parts of the United States, concrete is lumped into the linear foot rate for excavation; in these formations such a practice would put all of the risk of concrete overruns onto the contractor and thus necessitate a conservative estimate of concrete quantities on his part at bidding time. Some state highway departments provide for no cost differential between earth and hard rock drilling, but in pinnacle limestones it is extremely difficult to estimate how much rock excavation will be needed. With the unit cost approach, the contractor is neither penalized nor unfairly rewarded when directed to carry the hole deeper. In general, contractors, engineers, and owners have found this system to be fair and cost effective for all concerned.

SUMMARY

Drilled shaft foundations can provide a very cost-effective and high-quality foundation alternative in areas of hard pinnacle limestone. However, the uncertainties associated with this type of geology necessitate some special considerations with respect to construction and design. Particularly important is the requirement for flexibility in the specifications and bid documents. It is also essential to have well-trained and experienced personnel on site who are capable of making decisions relating to foundation capacity and construction. Attempts to construct rock sockets into sound hard limestone has not been a successful strategy; however, other strategies have evolved and are identified in the paper. The evolution of the local bidding structure into unit cost pricing is seen as a key element in the widespread acceptance and use of drilled shafts in these formations.

ACKNOWLEDGMENTS

The experiences reported in this paper have been shared with the author by a number of contractors and geotechnical engineers representing many years of construction work in the difficult geology of northern Alabama. The author expresses his gratitude to Paul Wilson, Hal Mckewen, and Danny Jennings of Russo Corp.; Bruce Long of Long Foundation Drilling Co.; Ed Munn of McKinney Drilling Co.; Luther Boudra and Bruce Bodner of Law Engineering, Inc.; Uday Bhate of Bhate Engineering Corp.; and Rick Bourquard and James Pegues of Ground Engineering and Testing Service, Inc. Financial support of the Alabama Highway Research Center is also gratefully acknowledged.

REFERENCES

1. L. C. Reese and M. W. O'Neill. *Drilled Shafts: Construction Procedures and Design Methods*. Report FHWA-HI-88-042. FHWA, U.S. Department of Transportation, Washington, D.C., 1988.
2. F. H. Kulhawy and R. E. Goodman. Design of Foundations on Discontinuous Rock. *Proc., International Conference on Structural Foundations on Rock*, Sydney, Australia, 1980, pp. 209–220.

Publication of this paper sponsored by Committee on Foundations of Bridges and Other Structures.

Development of an Expert System for Preliminary Selection of Pile Foundation

C. H. JUANG AND M. L. ULSHAFER

The development of an expert system for selection of pile type for design of a pile foundation is documented. The expert system, Pile Selection version 1.0 (PS1), incorporates many unique features. Among them are approximate reasoning with fuzzy logic, the blackboard architecture, and the emulated parallel processing of fuzzy production rules. An example using PS1 for pile selection is presented, and possible enhancement of the system is discussed.

Preliminary selection of pile type is an important step in the design and construction of pile foundation. Proper initial selection can shorten the design process and reduce the project cost. For experienced engineers, this initial task of choosing one or more piles for further design consideration may not be a problem. However, it may be quite challenging for persons with less experience because there are numerous uncertainties involved in several areas, including loading requirement, subsurface soil conditions, pile material properties, methods of construction, nuisance driving effects, and space and time constraints. An expert system that can provide a consistent and reliable selection of pile foundation, taking into account these factors, would certainly be very useful. This is the motivation for developing the system Pile Selection version 1 (PS1).

The PS1 system was written in FLOPS, a Fuzzy LOgic Production System created by Siler and Tucker (*1*). This paper will briefly describe FLOPS, followed by detailed discussion of the development of PS1.

FLOPS FEATURES

FLOPS is an expert system shell written in C language for use in the Microsoft Disk Operating System (MS-DOS) or compatible DOS environment on microcomputers. FLOPS has several unique features that provide a great deal of power and flexibility. A brief summary of the FLOPS features follows.

Approximate Reasoning with Fuzzy Logic

FLOPS uses fuzzy logic invented by Zadeh (*2,3*). Fuzzy sets and logic allow for a better model of an expert's reasoning process. The subject of civil engineering applications of fuzzy sets is beyond the scope of this paper and has been documented elsewhere (*4–9*).

Civil Engineering Department, Clemson University, Clemson, S.C. 29634.

Deductive and Inductive Reasoning

FLOPS is a production system and as such its basic element is a "rule." The deductive logic implemented in FLOPS is no different than most expert systems. It fires the production rules sequentially. If the data permits more than one rule to be "fireable," deductive systems select one rule for firing; other fireable rules are stacked for backtracking later. FLOPS, however, also implements inductive reasoning that considers many possible outcomes at once. FLOPS' parallel rule firing scheme for implementing the inductive reasoning is rather unique. All fireable rules are fired concurrently, and thus no rule remains to be stacked for backtracking. FLOPS adopts a weakly monotonic fuzzy logic for its truth maintenance to resolve the memory conflict problem. When applicable, the inductive mode of FLOPS is much faster than the deductive mode to reach a conclusion.

Blackboard Architecture

FLOPS employs a relational structure for data stored on a blackboard, a disk on microcomputers in the context of this paper. The ability of one FLOPS program to call another and to exchange data through the blackboard could overcome the memory limitations of small microcomputers.

Expert knowledge is divided into two classes in FLOPS. One is factual knowledge, which belongs in a data base. The other is expert skills, which belong in rules. One of these expert skills knows how to use the expert factual knowledge. The programmer-written rules can generate the production rules based on the factual knowledge during the program execution.

Two methods of communicating with external programs are available in FLOPS using a *call* command. One type of call transmits a command string to the called program in the DOS environment. The other is a call by reference to a C program and thus must follow calling convention used in the C language. Details of the above features as well as others can be found in FLOPS manual (*1*).

FACTORS AFFECTING SELECTION OF PILE TYPE

To arrive at the optimum pile foundation solution, the engineer must have thorough information and understanding of (1) foundation loads, (2) subsurface soil and rock conditions and properties, and (3) current practices in pile design and construction. Based on site conditions and design requirements, the designer may select two or more alternatives for further consideration. Analysis will be made to check out bearing capacity and settlement requirements. Comparison of the costs of acceptable alternatives then follows. This process might repeat one or more times to reach the optimum design.

Undoubtedly, the initial pile selection is an important step in the process. However, it is often not given proper coverage in the formal college engineering education. Years of apprenticeship seem to be the only way to acquire the needed experience for mastering this task. To bridge this gap, PS1 was created to assist the designers with various backgrounds on this very task of preliminary pile selection.

The selection of appropriate pile type for any given set of circumstances depends upon many variables. In particular, the type of subsoil, the groundwater condition, the topography of the site, the design loads, the construction concerns, and the location of the site in relation to nuisance effects, availability of pile material, and transportation costs are all of importance.

There are basically two routes to acquire expert knowledge. One is to work directly with an expert or a group of experts by conducting interviews necessary to extract expert knowledge. The other is to conduct an extensive literature review to extract rules of thumb and knowledge. The latter route was taken in this study. Extensive review of the literature on pile foundation was made during the course of this study. Major references on which PS1 was based are listed below (*10–28*). It is expected that the strength of the knowledge base will continue to grow as PS1 continues to evolve. Thus, the structure of PS1 was arranged in such a way that new or better expert opinions can be easily incorporated without any significant change in PS1.

DEVELOPMENT OF PS1

General Program Structure of PS1

The expert system PS1 was written in FLOPS, and as such it is often referred to as a FLOPS program in this paper. A FLOPS program may be grouped into three sections:

1. the declaration section, similar to that of C or PASCAL language;
2. the rules section, where the actual rules appear; and
3. the input section, in which actual values are assigned to the attributes described in the declaration section.

The basic structure of PS1 closely follows that of RMC, an expert system developed for rock mass classifications by Juang and Lee (*29*). Figure 1 shows its general architecture. PS1 first reads external "factual knowledge" files, which are referred

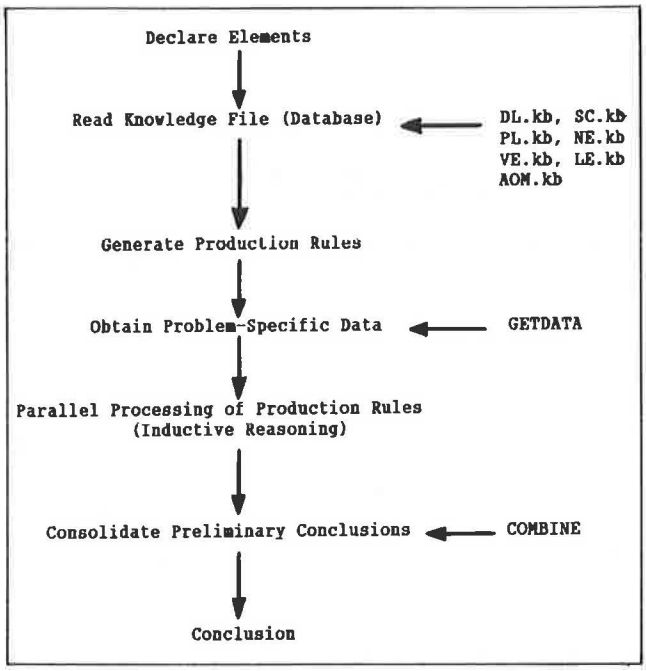

FIGURE 1 Overall structure of PS1.

to herein as knowledge data bases or simply data bases. The knowledge data bases required by PS1 include DL.kb (design load knowledge base), PL.kb (pile length knowledge base), SC.kb (soil condition knowledge base), NE.kb (noise effect knowledge base), VE.kb (vibration effects knowledge base), AOM.kb (availability of material knowledge base), and LE.kb (local experience knowledge base). Using this knowledge and some "meta-rules," PS1 can generate all needed production rules. Depending upon the sizes of these knowledge data bases, a total of several hundred rules may be generated with a few user-written rules.

After the rules are generated, the program will begin to ask for user input data by calling an external program GETDATA. The program GETDATA was written in C language and compiled with Microsoft C 5.1 compiler (*30*). It serves as a user interface that allows for the problem-specific data to enter PS1. Execution of GETDATA will create a data file called user.dat to store these user inputs. The user.dat file is then transferred to PS1 and matched with generated rules for determining rule fireability. (When input matches the premise of a generated rule, it makes that rule fireable.) Execution of the production rules then begins, which produces several preliminary conclusions. These conclusions are stored in a file named pile_type.dat. This new file serves as an input to COMBINE, another external program called by PS1. COMBINE, also written in the C language, consolidates the preliminary conclusions reached earlier. Result of the final conclusion reached is then reported to PS1.

It is noted that the expert system PS1 was written in parallel FLOPS. Thus, it does not involve backtracking of the rules. Instead, at any stage of rule firing, all fireable rules are fired at the same time. The problem of possible memory conflicts was resolved using weakly monotonic logic, a type of fuzzy logic in which the value of a datum may be replaced by a new

value, if the confidence in the new value is greater than or equal to the old confidence (*1*). However, the preliminary conclusions reached at different stages were treated as evidences, each based on a particular knowledge source. They were not combined with the weakly monotonic logic. Instead, an external program COMBINE was used to consolidate these evidences.

To use PS1, the user needs to have an idea of the design loads to be supported, subsurface soil condition, pile length requirement, availability of material, local contractor experience, and noise or vibration constraints. The interactive, menu-driven program GETDATA will direct the user through the creation of a user-supplied file, user.dat, which is required by PS1. On-line explanation features are provided in GETDATA to assure its user-friendly style. Also, the program GETDATA can be run as part of PS1, or it can be run separately before execution of PS1. This feature allows for maximum flexibility on the part of the user when consulting PS1.

Detailed Comments on PS1

As mentioned earlier, there are three major sections in a FLOPS program. Detailed comments on each section of PS1 follow.

Declaration Section

Elements declaration is the only task in the declaration section. Figure 2 shows an example of element declaration. The command *literalize* declares a memory element, xdata, with 28 attributes of the types *atm* and *flt*. In FLOPS, the data type *atm* is for character string, and the data types *flt* and *int* are for floating point and integer, respectively. The syntax for declaration is very similar to that of a structure in C or PASCAL language. An attribute is analogous to a variable in C or PASCAL. Notice that a semicolon is only needed at the end of the entire *literalize* command, and that separation of the *literalize* command into several lines is a programming style for ease of reading and maintaining of the code.

Element xdata is needed to store the user-supplied data. Other elements are declared to store factual knowledge data. Figure 3 shows another example of the element declaration. Element pile_type has seven attributes, criterion1 through criterion7, that are declared to be of data type *fzset*, which stands for fuzzy set. The fuzzy set data type in FLOPS is

```
:comment - user supplied (problem-specific) data

literalize xdata
  design_load        flt    avail_PC     atm   exp_PC     atm
  soil_type          atm    avail_PSC    atm   exp_PSC    atm
  strength           atm    avail_CIPM   atm   exp_CIPM   atm
  negative_friction  atm    avail_CIP    atm   exp_CIP    atm
  boulder            atm    avail_STL    atm   exp_STL    atm
  pile_length        flt    avail_TM     atm   exp_TM     atm
  noise              atm    avail_CPW    atm   exp_CPW    atm
  vibration          atm    avail_CPS    atm   exp_CPS    atm
                            avail_PIC    atm   exp_PIC    atm
                            avail_BP     atm   exp_BP     atm
```

FIGURE 2 Declaration of element xdata for PS1.

```
:comment - pile type selection according to each criterion

literalize pile_type
    criterion1   fzset (PC PSC CIPM CIP STL TM CPW CPS PIC BP)
    criterion2   fzset (PC PSC CIPM CIP STL TM CPW CPS PIC BP)
    criterion3   fzset (PC PSC CIPM CIP STL TM CPW CPS PIC BP)
    criterion4   fzset (PC PSC CIPM CIP STL TM CPW CPS PIC BP)
    criterion5   fzset (PC PSC CIPM CIP STL TM CPW CPS PIC BP)
    criterion6   fzset (PC PSC CIPM CIP STL TM CPW CPS PIC BP)
    criterion7   fzset (PC PSC CIPM CIP STL TM CPW CPS PIC BP)
```

FIGURE 3 Declaration of element pile_type for PS1.

unique. In common fuzzy set notation, using criterion1 as an example, it may be expressed as

criterion1 = {m1/PC, m2/PSC, m3/CIPM,
m4/CIP, m5/STL, m6/TM,
m7/CPW, m8/CPS, m9/PIC, m10/BP}

where m1 through m10 are the membership grades for the corresponding members PC through BP, respectively, which in turn are abbreviations for the following:

PC = precast concrete;
PSC = prestressed concrete;
CIPM = cast-in-place concrete with mandrel;
CIP = cast-in-place concrete without mandrel;
STL = steel pile (H, I section);
TM = timber;
CPW = composite wood-concrete;
CPS = composite steel-concrete;
PIC = pressure-injected concrete; and
BP = bored.

In FLOPS, these membership grades appear in the form of a confidence level. The confidence level is a unique data type, which is used to store the confidence toward a member of a fuzzy set. The attribute criterion1 is created to store the preliminary conclusion of pile selection based on design loads. The attributes criterion2 through criterion7 are declared in the same way, each based on a different pile selection factor incorporated in PS1. Although these seven attributes look alike, use of different attributes is necessary to preserve multiple preliminary conclusions reached at different stages in the inductive reasoning process in PS1. Otherwise, FLOPS' weakly monotonic logic could eliminate the desired membership values of these fuzzy set members before they can be combined.

Rule Section

For the PS1 system it was determined that a parallel (inductive) FLOPS program is more effective than a sequential (deductive) one. It was also decided to set up a block firing control, starting from block 0, to ensure the sequential firing of each block of rules. Within each block, however, the parallel processing ensures all rules that are fireable are fired at once.

The PS1 system starts with reading of expert knowledge files in block 0. With this knowledge, part or all of the block

0 rules become fireable and are fired at once. The actions of firing these rules generate the rules of blocks 2 through 8. It is noted that, without proper initiation of data, no rules can actually be fired.

As an example to explain how rules are generated, focus on rule r0, shown in Figure 4. The expert factual knowledge was stored in a file named DL.kb. As soon as it is transferred to the system (using the command *open*, explained below), the left hand side (LHS) of rule r0 will be satisfied. In other words, rule r0 becomes fireable; and when it is fired, the right hand side (RHS) of rule r0 will be executed. It is noted that LHS is generally referred to as premise part of a rule, while RHS is the action part of the rule.

For convenience of the further discussion, an example of the content of knowledge file DL.kb is shown in Figure 5. It basically consists of a set of *make* commands. The *make* command initiates a memory element and assigns values to its attributes. For example, when the file DL.kb is open, the first *make* command assigns the following data:

^lower1 = 0;
^upper1 = 20;
^fsmember = CIPM;
^confidence = 600.

Notice the ^ is the symbol used in FLOPS for the value of the attribute. Once these values are transferred to the system, the variables in the LHS of the rule r0 take on the following values:

⟨LB⟩ = 0;
⟨UB⟩ = 20;
⟨FSM⟩ = CIPM; and
⟨CONF⟩ = 600.

```
:comment - rule r0 to generate block 2 rules
rule 1000 ( DL  ^lower1 = <LB>  ^upper1 = <UB>  ^fsmember = <FSM>
                ^confidence = <CONF> )
    -->
    rule <CONF> 2 (xdata  ^design_load >= <LB>  ^design_load <= <UB>)
                  (pile_type  ^criterion.<FSM> = 0)
          -->
            modify 2  ^criterion1.<FSM> ;
```

FIGURE 4 The content of rule r0 of PS1.

```
:comment -- DL = design load (tons)
make DL    ^lower1  0.       ^upper1  20.  ^fsmember "CIPM"
           ^confidence  600;
make DL    ^lower1  0.       ^upper1   20.  ^fsmember "TM"
           ^confidence  1000;
  .
  .
  .
```

FIGURE 5 Partial list of contents of file DL.kb of PS1.

When rule r0 is fired, the action part (i.e., the RHS) of the rule yields a new rule, as shown in Figure 6. Whether the new rule is fireable depends on the actual attribute values in the elements xdata and pile_type. Notice how a membership grade of a member in a fuzzy set is represented. The term, ^criterion.CIPM, represents the confidence level (membership grade) toward the member CIPM of the fuzzy-set attribute criterion1.

Separation of factual knowledge data from the main part of PS1 is convenient for maintaining the system. When expert opinions change, we need only to change the content of the knowledge data file. We may even create a user interface to facilitate the editing of the knowledge data base. Figure 7 gives another example of knowledge data base that concerns soil conditions. Further discussion on the knowledge data bases will be presented later.

As a final note on rules in FLOPS, observe the first *rule* command of rule r0 (shown in Figure 4). A number, 1,000, appears immediately after the key word *rule*. This number is referred to as the priority of the rule or the prior confidence level of the rule. In FLOPS, the confidence level is encoded as an integer with a maximum value of 1,000, which actually means a confidence of 100 percent. When the LHS is evaluated, it also returns a confidence value. The smaller of the two confidence values is taken as the posterior confidence level. All actions involving memory updating in the RHS of that rule are assigned this posterior confidence value.

The PS1 system utilizes this feature to assign the membership grade of a member of a fuzzy set. The *modify* command in Figure 6 is an example. The generated rule shown in Figure 6 has a prior confidence level of 600. If the evaluation of LHS based on actual user input data returns a confidence of, say, 1,000, then the smaller of the two values would be 600, and this value is assigned to the fuzzy set member ^criterion.CIPM as its membership grade. The prior confidence level of the

```
rule 600 2 (xdata  ^design_load -)=  (0, 0, 0)
                   ^design_load -(=  (20, 2, 0.1))
           (pile_type  ^criterion1.CIPM = 0)
      -->
      modify 2  ^criterion1.CIPM;
```

FIGURE 6 An example of a rule generated by rule r0.

```
:comments
:factor1 = soil type (cohesive, cohesionless)
:factor2 = strength of bearing soil (low, medium, high)
:factor3 = negative skin friction (likely, unlikely)
:factor4 = presence of boulders (yes, no)
make SOIL   ^factor1 "cohesive"  ^factor2 "low"  ^factor3 "unlikely"
            ^factor4 "no"  ^fsmember "PC"  ^confidence 900;
make SOIL   ^factor1 "cohesive"  ^factor2 "low"  ^factor3 "unlikely"
            ^factor4  "no"    ^fsmember  "STL"    ^confidence  500;
  .
  .
  .
```

FIGURE 7 Partial list of contents of file SC.kb of PS1.

generated rule does not have to be 1,000. In the real world there often exists some essential knowledge that is less certain than other knowledge. It may be desirable to include this less-certain knowledge in the reasoning process. PS1 incorporates this desired feature by embedding the uncertainty (confidence value) in the knowledge data base.

The confidence (or uncertainty) of a piece of knowledge reflects an expert's opinion on that piece of knowledge. For a system to be efficient, it is necessary to set up a cutoff confidence value that determines whether a particular piece of uncertain knowledge should be incorporated into the system. If no prior experience exists, a sensitivity study should be conducted. This approach was taken in the development of PS1.

It is noted that the second *rule* command in Figure 4 has a number 2 beside 1,000. This is referred to as a block number. When that number does not appear, as in the case of the first *rule* command, the system assigns a number of 0. The block numbers are generally used to group rules for some rule firing control. It is a useful feature, especially for inductive reasoning in the FLOPS environment.

Input Section

The input section basically consists of at least a *make* command. The *make* command is used for noninteractive input or initiation of the elements and their attributes. The *run* command, although it can be issued from anywhere in FLOPS environment, is usually placed in the input section. This command causes execution of the rule section. The input section may include other FLOPS commands for specific purposes. All commands are executed sequentially in the input section.

As mentioned earlier, all production rules are grouped into blocks. By controlling the block firing sequence, the rules may be fired in some planned order. However, no particular order is set for the rules within a block. In fact, with parallel processing, all fireable rules will be fired at once, regardless their order of appearance.

The program structure shown in Figure 2 was implemented in this input section. First, the system reads in the knowledge data files with *open* command. It then sets up a control mechanism to execute each block of rules sequentially. The system begins with execution of block 0 under the command *run* The rules in block 0 generate all possible production rules. The system then executes block 1, which gathers problem-specific data by calling the external program GETDATA. Actions taken in block 1 also make blocks 2 through 8 fireable. These blocks are then fired sequentially under the next *run* command. An external data file, which contains the preliminary conclusions reached by PS1, is created after firing of these blocks. The last *run* command in the input section causes execution of block 9. This block calls an external program COMBINE to consolidate the preliminary conclusions. The final conclusion is then reported and the program stops.

Binary Logic vs. Fuzzy Logic

Notice that with the implemented structure described above, a rule will be actually fired if and only if all of the following conditions are met:

1. the block in which the rule resides is switched on;
2. the elements used in the LHS of the rule have been initiated with proper *make* commands; and
3. the LHS of the rule is evaluated to be "true."

The evaluation of the LHS of the rule begins with each individual comparison implemented in the LHS. Each comparison returns a truth value, which in binary logic takes the value of 0 (for false) or 1 (for true). The smallest of all values returned by the comparisons is taken as the confidence level of the LHS. In traditional comparison based on binary logic, this value will be either 0 or 1. In other words, the term "true" in the third condition stated above requires a confidence value of 1 (or in PS1 notion, 1,000/1,000 or simply 1,000).

The necessity of including uncertain but essential knowledge into the data base was discussed above. In a similar manner, PS1 adopts the fuzzy comparison feature whenever appropriate. The rule shown in Figure 6 provides an example of its potential advantage. The LHS consists of comparisons in two objects (elements), design_load and pile_type. The comparison in this rule is binary; it will return either 0 (false) or 1,000 (true). If a given datum of design_load is, say, 21, the comparison would return a value of 0 and the rule won't be fireable. On the other hand, a given datum of design_load of 19, although not much different from the value of 21, will return a value of 1,000 from the comparison. Such drastic change is a drawback of the binary logic, in which a proposition must be either true or false.

When fuzzy comparison is desired, the rule shown in Figure 6 may be revised into the one shown in Figure 8. A fuzzy comparison will return a value of between 1,000 (true) and 0 (false). In other words, a proposition can be partially true. Note that a fuzzy operation indicator, ~, preceding the comparison operators, such as $<$ and $\leq$, was used in the new rule. This indicator tells the program to make a fuzzy comparison. Also notice that for fuzzy comparison on two scalar numbers, FLOPS requires two additional data: an absolute uncertainty and a relative uncertainty. For example, the second fuzzy comparison in the LHS of the rule shown in Figure 8 is to be carried out using an absolute uncertainty of 2 and a relative uncertainty of 0.1. The confidence returned by this fuzzy comparison is calculated in the manner described in the next paragraph.

FLOPS assumes that the attribute—in this case, the design load—is a normal variate with a mean value of 20 and a standard deviation that is determined as follows:

$$s = [A^2 + (Rm)^2]^{1/2}$$

where

s = standard deviation,

```
rule 600 2 (xdata   ^design_load >= 0.    ^design_load <= 20. )
           (pile_type  ^criterion1.CIPM = 0)
      -->
     modify 2  ^criterion1.CIPM;
```

FIGURE 8 An example of generated rule with fuzzy comparison.

A = absolute uncertainty = 2 in this example,
R = relative uncertainty = 0.1 in this example, and
m = mean value = 20 in this example.

The confidence value resulting from such fuzzy comparison then becomes a simple matter of determining a probability. For a design load of much larger than 20, the value will be very close to 0; for a design load of about 20, the value will be about 0.5 (500/1,000); for a design load of much smaller than 20, the value will be very close to 1 (1,000/1,000).

EXTERNAL PROGRAMS OF PS1

External programs used in the PS1 system are treated as commands in the DOS environment and, as such, they communicated with the FLOPS program through a *call* command, with name of the executable program as the only argument. For example, the RHS of the rule shown in Figure 9 consists of two calls to the DOS commands. One is an executable program GETDATA, treated as a command. The other is a true DOS command *pause*. Although FLOPS allows for a direct call by reference (address) to a program written in C, it is considered to be advantageous to adopt the former method for this particular expert system.

The two external programs used are GETDATA and COMBINE, both written in C language and compiled by using Microsoft C 5.1 compiler (*30*) for use in the DOS environment. It should be noted that any DOS-based C compiler may be used for compiling. Once the program is compiled, it can run without the presence of the compiler.

The program GETDATA is used for gathering problem-specific data on a particular project. GETDATA is itself a complete program and can be run separately in the DOS environment. In fact, it is often run separately to create the data file to be used in PS1. The program GETDATA essentially serves as a user interface to the PS1 system. A segment of the screen output when running GETDATA is shown in Figure 10 to give the flavor of the program.

The program COMBINE is used for consolidating the preliminary conclusions reached by the PS1 system. The data needed for running the program COMBINE are created by the system and stored in an external file called pile_type.dat, which is an ASCII stream file. The data in file pile_type.dat represent the preliminary conclusions reached by the PS1 system. These data are the degrees of confidence toward each member of the fuzzy set attributes. As defined in the PS1

```
:comments
:block #1 - for gathering problem-specific data from the user
:rule r27

rule 1000 1 (start)
     -->
     write '\n*********************************************\n',
     write '   Begin to gather the problem_specific data. \n',
     write '*********************************************\n',
     call GETDATA,
     transfer xdata from user.dat,
     write '\nUser-supplied data have been loaded to PS1.\n',
     call pause,
     make pile_type;
```

FIGURE 9 An example of calling DOS commands from PS1.

```
Use previously-created data file ("user.dat")? (y/n)
n

ANSWER ALL QUESTIONS ASKED ...

Is data on DESIGN LOAD PER PILE known
or can be estimated? (y/n)
y

Estimated or required design load per pile (tons) =?
25
.
.
.
Which one of the descriptions is more-or-less the most
accurate on SUBSURFACE SOIL PROFILE?
  1) very deep soft layer, 2) soft layer underlain by
  medium to stiff layer, 3) soft layer underlain by hard
  stratum, 4) why?
(Enter 1, 2, 3, or 4):
2

What is the confidence of your answer on last question?
  1) absolutely sure, 2) very sure, 3) sure
(Enter 1, 2, or 3):
1
.
.
.
```

FIGURE 10 Segment of a screen output when running GETDATA.

system, the members of these attributes are PC, PSC, CIPM, CIP, STL, TM, CPW, CPS, PIC, and BP, as defined above. Each preliminary conclusion is reached based on each and every one of the seven factors (criteria) employed. An example of a possible conclusion is as follows:

criterion1 = {0.6/PC, 0.6/PSC, 0.95/CIPM, 0.5/CIP,
0.1/STL, 0.5/TM, 0.95/CPW, 0.9/CPS,
0.1/PIC, 0.2/BP}

where the values are the confidences toward the individual members. (In FLOPS notation, the value 0.6 is stored as 600, 1.0 as 1,000, and so on.) In the above example, it may be interpreted that the PS1 system strongly supports the selection of CIPM, CPW, and CPS piles; it gives moderate support to selection of PC, PSC, CIP, and TM piles, and almost no support to the others.

The algorithm implemented in the current version of the program COMBINE for consolidating the preliminary conclusions is a simple weighted average method. During the development of the PS1 system, other algorithms such as FLOPS' weakly monotonic logic, weighted fuzzy union, and fuzzy weighted average (*8,9*) were considered. It was decided to implement the above algorithm on this version of COMBINE for its simplicity. It was found that PS1 is working properly with this algorithm. Future versions of COMBINE might adopt other algorithms.

KNOWLEDGE DATA BASES OF PS1

The subject of extracting knowledge from experts is beyond the scope of this paper. However, a brief overview is in order for interested readers.

As mentioned earlier, knowledge may be extracted from relevant literature or through interviews with experts. In gen-

eral, the former may be used for fast prototyping of the desired system. It is generally done with intention to upgrade the knowledge data base later. This route is particularly suitable for cases where the system framework is more or less dependent on the knowledge data base. The system designer is also acting as a domain expert to determine what knowledge to incorporate, to what degree of certainty (or uncertainty) a piece of knowledge can become useful, and how to represent the knowledge (rule-based, frame-based, or others). This is the route taken in the development of PS1.

On the other hand, knowledge may be extracted from an expert or a group of experts. There are obvious advantages taking this route. For one, any system developed will perform only as well as the knowledge stored in it. This route requires very thorough planning and skillful interviews. There are some common methods in practice, but discussion of the subject is beyond the scope of this paper.

A comprehensive review of pile foundation literature was conducted during the development of PS1. It was decided that the first version of the system would deal only with the preliminary selection of pile type, and that the capacity to do design analysis and to make cost comparison will follow later. Findings of that review were documented in detail elsewhere (*31*). A summary is presented in the paragraphs that follow.

For the intended system, it was decided that 10 load-bearing piles will be covered. These pile types were listed above. The focus of the review is to determine under what circumstances a pile will be considered suitable for the project. Based on overall evaluation, seven factors (criteria) were identified as "knowledge" important to the preliminary selection. They are design load requirements, soil parameters, approximate pile length requirement, availability of pile material, local construction experience, vibration and noise effects. Obviously, on a given project these factors might weigh differently. It was decided that the weight will be handled in the system rather than in the knowledge data base. The current version of PS1 allows for the user to select the default setting or input these weights at run time. This feature makes a sensitivity study, if desired, easy to conduct.

Selection of pile type is based on the seven factors (criteria) mentioned above. Users of the developed system need only to input the required information concerning these factors through an interactive, menu-driven program. The rating scale for each criterion is stored in the knowledge base in terms of confidence level. Determination of the confidence level was based on "averaged opinions" obtained from literature review. A "preference rating" for each pile is obtained for a given set of site and design information according to each criterion. With the preference rating based on each criterion determined and weights among the seven criteria selected, the overall preference rating (in terms of a numerical index ranging from 0 to 1) can be computed for selecting each of the pile candidates considered for a given set of conditions. The user then has an option to print out the overall preference ratings of top three pile selections or all piles considered.

Among the seven factors adopted, the subsurface soil parameter is perhaps the most complicated one. Many soil characteristics might affect the selection of a pile, and indeed most of them were seriously considered for inclusion in the system. The current version of PS1, however, adopts only four general subfactors under this category: soil type, strength description, possibility of negative skin friction, and possibility of undesired conditions (such as presence of boulders). For other factors incorporated in the system, the situation is simpler. Only a rating scale, qualitative or quantitative, is needed.

Having established the system framework, it was decided that the factual knowledge will be coded in a data base like the one shown in Figure 5. The next task was to assign the confidence value for selecting each pile based on each factor under a given circumstance. It was decided any entry with a confidence value of less than 0.3 should be discarded. Also, the uncertainty associated with fuzzy comparison of the rules in PS1 was arbitrarily taken as a uniform 15 percent variation, although this datum could be directly included in the data base. Following the above general principles, a total of seven data bases were created as part of the PS1 system.

EXAMPLE

As a hypothetical example, consider a site consisting of a deep layer of loose sand overlying a deep layer of dense sand. Site investigation reveals no boulders in the ground. The design load per pile is estimated to be 25 tons. The length of pile is estimated to be 40 to 50 ft. There is no noise constraint, but a vibration constraint is present. The local contractor is knowledgeable in most types of piling construction except for auger-placed concrete piling, composite wood-concrete piling, and pressure-injected piling. No particular emphasis is placed on any pile selection criterion (factor).

With the above information input through the execution of GETDATA, the PS1 system began its internal reasoning process and reached a conclusion. The top selections recommended were a cast-in-place pile with mandrel and a timber pile. For this rather general description of the site, however, the support for other piles is also strong.

Although not shown in the paper, many examples were worked out with PS1 and the results were reasonable (*31*). For a preliminary pile selection, PS1 seems to be able to make right choice.

CONCLUDING REMARKS

The paper has documented details of the development of the expert system PS1. In particular, rule generation, inductive reasoning, combination of preliminary conclusions, and treatment of fuzzy comparison were discussed in depth. The experience gained and presented in this paper should be helpful to interested readers. Departing from the original intent because of space limit, the entire PS1 system and the screen output during its execution are not listed in this paper. However, the system can be obtained from the authors.

PS1 is working properly and is able to reach reasonable conclusions. However, further examination and calibration by experts is needed before it can be claimed as a reliable expert system. For that reason, the authors consider it at present a prototype of the intended system. Planned improvements to the system include additional quantitative soil parameters for the pile selection, as well as the design and cost analyses.

ACKNOWLEDGMENT

The writers wish to express their gratitude to the reviewers of this paper, whose comments have made it a better one.

REFERENCES

1. W. Siler and D. Tucker. *FLOPS Program and User Manual, Version 1.2c*. Kemp-Carraway Heart Institute, Birmingham, Ala., 1986.
2. L. A. Zadeh. *Fuzzy Sets. Information and Control*, Vol. 8, 1965, pp. 338–353.
3. L. A. Zadeh. Outline of A New Approach to the Analysis of Complex Systems and Decision Process. *IEEE Transactions on Systems, Man and Cybernetics SMCX-3*, 1973, pp. 28–44.
4. C. Brown. A Fuzzy Safety Measure. *Journal of Engineering and Mechanics*, ASCE, Vol. 105, No. EM5, 1979, pp. 855–872.
5. C. Brown and J. T. P. Yao. *Fuzzy Sets in Structural Engineering. Journal of Structural Engineering*, ASCE, Vol. 109, No. 5, 1983, pp. 1211–1225.
6. C. H. Juang and D. J. Elton. Fuzzy Logic for Estimation of Earthquake Intensity Based on Building Damage Records. *Civil Engineering Systems*, Vol. 3, 1986, pp. 187–191.
7. C. H. Juang, J. L. Burati, and S. N. Kalidindi. A Fuzzy System for Bid Proposal Evaluation Using Microcomputers. *Civil Engineering Systems*, Vol. 4, 1987, pp. 124–130.
8. C. H. Juang. Development of A Decision Support System Using Fuzzy Sets. *Journal of Microcomputers in Civil Engineering*, Vol. 3, 1988, pp. 157–166.
9. P. W. Mullarkey and S. J. Fenves. Fuzzy Logic in a Geotechnical Knowledge-Based System: CONE. *Proc., NSF Workshop on Civil Engineering Applications of Fuzzy Sets*, Purdue University, Lafayette, Ind., 1985, pp. 126–169.
10. J. E. Bowles. *Foundation Analysis and Design*, 4th ed., McGraw-Hill, New York, 1988.
11. J. L. Briaud and L. M. Tucker. Piles in Sand: A Method Including Residual Stresses. *Journal of Geotechnical Engineering*, ASCE, Vol. 111, No. 11, 1984, pp. 1666–1680.
12. Canadian Geotechnical Society. *Canadian Foundation Engineering Manual*, chaps. 19-21. BiTech Publishers, Vancouver, B.C., Canada, 1985.
13. R. D. Chellis. *Pile Foundation*, 2nd ed. McGraw-Hill, New York, 1961.
14. R. S. Cheney and R. G. Chassie. *Soils and Foundations Workshop Manual*. FHWA, U.S. Department of Transportation, Washington, D.C., 1982.
15. H. M. Coyle and R. Castello. New Design Correlations for Piles in Sand. *Journal of Geotechnical Engineering Division*, ASCE, Vol. 107, No. 7, 1981, pp. 965–986.
16. B. M. Das. *Principles of Foundation Engineering*, chap. 8. PWS Engineering, Boston, 1984.
17. B. H. Fellenius. *Negative Skin Friction on Long Piles Driven in Clay*. Report 18. Royal Swedish Academy of Engineering Science, Stockholm, 1971.
18. F. M. Fuller. *Engineering of Pile Installations*. McGraw-Hill, New York, 1983.
19. D. M. Greer and W. S. Gardner. *Construction of Drilled Pier Foundations*. John Wiley and Sons, New York, 1986.
20. G. G. Meyerhof. Bearing Capacity and Settlement of Pile Foundations. *Journal of Geotechnical Engineering*, ASCE, Vol. 102, No. GT3, 1976, pp. 195–228.
21. R. L. Nordlund. Bearing Capacity of Piles in Cohesionless Soils. *Journal of Soil Mechanics and Foundation*, ASCE, Vol. 89, No. 3, 1963, pp. 1–35.
22. *NAVFAC Design Manual, Foundations and Earth Structures*, Vol. 7.2. Naval Facilities Engineering Command, U.S. Department of Navy, Washington, D.C., 1982.
23. M. W. O'Neill. *Pile Group Prediction Symposium: Summary*. FHWA, U.S. Department of Transportation, Washington, D.C., 1987.
24. M. G. Spangler and R. L. Handy. *Soil Engineering*, 4th ed. Harper and Row, New York, 1982.
25. A. G. Thurman. Discussion of "Bearing Capacity of Piles in Cohesionless Soils," by R. L. Nordlund. *Journal of Soil Mechanics and Foundation*, ASCE, Vol. 90, No. 1, 1964, pp. 127–129.
26. S. N. Vanikar. *Manual on Design and Construction of Driven Pile Foundations*. FHWA, U.S. Department of Transportation, Washington, D.C., 1986.
27. A. S. Vesić. *NCHRP Synthesis of Highway Practice 42: Design of Pile Foundations*. TRB, National Research Council, Washington, D.C., 1977.
28. T. Whitaker. *The Design of Piled Foundations*. Pergamon, New York, 1976.
29. C. H. Juang and D. H. Lee. Development of an Expert System for Rock Mass Classification. Accepted for publication by *Journal of Civil Engineering Systems*, 1989.
30. *Microsoft C Compiler, Version 5.1*. Microsoft Corporation, Redmond, Wash., 1988.
31. C. H. Juang and M. L. Ulshafer. *Development of a Fuzzy Logic Expert System for Pile Selection*. Department of Civil Engineering, Clemson University, Clemson, S.C., 1989.

Publication of this paper sponsored by Committee on Foundations of Bridges and Other Structures.